

# **RAFT Dispersion Polymerisation in Silicone Oil**

**Matthew Joseph Rymaruk**



**The  
University  
Of  
Sheffield.**

The University of Sheffield  
Department of Chemistry

Thesis submitted for the degree of Doctor of Philosophy

September 2018

## **Declaration**

The work described in this thesis was carried out at the University of Sheffield under the supervision of Professor Steven P. Armes FRS between October 2014 and September 2018. It has not been submitted, either wholly or in part, for any other degree. All the work is the original work of the author, except where acknowledged by references.

Signature:.....

Matthew Joseph Rymaruk

September 2018

# Acknowledgements

I am indebted to a very large number of people, without whom much of the work described in this thesis would not be possible. First and foremost, I would like to thank my supervisor, Professor Steve Armes FRS, for giving me the opportunity to carry out my PhD under his supervision. I have learned a great deal over the last four years, and I cannot thank you enough for all the support and guidance you have given me.

My sponsors, Scott Bader and the EPSRC, are thanked for their very generous funding. In particular, I would like to express my gratitude to my industrial supervisors Clive Williams, Dr. Steven Brown and Dr. Vicki Cunningham, for all of their invaluable input during the course of my project. I would also like to thank the Scott Bader Company, in general, for letting me work there for six months during the course of my PhD. Not only was this a perspective-broadening experience, but everyone there was incredibly friendly and made me feel welcome.

I have been fortunate enough to travel to some amazing places during the course of my PhD studies, something else I would like to thank you for, Steve. A particular highlight was a 3-month secondment spent working at the University of Newcastle (Australia, not UK!). Professor Erica Wanless is thanked for allowing me the opportunity to work in her group.

I'm grateful to Svet and Chris, for their help with TEM, and Sandra for her help with NMR. A number of technical and support staff must also be thanked for making day-to-day running of the Chemistry Department possible. In particular, Denise Richards, Nick Smith, Sharon Spey, Stephen Atkin, Craig Robertson, Richard Bottomley, Simon Thorpe, Richard Wilkinson and Rob Hanson.

A big thanks goes to Liam Ratcliffe for helping me get started in the lab, and for being a great friend over the past four years. In addition, everyone in the Armes group & F3 (past and present) for being great people. Thanks goes to Derry, Beulah, Fiona, Joe, Penners, Byard (Wilson), Saul, Erik, Yin, Amy, Vicki, Lizzy, Simon, Nick Warren, Lee, Mark, Tom, Shannon, Olly, Reb, Debs, Canning, Gwen, Mable (Morse), Dave, Christoph, Derek, Rheanna, Emma, Jasmine, Anna, Kate Thompson, Greg Smith, Craig, Paul and Izzy.

The centre for doctoral training (CDT) program has been a fantastic addition to my PhD studies, and I've thoroughly enjoyed all of the activities that came with it. All of these would not have been possible without Dr. Joe Gaunt. Thank you for putting in huge amounts of work to organise everything, and for always being available to lend an ear. I would also like to thank every CDT student for being generally friendly and helpful. A special mention goes to Kat, Dom, Amy, Luke and Ste, our regular(ish) coffee breaks really helped put things into perspective.

Thank you to all of my family, for always being there for me. To my mum and big sister, thank you so much for the unconditional love and support. You've always encouraged me to do my best, and this thesis is dedicated to you both.

Finally, to Cate, thank you for being the incredible person that you are. These past (almost!) two years have been the happiest I've been, and I can't wait to see what the future holds for us. Also, you probably deserve a medal for the amount of proof reading you've done, I'll see what I can do.

## Publications

### Primary Publications

(1) **Rymaruk, M. J.**; Thompson, K. L.; Derry, M. J.; Warren, N. J.; Ratcliffe, L. P. D.; Williams, C. N.; Brown, S. L.; Armes, S. P. Bespoke Contrast-Matched Diblock Copolymer Nanoparticles Enable the Rational Design of Highly Transparent Pickering Double Emulsions. *Nanoscale* **2016**, *8*, 14497-14506

### Secondary Publications

(2) Lopez-Oliva, A. P.; Warren, N. J.; Rajkumar, A.; Mykhaylyk, O. O.; Derry, M. J.; Doncom, K. E. B.; **Rymaruk, M. J.**; Armes, S. P. Polydimethylsiloxane-Based Diblock Copolymer Nano-Objects Prepared in Nonpolar Media via RAFT-Mediated Polymerization-Induced Self-Assembly. *Macromolecules* **2015**, *48*, 3547–3555.

### Abstract

The work described in this thesis involves reversible addition-fragmentation chain transfer (RAFT) dispersion polymerisation conducted primarily in silicone oil. This is an example of polymerisation-induced self-assembly (PISA), which provides a convenient and facile route to the reproducible synthesis of range of polymer nanoparticles.

In Chapter 2, a silicone oil-soluble PDMS<sub>66</sub> macromolecular chain transfer agent (macro-CTA) is prepared *via* esterification of a carboxylic acid-based RAFT CTA with monohydroxy-terminated PDMS<sub>66</sub>. This macro-CTA is then chain-extended with a range of methacrylic monomers directly in decamethylcyclopentasiloxane (D5). Spherical nanoparticles are obtained in all cases, except when using 2-(dimethylaminoethyl) methacrylate (DMA). In this case, spheres, worms or vesicles can be obtained in D5. In addition, PDMS-PDMA worms are also synthesised in three other solvents, hexadimethyldisiloxane, *n*-dodecane and octamethylcyclotetrasiloxane (D4). Furthermore, these PDMS-PDMA worms form soft free-standing gels at ambient temperature owing to multiple inter-worm contacts. This gelation behaviour is characterised by oscillatory and rotational rheometry, which suggests that PDMS-PDMA worms may have potential application as thickeners for non-polar solvents, specifically silicone oil.

When PDMS-PDMA worms are heated to 110 °C in D5, they undergo a worm-to-sphere transition. This is attributed to surface plasticisation of the nanoparticle core by the hot solvent. This transition is probed using <sup>1</sup>H NMR, transmission electron microscopy, rheology and small-angle X-ray scattering. The effect of incorporating a cross-linking agent, 1,2bis(2-iodoethoxy)ethane (BIEE) into these PDMS-PDMA nanoparticles is also investigated. Covalent cross-linking has the most demonstrable effect on the worms: not only do they form significantly stronger gels, they are also no longer thermoresponsive.

To produce spheres, worms or vesicles in D5 with a monomer other than DMA, a new silicone-containing macro-CTA is prepared *via* RAFT solution polymerisation of 3-[tris(trimethylsiloxy)silyl]propyl methacrylate (SiMA). The resulting PSiMA macro-CTA enables the formation of spheres, worms, or vesicles when chain-extended with benzyl methacrylate (BzMA) in D5. Two phase diagrams are constructed in order to facilitate the reproducible synthesis of these morphologies, with the copolymer concentration, PSiMA DP and PBzMA DP being important parameters.

PSiMA-PBzMA spherical nanoparticles can also be prepared in a low molecular weight silicone oil with a viscosity of 5 cSt (DM5). The ability of such nanoparticles to stabilise oil-in-DM5 Pickering emulsions is explored. A range of natural oils can be utilised for the dispersed phase, such as sunflower oil or castor oil, with the resulting emulsions stable for at least 2 months. Moreover, by statistically copolymerising lauryl methacrylate (LMA) with BzMA to form the nanoparticle cores, a much wider range of oils can be used as the dispersed phase. It is hypothesised that this is owing to the enhanced wettability of the resulting PSiMA-P(BzMA-stat-LMA) spherical nanoparticles by the various different vegetable oils examined.

RAFT aqueous emulsion polymerisation is used to prepared to spherical nanoparticles with a semifluorinated core-forming block. Such nanoparticles have a relatively low refractive index, which can be matched to the aqueous phase by adding either sucrose or glycerol. Such isorefractive particles facilitate the production of highly transparent Pickering emulsions when an isorefractive oil (*n*-dodecane) is used as the dispersed phase. Finally, when these hydrophilic particles are used in conjunction with similar oil-dispersed particles comprising the same semifluorinated core-forming block, highly transparent Pickering double emulsions can be produced.

## Terminology

---

AIBN	-	2,2' Azobisisobutyronitrile
ATRP	-	Atom transfer radical polymerisation
BzMA	-	Benzyl methacrylate
BIEE	-	1,2-Bis(2-iodoethoxy)ethane
CGC	-	Critical gelation concentration
CGT	-	Critical gelation temperature
CTA	-	Chain transfer agent
Đ	-	Dispersity
DLS	-	Dynamic light scattering
DP	-	Degree of polymerisation
FRP	-	Free radical polymerisation
G'	-	Dynamic storage modulus
G''	-	Dynamic loss modulus
GMA	-	Glycerol monomethacrylate
GPC	-	Gel permeation chromatography
HPMA	-	2-Hydroxypropyl methacrylate
LAP	-	Living anionic polymerisation
LMA	-	Lauryl methacrylate
M <sub>n</sub>	-	Number-average molecular weight
M <sub>w</sub>	-	Weight-average molecular weight
MAA	-	Methacrylic acid
Macro-CTA	-	Macromolecular chain transfer agent
MMA	-	Methyl methacrylate
MWD	-	Molecular weight distribution
NMP	-	Nitroxide-mediated polymerisation
NMR	-	Nuclear magnetic resonance
PAO	-	Poly( $\alpha$ -olefin)
PETTC	-	4-Cyano-4-(2-phenylethanesulfanylthiocarbonyl) sulfanylpentanoic acid
PISA	-	Polymerisation-induced self-assembly
PRE	-	Persistent radical effect
RAFT	-	Reversible addition-fragmentation chain transfer
RDRP	-	Reversible deactivation radical polymerisation
SAXS	-	Small-angle X-ray scattering
SIPLI	-	Shear-induced polarised light imaging

## Terminology

---

SiMA	-	3-[Tris(trimethylsiloxy)silyl]propyl methacrylate
SMA	-	Stearyl methacrylate
T21s	-	<i>Tert</i> -butyl peroxy-2-ethylhexanoate
TEM	-	Transmission electron microscopy
TFEMA	-	2,2,2-Trifluoroethyl methacrylate
UCST	-	Upper critical solution temperature
$\omega$	-	Angular frequency
$\sigma$	-	Stress
$\varepsilon$	-	Strain
$\eta$	-	Viscosity

## Table of contents

---

# Table of contents

### Chapter 1: Introduction

1.1	Polymer science	2
1.2	Polymer characterisation	4
1.2.1	Gel permeation chromatography	4
1.3	Chain growth polymerisation	6
1.3.1	Free radical polymerisation	6
1.3.2	Living anionic polymerisation	9
1.3.3	Reversible deactivation radical polymerisation	12
1.4	Polymerisation conditions	21
1.4.1	Dispersion polymerisation	21
1.4.2	Emulsion polymerisation	23
1.5	Self-assembly	25
1.5.1	Self-assembly of diblock copolymers in bulk	25
1.5.2	Self-assembly of diblock copolymer in solution	28
1.6	Polymerisation-induced self-assembly	31
1.6.1	RAFT aqueous dispersion polymerisation	31
1.6.2	RAFT dispersion polymerisation in non-polar media	35
1.6.3	RAFT aqueous emulsion polymerisation	41
1.7	Particle characterisation techniques	43
1.7.1	Dynamic light scattering	44
1.7.2	Rheology	44
1.7.3	Shear-induced polarised light imaging	48
1.7.4	Small-angle X-ray scattering	52
1.8	Thesis outline	54
1.9	References	55

### Chapter 2: Synthesis of Diblock Copolymer Nanoparticles in Silicone Oils

2.1	Introduction	65
2.2	Experimental Section	66
2.2.1	Materials	66
2.2.2	Methods	67
2.2.3	Characterisation	68
2.3	Results and discussion	70
2.3.1	Synthesis of diblock copolymers in D5 silicone oil	72

## Table of contents

---

2.4	Conclusions	83
2.5	References	84

### Chapter 3: Effect of Cross-linking on the Thermoresponsive Behaviour of PDMS-PDMA Nanoparticles in Silicone Oil

3.1	Introduction	88
3.2	Experimental	91
3.2.1	Materials	91
3.2.2	Methods	91
3.2.3	Characterisation	91
3.3	Results and discussion	93
3.3.1	Synthesis of PDMS <sub>66</sub> -PDMA <sub>x</sub> diblock copolymer nanoparticles in D5	93
3.3.2	Thermoresponsive behaviour of PDMS <sub>66</sub> -PDMA <sub>100</sub> worms	94
3.3.3	Cross-linking PDMS <sub>66</sub> -PDMA <sub>100</sub> worms with BIEE	96
3.3.4	Kinetics of cross-linking	98
3.3.5	Variable temperature DLS	103
3.3.6	Rheology of cross-linked worm gels	104
3.3.7	Shear-induced polarised light imaging	107
3.3.8	Small-angle x-ray scattering	109
3.3.9	Influence of cross-linking on CGC	111
3.4	Conclusions	112
3.5	References	113

### Chapter 4: RAFT Dispersion Polymerisation in Silicone Oil Using a Silicone-Based Methacrylic Stabiliser

4.1	Introduction	119
4.2	Experimental	121
4.3	Results and discussion	123
4.3.1	Chain-extension of P <i>Si</i> MA macro-CTAs with BzMA in D5 silicone oil	127
4.3.2	Construction of a P <i>Si</i> MA <sub>x</sub> -PBzMA <sub>y</sub> phase diagram	129
4.3.3	Influence of concentration upon copolymer morphology	132
4.3.4	Spontaneous cross-linking of P <i>Si</i> MA <sub>x</sub> -PBzMA <sub>y</sub> nanoparticles over time	134
4.4	Conclusions	137
4.5	References	137

## Table of contents

---

### Chapter 5: Oil-in-Oil Pickering Emulsions Stabilised by Polymeric Nanoparticles

5.1	Introduction	141
5.2	Experimental section	145
5.2.1	Materials	145
5.2.2	Methods	145
5.2.3	Characterisation	147
5.3	Results and discussion	149
5.3.1	Nanoparticle synthesis	149
5.3.2	Determination and characterisation of immiscible oils	152
5.3.3	PSiMA-PBzMA spherical nanoparticles as Pickering emulsifiers	153
5.3.4	Droplet diameter as a function of PSiMA <sub>19</sub> -PBzMA <sub>200</sub> concentration	156
5.3.5	Droplet diameter as a function of time	158
5.3.6	Tuning the nanoparticle wettability to improve emulsifier performance	162
5.4	Conclusions	168
5.5	References	168

### Chapter 6: Bespoke Isorefractive Diblock Copolymer Nanoparticles Enable the Rational Design of Highly Transparent Pickering Emulsions

6.1	Introduction	172
6.2	Experimental	173
6.2.1	Materials	173
6.2.2	Methods	174
6.2.3	Characterisation	177
6.3	Results and discussion	179
6.3.1	Nanoparticle synthesis and refractive index matching	179
6.3.2	Preparation of isorefractive Pickering emulsions	183
6.3.3	Control experiments with non-isorefractive nanoparticles	186
6.3.4	Isorefractive Pickering double emulsions	188
6.4	Conclusions	191
6.5	References	191

### Chapter 7: Conclusions and future work

7.1	References	200
-----	------------	-----

# Chapter 1: Introduction

## 1.1 Polymer science

A polymer (from the Greek “poly” meaning “many”, and “mer” meaning “parts”) is a macromolecule comprising smaller repeat units linked together. The repeat units that combine to form the polymer chain are known as *monomers*, the reactions by which they combine are termed *polymerisations*, and the number of repeat units per polymer chain is defined as the degree of polymerisation (DP).<sup>1</sup> Polymers play a huge role in modern-day living. Plastics can be found in every facet of our lives, from clothing and food packaging to aerospace components, contact lenses and medical implants.<sup>2</sup> Human history is often categorised chronologically as, for example, the stone age, the bronze age, and the iron age; today we are living in the plastic age.

The macromolecular structure of polymer chains was first elucidated by Staudinger in a landmark paper in 1920, for which he later received the Nobel Prize in Chemistry.<sup>3</sup> However, many of his colleagues still challenged his assertions for almost a decade. Ultimately, the proof of the long-chain nature of polymers was provided by Mark and Carothers independently. Mark used the newly-developed technique of X-ray crystallography to demonstrate that cellulose was composed of giant fibres, each containing thousands of atoms.<sup>4,5</sup> This discovery overturned the commonly held notion at the time that molecular weights could be no more than a few hundred Daltons. Similarly, Carothers demonstrated that polymers such as nylon and polyesters could be prepared using well-understood synthetic organic chemistry.<sup>6,7</sup>

To form a polymer chain, a monomer must possess at least two sites available for bonding. Unsurprisingly, a large number of different compounds satisfy this broad criterion and have been used to prepare polymer chains. Consequently, polymers with many different compositions and architectures have been reported over the last century. A schematic representation of the most commonly encountered polymeric architectures, ranging from simple linear homopolymers to block, star and graft copolymers, are depicted in **Figure 1.1**.

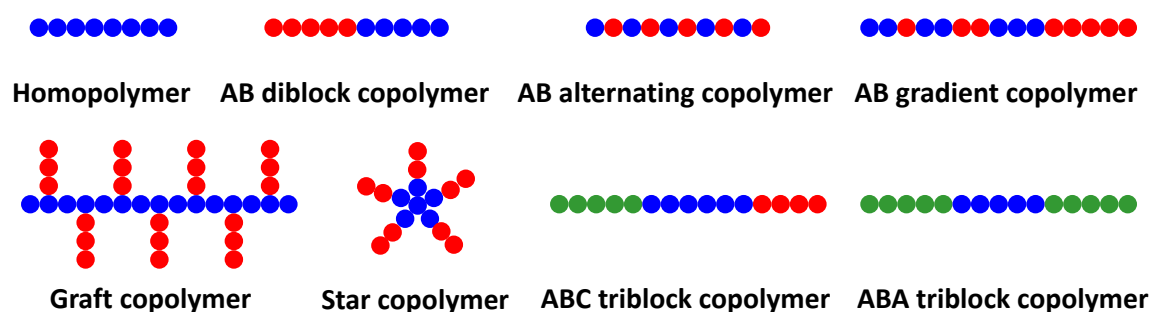


**Figure 1.1:** Schematic representation of a range of various (co)polymer architectures. The filled coloured circles represent monomer units of a particular chemical identity.

Of the different polymers depicted in **Figure 1.1**, the ones of most relevance to this thesis are linear homopolymers and diblock copolymers. In general, a polymer is described as linear when it is formed from monomer units that are linked together to form a long, straight chain. Typically, linear synthetic polymers contain a distribution of chain lengths (DPs) centred around an average value. A direct consequence of this distribution is that polymers do not have a unique molecular weight and instead possess a molecular weight distribution (MWD). For polymers possessing a normal distribution of molecular weights, there are two parameters used to describe them.<sup>1</sup> The first is the number-average molecular weight,  $M_n$ , which is given by equation (1.1):

$$M_n = \frac{\sum N_i M_i}{\sum N_i} \quad (1.1)$$

Here  $N_i$  is the number of molecules with weight  $M_i$ . The  $M_n$  of a polymer is the ordinary arithmetic mean, or the average molecular weight of all of the individual polymer chains. The second useful descriptor is the weight-average molecular weight,  $M_w$ , which is defined according to equation (1.2):<sup>1</sup>

$$M_w = \frac{\sum N_i M_i^2}{\sum N_i M_i} \quad (1.2)$$

$M_w$  is biased towards longer (more massive) chains. Therefore, for any polymer possessing a distribution of molecular weights, it follows that  $M_w > M_n$  and  $M_w / M_n$  will always be greater than unity. In fact,  $M_w / M_n$  is a useful, albeit crude, description of the breadth of a molecular weight distribution and is commonly known as the dispersity ( $\mathfrak{D}$ ) or, historically, the polydispersity index (PDI):

$$\mathfrak{D} = \frac{M_w}{M_n} \quad (1.3)$$

For polymers with narrow MWDs,  $M_w / M_n$  will be close to unity, typically of the order of 1.1 - 1.2. Conversely, for polymers with broad MWDs, which are composed of chains with vastly different DPs,  $M_w / M_n$  will be large, typically greater than 2.

### 1.2 Polymer characterisation

In addition to the chemical structure of a polymer, its molecular weight and dispersity also play a huge role in determining its physical characteristics. Properties such as viscosity, solubility, intrinsic viscosity and glass transition temperature ( $T_g$ ) can all be influenced by  $M_n$ . Therefore, it is crucial that these parameters can be determined for a given polymer. A number of techniques are available for such a purpose, such as nuclear magnetic resonance (NMR) spectroscopy, static light scattering, and osmometry. However, arguably the most utilised is gel permeation chromatography (GPC), otherwise known as size exclusion chromatography.<sup>8</sup>

#### 1.2.1 Gel permeation chromatography

GPC is a chromatographic technique that separates polymers according to their hydrodynamic volume ( $V_h$ ).<sup>8</sup> This is achieved by passing a polymeric solution through a column packed with porous beads (typically cross-linked polystyrene beads) which act in essence as a reverse filtration system. As the solution flows through the column, molecules with a small  $V_h$  will diffuse into the pores and spend longer in the column, thus increasing their retention time. Molecules with a larger  $V_h$  cannot access the pores and so elute first. The range of pore sizes in the column dictates the range of hydrodynamic volumes that can be fractionated, and in turn the range of molecular weights. Unlike conventional chromatography, it is crucial that the analyte and stationary phase are non-interacting, otherwise the elution time and  $V_h$  will not be directly correlated. Once eluted from the column, the polymer chains are analysed *via* a refractive index, light scattering, ultraviolet, or viscosity detector.

Typically, GPC is a relative technique and so it must be calibrated using a series of low dispersity standards of a known molecular weight (usually polystyrene, PMMA or PEG).<sup>8</sup> Once the analyte of interest has eluted from the column, its elution time is matched with the equivalent elution time of the calibrants and a molecular weight, expressed *relative to the calibration standard*, is obtained. Selection of an appropriate standard is crucial to obtaining meaningful results *via* GPC. For two different polymers of equal molecular weight,  $V_h$  will *not* be identical. Therefore, the extent to which  $V_h$  differs for a given molecular weight will determine how appropriate the calibration standards are judged to be.

For reasons described above, obtaining accurate molecular weights from GPC typically requires that the unknown analyte and calibrant have the same chemical structure. However, the range of commercially available calibration standards is rather narrow, so it is rare that a suitable calibrant will be available for the polymer of interest. One way in which to overcome this problem is to use

a method known as universal calibration. In the 1960s, Benoit and co-workers demonstrated that it is possible to use low-dispersity standards of one type of polymer to provide absolute molecular weight values for an unknown second polymer.<sup>9</sup> This is made possible using the Einstein-Simha viscosity law:<sup>10</sup>

$$[\eta] = C \frac{V_h}{M} \quad (1.4)$$

Here  $[\eta]$  is the intrinsic viscosity,  $M$  is the molecular weight and  $C$  is a constant. This equation demonstrates that the product of  $[\eta]$  and  $M$  is a direct measure of  $V_h$ . Therefore, for two different polymers possessing the same  $V_h$  but different molecular weights, Benoit *et al.* demonstrated that:<sup>9</sup>

$$[\eta]_a M_a = [\eta]_b M_b \quad (1.5)$$

Hence, in principle, this simple relationship can be used to determine the molecular weight of an unknown analyte using a standard. However, for this method to work in practice, one must know the intrinsic viscosity of each slice of the molecular weight distribution of the analyte, which is hugely time intensive. Therefore, equation (1.5) is modified in order to make this approach more practical. This can be achieved by using the Mark-Houwink relationship:<sup>8</sup>

$$[\eta] = KM^\alpha \quad (1.6)$$

Here,  $K$  and  $\alpha$  are constants for a particular polymer-solvent pair at a given temperature. This method, known as universal calibration, is based upon two principles. Firstly, having a GPC with a dual detection system, i.e. a concentration detector and viscosity detector (to measure  $[\eta]$ ) connected in parallel. Secondly, the  $K$  and  $\alpha$  values must be known for *both* the standard *and* the analyte. If these conditions are satisfied, equation (1.6) can be substituted into equation (1.5) which results in equation (1.7) for the absolute molecular weight of the analyte (expressed in known quantities, without needing to know the intrinsic viscosity of each slice of the MWD):<sup>8</sup>

$$M_2 = \left( \frac{K_1 M_1^{\alpha_1 + 1}}{K_2} \right)^{\frac{1}{\alpha_2 + 1}} \quad (1.7)$$

However, needing prior knowledge of  $K$  and  $\alpha$  for the unknown sample means that molecular weights must be measured *via* other methods initially. Techniques such as membrane osmometry and light scattering have been traditionally used for this purpose.<sup>1</sup> In summary, GPC is a versatile and convenient technique that has become invaluable in modern-day polymer characterisation.

---

### 1.3 Chain growth polymerisation

In 1929, Carothers classified polymers as either *condensation* or *addition* polymers, based on compositional differences between the polymer and its corresponding monomer(s).<sup>7</sup> Condensation polymers were defined as those formed *via* condensation reactions, which typically involved elimination of a small molecule (e.g. water). Addition polymers, on the other hand, were defined as those formed *without* loss of a small molecule. In other words, the repeat units of addition polymers have the same composition as the monomer(s) from which they are composed. The problem with this definition, however, is that it can lead to certain discrepancies. Polyurethanes, for example, would be classified as addition polymers under this definition yet they are more structurally similar to condensation polymers. To avoid this discrepancy, in 1953 Flory reclassified polymers based on their mechanism of formation.<sup>11</sup> *Step polymerisations* are hence defined as those which occur *via* repeating stepwise reactions of functional groups. In contrast, *chain polymerisations* involve successive addition of monomer units to a propagating active centre, typically a radical, cation or anion. Step polymerisations will not be reviewed in this thesis, but chain polymerisations will be discussed in detail.

#### 1.3.1 Free radical polymerisation

Free-radical polymerisation (FRP) is a robust type of chain-growth polymerisation, responsible for the production of almost 50 % of commercially-available synthetic polymers.<sup>2</sup> Radical polymerisation, in its broadest sense, involves the sequential addition of monomer units to a propagating free radical, in order to produce polymer chains. The wide-spread application of FRP can be attributed to a number of factors: the broad range of radically polymerisable monomers, the relatively mild reaction conditions required (up to 100 °C and ambient pressure) and its excellent tolerance towards protic impurities and solvents, such as water. Purification requirements for FRP are also minimal; the only necessity being that the polymerisation should be conducted under deoxygenated conditions because O<sub>2</sub> is a known radical retarder that would otherwise inhibit polymerisation. The compatibility of FRP with monomers containing carboxylic acids, hydroxyl and amine moieties ensures it has the greatest versatility when compared with all other forms of chain-growth polymerisation.

The mechanism of FRP is divided into four fundamental steps: initiation, propagation, termination and transfer (**Figure 1.2**).<sup>1</sup> In FRP, initiation usually comprises two stages: i) the generation of primary initiating radicals, and ii) the reaction of these primary radicals with monomer, resulting in a new active centre. Typically, the generation of the primary initiating radicals occurs *via* the decomposition of an added initiator species such as an azo or peroxide compound.

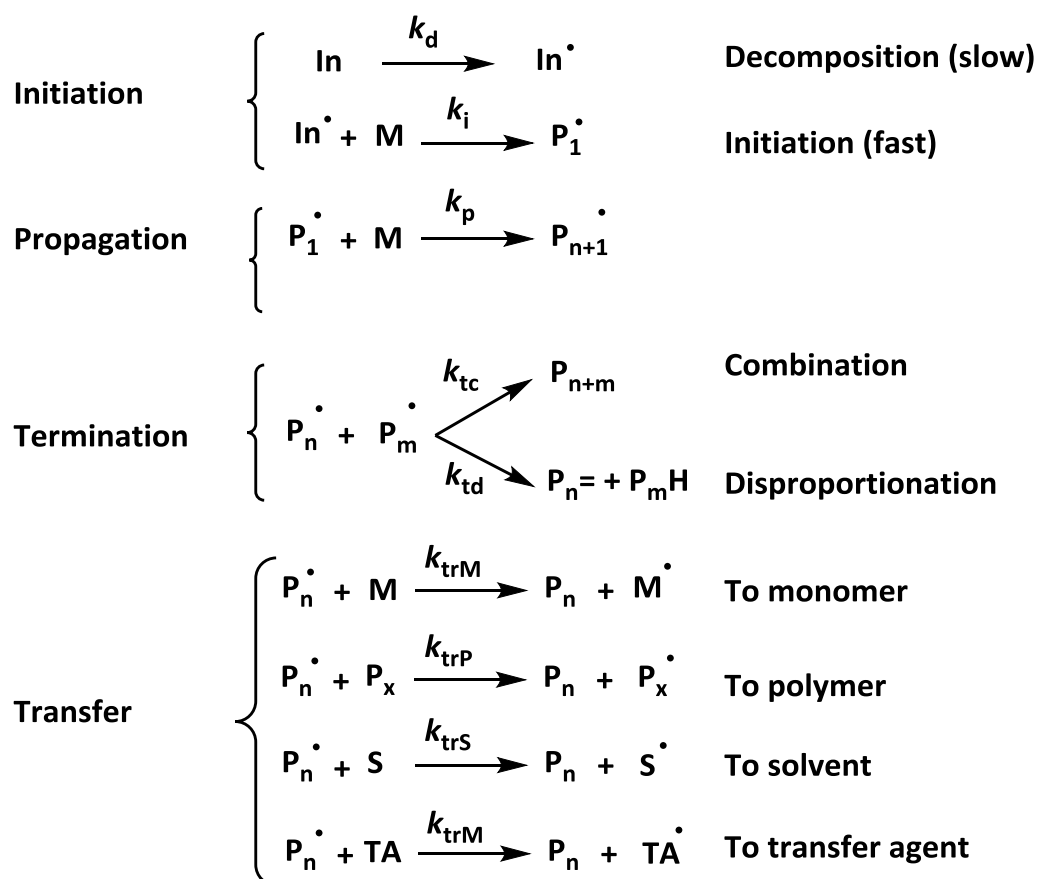


**Figure 1.2:** The four stages of a free radical polymerisation: initiation, propagation, termination and transfer, and accompanying rate constants. In = initiator, M = monomer, P = polymer, S = solvent, TA = transfer agent

Generally, the polymerisation temperature is selected to be approximately equal to the ten hour half-life of the initiator, in order to ensure a constant supply of radicals is available during the course of the polymerisation. Consequently, the decomposition of the initiator is very slow with respect to the initiation of the monomer. One important factor to consider when selecting an initiator for FRP is the initiator efficiency, ( $f$ ), which is defined as the ratio of the number of radicals that initiate polymerisations to the total number of radicals generated. Ideally,  $f$  should be equal to unity, but owing to various side reactions, typical  $f$  values range from 0.3 – 0.8.<sup>12</sup>

After the primary radicals have been generated and reacted with a monomer unit, further monomer units can react sequentially, resulting in the propagation of a polymer chain. The final stage of the polymerisation, termination, occurs between two active radicals and results in dead polymer chains. Termination can occur *via* one of two pathways: combination or disproportionation. Combination is favoured for less sterically-hindered radicals such as styrene or acrylates. Conversely, disproportionation is favoured for more hindered radicals such as methacrylates. The overall rate laws for the various stages of a FRP are summarised in **Table 1.1**

Rate of decomposition	$R_d = -\frac{d[\text{In}]}{dt} = k_d[\text{In}]$
Rate of initiation	$R_i = \frac{d[P_1^\bullet]}{dt} = 2fk_d[\text{In}]$
Rate of propagation	$R_p = -\frac{d[\text{M}]}{dt} = k_p[\text{M}][P_n^\bullet]$
Rate of termination <i>via</i> combination	$R_{tc} = k_{tc}[P_n^\bullet]^2$
Rate of termination <i>via</i> disproportionation	$R_{td} = k_{td}[P_n^\bullet]^2$
Overall rate of termination	$R_t = 2(k_{tc} + k_{td})[P_n^\bullet]^2$
Rate of transfer to monomer	$R_{trM} = k_{trM}[\text{M}][P_n^\bullet]$
Rate of transfer to solvent	$R_{trS} = k_{trS}[\text{S}][P_n^\bullet]$
Rate of transfer to Polymer	$R_{trM} = k_{trP}[P_x][P_n^\bullet]$
Rate of transfer to transfer agent	$R_{trTA} = k_{trP}[\text{TA}][P_n^\bullet]$

**Table 1.1:** Rate equations associated with the major steps of a free radical polymerisation.<sup>1</sup>

In addition to initiation, propagation and termination, transfer reactions also play a role in FRP. Transfer occurs when a propagating polymer radical,  $P_n^\bullet$ , reacts with a non-radical species such as monomer, a dead polymer or solvent. This process results in the formation of a new radical centre,  $R^\bullet$ , and a dead polymer chain. Typically, these reactions have little influence on the polymerisation kinetics because no radicals are consumed. However, they do serve to reduce the final molecular weight of the polymer and are therefore usually undesirable. If one makes the assumption that transfer reactions do not influence the kinetics of FRP, it is possible to derive an equation for the rate of polymerisation based solely on the rate laws for initiation, propagation and termination:<sup>12</sup>

$$R_{\text{polym}} = k_p[\text{M}] \sqrt{\frac{fk_d[\text{In}]}{k_t}} \quad (1.8)$$

Here  $f$  is the initiator efficiency,  $k_d$  is the rate constant for decomposition,  $[\text{In}]$  is the initiator concentration,  $k_t$  is the rate constant for termination,  $[\text{M}]$  is the monomer concentration and  $k_p$  is the rate constant for propagation. In order to derive equation (1.8), a number of assumptions must be made. Specifically, it is assumed that the rate of initiation and termination is the same (i.e. the steady-state approximation) *and* that the fraction of monomer consumed during initiation is negligible.<sup>12</sup> Granted these assumptions, equation (1.8) indicates that the rate of polymerisation is dependent upon  $[\text{M}]$  and  $[\text{In}]^{1/2}$ . Thus, one can predict that increases to both the monomer and

initiator concentration should result in a faster polymerisation rate, which has been experimentally verified.<sup>13</sup>

At this point, it is important to introduce the concept of kinetic chain length,  $\nu$ , which is defined as the average number of monomer units consumed per initiating radical.<sup>12</sup> This is given by the ratio of the rate of propagation to the rate of initiation ( $\nu = R_p/R_i$ ) and describes how the molecular weight varies with  $[M]$  and  $[In]$ . Assuming that the rate of initiation is equal to the rate of termination, then  $\nu = R_p/R_t$ . From the steady-state approximation we know that  $[P_n^*] = (k_d f [In] / k_t)^{1/2}$ . Therefore, combining the relevant rate laws for  $R_p/R_t$  and substituting in the equation for  $[P_n^*]$  we arrive at the following expression:

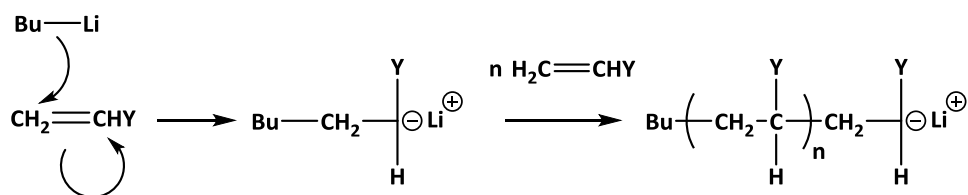
$$\nu = \frac{R_p}{R_t} = \frac{k_p [M]}{2(f k_d k_t [In])^{1/2}} \quad (1.9)$$

Hence, larger molecular weights are proportional to  $[M]$  but also to  $[In]^{-0.5}$ . Therefore, there is an inherent trade-off between polymerisation rate and the molecular weight that can be obtained by FRP. In addition to  $\nu$ , the method of termination also plays a role in determining the final DP of the polymers. If disproportionation is the sole method of termination, the final DP will be simply equal to the kinetic chain length. Conversely, if termination is exclusively *via* combination, then the DP is equal to  $2\nu$ .

Despite the many advantages associated with FRP, there are some inherent drawbacks. Firstly, in order to produce high molecular weight polymers, the concentration of active propagating polymer radicals must be kept very low in order to minimise termination reactions. Consequently, the rate of initiation must be much slower than the rate of propagation. As a result, initiation is not limited to the start of the polymerisation and instead occurs throughout. Therefore, the time at which polymers chains will initiate, propagate and terminate, are all governed by statistical factors. Hence, FRP offers very little control over the dispersity and copolymer architecture.

### 1.3.2 Living anionic polymerisation

Living anionic polymerisation (LAP) is another category of chain-growth polymerisation first reported in 1956 by Szwarc.<sup>14</sup> LAP involves the growth of polymer chains *via* a propagating anionic centre. In the pioneering work of Szwarc, styrene was polymerised using a sodium naphthalenide initiator in dry tetrahydrofuran solvent. For a more generic representation of a LAP formulation, see **Scheme 1.1**<sup>2</sup>



**Scheme 1.1:** Reaction scheme for a living anionic polymerisation of a vinyl monomer initiated by *n*-butyl lithium. The Y group represents any functionality that may be attached to the alkene bond.

Unlike FRP, LAP does not suffer from intrinsic termination reactions because the propagating anionic centres cannot react with each other. As a result, the kinetics of a LAP are more straightforward to describe, with the rate of polymerisation being given by equation (1.10). In practice, the kinetics also depend on additional factors such as the choice of initiator and solvent.

$$R_{\text{polym}} = k_p [M^-][M] \quad (1.10)$$

Here  $k_p$  is the rate constant for propagation,  $[M^-]$  is the concentration of propagating anionic centres, and  $[M]$  is the monomer concentration. In LAP, initiation is restricted to a short time interval at the start of the polymerisation. Therefore, all polymer chains will begin propagating at the same time. Similarly, all chains have the same rate constant for propagation and hence grow at the same rate. It is for this reason that the evolution of molecular weight in a LAP varies linearly with monomer conversion (Figure 1.3).

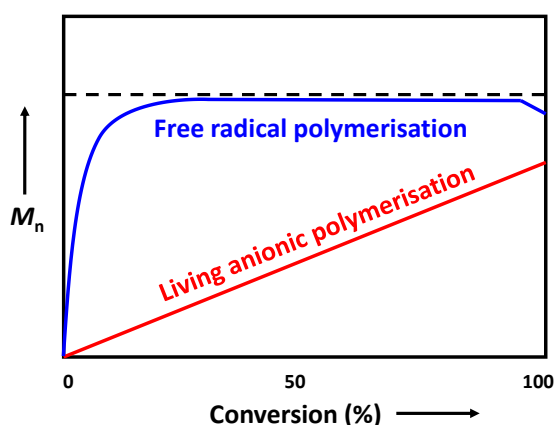


**Figure 1.3:** Schematic representation of the evolution of molecular weight during (i) a free radical polymerisation (blue curve) and (ii) a living anionic polymerisation (red curve).

In addition, the typical dispersity of polymers produced by LAP is exceptionally low ( $\mathcal{D} \sim 1.1$ ). This behaviour strongly contrasts with that for FRP, whereby high molecular weight species with high dispersity are formed in the early stages of the polymerisation. Furthermore, in FRP the

molecular weight of polymers produced at the end of the polymerisation decreases slightly, owing to monomer depletion. This effect is not observed in LAP.

If it is assumed that each initiator produces a propagating polymer chain, then the target degree of polymerisation is simply given by the initial molar ratio of the monomer to the initiator. Hence, molecular weights can be readily predetermined. Furthermore, the actual DP at any point during the polymerisation is given by equation (1.11):

$$DP = \frac{[M]_0}{[In]_0} p \quad (1.11)$$

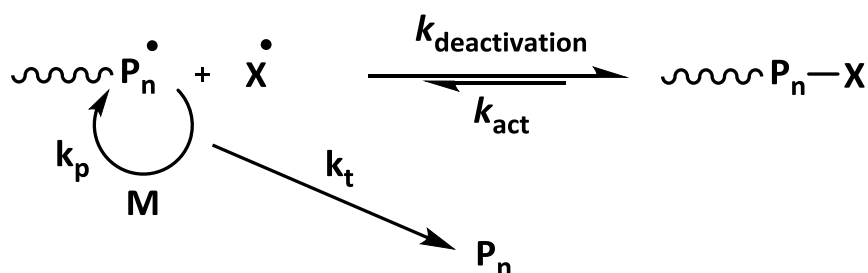
Here,  $p$  is the fractional monomer conversion,  $[M]_0$  is the initial molar monomer concentration and  $[In]_0$  is the initial molar initiator concentration. One final advantage of LAP compared to FRP is that in the absence of termination, the chains remain active once the polymerisation has finished. Consequently, further monomer can be added to the reaction mixture, and the polymerisation will resume (hence the term ‘living’). If a different monomer is added, a well-defined diblock copolymer will be produced. Such diblock copolymers cannot be prepared *via* FRP.<sup>2</sup>

LAP does, however, suffer from several major drawbacks. Perhaps the most obvious is its incompatibility with any monomers, solvents and impurities containing protic functional groups. If present, such labile protons would rapidly react with the organometallic initiator and destroy it. As discussed earlier, the target DP of polymers synthesised *via* LAP is *inversely* proportional to the initial initiator concentration (target DP =  $[M]_0/[In]_0$ ). Hence, any unintended reduction of the initiator concentration will directly influence the final molecular weight of the polymers. This effect is especially serious when targeting very high molecular weight polymers, which require low initial concentrations of initiator. This is because the initial initiator concentration may become comparable to that of the background protic impurities. This drawback places stringent purification requirements upon LAP that makes it much more demanding and energy-intensive than other techniques such as FRP. Similarly, unless expensive and time consuming protecting group chemistry is used to mask functional groups, the choice of monomer available for LAP is limited. Although there are other living techniques that avoid some of these issues, they lie outside of the scope of this thesis and consequently will not be discussed further.<sup>15–18</sup>

### 1.3.3 Reversible deactivation radical polymerisation

#### 1.3.3.1 General concepts

In order for a polymerisation to be considered ‘living’ it must fulfil three criteria.<sup>19</sup> Firstly, initiation must be limited to a very short interval at the start of the polymerisation (all chains must begin their growth at approximately the same time). Secondly, all chains must propagate at the same rate. Finally, there must be no irreversible termination. Reversible deactivation radical polymerisation (RDRP) is an umbrella term used to describe a number of techniques that attempt to impart these ‘living’ characteristics to FRP.<sup>20–23</sup> Sometimes referred to as living radical polymerisation (LRP) or controlled radical polymerisation (CRP), RDRP has received much attention, especially in the past two decades. The main attraction of RDRP techniques is that they combine many of the advantages of FRP and LAP while eliminating most of the disadvantages. For example, the ease of implementation and functional-group tolerance of FRP is maintained in RDRP. This means that RDRP can be carried out in cost-effective solvents such as water, using protic monomers, without strict purification requirements. Similarly, good control over molecular weight, dispersity and copolymer architecture, typically associated with LAP, is also incorporated into RDRP. There are a number of different techniques that fall under the definition of RDRP, but the three which are most utilised are atom transfer radical polymerisation (ATRP),<sup>24</sup> nitroxide-mediated polymerisation (NMP)<sup>21</sup> and reversible addition-fragmentation chain transfer polymerisation (RAFT).<sup>25</sup> The key principle for all of these techniques is a rapid, reversible equilibrium between active polymer radicals, and deactivated dormant chains. However, the mechanism by which this is achieved differs in each case.<sup>2</sup> One way in which this equilibrium can be established is *via* the reversible activation/deactivation of polymer radicals with a capping agent (Scheme 1.2).

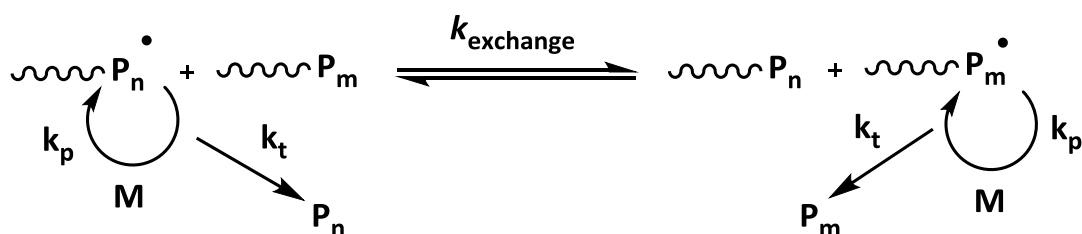


**Scheme 1.2:** Reversible deactivation of a propagating polymer radical ( $\text{P}_n^\bullet$ ) with a capping agent  $\text{X}^\bullet$

The crux of the reversible activation/deactivation mechanism is the persistent radical effect (PRE), which forms the basis for NMP and ATRP.<sup>2</sup> Following the PRE, radicals generated during initiation ( $\text{R}^\bullet$ ) are rapidly deactivated by a capping species  $\text{X}^\bullet$ , resulting in a dormant species.

Typically,  $X^{\bullet}$  is a highly stable radical such as a nitroxide or organometallic complex. When the dormant species is reactivated (*via* homolytic fission of the R-X bond), propagation and termination can occur to produce polymer chains. It is important to note that due to steric effects, the persistent radical  $X$  cannot self-terminate; it can only cross-couple with an active polymer radical. Therefore, any termination between two polymeric radicals leads to an irreversible accumulation of  $X^{\bullet}$ . Hence, as the polymerisation progresses and the concentration of  $X^{\bullet}$  gradually increases, the concentration of active polymer radicals *decreases* (due to a shift in the equilibrium shown in **Scheme 1.2** towards the dormant species). As a result, the rate of termination is suppressed relative to propagation (because  $R_p \propto [P_n^{\bullet}]$  yet  $R_t \propto [P_n^{\bullet}]^2$ , see **Table 1.1**). Furthermore, in systems based on the PRE, initiation is much quicker than termination. In practice, this means that all chains begin their growth at the same time at the start of the polymerisation. The rapid initiation combined with the suppression of termination results in the production of polymers with narrow MWDs. It is worth noting here that unlike FRP, in which the steady-state of active radicals is determined by the relative rates of initiation/termination, it is the relative rates of activation/deactivation that are important for PRE.

A second mechanism, by which the equilibrium between active and dormant polymer chains can be established, is *via* degenerative transfer (DT) (**Scheme 1.3**).<sup>2</sup>

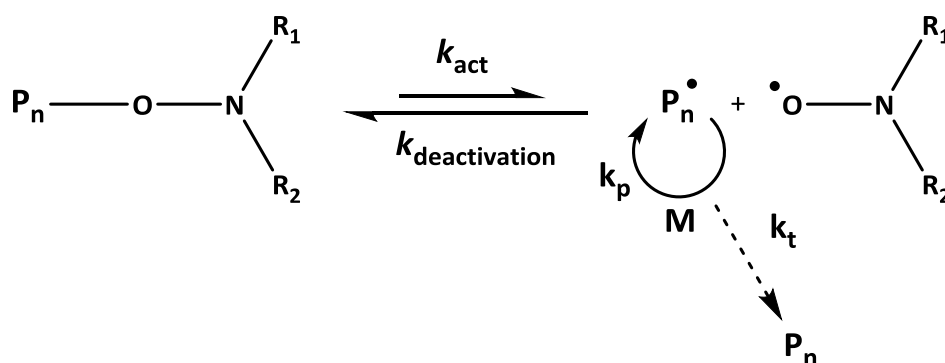


**Scheme 1.3:** Degenerative transfer equilibrium between an active propagating polymers  $P_n^{\bullet}$  and  $P_m^{\bullet}$  and dormant polymers  $P_n$  and  $P_m$

For processes based on DT, namely RAFT, the PRE is *not* involved. Instead, conventional free radical initiators are used, and control is provided by an added chain transfer agent (CTA). This CTA facilitates the exchange of radicals between polymer chains. During RAFT polymerisation, the concentration of the dormant species is much greater ( $\sim 10^6$ ) than the active propagating chains. Because the CTA partitions the available free-radicals equally amongst all polymer chains, all chains have an equal opportunity for growth. This results in the synthesis of chains of similar DPs and, consequently, low dispersity.

### 1.3.3.2 Nitroxide-mediated polymerisation

NMP is a type of RDRP based on the PRE that was first discovered in the 1980s.<sup>26,27</sup> Mechanistically the most straightforward of the RDRP techniques, NMP requires the reversible capping of propagating radicals with a nitroxide compound (**Scheme 1.4**).<sup>21</sup> Initiation in NMP can be achieved in one of two ways (i) the addition a nitroxide compound and a conventional FRP initiator or (ii) the addition of an alkoxyamine compound that decomposes into a nitroxide compound and a radical initiator. Although NMP has been used with great success to control the polymerisation of a range of monomers, it suffers from two important drawbacks that have limited its widespread use.<sup>21</sup> First, common alkoxyamine compounds used with NMP typically require temperatures in excess of 120 °C to achieve useful rates of polymerisation. This prohibits polymerisations in low-boiling solvents such as water under normal pressures. Second, NMP cannot be used to control the polymerisation of methacrylic monomers, due to cross disproportionation reactions and/or large activation/deactivation equilibrium constants.<sup>28</sup>

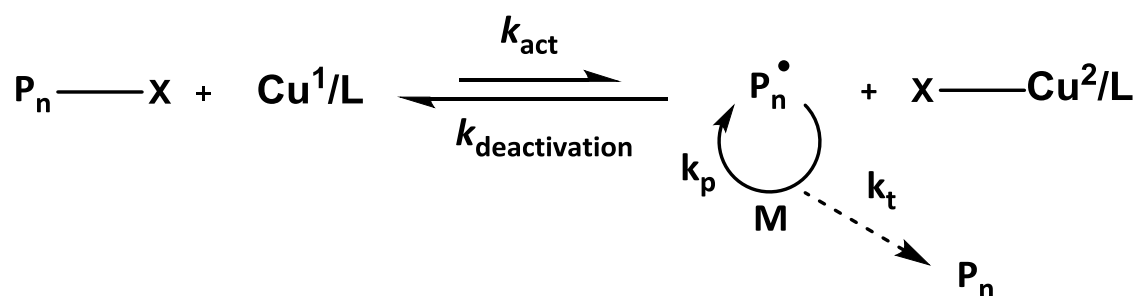


**Scheme 1.4:** Reversible activation/deactivation equilibrium for a typical NMP synthesis mediated *via* a generic nitroxide compound.

Considerable effort has been spent in recent years addressing both of these issues.<sup>29,30</sup> The synthesis of new nitroxide/alkoxyamine compounds with high dissociation rate constants has facilitated polymerisations at temperatures below 100 °C. This has removed the high temperature polymerisation requirement for acrylic monomers, although methacrylates remain problematic.<sup>31</sup> In addition, Charleux and co-workers have reported that NMP can be used to control the polymerisations of MMA as long as a small (~ 8 mol %) amount of styrene is present.<sup>32</sup> More recently, bespoke nitroxides have been synthesised that can exert control over the *bulk* polymerisation of MMA at ~ 100 °C.<sup>33</sup> However, preparation of these compounds typically requires significant synthetic expertise and/or comes at much greater cost.

### 1.3.3.3 Atom transfer radical polymerisation

First discovered in 1995, ATRP is another RDRP technique that relies upon the PRE (**Scheme 1.5**).<sup>34–36</sup> The mechanism of ATRP relies upon the homolytic cleavage of an alkyl halide bond (R-X) by a transition metal complex ( $M^n-L_y$ ), to generate an alkyl radical  $R^\bullet$  and the corresponding transition metal halide complex with a higher oxidation state ( $M^{n+1}L_yX$ ). Once generated, the alkyl radical can propagate, terminate, or be reversibly deactivated by this complex. As the polymerisation progresses, irreversible termination is suppressed owing to the PRE (see earlier). Again, this results in the shift of the equilibrium towards the dormant form. Unlike NMP, the kinetics depend not only on the persistent radical, but also on the activating species ( $M^n-L_y$ ). Furthermore, the DP of polymers synthesised *via* ATRP is determined by the molar ratio of the monomer to the alkyl halide initiator ( $DP = [M]_0/[RX]_0$ ).



**Scheme 1.5:** Reversible activation/deactivation equilibrium for a typical ATRP synthesis mediated *via* a copper(I) transition metal complex.

A range of different transition metals have been used as an activator in ATRP,<sup>37–40</sup> but copper is by far the most reported.<sup>41</sup> Typical ligands include multidentate alkylamines, pyridines, phosphines and ethers.<sup>20</sup> The range of monomers that are amenable to ATRP includes styrene, (meth)acrylates, (meth)acrylamides, acrylonitrile and others.<sup>20</sup> Furthermore, ATRP can be carried out over a wide range of temperatures ( $< 0\text{ }^\circ\text{C}$  and  $> 130\text{ }^\circ\text{C}$ ).

Despite the broad applicability of ATRP, there are inherent problems associated with this process. Copper compounds can be highly toxic and therefore require removal from the final polymer. This issue has been partially addressed by the development of new methods that enable the activator to be regenerated, *in situ*, and therefore used at catalytic concentrations ( $\sim 50\text{ ppm}$ ). Examples of this approach are ‘activator regenerated by electron transfer’ (ARGET) ATRP<sup>42</sup> and ‘initiators for continuous activator regeneration’ (ICAR) ATRP.<sup>43</sup> In the former case, a reducing agent is used to regenerate the activator species, while with ICAR ATRP, a free-radical initiator



to initiate a new propagating polymer chain ( $P_m^\bullet$ ). The rapid equilibrium between  $P_m^\bullet$  and  $P_n^\bullet$  via intermediate **4** (**Figure 1.4**) provides equal probability for each polymer chain to grow, and hence, similar DPs and low dispersities are obtained. One major difference between RAFT and FRP is the lifetime of an individual chain. In FRP, chains will typically initiate, propagate and terminate in a fraction of a second. In a RAFT polymerisation, however, chains can remain active for hours, albeit in a dormant form the majority of the time. Similarly, whilst the concentration of propagating polymer radicals in a RAFT polymerisation may be the same as it is in an equivalent FRP, the cumulative lifetime of each polymer radical in a RAFT polymerisation will be lower, as each chain only grows intermittently.<sup>19</sup> Finally, because most of the chains retain their RAFT end group post-polymerisation, these chains can be isolated and further extended with additional monomers. Therefore, RAFT enables a convenient route by which to synthesis well-defined block copolymers with well-defined sequences and architectures.<sup>49-51</sup>

For a successful RAFT polymerisation, there are various criteria that the CTA must satisfy. Firstly, the CTA should have a high rate constant for addition,  $K_{add}$ , so  $P_n^\bullet$  should react rapidly with the CTA to form intermediate **2** (**Figure 1.4**). Once formed, **2** should then fragment quickly and partition in favour of the  $R^\bullet$  leaving group (i.e. the partition coefficient  $K_\beta / (K_\beta + K_{add})$  should be as close to unity as possible). Finally,  $R$  must be a good free-radical leaving group *and* a good initiator for the monomer to be polymerised ( $K_i > K_p$ ).<sup>19</sup>

Whether these criteria are met depends on the nature of the  $Z$  and  $R$  groups attached to the RAFT agent.<sup>52,53</sup> For example, to polymerise methacrylic monomers,  $R^\bullet$  should be a tertiary propagating radical, otherwise it will be a poor leaving group with respect to the monomer. Unlike the  $R$  group, the  $Z$  group remains attached to the CTA throughout the polymerisation and influences both the reactivity of the  $C=S$  double bond and the stability of the intermediates (labelled **2** and **4**, **Figure 1.4**). In doing so, the  $Z$  group controls the rate of addition to the CTA. Moad *et al.* published a series of guidelines regarding RAFT agent choice and design depending on the monomer class to be polymerised (**Figure 1.5**).<sup>49</sup> For appropriate RAFT agent selection, monomers are sub-divided into two categories: more-activated monomers “MAMs”, such as methacrylates, acrylates, methacrylamides and styrene, and less activated monomers “LAMs” such as vinyl acetate and *n*-vinylformamide. This nomenclature indicates the ease with which a monomer undergoes a reaction with a free radical rather than its reactivity. MAMs typically produce more stabilised and less reactive radicals, due to steric and stereoelectronic factors, as well as the presence of neighbouring groups capable of radical delocalisation. Conversely, LAMs typically result in non-stabilised highly reactive radicals.



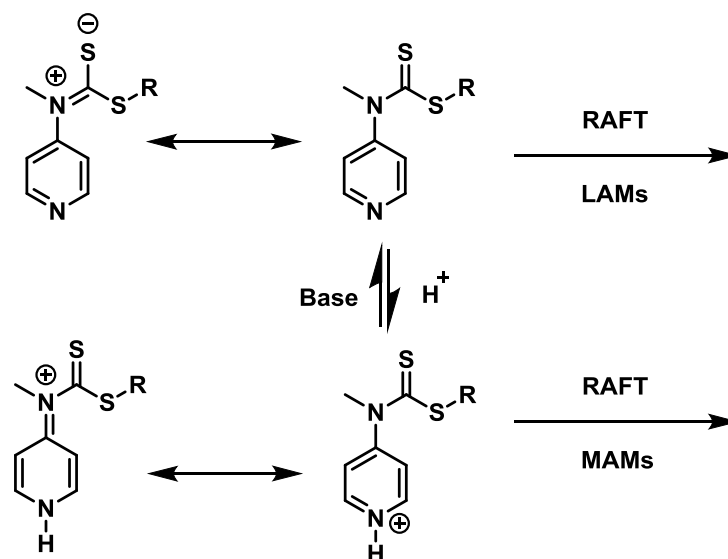


**Figure 1.6:** A switchable or ‘universal’ RAFT agent. In the deprotonated form it is suitable for the polymerisation of MAMs, in its protonated form it becomes compatible with LAMs.<sup>54</sup>

In its deprotonated form, the nitrogen lone-pair delocalises with the C=S double bond and the RAFT agent is suitable for the polymerisation of LAMs (see **Figure 1.6**). Conversely, upon addition of acid the second nitrogen becomes protonated, which then serves to draw electron density away from the C=S double bond. Hence, the RAFT agent becomes activated towards the polymerisation of MAMs.

In an ideal RAFT synthesis, the CTA behaves as an ideal transfer agent, i.e. the steady-state concentration of radicals is the same as it would be in an equivalent FRP synthesis.<sup>51</sup> Therefore, the kinetics of the polymerisation should be unaffected (excluding differences due to the differing molecular weights of the reacting polymer radicals). However, this is not always the case and retardation is often observed.<sup>55</sup> Typically, this retardation manifests as an induction period at the start of the polymerisation, or as slower overall reaction rate. The precise reason for the retardation observed in *some* RAFT polymerisations is still a matter of debate.<sup>55</sup> However, several explanations have been postulated. One hypothesis, named the slow-fragmentation (SF) hypothesis, states that fragmentation of intermediates **2** and/or **4** (**Figure 1.4**) is sufficiently slow enough to account for the observed retardation by itself.<sup>19</sup> If this hypothesis were true, it would require that the fragmentation rate of **2** and **4** be very low and therefore the concentrations of **2** and/or **4** be very high ( $\sim 10^{-4}$  M). Thang and co-workers have used electron paramagnetic resonance (EPR) spectroscopy to demonstrate that this in fact not the case for the polymerisation of methacrylic monomers with cumyl dithiobenzoate (the polymer radical concentration is around  $10^{-7}$  M).<sup>56</sup> As a result, the SF hypothesis has been discounted as the lone cause of retardation, at least for the dithiobenzoate mediated polymerisations investigated.

A second potential source of retardation is the slow initiation of the monomer by the initiator and/or the R group. If this is the case, the polymerisation will proceed very slowly until the entire RAFT agent has been consumed and the monomer becomes the active propagating radical (as opposed to  $\text{In}^\cdot$  or  $\text{R}^\cdot$ ). Such behaviour has been documented for the cumyl dithiobenzoate-mediated polymerisations of *n*-butyl acrylate (BA).<sup>57</sup> A third hypothesis is the intermediate radical termination (IRT) hypothesis. This states that the irreversible termination of intermediates (**2** or **4**) either with themselves and/or with other radical sources (propagating polymeric radicals or initiator) is the main source of retardation. IRT results in the formation of multi-armed star compounds (**Figure 1.7**), of which there is undeniable evidence in the literature.<sup>58,59</sup> However, the extent to which IRT contributes to retardation remains unclear. Finally, a more obvious source for retardation in some RAFT polymerisations is an inappropriate choice of CTA or initiator. For example, RAFT polymerisations initiated by lauryl peroxide feature undecyl initiating radicals. The addition of undecyl-based radicals to a RAFT agent is typically irreversible under normal conditions, and results in deactivation. This issue may be avoided when targeting very high DPs, as the concentration of the RAFT agent is minimal in comparison to the monomer, and therefore, a reaction between the initiator and CTA is very unlikely. However, it may become significant working at high initiator concentrations or when targeting shorter DPs.<sup>55</sup>

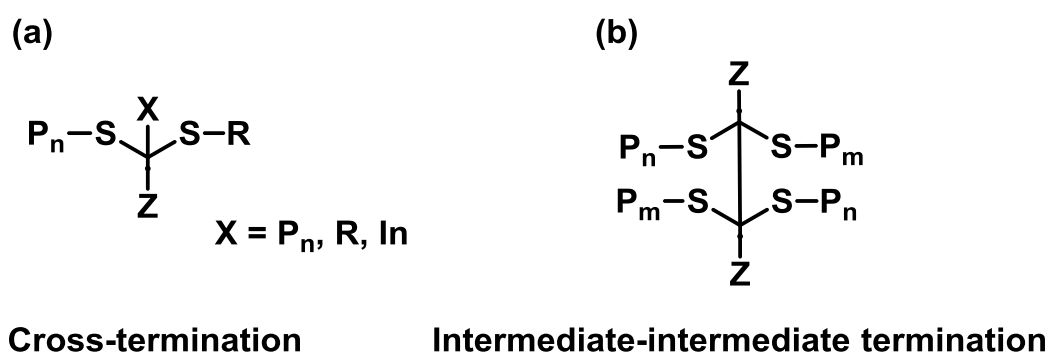


**Figure 1.7:** Multi-armed star compounds resulting from irreversible intermediate termination during a RAFT polymerisation.

Although RAFT polymerisation manages to avoid many issues that plague other RDRP techniques, such as toxic catalysts or very high polymerisation temperatures, this technique also suffers from certain disadvantages. The most obvious of these are associated with the sulfur-based CTA, which is both highly coloured and malodorous.<sup>46,60</sup> As a result, a number of methods have been devised to cleave or functionalise the CTA end-group. One very effective way in which to achieve this is to react the thiocarbonylthio group with a nucleophile.<sup>61,62</sup> In doing so, the CTA end group is converted to a thiol and the characteristic colour is removed. Other common methods

include a reaction with free-radicals,<sup>63,64</sup> dienes,<sup>65,66</sup> hydrogen peroxide<sup>67</sup> or heat.<sup>68</sup> Some of these different end-group removal/functionalisation strategies are shown in **Figure 1.8**.

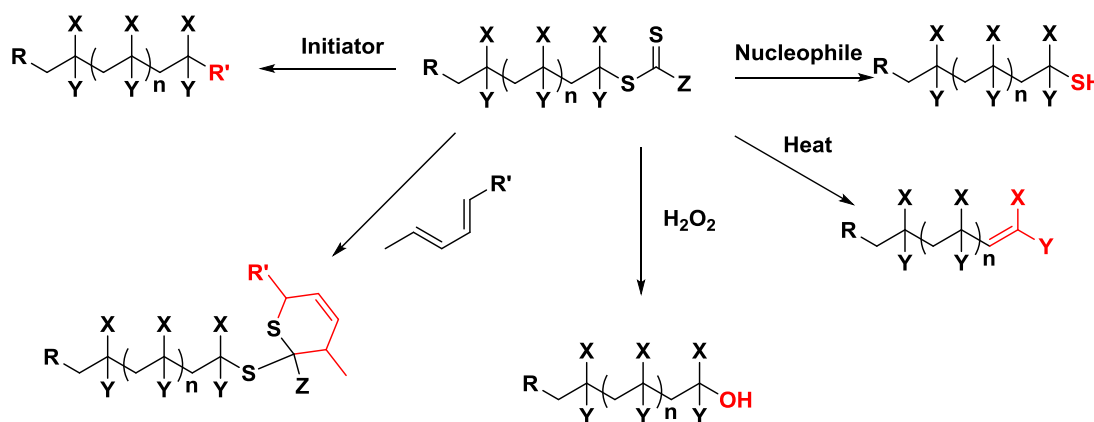


**Figure 1.8:** Schematic representation of the main methods of RAFT end group modification.<sup>60</sup>

## 1.4 Polymerisation conditions

Thus far, various radical polymerisation techniques have been discussed. However, the physical conditions under which these polymerisations are conducted are also important. Arguably, the simplest form of radical polymerisation is bulk polymerisation. In a bulk polymerisation, initiation takes place directly in bulk monomer i.e. in the absence of solvent.<sup>1</sup> As the polymerisation proceeds, the unreacted monomer acts as a solvent for the growing polymer chains. If the polymerisation proceeds to full conversion, pure polymer remains. In solution polymerisation, a good solvent for both the monomer and the resulting polymer chains is added. After the polymerisation is finished, a solution of the desired polymer is obtained.<sup>12</sup> In addition to bulk and solution polymerisations, there are a number of more complex polymerisation techniques that exist, such as suspension, precipitation, dispersion and emulsion polymerisation. Each technique has its advantages and disadvantages depending on the final desired application. Whilst suspension and precipitation polymerisation are not relevant to this thesis, dispersion and emulsion polymerisation will be discussed in more detail.

### 1.4.1 Dispersion polymerisation

Dispersion polymerisation was first reported in the early 1960s by workers at Imperial Chemical Industries (ICI).<sup>69</sup> Initially developed for coatings applications, dispersion polymerisation facilitates the production of well-defined spherical particles in the range of 0.1 to 10  $\mu\text{m}$ .<sup>70,71</sup> Although historically limited to non-polar organic media such as petroleum ether,<sup>72</sup> the technique has now been applied to more polar solvents, such as water<sup>73</sup> and alcohols.<sup>74–76</sup> Dispersion

polymerisation, like precipitation polymerisation, involves polymerising an initially soluble monomer to form an insoluble polymer. The distinction between dispersion and precipitation polymerisation is that dispersion polymerisations are conducted in the presence of a suitable (usually polymeric) stabiliser. The four main components of a typical dispersion polymerisation are: (i) a solvent (ii) a soluble monomer that polymerises to give an insoluble polymer, (iii) an initiator and (iv) a suitable stabiliser (usually a polymer/surfactant, or macro-CTA in the case of RAFT dispersion polymerisation). The currently accepted mechanism of dispersion polymerisation (**Figure 1.9**) is divided into approximately six distinct regimes.<sup>77</sup> To begin with, before the polymerisation is initiated, all components are dissolved in the solvent resulting in a homogeneous solution. In the second stage, decomposition of the initiator is induced *via* heating or exposure to radiation. This results in the formation of initiator radicals, which react with monomer units to form propagating oligomeric radicals.

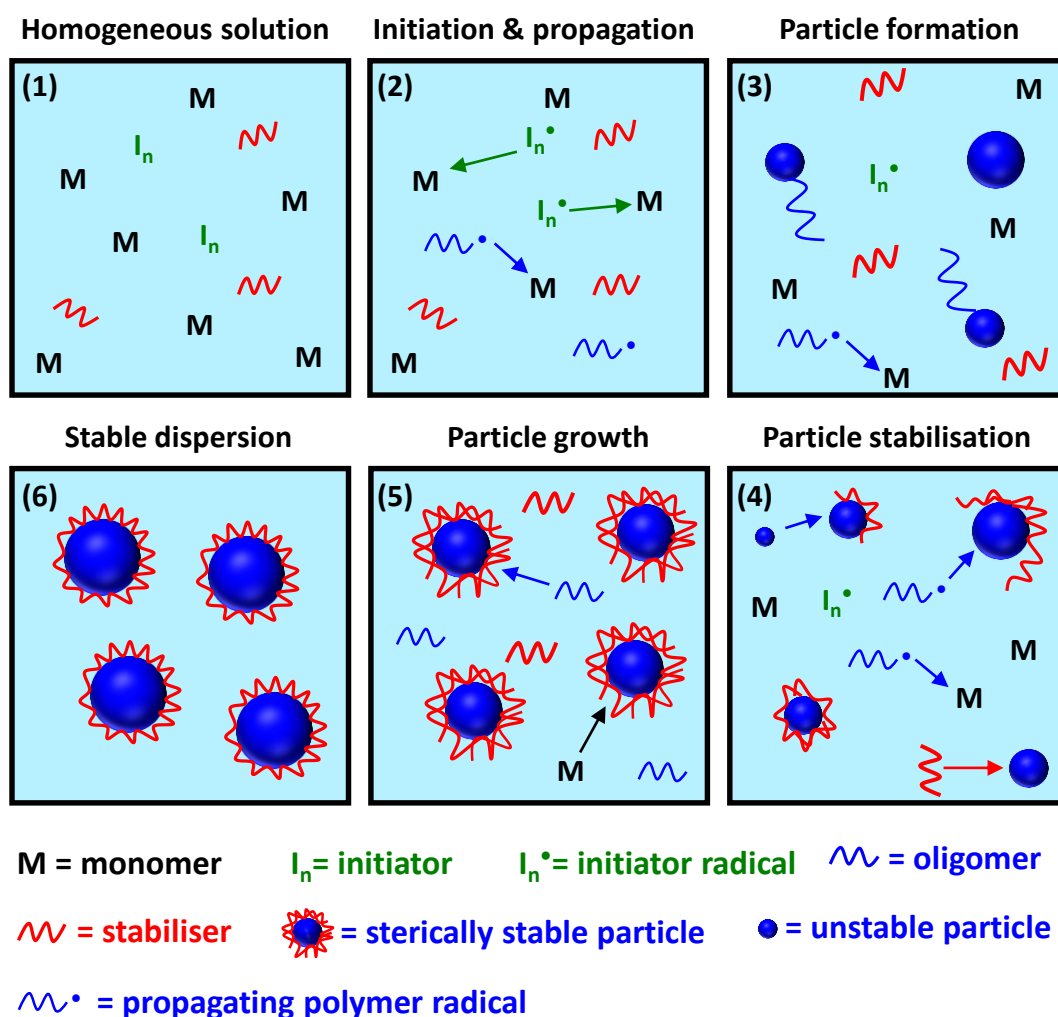


**Figure 1.9:** The accepted mechanism of a typical dispersion polymerisation.<sup>77</sup>

The solubility of these oligomers is molecular-weight dependent. They are initially soluble, but a critical DP is eventually reached at which they begin to precipitate to form nascent, unstable particles (stage 3). After the particles have begun to form, the stabiliser begins to physically adsorb onto them, thus providing initial colloidal stability (stage 4). The diameter of the resulting particles continuously increases at this stage, as monomer and oligomers enter the nascent particles, in addition to particle-particle fusion. The penultimate stage of the polymerisation represents the point at which all particles have acquired sufficient stabiliser to be colloidally stable. At this stage, it is assumed that no new nuclei are formed (and therefore the number of particles remains constant). Instead, the polymerisation progresses by the diffusion of oligomers and monomer units into pre-existing particle cores. The final stage of the polymerisation is reached once the polymerisation ceases and a stable dispersion of particles is obtained. The mean particle diameter obtained from a dispersion polymerisation, in addition to the particle size distribution, can be tuned by adjusting various parameters.<sup>78-80</sup> Firstly, the temperature at which the polymerisation is conducted may have profound effects. Varying the polymerisation temperature will influence the solubility of the propagating oligomers in the continuous phase, and therefore influence the critical DP at which they precipitate. Moreover, changes in temperature can influence the solvation of the stabiliser, and hence its rate of adsorption onto the growing particles. Also, for a given initiator, varying the temperature affects both the concentration of precipitating oligomers *and* the rate at which they are generated. Finally, changing the polymerisation temperature will affect the viscosity of the continuous phase. Other than the reaction temperature, the monomer and initiator concentrations can be hugely important in determining the final diameter of the particles.<sup>79</sup> Increasing the monomer concentration increases the solvency of the medium towards the polymer being formed, hence the critical chain DP required for precipitation should increase (assuming the monomer is a good solvent for the polymer). Similarly, increasing the initiator concentration results in a greater concentration of radicals. As a result, the concentration of precipitating oligomers increases. Because the adsorption of the stabiliser is relatively slow, aggregation of nuclei is enhanced, which ultimately results in the formation of larger particles.

### 1.4.2 Emulsion polymerisation

Like dispersion polymerisation, emulsion polymerisation is a form of radical polymerisation used to prepare polymer latexes.<sup>81-84</sup> A typical aqueous emulsion polymerisation formulation comprises: a continuous phase (water), a water-soluble initiator, a surfactant/copolymer as a stabiliser and emulsifying agent, and a water-immiscible monomer. In the case of a RAFT emulsion polymerisation, a macro-CTA can be used in place of the surfactant. Known since at

least the 1920s, emulsion polymerisation is hugely popular within the chemical industry for a number of reasons. Firstly, high molecular weight polymers can be synthesised within short reaction times. In addition, the final form of the aqueous-based polymer latex is low-viscosity and environmentally-friendly. Furthermore, tunable parameters such as the surfactant/stabiliser concentration allow for the synthesis of well-defined particles in the 50-1000 nm range.<sup>70</sup> The mechanism of emulsion polymerisation (**Figure 1.10**) is usually divided into three separate intervals.<sup>82,85</sup> The first interval begins with an aqueous continuous phase containing dispersed surfactant micelles and emulsified monomer droplets (of the order of a few microns). The vast majority of the monomer present is contained within these droplets. However, a minor fraction is located within the surfactant micelles, and even smaller quantities are dissolved in the aqueous phase. At this stage, all components are in dynamic equilibrium. Monomer continuously diffuses out of the larger droplets into the smaller, more numerous surfactant micelles. Once the water-soluble initiator begins to decompose to form radicals, initiation can take place in one of two ways. Either a radical diffuses into a monomer-swollen surfactant micelle and initiates polymer chains (heterogeneous nucleation) or it will initiate dissolved monomer (homogeneous nucleation). If the dissolved monomer is initiated, it propagates until a critical chain DP is reached, at which point it becomes insoluble and diffuses into an existing micelle (or associates with excess surfactant to form a new micelle).

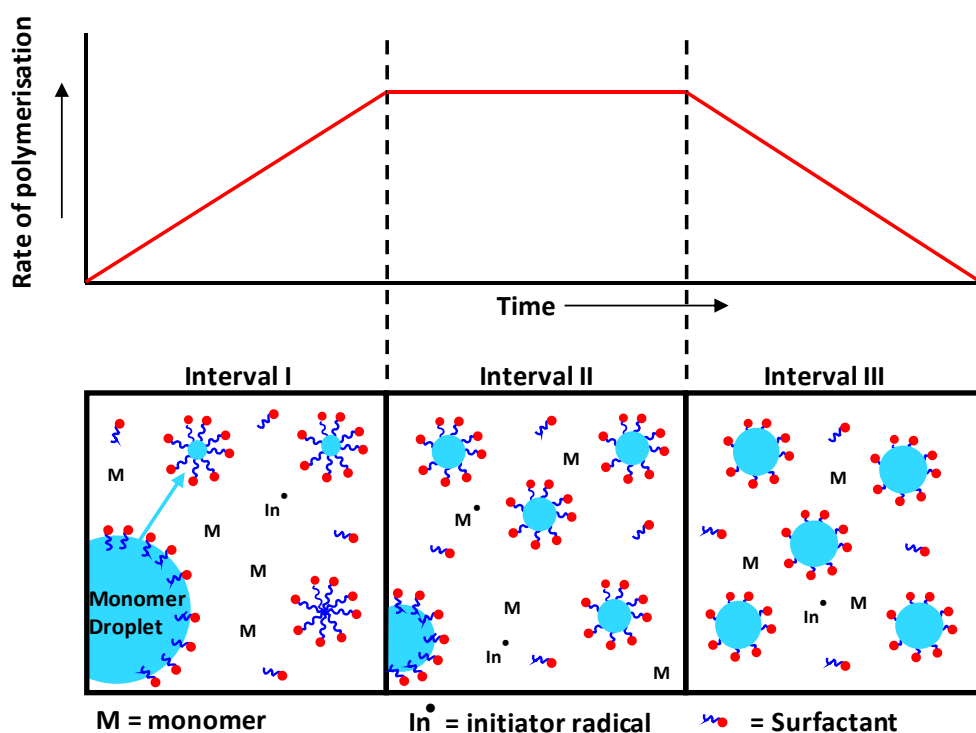


**Figure 1.10:** Schematic representation of the mechanism of an emulsion polymerisation from interval I to III. The accompanying rate of polymerisation is depicted above. The duration of each time interval is not necessarily representative as shown.<sup>85</sup>

The total number of polymer particles present in the system continuously increases until all of the available surfactant has been adsorbed. Once this is the case, nucleation finishes and the second interval begins. After this point, the number of particles present remains relatively constant. The particles grow by the continuous diffusion of monomer from the droplets into the micelles (which contain the propagating chains). This stage proceeds with a relatively constant reaction rate until all of the monomer droplets are used up. Finally, during the third interval, only monomer-swollen latex particles and residual dissolved monomer are present.<sup>85</sup> The reaction rate steadily declines over time as the remaining monomer is polymerised. This proceeds until all of the available monomer is used up. At the end of the polymerisation, a stable surfactant-stabilised latex is obtained.

## 1.5 Self-assembly

Self-assembly describes a process by which an initially disordered system reorganises to an ordered state without external influence.<sup>86,87</sup> There are many phenomena found throughout nature which rely upon self-assembly, including the formation of the cell wall, the folding of proteins and nucleic acids, and the formation of micelles by amphiphilic surfactants. In recent years, the invention of controlled/living polymerisation techniques has enabled the convenient synthesis of amphiphilic block copolymers. Like small-molecule surfactants, block copolymers also display interesting self-assembly behaviour, in both solution and the bulk. This will be reviewed in the next section.<sup>86,87</sup>

### 1.5.1 Self-assembly of diblock copolymers in bulk

Before the self-assembly of diblock copolymers can be discussed, the thermodynamics of mixing of polymers in general must be considered. The parameter that determines whether or not two pure substances will mix spontaneously is the Gibbs free energy of mixing:<sup>88</sup>

$$\Delta_{mix}G = \Delta_{mix}H - T\Delta_{mix}S \quad (1.12)$$

Here  $\Delta_{mix}G$  is the Gibbs free energy of mixing,  $\Delta_{mix}H$  is the enthalpy of mixing,  $T$  is the absolute temperature and  $\Delta_{mix}S$  is the entropy of mixing. If mixing two substances results in a negative  $\Delta_{mix}G$ , this is a spontaneous process. Examination of equation (1.12) reveals that the Gibbs free energy of mixing depends on the entropy and enthalpy of mixing. In general, when mixing two pure small-molecule substances A and B, the entropic term will be positive, i.e. entropy favours mixing. This is perhaps easiest to conceptualise in terms of the increase in disorder brought about

*via* mixing. Consequently, if two pure substances do not mix, this is typically an enthalpic effect. If we consider the same two substances (A and B), the enthalpy of mixing is given by the energy of interaction between A and B, minus the energy of interaction that A has with itself and that B has with itself. This is described by equation (1.13).<sup>88</sup>

$$\Delta_{mix}H = 2\Delta_{mix}H_{a-b} - \Delta_{mix}H_{a-a} - \Delta_{mix}H_{b-b} \quad (1.13)$$

This explains why certain dissimilar substances, such as *n*-hexane and ethylene glycol do not mix: although the entropy of mixing is favourable, the enthalpic term is strongly unfavourable ( $2\Delta_{mix}H_{a-b} \ll \Delta_{mix}H_{a-a} + \Delta_{mix}H_{b-b}$ ). The physical explanation is that ethylene glycol can hydrogen bond with itself but not with hexane.

Polymers, however, behave very differently to small molecules. In general, any two homopolymers *do not* mix in the solid state.<sup>89</sup> Phase separation is almost invariably observed even when the two polymers are chemically very similar. For example, at sufficiently large molecular weights, polystyrene and deuterated polystyrene do not mix. Given the above discussion regarding the mixing of small molecules, this behaviour seems counter-intuitive. The explanation lies in the entropy of mixing. For a generic amorphous polymer, its entropy is already very high. Each individual chain can adopt a huge number of conformations. Therefore, when mixing two amorphous polymers, the entropy change of mixing per unit volume is small. Without this driving force, mixing relies solely upon the enthalpy. If this is insignificant, then the polymers simply do not mix. This also explains why certain polymers such as polystyrene and poly(phenylene oxide) can mix: they both contain aromatic rings which interact with each other, providing an enthalpic incentive.<sup>90</sup>

The situation becomes more interesting when the two immiscible polymers are covalently bound together, to form an AB diblock copolymer. Now, the two chains still do not mix but they cannot escape one another. In this case, the copolymer undergoes microphase separation (or self-assembly) to produce a range of different copolymer morphologies.<sup>91–94</sup> This process can occur either in the bulk, or in a solvent that is selective for only one of the two blocks.<sup>95</sup> In bulk, there are three parameters which dictate the self-assembly behaviour of AB diblock copolymers.<sup>89</sup> The first parameter is the total degree of polymerisation of the copolymer (*N*). As described above, the entropy of mixing chemically dissimilar polymers is very small. Moreover, this varies inversely with molecular weight. Hence, as the degree of polymerisation of the copolymer increases, self-assembly becomes increasingly favourable. The second parameter that is important

for self-assembly is the Flory-Huggins interaction parameter, which is described by equation (1.14):<sup>96</sup>

$$\chi_{AB} = \left( \frac{z}{k_B T} \right) \left[ \varepsilon_{AB} - \frac{1}{2} (\varepsilon_{AA} + \varepsilon_{BB}) \right] \quad (1.14)$$

Here  $\chi_{AB}$  is the Flory-Huggins interaction parameter,  $z$  is the number of nearest-neighbour monomers,  $k_B$  is the Boltzmann constant,  $T$  is the absolute temperature and  $\varepsilon_{AB}$ ,  $\varepsilon_{AA}$  and  $\varepsilon_{BB}$  are the interaction energies between repeat units AB, AA and BB respectively. In essence, the Flory-Huggins interaction parameter describes the extent to which two polymers can mix together. Negative values of  $\chi_{AB}$  indicate that mixing of the A and B blocks is preferred, whilst positive  $\chi_{AB}$  implies self-assembly is favoured. In fact, the product of  $N$  and  $\chi_{AB}$ , known as the segregation product ( $\chi N$ ), is very useful in determining the degree of microphase separation of diblocks, see below. Inspection of equation (1.14) reveals two important considerations. Firstly,  $\chi_{AB}$  has an inverse dependence on the temperature, meaning that mixing is promoted at higher temperatures. Second, if the A-B interaction energy is greater than the combination of A-A and B-B interactions [i.e., if  $\varepsilon_{AB} > 1/2(\varepsilon_{AA} + \varepsilon_{BB})$ ] then  $\chi_{AB}$  must be negative, which means that mixing is favoured. Therefore, to encourage microphase separation, the A and B blocks should be chosen such that they have no specific interactions (e.g. hydrogen bonding or electrostatics).

The third parameter that is important for microphase separation is the relative volume fractions of the A block ( $f_a$ ) and B block ( $f_b$ ). While the segregation product describes the extent to which a diblock copolymer undergoes microphase separation, the relative volume fractions dictate the final morphology into which it will self-assemble. To date, a lot of effort has been devoted to modelling the behaviour of diblock copolymers in the bulk. In fact, theoretical predictions now agree rather well with the experimental observations.<sup>89</sup> For example, **Figure 1.11b** depicts the phase diagram of an AB diblock copolymer as predicted by self-consistent mean-field theory (SCMF),<sup>89,94,95</sup> and **Figure 1.11c** depicts an experimentally-determined phase diagram for a series of polyisoprene-polystyrene diblock copolymer.<sup>89,95,97</sup> Both phase diagrams depict the variation in the self-assembled copolymer morphology with ( $f_A$ ) and  $\chi N$ .

At very high values of the segregation product ( $\chi N \gg 10$ ), which is known as the hard segregation limit, there is a strong driving force for self-assembly.<sup>89,95</sup> This results in the formation of separate domains of A and B, both of which are essentially pure. At lower values of  $\chi N$ , the driving force for self-assembly is reduced. Eventually, a critical value of  $\chi N$  is reached (the soft segregation limit) for which self-assembly is no longer favourable and the diblock becomes disordered

(homogeneous). The point at which this occurs is known as the order-disorder transition (ODT). **Figure 1.11a** shows how the copolymer morphology evolves upon increasing the ( $f_a$ ) at a fixed  $\chi N$  above the ODT. At very asymmetric volume fractions ( $f_a \gg f_b$ ) closed packed spheres (CPS) are observed. This separates the disordered state from the body-centred cubic (S) phase. Then, a series of order-order transitions (OOT) are observed, passing through hexagonally-packed cylinders, bicontinuous gyroids (G) and finally ending with lamellae (L) when  $f_a = f_b$ . As the block composition then becomes rich in block A ( $f_a > f_b$ ), the reverse morphological sequence is observed, ultimately ending with disordered chains.

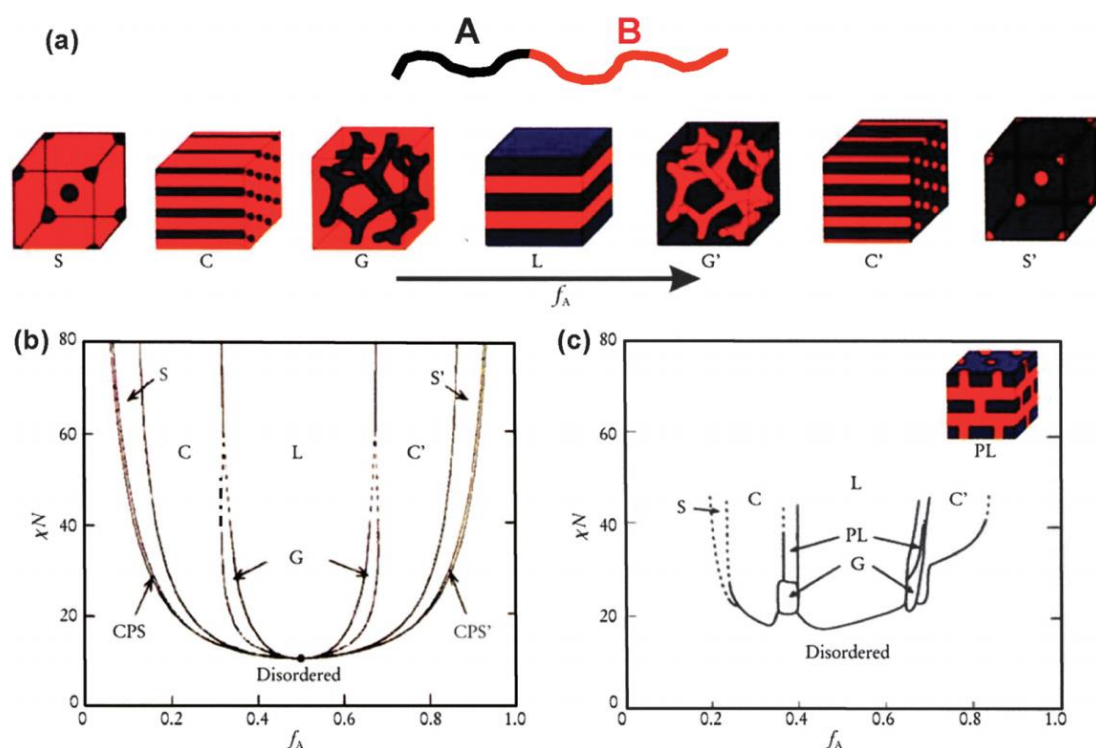


**Figure 1.11:** (a) Equilibrium morphologies for a series of AB diblock copolymers in the bulk:  $f_A$  represents the volume fraction of the A block, S & S' = body-centred cubic, C & C' = hexagonally-packed cylinders, G & G' = bicontinuous gyroid and L = lamellae.<sup>89</sup> (b) Theoretical phase diagram of AB diblock copolymer self-assembly as predicted by self-consistent mean-field theory, varying with both  $f_A$  and the segregation product  $\chi N$  (where N = the degree of polymerisation and  $\chi$  is the Flory-Huggins interaction parameter). CPS & CPS' = close-packed spheres.<sup>94</sup> (c) Experimentally-determined phase diagram for polyisoprene-block-polystyrene (where  $f_A$  = volume fraction of polyisoprene) and PL = perforated lamellae.<sup>95,97</sup>

### 1.5.2 Self-assembly of diblock copolymer in solution

So far, only diblock copolymer self-assembly in the bulk has been discussed. However, block copolymer self-assembly in solution has also been well documented.<sup>98–101</sup> To date, a broad range of copolymer morphologies have been obtained by solution-based self-assembly, such as spheres, rods (or worms), vesicles, and lamella.<sup>95</sup> Perhaps the most well-known example of this type of behaviour was reported by Eisenberg and co-workers for polystyrene-block-poly(acrylic

acid)<sup>102,103</sup> (PS-PAA) (**Figure 1.12**) and polystyrene-block-poly(ethylene oxide) (PS-PEO)<sup>104</sup>. In general, for a diblock copolymer to self-assemble in solution, it must be dissolved in a solvent that is good for only one of the blocks.

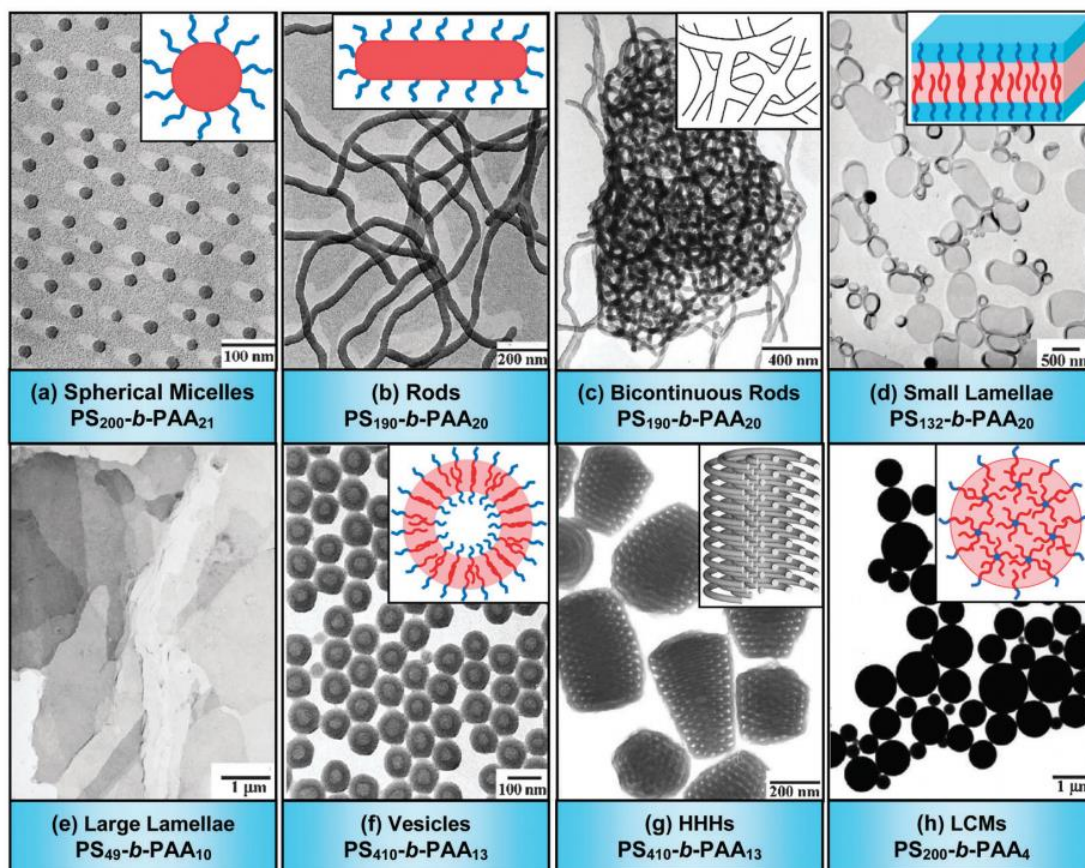


**Figure 1.12:** Transmission electron micrographs (TEMs) and corresponding schematics for various copolymer morphologies formed from PS<sub>X</sub>-PAA<sub>Y</sub> copolymers (red = PS, blue = PAA). HHH= hexagonally packed hollow hoops, LCM = large compound micelle.<sup>95</sup>

To understand the self-assembly behaviour of diblock copolymers in solution, the fractional packing parameter ( $p$ ) is a very useful concept:<sup>86</sup>

$$p = \frac{v_c}{al_c} \quad (1.15)$$

Here,  $p$  is the fractional packing parameter,  $v_c$  is the volume of the solvophobic core,  $l_c$  is the critical chain length of the solvophobic tail and  $a$  is the area occupied by the solvophilic head group. Originally developed by Israelachvili to explain the various morphologies adopted by surfactant micelles,<sup>87</sup> the packing parameter is also loosely applicable to diblock copolymer self-assembly.<sup>95,105</sup> The packing parameter is a measure of the shape pervaded by an amphiphilic molecule (**Figure 1.13**). If the head group of an amphiphile is very large and the tail very small,

a conical shape results. The value of  $p$  for such a molecule would be relatively low. In fact, when the packing parameter of an amphiphile is less than  $1/3$ , then spherical micelles are the geometrically favoured morphology. Conversely, if the head-group and tail have equal volume fractions, a cylindrical shape results. In this case, the packing parameter has a numerical value of unity and bilayers are the preferred morphology. For situations between these two extremes, i.e.  $1/3 < p < 1$ , rod/worms and vesicles are geometrically preferred.<sup>86,87</sup>

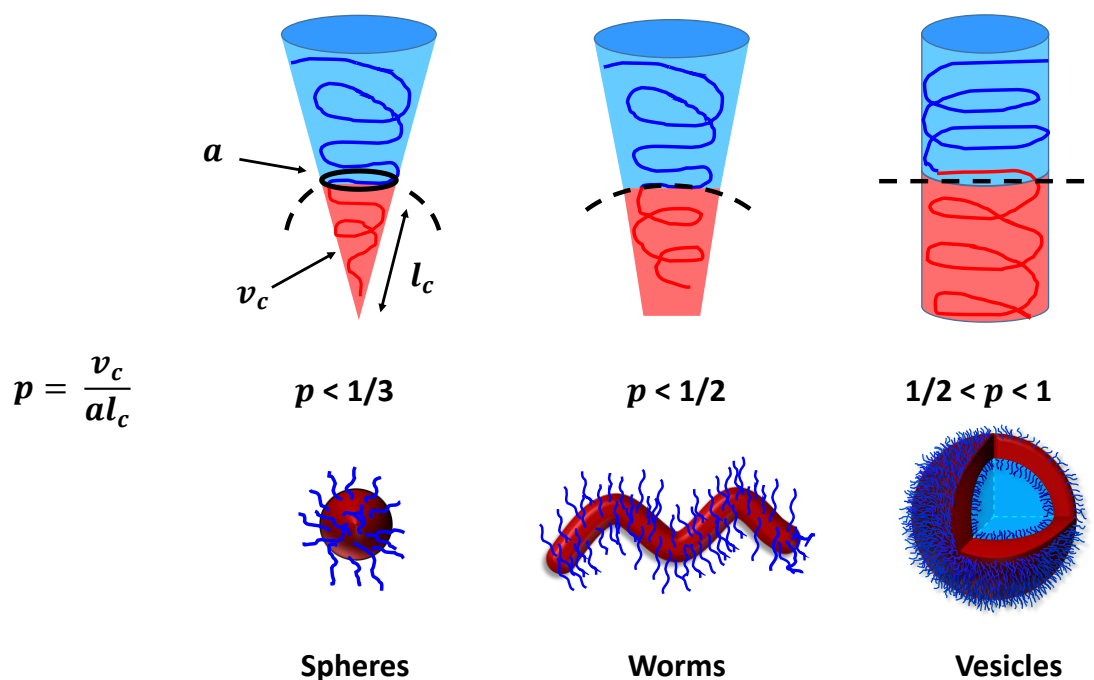


**Figure 1.13:** Schematic representation of how the dimensionless packing parameter,  $p$ , relates to the molecular curvature of amphiphilic polymers.  $v_c$  is the volume of the solvophobic core,  $l_c$  is the critical chain length of the solvophobic tail and  $a$  is the area occupied by the head group

Although block copolymers and surfactants have some important similarities, they also exhibit some distinct differences. Firstly, the kinetic exchange between unimers/aggregates for block copolymers is relatively slow. This is owing to the large enthalpic penalty required to produce a free chain in solution, combined with the relatively high viscosity inside the micelle core. Thus, copolymer chains typically exhibit much longer residence times within micelles than surfactants do. Consequently, copolymer micelles are more stable than surfactant micelles.<sup>2</sup> Moreover, critical micelle concentrations (CMCs) observed for block copolymers are usually much lower than for surfactants. For example, PS-PAA diblock copolymers exhibit CMCs that are approximately 6 orders of magnitude lower than sodium dodecylsulfate (SDS) does.<sup>2</sup>

To prepare diblock copolymer micelles, a number of processing techniques have been reported. Perhaps the two most common involve either a solvent switch or rehydration of a thin film.<sup>95</sup>

However, both of these techniques are only applicable for low copolymer concentrations (~ 1 % w/w), which places limits on the final application of the block copolymer micelles. This restriction has been largely addressed in recent years with the development of polymerisation-induced self-assembly (PISA).

### 1.6 Polymerisation-induced self-assembly

PISA facilitates the synthesis of block copolymer nanoparticles at very high concentrations (~ 50 % w/w) without the requirement of a post-polymerisation processing step.<sup>106</sup> As a result, PISA has attracted significant attention over the past decade, both from academia *and* industry.<sup>107–110</sup> The basic principle of PISA is relatively straightforward. Firstly, a suitable polymer is selected as a stabiliser block and dissolved in a good solvent. Then, a second monomer is polymerised from one end of this soluble precursor, such that it forms an insoluble polymer. As the second block grows and becomes increasingly insoluble, the block copolymer chains undergo *in situ* self-assembly to form micelles (**Figure 1.14**).<sup>111</sup> Typically, the range of copolymer morphologies obtained is very similar to those reported for traditional self-assembly in dilute solution, i.e. spheres, worms and vesicles. The critical DP at which nucleation occurs varies significantly between PISA formulations and depends largely on the choice of the polymers/solvent.<sup>112</sup> It is perhaps important to emphasise that although any living/controlled polymerisation technique can in practice facilitate PISA,<sup>113–116</sup> the vast majority of the published literature utilises RAFT polymerisation.<sup>111</sup>

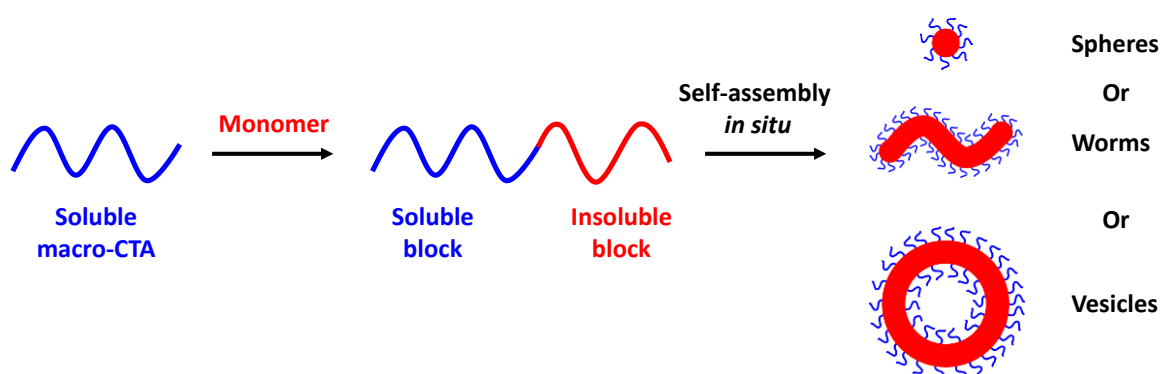


**Figure 1.14:** Schematic representation of polymerisation-induced self-assembly (PISA). A soluble macromolecular chain transfer agent (macro-CTA) is used to polymerise a second monomer, which results in an insoluble core-forming block.

#### 1.6.1 RAFT aqueous dispersion polymerisation

Of all the PISA formulations thus far reported, the most studied are based on RAFT aqueous dispersion polymerisation.<sup>106,111</sup> As described earlier, this involves the polymerisation of a water

miscible monomer to give a *water-insoluble* polymer, which acts as the core-forming block. The archetypical example of this behaviour is 2-hydroxypropyl methacrylate (HPMA).<sup>111</sup> Indeed, HPMA has been used as a core-forming block in water with various steric stabiliser blocks.<sup>117–120</sup>

The precise nanoparticle morphology obtained from a PISA synthesis depends on the DP of the stabiliser block, the DP of the core-forming block and also the copolymer concentration at which the synthesis is conducted. In general, increasing the core-forming block DP for a fixed stabiliser DP results in an evolution of copolymer morphology from spheres to worms to vesicles.<sup>120</sup> Qualitatively, this can be explained using the packing parameter concept, see equation (1.15). For a fixed stabiliser DP, increasing the core-forming DP results in a larger volume fraction for the core-forming block. As a result, the packing parameter increases and hence a morphological transition is observed. However, although this argument is a useful guideline, it does not tell the whole story. For example, in many cases, utilising a relatively long stabiliser block limits the resulting nanoparticle morphology to spheres.<sup>106</sup> A similar effect is observed if the PISA synthesis is conducted at low copolymer concentrations (< 5 % w/w), i.e. there is a strong concentration effect. Neither of these phenomena can be explained by the packing parameter, which is simply based on geometric considerations.

The first attempt to understand the morphological transitions observed during PISA, from a mechanistic standpoint, were made by Blanazs *et al.*<sup>121</sup> In this study, a poly(glycerol monomethacrylate)<sub>47</sub> (PGMA)<sub>47</sub> stabiliser was used to polymerise HPMA in water. The polymerisation was conducted at 10 % w/v and a core-forming PHPMA DP of 200 was targeted, corresponding to vesicles. During the HPMA polymerisation, aliquots were removed at regular intervals and analysed by TEM. In the early stages of the polymerisation (i.e. at a HPMA conversion of < 40 %) no particles were observed. This was because the PHPMA chains were insufficiently hydrophobic to induce particle nucleation. However, once a critical threshold DP of 92 had been reached, nucleation and spheres were observed *via* TEM (**Figure 1.15**). Furthermore, nucleation was also accompanied by a five-fold polymerisation rate enhancement. This increase in polymerisation rate was attributed to the unreacted HPMA monomer swelling the nascent spherical micelles, thus increasing the local concentration of HPMA monomer within

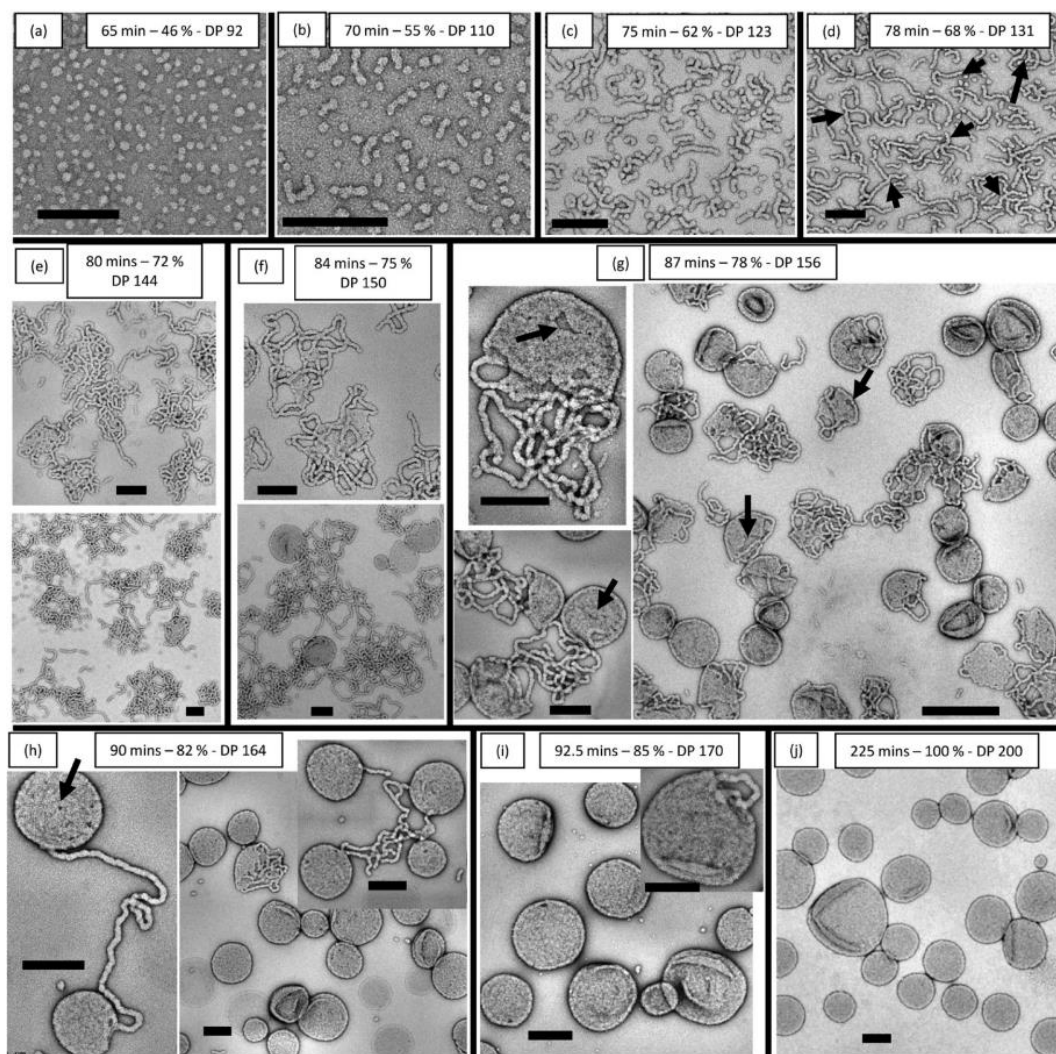


**Figure 1.15:** Intermediate nanostructures observed during the synthesis of PGMA<sub>47</sub>-PPHMA<sub>200</sub> vesicles at 10 % w/v in water. The percentage values indicate the HPMA monomer conversion at the time the polymerisation was sampled. Transmission electron micrographs represent (a) spheres, (b) short worms (c) long worms (d) branched worms (e,f) partially coalescence/branched worms (g) jellyfish, and (h-j) vesicles. The scale bars correspond to 200 nm.<sup>121</sup>

the nanoparticle core. Based on TEM images, it was suggested that during a PISA synthesis, worm-like micelles are formed by the 1D stochastic fusion of spherical micelles. Then, as the polymerisation and the core-forming block grows, the worms begin branching and coalescing before wrapping-up to form block copolymer vesicles. If correct, this hypothesis would also explain why relatively long stabiliser blocks and low copolymer concentrations typically limit PISA formulations to kinetically-trapped spheres. If the stabiliser DP is too large, the kinetic barrier to sphere fusion is insurmountable. Furthermore, if the synthesis concentration is too low, sphere fusion events are too infrequent on the time scale of the HPMA polymerisation. More recently, Derry *et al.* have reported similar behaviour for poly(stearyl methacrylate)-poly(benzyl methacrylate) (PSMA-PBzMA) nanoparticles prepared *via* PISA in mineral oil.<sup>122</sup> This suggests

that the evolution of spheres to form worm and vesicles is limited to water and is likely to be universal to all PISA formulations.

Although much is now known about the mechanism of PISA, there are still considerable gaps in our understanding. For example, even if the core-forming DP, the stabiliser DP and the copolymer concentration are all precisely known for a PISA formulation of interest, the resulting copolymer morphology cannot be predicted *a priori*. To address this problem, the typical strategy is to construct a phase diagram for the PISA system of interest. Typically, the DP of the stabiliser block is fixed and a large number of PISA syntheses are conducted at various copolymer concentrations targeting a range of core-forming DPs.<sup>123</sup> The copolymer morphology is then determined by TEM post-polymerisation, in order to map out the boundaries of each phase. As PISA syntheses are typically highly reproducible, these phase diagrams then serve as road map to target the desired copolymer morphology. A typical example of a phase diagram, constructed for PGMA<sub>78</sub>-PHPMA<sub>x</sub> copolymers, is shown in **Figure 1.16**.<sup>123</sup>

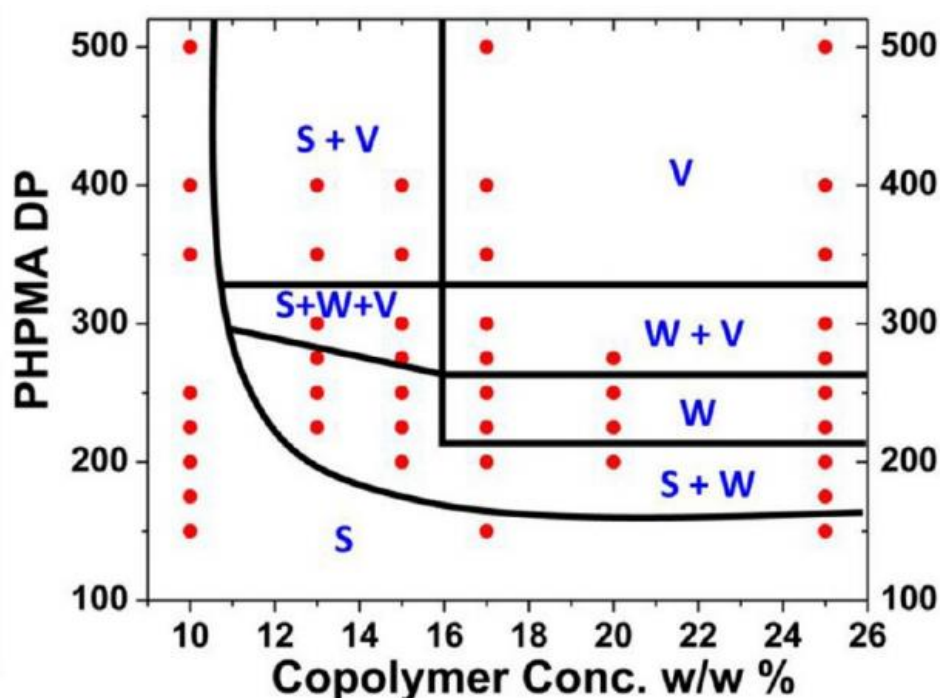


**Figure 1.16:** Phase diagram for a series of PGMA<sub>78</sub>-PHPMA<sub>x</sub> copolymer synthesised by RAFT aqueous dispersion polymerisation at concentrations ranging between 10 and 25 % w/w. S = spheres, W = worms and V = vesicles.<sup>123</sup>

As already described, PISA *via* RAFT aqueous dispersion polymerisation comprises the majority of the PISA literature. However, it is also the least pertinent to the work described in this thesis. As such, this topic will not be discussed further. Instead, the remainder of this section will be

spent highlighting the latest developments in RAFT PISA syntheses based on dispersion polymerisation in *non-polar* solvents. This is followed by a brief review of RAFT PISA *via* aqueous emulsion polymerisation.

### 1.6.2 RAFT dispersion polymerisation in non-polar media.

Although far less common than RAFT aqueous dispersion or emulsion polymerisation, RAFT dispersion polymerisation in non-polar media is still well documented.<sup>124</sup> To highlight the broad range of the various CTAs, stabiliser blocks and core-forming blocks that have been used for this purpose, a selection of such reagents is depicted in **Figure 1.17**.<sup>124</sup>

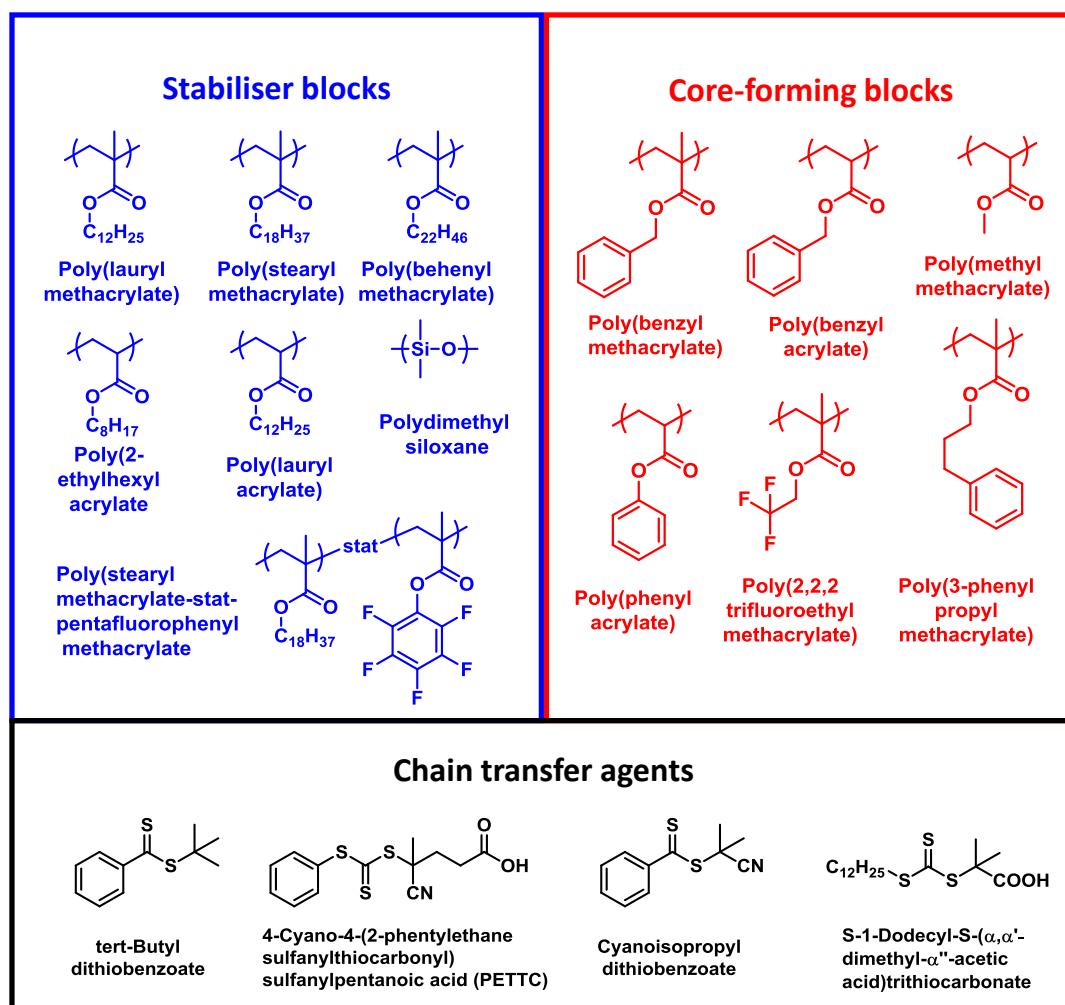


**Figure 1.17:** Chemical structures of the various stabiliser blocks (blue), core-forming blocks (red) and chain transfer agents (black) that have been used in various RAFT dispersion polymerisations performed in non-polar media reported in the literature.<sup>124</sup>

The first examples of PISA conducted by RAFT dispersion polymerisation in non-polar media were reported by Charleux *et al.*<sup>125–127</sup> Initially, a poly(2-ethylhexyl acrylate)<sub>114</sub> (PEHA)<sub>114</sub> macro-CTA was prepared *via* bulk polymerisation. This macro-CTA was then chain-extended with methyl acrylate (MA), directly in *iso*-dodecane, in order to form PEHA-PMA diblock copolymers

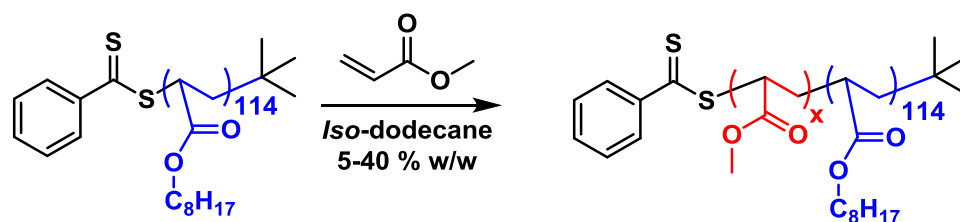


**Figure 1.18:** Polymerisation of methyl acrylate with a poly(2-ethylhexyl acrylate)<sub>114</sub> macro-CTA, directly in *iso*-dodecane.<sup>127</sup>

(see **Figure 1.18**). The insolubility of the PMA block in *iso*-dodecane resulted in PISA, and the formation of small well-defined spherical micelles was observed. Perhaps surprisingly, this prototype system was plagued with a number of problems, including poor RAFT control, incomplete conversions and significant rate retardation. GPC studies indicated multimodal GPC traces, suggesting incomplete chain extension of the macro-CTA, and very broad molecular weight distributions ( $\bar{M}_w/\bar{M}_n \sim 6$ ). These issues could be alleviated somewhat by changing the CTA type from a dithiobenzoate to a trithiocarbonate, but, the molecular weight distributions still remained broad. Therefore, given these inherent problems, it seems likely that the RAFT polymerisation was not actually well controlled. Nevertheless, the resulting particles were still well-defined with narrow size distributions.

The first report of a well-controlled RAFT non-polar dispersion polymerisation was reported in 2013 by Fielding and co-workers.<sup>128</sup> Firstly, a cumyl dithiobenzoate CTA was used to polymerise lauryl methacrylate (LMA) *via* RAFT solution polymerisation in toluene. The resulting PLMA macro-CTAs were then chain-extended in *n*-heptane with benzyl methacrylate (BzMA). When a relatively long PLMA DP of 37 was used, only spherical nanoparticles were obtained. The Z-average diameters of these particles ranged from 41 nm to 139 nm, with PBzMA core-forming DPs of 97 and 873 respectively. Moreover, the diameter could be precisely tuned within this range by targeting appropriate PBzMA core-forming DPs. This was consistent with the reported PISA literature, in that very long stabiliser DPs limit the nanoparticle morphology to spheres. As described earlier, this is most likely due to a large kinetic barrier preventing 1D sphere fusion. When a shorter PLMA DP of 17 was utilised, the full range of copolymer morphologies were observed, i.e. spheres worms and vesicles. Also, BzMA polymerisations proceeded to very high BzMA conversions ( $\sim 97\%$ ) and dispersities remained reasonably low throughout ( $\bar{M}_w/\bar{M}_n < 1.34$ ).

In a follow-up publication, Fielding *et al.* explored the synthesis of PLMA-PBzMA in *n*-dodecane rather than *n*-heptane.<sup>129</sup> At first glance, this appears to be a rather trivial change. However, the relatively high boiling point of *n*-dodecane compared to *n*-heptane facilitated a number of high-temperature studies to be performed, that were previously not feasible. Firstly, the rheology of

PLMA<sub>16</sub>-PBzMA<sub>37</sub> worm gels prepared at 20 % w/w was examined. Upon performing a heating cycle from 20 °C to 90 °C, reversible degelation was observed around 47 °C, albeit with some minor hysteresis. TEM studies were used to probe this transition further, and it was determined that a reversible worm-to-sphere transition was responsible (**Figure 1.19**).

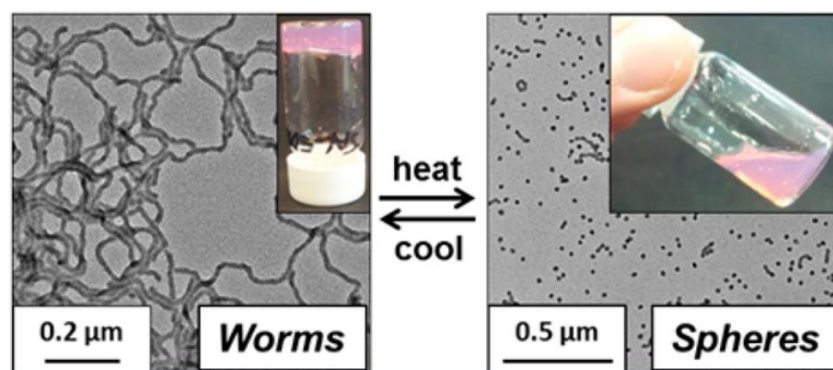


**Figure 1.19:** Transmission electron micrographs (TEMs) and accompanying digital photographs obtained upon heating a dispersion of PLMA<sub>16</sub>-PBzMA<sub>37</sub> worms from 20 °C to 90 °C. TEM images were obtained for a dilute (0.1 % w/w) dispersion of PLMA<sub>16</sub>-PBzMA<sub>37</sub> spheres/worms. Digital images were recorded (see inset) for a concentrated (20 % w/w) dispersion.<sup>129</sup>

Interestingly, although rheology studies indicated degelation occurred at 47 °C, small-angle X-ray scattering (SAXS) indicated that heating up to 160 °C was required to fully convert worms into spheres. As such, it was concluded that the critical gelation temperature (CGT) observed *via* rheology was the result of a reduction in the mean worm contour length upon heating. This would result in fewer inter-worm contacts *per worm* and, ultimately, degelation.<sup>130</sup> Two mechanisms were hypothesised for the way in which this transition might occur: (i) random worm cleavage to produce increasingly shorter worms or (ii) sequential budding of spheres from the worm ends (**Figure 1.20**). Variable temperature SAXS studies suggested that the latter mechanism was most likely the dominant one.<sup>129</sup>

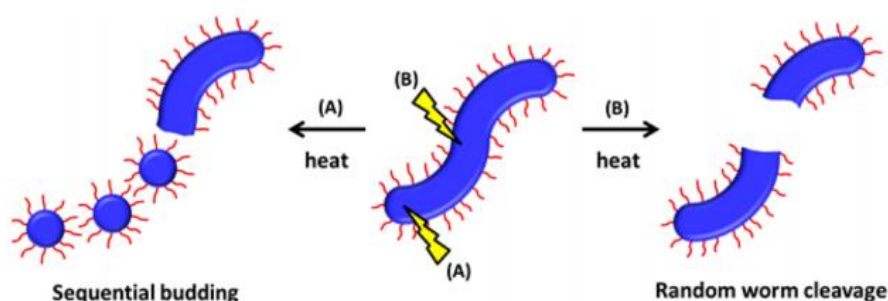


**Figure 1.20:** Two proposed mechanisms by which the thermally induced worm-to-sphere transition might take place. (A) sequential budding of spheres from the worm-ends (B) random worm cleavage.<sup>129</sup>

Variable temperature  $^1\text{H}$  NMR experiments, conducted on a 5 % w/w dispersion of PLMA<sub>16</sub>-PBzMA<sub>37</sub> worms in *n*-dodecane- $\text{d}_{26}$  provided useful insights regarding the physical origin of the worm-to-sphere transition. As the temperature was increased, the PBzMA core-forming block became increasingly solvated. This is understandable as such upper-critical solution temperature (UCST)-like behaviour for hydrophobic polymers in organic media is well documented.<sup>129</sup> Based on this observation, it was proposed that surface plasticisation of the PBzMA core was responsible for the worm-to-sphere transition. In other words, ingress of hot *n*-dodecane into the surface of the nanoparticle cores results in a longer effective stabiliser DP. This reduces the effective packing parameter for the copolymer chains and hence spherical micelles become the preferred copolymer morphology.

More recently, Derry *et al.* revisited this PLMA-PBzMA formulation. This time, PISA syntheses were conducted in *n*-dodecane, mineral oil and poly( $\alpha$ -olefin) (PAO) oil.<sup>110</sup> The motivation behind this work stemmed from an earlier publication by Zheng *et al.*<sup>131</sup> In this tribological study it was demonstrated that diblock copolymer spheres, when dispersed in lubricant base oils, can significantly reduce the friction coefficient of such oils operating under boundary lubrication conditions. However, ATRP chemistry was used to synthesise the diblock copolymers, before dispersing them in oil. This multi-step process involved both post-polymerisation processing, protecting group chemistry and photo-cross-linking purification, thereby reducing its industrial applicability. This was addressed by Derry *et al.*, who demonstrated that RAFT PISA can be used to synthesise similar-sized PLMA-PBzMA spheres directly in the oil of interest *via* a one-pot synthesis. As a result, the need for post-polymerisation processing steps are removed and the formulation becomes more industrially relevant.

As an alternative to PLMA, it has been demonstrated that PSMA can also act as a stabiliser block for nanoparticles in non-polar media. This was first demonstrated by Lowe and co-workers, who chain-extended a PSMA<sub>19</sub> macro-CTA with 3-phenylpropyl methacrylate (3-PPMA) directly in *n*-tetradecane.<sup>132</sup> Spheres, worms and vesicles were all accessible with this formulation at a copolymer concentration of 20 % w/w. Moreover, good RAFT control was observed for each polymerisation, with dispersities remaining below 1.2. Perhaps unsurprisingly, given the similarities between 3-PPMA and BzMA, a worm-to-sphere transition was observed for this system which was analogous to that reported by Fielding *et al.*<sup>129</sup> Although high-temperature SAXS studies were not performed upon these diblock copolymers, TEM indicated that a full worm-to-sphere transition occurred at 95 °C. Again, variable temperature  $^1\text{H}$  NMR indicated that this transition was the result of increased solvation, and hence surface plasticisation, of the

P(3-PPMA) core at elevated temperatures. This formulation was also successfully extended to include *n*-octane in a follow-up publication.<sup>133</sup>

The use of PSMA as a steric stabiliser in RAFT dispersion polymerisation was explored further by Derry *et al.* In this study, PSMA macro-CTAs of varying DP were used to polymerise BzMA in mineral oil.<sup>122</sup> A relatively short PSMA DP of 13 allowed spheres, worms or vesicles to be synthesised. On the other hand, PSMA DPs of 18 and 31 resulted solely in kinetically-trapped spheres, even at PBzMA target DPs of 2000. A phase diagram was constructed for PSMA<sub>13</sub>-PBzMA<sub>x</sub>, for a range of copolymer concentrations, in order to facilitate the reproducible targeting of each copolymer morphology. Surprisingly, it was discovered that worms could be synthesised at a copolymer concentration as low as 5 % w/w. This is consistent with PISA formulations reported in water,<sup>111</sup> but it is unusual for a non-polar PISA formulation for which worms are typically only accessible at copolymer concentrations in excess of 10 % w/w.<sup>124</sup> Perhaps most noteworthy, SAXS was used for the first time by Derry *et al.* to monitor PISA syntheses *in situ* at a copolymer concentration of 10 % w/w. By conducting the BzMA polymerisations directly in the X-ray beam, the evolution in copolymer morphology from spheres to worms to vesicles was observed. Moreover, the mean aggregation number, the number of copolymer chains per unit surface area, and the distance between adjacent copolymer chains at the core/shell interface were calculated during the polymerisation. Furthermore, these SAXS studies also provided important insights regarding the mechanism of vesicle growth during these PISA syntheses. Once vesicles had been formed, their overall mean diameter remained approximately constant. As the unreacted BzMA monomer continued to polymerise, the vesicle membrane thickness increased monotonically. A constant overall diameter coupled with an increasing membrane thickness implies that vesicles grow inward, progressively reducing the lumen volume. This is highlighted by the cartoon schematic shown in **Figure 1.21**.<sup>122</sup>

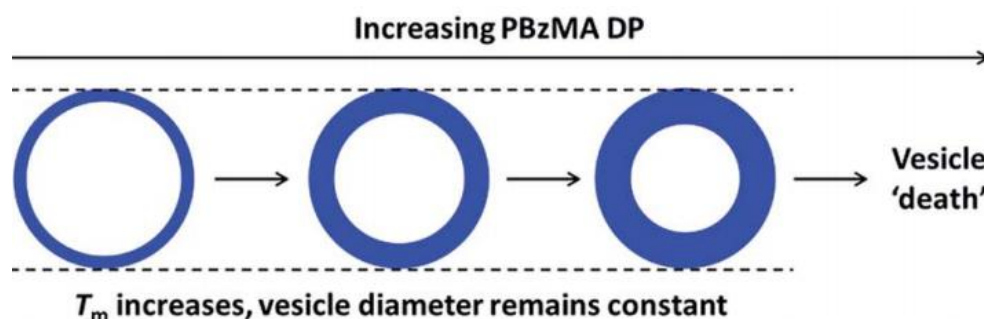


**Figure 1.21:** Schematic representation of vesicle growth observed during *in situ* small-angle X-ray scattering studies of poly(stearyl methacrylate)-poly(benzyl methacrylate). The overall vesicle diameter remains approximately constant, the membrane thickness increases, indicating that the vesicles grow inward.  $T_m$  = membrane thickness.<sup>122</sup>

Obviously, inward growth of the membrane cannot continue indefinitely. At a certain critical PBzMA DP, the vesicle morphology becomes unstable resulting in ‘vesicle death’. Similar behaviour was also observed for aqueous PISA formulations by Warren *et al.*,<sup>134</sup> suggesting that this vesicle growth mechanism may be universal to PISA. It was hypothesised that the vesicles grow *via* this mechanism because it reduces their interfacial area and, hence, minimises their free energy.

Discussed earlier, PLMA-PBzMA worms undergo a reversible worm-to-sphere on heating, owing to surface plasticisation of the core-forming block by the hot solvent. Recently, it has been reported that PSMA-PBzMA vesicles undergo an analogous vesicle-to-worm transition.<sup>135</sup> More specifically, Derry *et al.* prepared PSMA-PBzMA vesicles at 10 % w/w in *n*-dodecane before heating this dispersion to 150 °C. TEM studies confirmed that a vesicle-to-worm transition had taken place. To characterise this transition further, a 10 % w/w vesicle dispersion was analysed *via* oscillatory rheology. At 20 °C, the vesicles behaved as a low-viscosity free-flowing fluid. However, on heating to 130 °C, a significant increase in viscosity observed. This can be explained by the presence of diblock copolymer worms, which are known to form free-standing gels at 10 % w/w in mineral oil at 20 °C. One potential application for this new discovery is in high-temperature oil thickening, which may be of high interest in the automotive industry.

The majority of the PISA literature regarding non-polar dispersion polymerisation is based on alkyl-(meth)acrylate stabilisers. One exception was the use of a polydimethylsiloxane<sub>66</sub> (PDMS)<sub>66</sub> stabiliser, as reported by Lopez-Oliva *et al.*<sup>136</sup> In this study, a PDMS<sub>66</sub> chain containing a single terminal hydroxyl group was esterified with 4-cyano-4-(2-phenylethanesulphonylthiocarbonyl) sulphonylpentanoic acid (PETTC) (**Figure 1.22**).

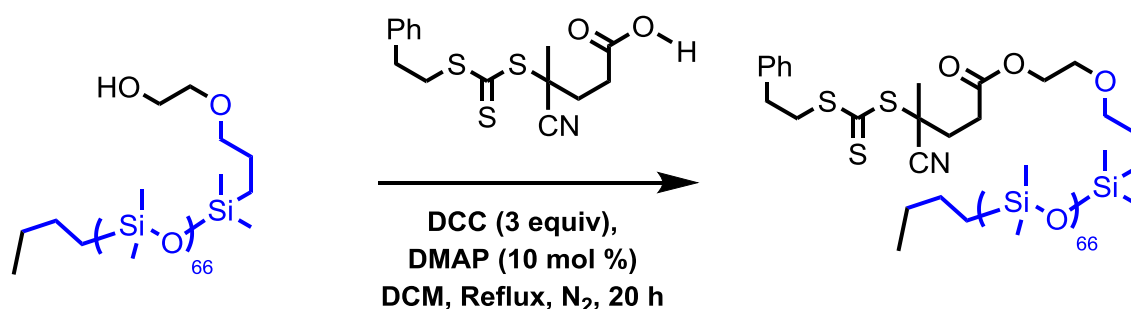


**Figure 1.22:** Esterification of monofunctionalized PDMS with 4-cyano-4-(2-phenylethanesulphonylthiocarbonyl)sulphonylpentanoic acid (PETTC) using dimethylaminopyridine (DMAP) and N, N'-dicyclohexylcarbodiimide (DCC).<sup>136</sup>

The resulting PDMS<sub>66</sub> macro-CTA had an end-group functionality of 92 % as determined by <sup>1</sup>H NMR. It was then chain-extended with BzMA in *n*-heptane at 70 °C, targeting various PBzMA

DPs. Each polymerisation was well controlled, with dispersities remaining below 1.25. Furthermore, spheres, worms or vesicles were accessible using this new macro-CTA, albeit only at relatively high copolymer concentrations. A phase diagram was constructed for this PISA formulation, to allow the reproducible targeting of each morphology (**Figure 1.23**). However, it is worth emphasising that, although worms could be reproducibly synthesised, the worm phase was exceptionally narrow, comprising a single PBzMA DP.

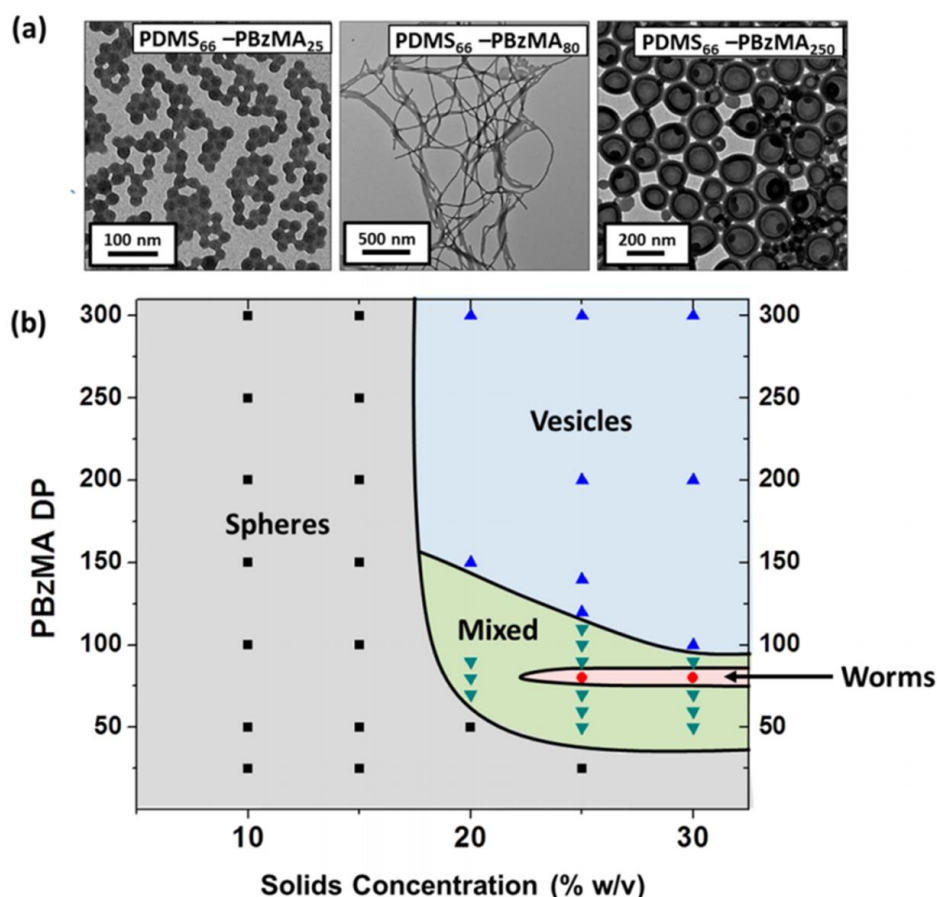


**Figure 1.23:** (a) Representative transmission electron micrographs obtained for polydimethylsiloxane<sub>66</sub>-poly(benzyl methacrylate)<sub>x</sub> diblock copolymer nano-objects synthesised at 25 % w/w in *n*-heptane. (b) Phase diagram reported for the same system.<sup>136</sup>

### 1.6.3 RAFT aqueous emulsion polymerisation

As discussed in section 1.4.2, aqueous emulsion polymerisation offers a convenient route by which to synthesise well-defined spherical particles in the 50 – 1000 nm region. Typically, this is accomplished with the use of surfactant stabilisers. In principle, RAFT emulsion polymerisation offers a convenient surfactant-free route to well-defined sterically-stabilised nanoparticles.<sup>112</sup> This is achieved by simply replacing the surfactant in the formulation with a macro-CTA. The first reports of well-controlled RAFT aqueous emulsion polymerisation were by Hawket and co-

workers.<sup>137</sup> In this seminal work, a PAA macro-CTA was prepared and then chain-extended with *n*-butyl acrylate (BA) in water. The resulting PAA-PBA spherical nanoparticles were well-defined, with a mean diameter of 60 nm. Moreover, GPC analysis confirmed that dispersities remained below 1.5 throughout the BA polymerisation. Since this seminal study, the Charleux group have been most active in this area, reporting a wide range of PISA formulations mediated *via* RAFT aqueous emulsion polymerisation. These formulations utilise various macro-CTAs, typically based on methacrylic,<sup>138</sup> acrylic,<sup>139</sup> acrylamide<sup>140</sup> or PEO polymers<sup>141</sup> (or a binary combination of these).<sup>142</sup> Moreover many core-forming monomers have been used, such as styrene,<sup>141</sup> BA,<sup>141</sup> BzMA<sup>142</sup> and MMA.<sup>143</sup> To highlight one example in particular, Zheng *et al.*<sup>144</sup> reported the use of a statistical copolymer macro-CTA, namely poly(methacrylic acid-co-poly(ethylene oxide)methyl ether methacrylate), P(MAA-co-PEOMA), for the aqueous emulsion polymerisation of styrene. This formulation facilitated the synthesis of well-defined spherical, worm-like or vesicular morphologies. (Figure 1.24).

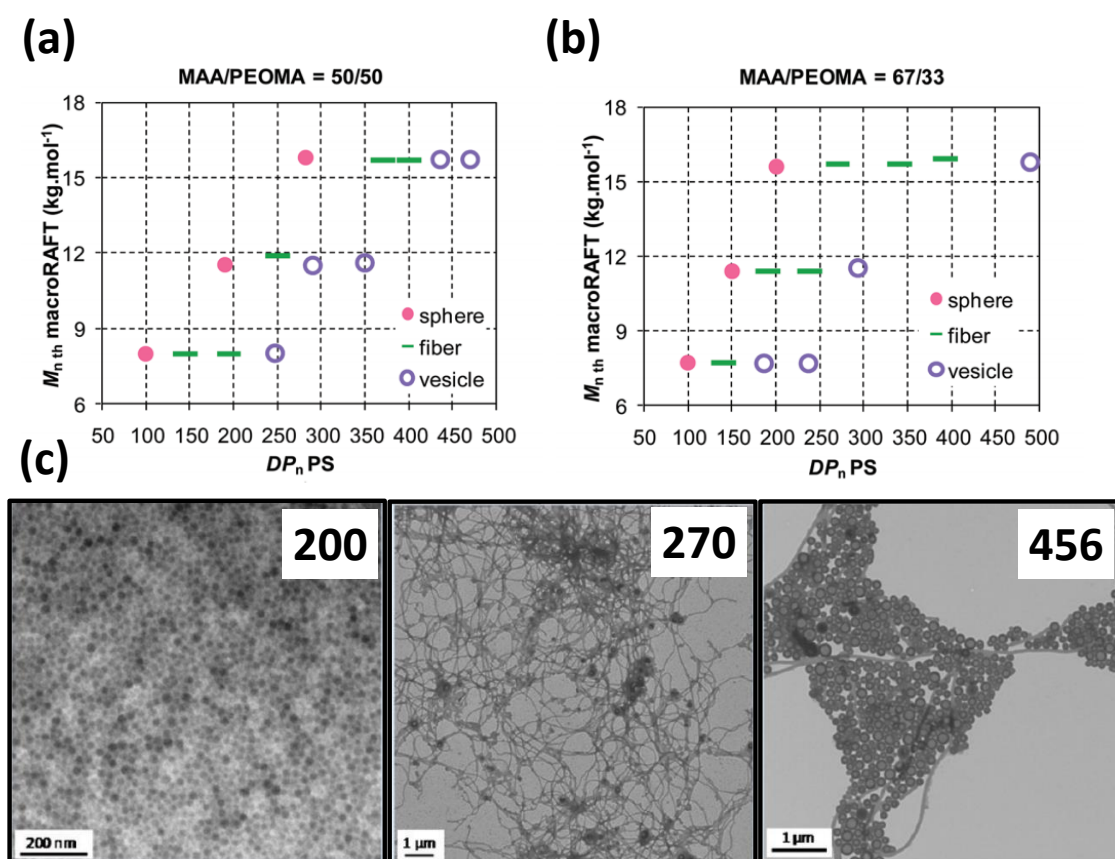


**Figure 1.24:** Phase diagrams reported by Zheng *et al.* for polystyrene nanoparticles stabilised with poly(methacrylic acid-co-poly(ethylene oxide) methyl ether methacrylate), P(MAA-co-PEOMA). (a) the MAA/EOMA molar ratio = 50/50 (b) the MAA/EOMA molar ratio = 67/33. (c) Representative examples of spheres, worms and vesicles indicated by transmission electron microscopy obtained when the MAA/EOMA ratio = 50/50. The number in the right-hand corner indicates the DP of the core-forming polystyrene block.<sup>144</sup>

This particular example is of interest because the full range of copolymer morphologies were accessible. This is rather unusual for a RAFT aqueous emulsion polymerisation, with most formulations resulting only in kinetically-trapped spheres.<sup>106</sup> The explanation for this strange phenomenon, however, remains unclear. Recently, it has been suggested that the aqueous solubility of the monomer may play a role in determining which morphologies are accessible.<sup>145</sup> This was highlighted in a recent study by Cockram *et al.*, who reported the RAFT aqueous emulsion polymerisation of 2-hydroxybutyl methacrylate (HBMA) with a PMAA macro-CTA.<sup>146</sup> HBMA is an interesting monomer to study by RAFT aqueous emulsion polymerisation because its water solubility is relatively high ( $20 \text{ g dm}^{-3}$  at  $70 \text{ }^\circ\text{C}$ ).<sup>146</sup> When low PHBMA core-forming DPs of less than 130 were targeted, spherical particles were obtained. On increasing the core-forming PHBMA DP an unusual anisotropic ‘monkey-nut’ morphology was observed (**Figure 1.25**). Further increases to the PHBMA DP resulted, rather surprisingly, in a spherical morphology again, i.e. a traditional worm or vesicle phase could not be prepared. As such, this work represents a useful first step in our efforts to understand RAFT PISA formulations based on aqueous emulsion polymerisation. However, our current understanding remains incomplete.

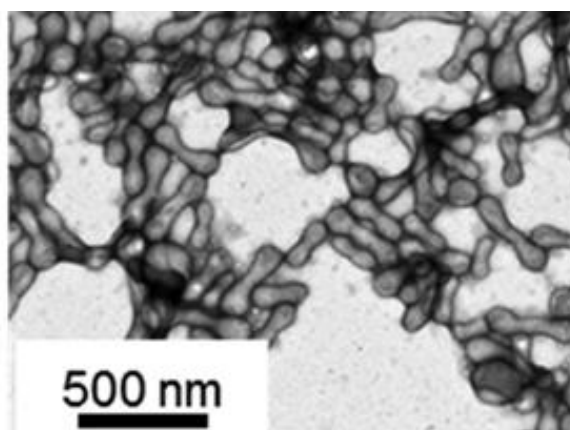


**Figure 1.25:** Transmission electron micrograph (TEM) obtained for poly(methacrylic acid)<sub>56</sub>-poly(2-hydroxybutyl methacrylate)<sub>150</sub> monkey nuts synthesised at 20 % w/w *via* RAFT aqueous emulsion polymerisation of PHBMA at  $70 \text{ }^\circ\text{C}$  and pH 5.<sup>146</sup>

## 1.7 Particle characterisation techniques

The number of techniques available for the characterisation of colloids is very large, with each providing different information about the particles under analysis. These range from microscopic techniques, such as electron microscopy, atomic force microscopy and confocal microscopy, to scattering techniques such as light, x-ray and neutron scattering. Furthermore, there also methods by which to analyse the emergent properties of a colloidal system as a whole, such as rheometry or viscometry. This section will briefly outline some of the different techniques utilised in this thesis.

### 1.7.1 Dynamic light scattering.

DLS is a technique used to determine the hydrodynamic diameter of a dilute dispersion of colloidal particles, typically in the sub-micron size range. DLS measures the translational diffusion coefficient,  $D$  and then the hydrodynamic diameter is calculated using the Stokes-Einstein relationship shown in equation (1.16):<sup>147</sup>

$$D = \frac{k_B T}{6\pi\eta r} \quad (1.16)$$

Here,  $k_B$  is the Boltzmann constant,  $T$  is the absolute temperature,  $\eta$  is the viscosity of the solvent,  $\pi$  is the well-known mathematical constant and  $r$  is the hydrodynamic particle radius. In a typical DLS experiment colloidal particles are irradiated with a laser. The particles then scatter the incident laser light, which is detected as a speckle pattern.<sup>148</sup> If the particles were motionless, this speckle pattern would remain unchanged with respect to time. However, the particles undergo constant Brownian motion owing to their random bombardment by the surrounding solvent molecules.<sup>148</sup> Therefore, the intensity of the scattered light fluctuates as the particles diffuse, which leads to the speckle pattern changing over time. If the particles are relatively large, Brownian motion is slow and the speckle pattern changes slowly. Similarly, if the particles are relatively small, Brownian motion is very fast and the speckle pattern changes more rapidly. Using an autocorrelation function, which compares how well a signal correlates to itself after a specified time delay, the rate of change of the speckle pattern can be determined.<sup>148</sup> From this information,  $D$  can be calculated, which can then be used to obtain  $r$  using equation (1.16). One limitation of DLS is that the Stokes-Einstein relationship is only strictly valid for spherical particles. Therefore, if non-spherical particles are analysed *via* DLS, a sphere-equivalent diameter is obtained. Therefore, although DLS is useful for sizing spheres and vesicles, caution must be exercised when interpreting DLS data for worm-like micelles.<sup>147</sup>

### 1.7.2 Rheology

Rheology is the study of the flow and deformation of materials.<sup>149</sup> Two important rheological concepts are stress ( $\sigma$ ) and strain ( $\varepsilon$ ). Stress describes the applied force per unit area. However, from the perspective of the material, stress can be considered the sum of the internal forces that resist the applied force. Strain, on the other hand, describes the deformation of a material upon the application of a force, typically relative to its original dimensions.<sup>149</sup> For example, when an elastic band is stretched, the strain describes the amount of stretching, and the stress describes how much force is required to produce it (or the internal forces within the band that resist the applied load). These two parameters are usually inter-related, but this is not always the case. For

example, a force applied to a perfectly rigid material will result in the generation of stress but no strain, because the dimensions remain unchanged. Similarly, when a material is heated and thermally expands, strain will result without any associated stress.

For a purely elastic (Hookean) solid, application of a shear stress results in deformation of the material (shear strain).<sup>150</sup> For example, if an elastic solid is sandwiched between two metal plates and the top plate is moved laterally, the material deforms. Once the applied stress is removed, the material regains its original dimensions. The tendency of materials to deform elastically in this way is described by their shear modulus ( $G$ ), which is defined as  $\sigma/\epsilon$ .<sup>149,150</sup> Eventually, a yield point will be reached after which the stress is sufficient to cause permanent, non-reversible deformation. This concept is illustrated in **Figure 1.26**.

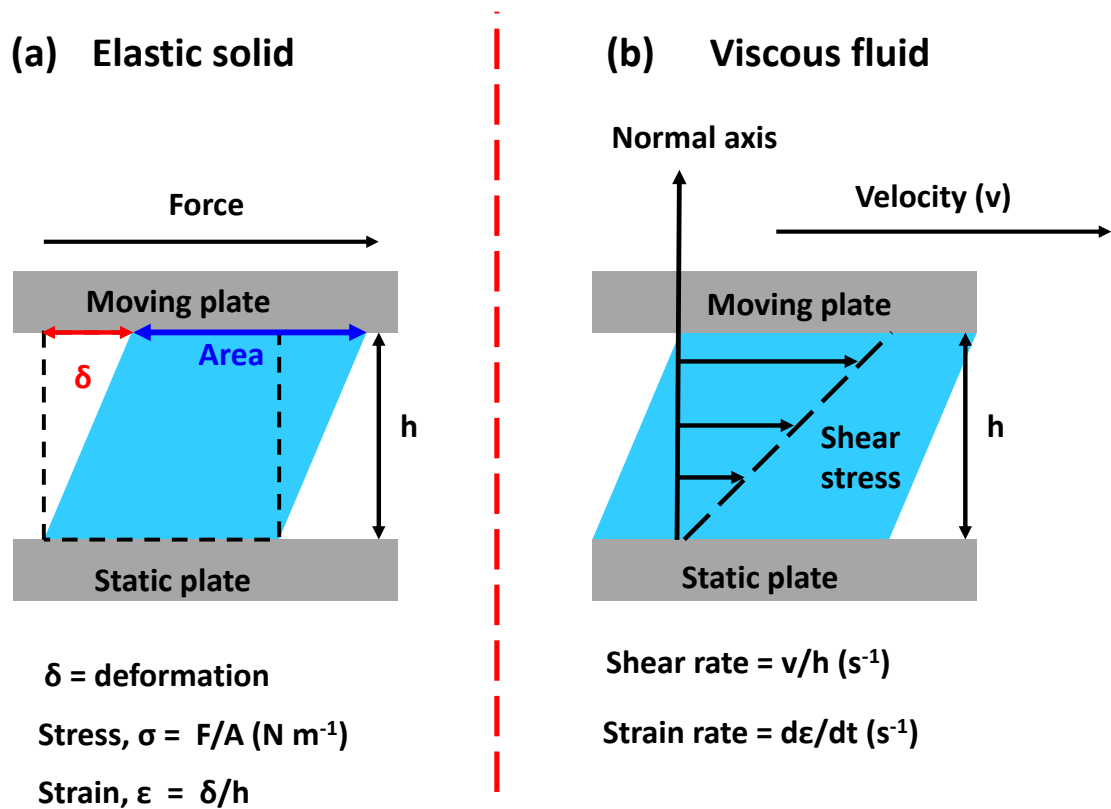


**Figure 1.26:** Schematic representation of the application of a shear force to either (a) an elastic solid or (b) a viscous fluid, sandwiched between two metal plates. For an elastic solid, the force results in a deformation. For the fluid, the force results in a velocity gradient throughout the fluid and therefore an associated flow.<sup>149</sup>

Newtonian Liquids, which are defined as those liquids which exhibit shear rate-independent viscosity ( $\eta$ ), behave differently when compared to elastic solids. Unlike solids, the molecules within a Newtonian liquid are not confined to a particular position in space and so can move freely past each other. Therefore, when a liquid is placed between two parallel plates, and the top plate

is moved laterally, different behaviour is observed. When considering Newtonian liquids, it is useful to think of the liquid comprising many different layers stacked on top of each other, all capable of moving over one another (laminar flow).<sup>149</sup> When a shear force is applied, the top layer begins to move with a velocity,  $v$ . This mobile top layer causes the layers below it to begin moving too, such that a velocity gradient is established throughout the fluid reaching zero at the stationary plate. As a result, when a shear force is applied to a liquid, the liquid continually deforms (flows) until the external force is removed. The shear rate ( $\dot{\gamma}$ ) at any point in the fluid is simply the difference in velocity between these different layers. This can be calculated by dividing the velocity at the top plate (the bottom plate remains stationary) by the distance between the plates, see **Figure 1.26**.<sup>149</sup> Another important parameter is the viscosity, which describes the resistance of the fluid to these shear forces. Highly viscous fluids resist shear force more than less viscous fluids and consequently flow less. Given that a Newtonian liquid cannot remain at rest under a shear force like an elastic solid, it is actually the rate of strain ( $d\varepsilon/dt$ ) that dictates how much stress is generated. This differs from an elastic solid for which the magnitude of the strain that dictates the stress.<sup>149</sup>

Generally, most polymeric materials display behaviour that is intermediate between that of an elastic solid and a viscous liquid, i.e. they exhibit viscous and elastic character.<sup>151</sup> As a result, these materials are said to be viscoelastic. There are many different rheological techniques by which these viscoelastic materials can be characterised, but perhaps the most useful is oscillatory rheology.<sup>149</sup> In an oscillatory rheology experiment, the input strain is applied sinusoidally, and the resulting stress is measured. This type of experiment is often performed using a rheometer equipped with a cone-and-plate geometry (**Figure 1.27**). This geometry is selected because the shear rate remains uniform across the whole sample.<sup>149</sup> For an oscillating cone, the velocity at any point on the rotating surface is given by the angular velocity multiplied by the radius from the centre ( $\omega r$ ). Similarly, the height between the cone and plate at any given  $r$  is given by the radius at that point, multiplied by the cone angle  $\Phi$ , or  $\Phi r$ . This is valid provided that the cone angle is small, such that  $\tan\Phi \sim \Phi$ . The shear rate at any point in this fluid is given by  $v/h$ , or in this case  $\omega r / r\Phi$ , or simply  $\omega/\Phi$ . Since this value is constant, it follows that the shear rate is also constant across the whole sample.

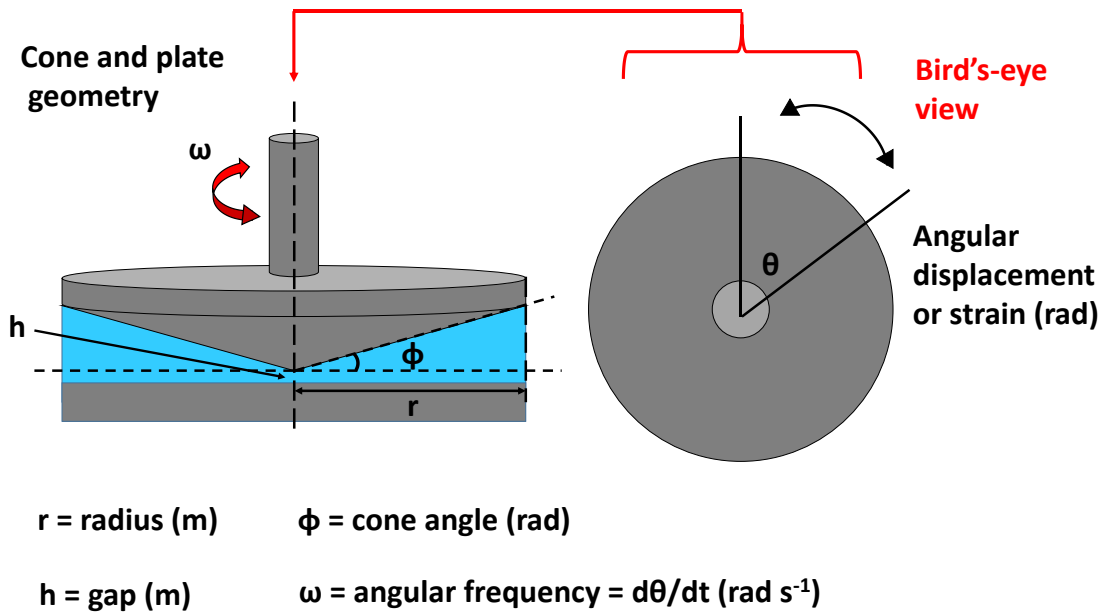


**Figure 1.27:** Schematic representation of the cone-and-plate geometry used for a typical oscillatory rheology experiment.

When characterising viscoelastic materials, perhaps the two most useful parameters are the dynamic storage modulus,  $G'$ , and the dynamic loss modulus,  $G''$ .  $G'$  describes the elastic character of the material by relating the input strain to the resulting stress. Similarly,  $G''$  represents the viscous character of a material by describing the change in the strain over time that occurs when an applied stress is removed. Therefore, it is worth emphasising that the elastic character and viscous character of a material have different time dependencies, which is why they can be separated by oscillatory rheology. For purely elastic behaviour, the removal of strain results in the instantaneous loss of stress. For viscous Newtonian liquids, on the other hand, once the applied stress is removed, the flow does not stop instantaneously but after some time.<sup>151</sup> Therefore, for purely elastic behaviour, the stress/strain sinusoidal curves will be precisely in phase. However, for liquids the maximum stress occurs with the maximum rate of strain, hence the resulting stress/strain curves are 90° out of phase. For viscoelastic materials, this phase difference will be located somewhere between these two extremes. Materials that exhibit more liquid-like character than elastic ( $G'' > G'$ ) are often called Maxwell materials. Similarly, materials that exhibit more elastic character than viscous ( $G' > G''$ ) are referred to as Kelvin-Voigt materials.<sup>151</sup>

In the context of polymeric nanoparticles prepared by PISA, the various morphologies often display distinctly different rheological properties. For example, worms will usually form free-standing gels when at sufficiently high copolymer concentration.<sup>110,129</sup> This gelation can be

determined by oscillatory rheology by examining the difference between  $G'$  and  $G''$ . It is generally accepted that gels exhibit substantially greater  $G'$  values than  $G''$  values, i.e. they have more elastic-like character than viscous-like character.<sup>151</sup> Moreover, for a true gel,  $G'$  and  $G''$  should be relatively linear over a broad frequency range. On the other hand, spheres and vesicles are free-flowing fluids for which  $G'' > G'$ .<sup>135</sup> Given these rheological differences between worms and spheres/vesicles, the rheological changes that occur during morphological transitions can be monitored conveniently by performing variable temperature experiments.

### 1.7.3 Shear-induced polarised light imaging

Light appears to travel more slowly through a medium such as water or air than it does through a vacuum.<sup>152</sup> This phenomenon is described by the index of refraction,  $n$ , which is defined as follows:

$$n = \frac{c}{v} \quad (1.17)$$

Here,  $c$  is the speed of light in a vacuum and  $v$  is the phase velocity of light in the medium. The refractive index of a particular material can be resolved into three orthogonal components, corresponding to the  $x$ ,  $y$  and  $z$  axes respectively. For most commonly encountered materials, these axes are all equivalent and therefore the material possesses a single index of refraction.<sup>152</sup> However, in certain materials, these components are not equivalent and therefore there is more than one index of refraction, each depending on the polarisation and propagation direction of the light. This phenomenon, known as birefringence, often arises in crystals with a non-cubic structure (such as calcite) or polymeric materials.<sup>152,153</sup> The most simple case of birefringence arises in uniaxial materials, which have just one axis of optical inhomogeneity with all other axes being equivalent. This axis is known as the optic axis. Consider, for example, light incident upon a worm-like micelle. Light travelling parallel to the long axis of the worm will experience a different refractive index compared to light travelling *via* the two axes perpendicular to the worm length (**Figure 1.28**). Birefringence is defined as the difference between these two indices of refraction ( $\Delta n = n_1 - n_2$ ).<sup>152</sup> However, in order to observe this birefringence experimentally, two additional conditions must be satisfied: (i) the sample must have a net orientation to yield a primary refractive index, and (ii) polarised light must be used. If the anisotropic particles are

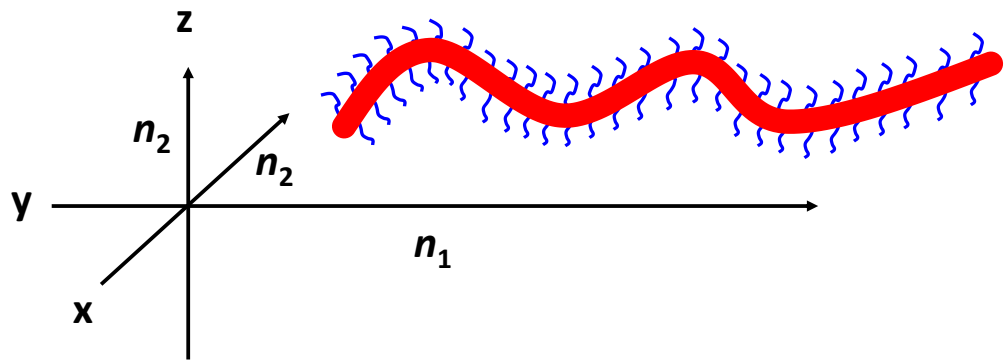


**Figure 1.28:** The three different refractive indices that characterise a worm-like micelle.

randomly orientated, the light still experiences an overall homogeneous path through the sample (**Figure 1.29**). Similarly, the light must be polarised because otherwise it would not be possible to determine which emerging photons had experienced birefringence.

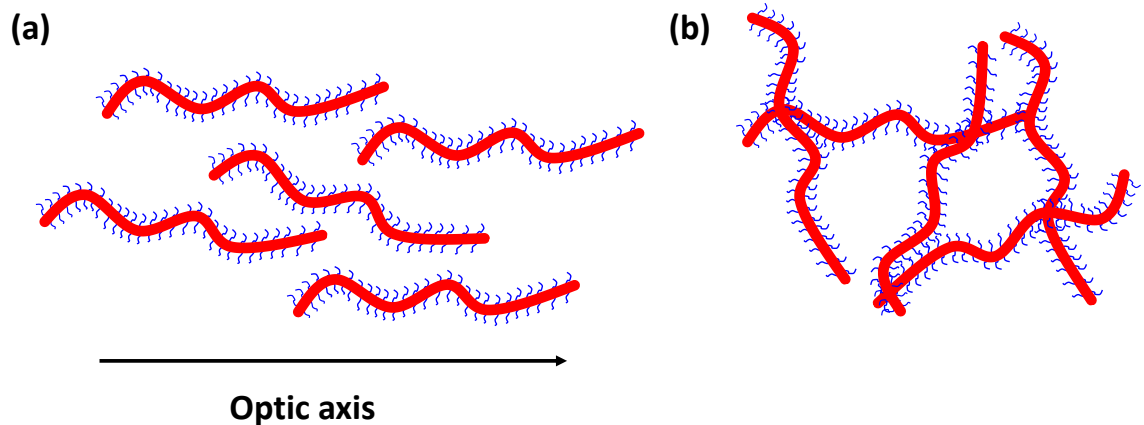


**Figure 1.29:** (a) Worm-like micelles orientated at a critical shear rate exhibit birefringence. (b) Randomly orientated worms exhibit no birefringence

In a uniaxial material, light with a polarisation angle parallel to the optic axis experiences only one environment and therefore is transmitted at a single velocity. Light with polarisation perpendicular to the optic axis behaves similarly (because all of the other axes are equivalent). However, an interesting situation arises when the angle of polarisation is intermediate (say  $45^\circ$ ). In this case, the light experiences two refractive indices leading to the rotation of the plane of polarisation. To understand how this rotation arises, it is useful to note that a polarised light wave can be represented as a superposition of two other orthogonal waves that are in phase. Therefore, when the polarised light travels through the birefringent sample, the waves become decoupled into these two orthogonal components. The component travelling parallel to the optic axis will be

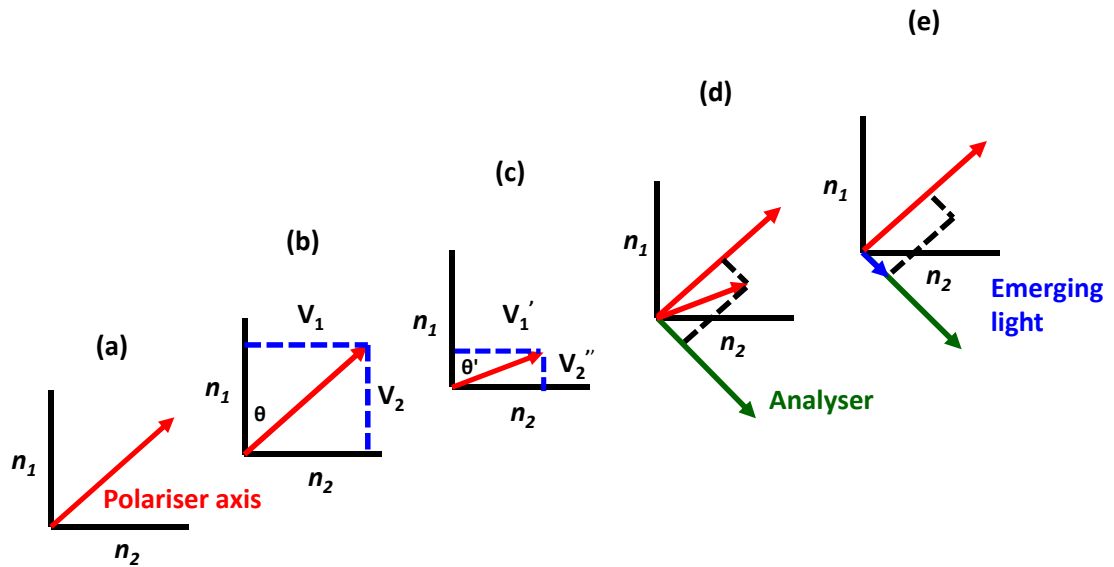


**Figure 1.30:** Schematic representation of the rotation of polarised light by a uniaxial material with two refractive indices,  $n_1$  and  $n_2$ . Here,  $n_2$  represents the optic axis. (a) The axis of the polariser is orientated at an angle  $\theta$  between the two axes of the sample. (b) The polarised light, represented by two orthogonal vectors  $V_1$  and  $V_2$ , enters the sample. (c)  $V_2$  is retarded by the refractive index  $n_2$  and  $V_1$  is retarded by the refractive index  $n_1$ , leading to a new pair of vectors  $V_1'$  and  $V_2''$  and a rotation of the angle of polarisation to  $\theta'$ . The analyser is placed orthogonal to the initial axis of polarisation; hence, the rotated light has a small component in the direction of the analyser. (e) The rotated light due to birefringence passes through the second polariser and is detected.

retarded more than the component travelling perpendicular to the optic axis. This results in a rotation of the plane of polarisation (**Figure 1.30**). Therefore, if the light emerging from the birefringent sample is analysed at  $90^\circ$  to the initial polarisation angle, only birefringent light is detected. A typical experimental set-up for such an experiment is shown schematically in **Figure 1.31**.

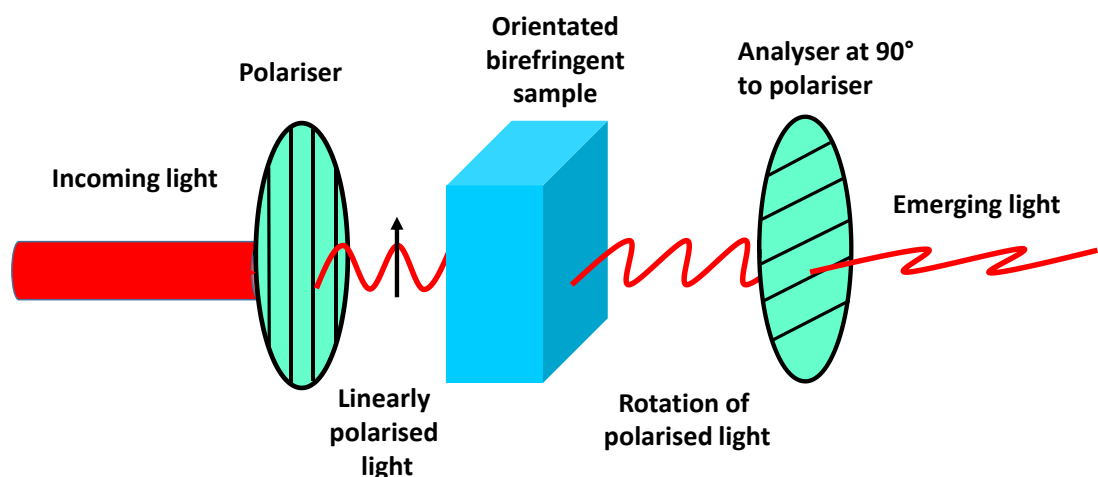


**Figure 1.31:** Schematic representation of a typical experiment to observe birefringence. White light is linearly polarised before entering a birefringent sample. As a result of the birefringence, the plane of polarisation is rotated. The emerging rotated light is then passed through a polariser orientated at  $90^\circ$  to the original angle of polarisation prior to its detection.<sup>152</sup>

As the two polarisers are orthogonal, any light which emerges from the sample without rotation is blocked. This can occur when the optic axis of the sample is orientated  $0^\circ$  to the initial polarisation angle i.e. the light travels parallel to the optic axis. The light will also experience no rotation when the sample is orientated  $90^\circ$  to the initial polarisation angle, i.e. if the light travels solely perpendicular to the optic axis. This absence of light manifests as a dark cross in the middle of the detector. On the other hand, maximum birefringence is observed when the polarisation angle is  $45^\circ$  relative to the two axes. This corresponds to a sample orientation of  $45^\circ$  relative to the initial polariser, and results in a characteristic bright Maltese cross in the detector.<sup>153</sup>

Shear-induced polarised-light imaging (SIPLI) is a technique that combines this birefringence principle with a rheometer equipped with a parallel plate geometry (Figure 1.32), operating in rotational mode.<sup>153,154</sup>

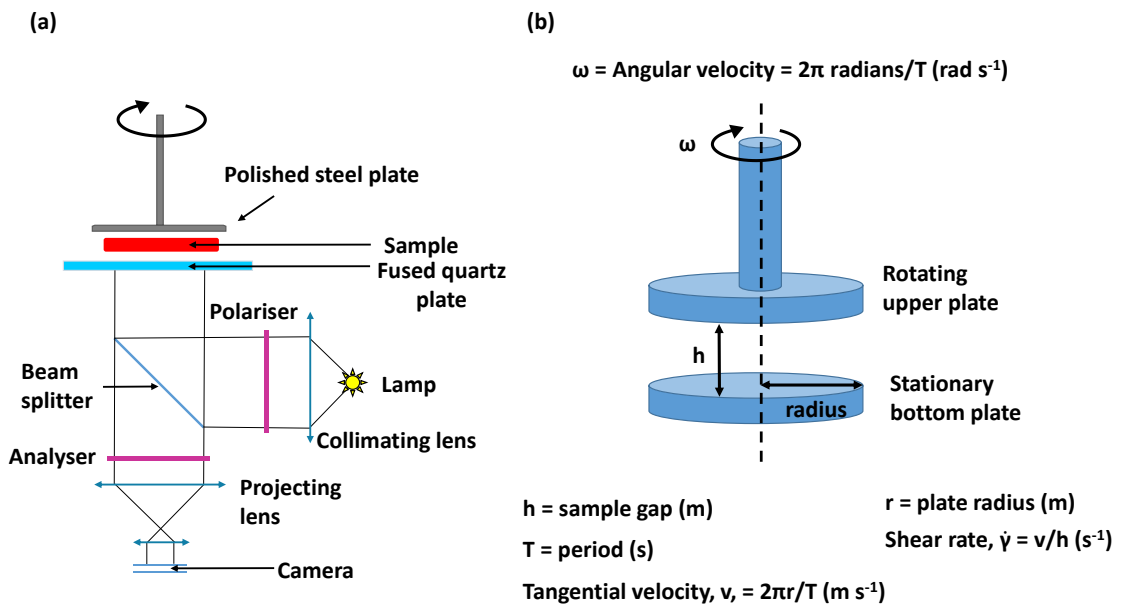


**Figure 1.32:** (a) Schematic representation of a SIPLI rheometer utilising a parallel plate geometry. The sample is sheared by the rotating top plate and, simultaneously, polarised light is passed through the sample from the bottom fused quartz plate. The light is reflected off the polished steel top plate, passes back through the sample and is then analysed at  $90^\circ$  to the original angle of polarisation. (b) Schematic representation of a parallel plate geometry. The sample is loaded between two plates, the bottom one then remains stationary and the top one rotates at a specified shear rate. The specified shear rate corresponds to the outer edge of the plate.<sup>153,154</sup>

In rotational rheometry, a directional shear stress is applied to the sample as the top plate rotates around a defined axis. This differs from oscillatory rheology in which the shear force is applied sinusoidally. Generally, when anisotropic objects are subject to a directional shear force, they align under shear.<sup>153,154</sup> This is important for birefringence experiments because net orientation is required. In a SIPLI rheometer, the top rotating plate is made from polished steel, and so acts as

a mirror. Similarly, the bottom plate is prepared from fused quartz, and so it is transparent towards incoming polarised light. When a SIPLI experiment is performed, polarised light is directed upwards through the fused quartz bottom plate. The polarised light then passes through the sample as it is being sheared, is reflected off the top plate back through the sample and is analysed at  $90^\circ$  to the initial angle of polarisation. Consequently, if any anisotropic particles are present that are aligned under shear, a Maltese cross is observed at a certain critical shear rate indicating birefringence. Furthermore, because the gap between the two parallel plates is fixed and  $\dot{\gamma} = v/h$ , a shear rate gradient is established which is at a maximum at the periphery and is zero at the centre. Consequently, in addition to the presence of shear-aligned anisotropic particles, SIPLI also provides information about the critical shear rate required to achieve alignment. Below this critical shear rate no alignment (and hence no birefringence) will be observed. This manifests as a dark spot at the centre of the Maltese cross. In addition, cessation of applied shear enables characteristic relaxation times to be determined. This is the time required for complete loss of orientation of the anisotropic worms.<sup>153,154</sup>

### 1.7.4 Small-angle X-ray scattering

SAXS is a powerful analytical technique that can be used to determine, amongst other things, the average size and shape of nanoparticles within a dispersion.<sup>155–157</sup> SAXS offers a significant advantage over number-averaged analytical techniques, such as TEM, because it provides structural information averaged over millions of particles in their native environment. In a typical SAXS experiment for colloidal dispersions, the sample is placed in a capillary and irradiated with a collimated monochromatic X-ray beam. The electrons present within a sample scatter the incident X-rays, the intensity of which is then recorded by a photon detector.<sup>157</sup> The scattering pattern of the pure solvent and empty capillary are also collected and subtracted from the sample scattering pattern, which leaves the pattern solely owing to the particles. This pattern is characteristic of the size and shape of the particles under analysis. A schematic representation of a SAXS experiment is shown in **Figure 1.33**.

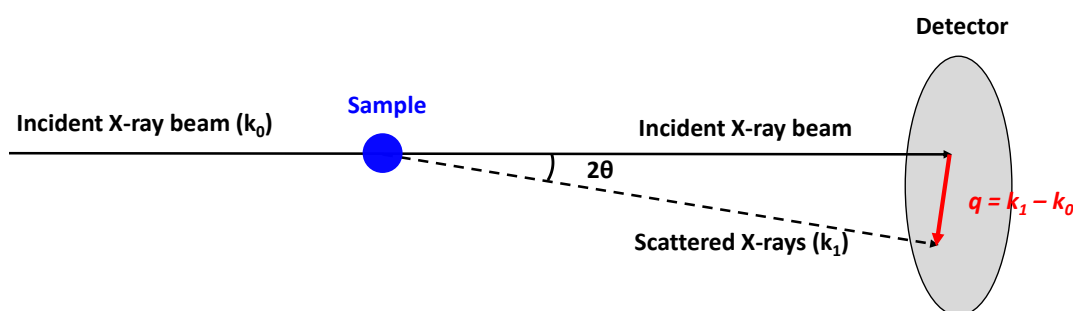


**Figure 1.33:** Schematic representation of a SAXS experiment. The vector  $k_0$  represents the incoming X-rays,  $k_1$  represents the scattered X-rays,  $q$  represents the scattering vector and  $\theta$  is one half of the scattering angle.<sup>157</sup>

The scattering vector,  $q$ , is a measure of the magnitude and direction of scattering and is given by the following expression:

$$q = \frac{4\pi\sin\theta}{\lambda} \quad (1.18)$$

Here,  $\theta$  is one-half of the scattering angle and  $\lambda$  is the wavelength of the incident X-rays. The scattering from an individual particle (which is composed of many atoms) can be explained as the interference pattern produced by all of the waves emanating from the electrons within the particle.<sup>155</sup> As such, this pattern is dependent upon the shape of the scattering object and is called the form factor, or  $P(q)$ . For densely packed particle systems, the inter-particle distance approaches the same order of magnitude as the distances within a particle. Therefore, the interference pattern also contains information about neighbouring particles. This additional interference pattern multiplies with the form factor, and is known as the structure factor  $S(q)$ .<sup>155</sup> The scattering intensity at a given value of  $q$ ,  $I(q)$ , is then given by following equation:<sup>155</sup>

$$I(q) = NV^2\Delta\xi^2P(q)S(q) \quad (1.19)$$

Here,  $N$  is the number density of particles,  $V$  is the volume of particles and  $\Delta\xi$  is the difference in scattering length density between the particles and the solvent. However, if the dispersion is very dilute then the inter-particle distance is large and  $S(q) = 1$ , which eliminates the structure factor from the SAXS pattern. In a typical SAXS experiment on such a dilute dispersion, the scattering pattern is recorded using a two-dimensional detector. As the particles are randomly orientated, the resulting scattering pattern is isotropic and can be radially averaged. Usually, this is presented as an  $I(q)$  vs.  $q$  plot. Even without sophisticated models, such a plot is rich with structural information about the particles under analysis. For example, inspecting the gradient of an  $I(q)$  vs.  $q$  plot indicates the dominant particle morphology. A gradient of 0 indicates spheres, a gradient of -1 indicates worms and a gradient of -2 indicates vesicles (or disks/lamellae). **Figure 1.34** shows a schematic  $I(q)$  vs.  $q$  plot obtained for monodisperse spheres worms and vesicles. SAXS has been used to characterise a range of different nanoparticle morphologies prepared *via* PISA syntheses in a range of different solvents. Moreover, SAXS can be used to observe PISA syntheses *in situ* and extract a range of useful parameters, such as the nanoparticle morphology, overall mean diameter and aggregation number (or number of polymer chains per nanoparticle).

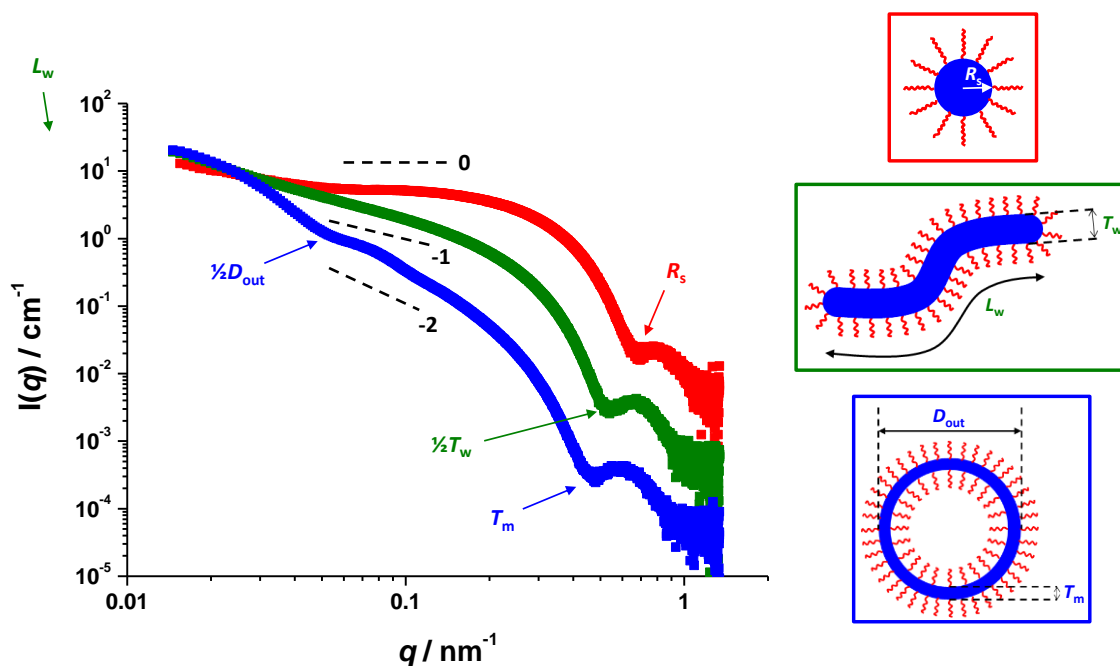


**Figure 1.34:** Schematic  $I(q)$  vs.  $q$  plot obtained for spheres (red), monodisperse worms (green) and vesicles (blue). The gradient of the slope at low  $q$  (displayed on the graph) indicates the nanoparticle morphology. A gradient of 0 = spheres, -1 = worms and -2 = vesicles. Image courtesy of Dr. M. J. Derry.

## 1.8 Thesis outline

This thesis focuses primarily on the preparation of well-defined diblock copolymer nanoparticles in silicone oil. This is achieved via RAFT dispersion polymerisation, which involves PISA. Chapter 2 describes the esterification of a monohydroxylated PDMS<sub>66</sub>, with a carboxylic acid-functional RAFT agent. Subsequent chain extension of this precursor with DMA in silicone oil results in the formation of well-defined spheres, worms and vesicles. Moreover, the PDMS-PDMA worms can also be synthesised in several other non-polar solvents, such as *n*-dodecane, and hexmethylsiloxane, and can act as viscosity modifiers. In Chapter 3, the temperature-responsive nature of these PDMS-PDMA worm gels is examined. Furthermore, cross-linking of the tertiary amine-functional cores is explored. In Chapter 4, the synthesis of a new silicone-based macro-CTA, comprising 3-[tris(trimethylsiloxy)silyl]propyl methacrylate (SiMA), is outlined. This macro-CTA is used as a steric-stabiliser to achieve higher-order morphologies in silicone oil *via* the RAFT dispersion polymerisation of BzMA. Chapter 5 outlines results obtained during a 6-month industrial secondment undertaken at the Scott Bader Company. More specifically, the ability of PSiMA-PBzMA spherical nanoparticles to stabilise Pickering emulsions comprising two immiscible non-polar oils was examined. Finally, Chapter 6 deals with the synthesis of diblock copolymer spherical micelles with cores comprising a semi-fluorinated monomer, namely 2,2,2-trifluoroethyl methacrylate (TFEMA). Such semi-fluorinated polymers typically exhibit relatively low refractive indices. As such, the feasibility of matching the refractive index these

particles to that of the solvent is demonstrated. Furthermore, it is shown that such highly transparent dispersions, when used in conjunction with a refractive-index-matched oil (*n*-dodecane), can be used to prepare transparent Pickering emulsions and Pickering double emulsions.

### 1.9 References

- (1) Odian, G. *Principles of Polymerization*, 4th ed.; John Wiley & Sons, Inc.: Hoboken, 2004.
- (2) Matyjaszewski, K.; Gnanou, Y.; Leibler, L. *Macromolecular Engineering: Precise Synthesis, Materials Properties, Applications*; Wiley: Weinheim, Germany, 2011; Vol. 1.
- (3) Staudinger, H. Über Polymerisation. *Berichte der Dtsch. Chem. Gesellschaft* **1920**, *53*, 1073–1085.
- (4) Meyer, K. H.; Mark, H. Über Den Kautschuk. *Berichte der Dtsch. Chem. Gesellschaft* **1928**, *61*, 1939–1949.
- (5) Meyer, K. H.; Mark, H. Über Den Bau Des Krystallisierten Anteils Der Cellulose. *Berichte der Dtsch. Chem. Gesellschaft* **1928**, *61*, 593–614.
- (6) Carothers, W. H. Linear Condensation Polymers, United States Patent. No. 2,071,253 **1937**.
- (7) Carothers, W. H. Studies on Polymerization and Ring Formation. I. An Introduction to the General Theory of Condensation Polymers. *J. Am. Chem. Soc.* **1929**, *51*, 2548–2559.
- (8) Himmel, M.; Mlynár, J.; Sarkanen, S.; Wu, C. *Handbook of Size Exclusion Chromatography*; Marcel Dekker: New York, 1995; Vol. 52.
- (9) Grubisic, Z.; Rempp, P.; Benoit, H. A Universal Calibration for Gel Permeation Chromatography. *J. Polym. Sci. Part B Polym. Lett.* **1967**, *5*, 753–759.
- (10) Simha, R. The Influence of Brownian Movement on the Viscosity of Solutions. *J. Phys. Chem.* **1940**, *44*, 25–34.
- (11) Flory, P. *Principles of Polymer Chemistry*; Cornell University Press: Ithaca and London, 1953.
- (12) Cowie, J. M. G. *Polymers: Chemistry and Physics of Modern Materials, 2nd Edition*; Taylor & Francis, 1991.
- (13) Kobatake, S.; Yamada, B.; Aoki, S. Radical Polymerization and Copolymerization of Methyl 2-(Acyloxymethyl)acrylate as Hindered 2-Substituted Acrylate. *Polymer* **1995**, *36*, 413–419.
- (14) Szwarc, M. “Living” Polymers. *Nature* **1956**, *178*, 1168–1169.
- (15) Miyamoto, M.; Sawamoto, M.; Higashimura, T. Living Polymerization of Isobutyl Vinyl Ether with the Hydrogen Iodide/Iodine Initiating System. *Macromolecules* **1984**, *17*, 265–268.
- (16) Kato, M.; Kamigaito, M.; Sawamoto, M.; Higashimura, T. Polymerization of Methyl Methacrylate with the Carbon Tetrachloride/Dichlorotris-(triphenylphosphine)ruthenium(II)/ Methylaluminum Bis(2,6-Di-Tert-Butylphenoxy) Initiating System: Possibility of Living Radical Polymerization. *Macromolecules* **1995**, *28*, 1721–1723.
- (17) Bielawski, C. W.; Grubbs, R. H. Living Ring-Opening Metathesis Polymerization. *Prog. Polym. Sci.* **2007**, *32*, 1–29.
- (18) Yokozawa, T.; Yokoyama, A. Chain-Growth Polycondensation: The Living Polymerization Process in Polycondensation. *Prog. Polym. Sci.* **2007**, *32*, 147–172.
- (19) Moad, G.; Rizzardo, E.; Thang, S. H. Living Radical Polymerization by the RAFT Process. *Aust. J. Chem.* **2005**, *58*, 379–410.
- (20) Matyjaszewski, K.; Xia, J. Atom Transfer Radical Polymerization. *Chem. Rev.* **2001**, *101*, 2921–2990.

- (21) Hawker, C. J.; Bosman, A. W.; Harth, E. New Polymer Synthesis by Nitroxide Mediated Living Radical Polymerizations. *Chem. Rev.* **2001**, *101*, 3661–3688.
- (22) Jenkins, A. D.; Jones, R. G.; Moad, G. Terminology for Reversible-Deactivation Radical Polymerization Previously Called “controlled” radical Or “living” radical Polymerization (IUPAC Recommendations 2010). *Pure Appl. Chem.* **2009**, *82*, 483–491.
- (23) Moad, G.; Rizzardo, E.; Thang, S. H. Toward Living Radical Polymerization. *Acc. Chem. Res.* **2008**, *41*, 1133–1142.
- (24) Matyjaszewski, K. Atom Transfer Radical Polymerization (ATRP): Current Status and Future Perspectives. *Macromolecules* **2012**, *45*, 4015–4039.
- (25) Chiefari, J.; Chong, Y. K. B.; Ercole, F.; Krstina, J.; Jeffery, J.; Le, T. P. T.; Mayadunne, R. T. A.; Meijs, G. F.; Moad, C. L.; Moad, G.; et al. Living Free-Radical Polymerization by Reversible Addition–Fragmentation Chain Transfer: The RAFT Process. *Macromolecules* **1998**, *31*, 5559–5562.
- (26) Bertin, D.; Gimes, D.; Marque, S. R. A.; Tordo, P. Kinetic Subtleties of Nitroxide Mediated Polymerization. *Chem. Soc. Rev.* **2011**, *40*, 2189–2198.
- (27) Georges, M. K.; Veregin, R. P. N.; Kazmaier, P. M.; Hamer, G. K. Narrow Molecular Weight Resins by a Free-Radical Polymerization Process. *Macromolecules* **1993**, *26*, 2987–2988.
- (28) Greene, A. C.; Grubbs, R. B. Nitroxide-Mediated Polymerization of Methyl Methacrylate and Styrene with New Alkoxyamines from 4-Nitrophenyl 2-Methylpropionat-2-Yl Radicals. *Macromolecules* **2010**, *43*, 10320–10325.
- (29) Benoit, D.; Chaplinski, V.; Braslau, R.; Hawker, C. J. Development of a Universal Alkoxyamine for “Living” Free Radical Polymerizations. *J. Am. Chem. Soc.* **1999**, *121*, 3904–3920.
- (30) Benoit, D.; Harth, E.; Fox, P.; Waymouth, R. M.; Hawker, C. J. Accurate Structural Control and Block Formation in the Living Polymerization of 1,3-Dienes by Nitroxide-Mediated Procedures. *Macromolecules* **2000**, *33*, 363–370.
- (31) Cameron, N. R.; Lagrille, O.; Lovell, P. A.; Thongnuanchan, B. A Nitroxide for Effecting Controlled Nitroxide-Mediated Adical Polymerization at Temperatures  $\geq 90$  °C. *ACS Macro Lett.* **2012**, *1*, 1262–1265.
- (32) Nicolas, J.; Dire, C.; Mueller, L.; Belleney, J.; Charleux, B.; Marque, S. R. A.; Bertin, D.; Magnet, S.; Couvreur, L. Living Character of Polymer Chains Prepared via Nitroxide-Mediated Controlled Free-Radical Polymerization of Methyl Methacrylate in the Presence of a Small Amount of Styrene at Low Temperature. *Macromolecules* **2006**, *39*, 8274–8282.
- (33) Guillaneuf, Y.; Gimes, D.; Marque, S. R. A.; Astolfi, P.; Greci, L.; Tordo, P.; Bertin, D. First Effective Nitroxide-Mediated Polymerization of Methyl Methacrylate. *Macromolecules* **2007**, *40*, 3108–3114.
- (34) Wang, J. S.; Matyjaszewski, K. “Living”/Controlled Radical Polymerization. Transition-Metal-Catalyzed Atom Transfer Radical Polymerization in the Presence of a Conventional Radical Initiator. *Macromolecules* **1995**, *28*, 7572–7573.
- (35) Wang, J. S.; Matyjaszewski, K. Controlled/“Living” Radical Polymerization. Halogen Atom Transfer Radical Polymerization Promoted by a Cu(I)/Cu(II) Redox Process. *Macromolecules* **1995**, *28*, 7901–7910.
- (36) Wang, J. S.; Matyjaszewski, K. Controlled/“Living” Radical Polymerization. Atom Transfer Radical Polymerization in the Presence of Transition-Metal Complexes. *J. Am. Chem. Soc.* **1995**, *117*, 5614–5615.
- (37) Gibson, V. C.; O’Reilly, R. K.; Reed, W.; Wass, D. F.; White, A. J. P.; Williams, D. J. Four-Coordinate Iron Complexes Bearing  $\alpha$ -Diimine Ligands: Efficient Catalysts for Atom Transfer Radical Polymerisation (ATRP). *Chem. Commun.* **2002**, *2*, 1850–1851.
- (38) Moineau, G.; Minet, M.; Dubois, P.; Teyssié, P.; Senninger, T.; Jérôme, R. Controlled Radical Polymerization of (Meth)acrylates by ATRP with  $\text{NiBr}_2(\text{PPh}_3)_2$  as Catalyst  $\dagger$ . *Macromolecules* **1999**, *32*, 27–35.

- (39) Asandei, A. D.; Moran, I. W. The Ligand Effect in Ti-Mediated Living Radical Styrene Polymerizations Initiated by Epoxide Radical Ring Opening. 2. Scorpionate and Half-Sandwich  $\text{LTiCl}_3$  Complexes. *J. Polym. Sci. Part A Polym. Chem.* **2005**, *43*, 6039–6047.
- (40) Le Grogne, E.; Claverie, J.; Poli, R. Radical Polymerization of Styrene Controlled by Half-Sandwich Mo(III)/Mo(IV) Couples: All Basic Mechanisms Are Possible. *J. Am. Chem. Soc.* **2001**, *123*, 9513–9524.
- (41) Di Lena, F.; Matyjaszewski, K. Transition Metal Catalysts for Controlled Radical Polymerization. *Prog. Polym. Sci.* **2010**, *35*, 959–1021.
- (42) Pietrasik, J.; Dong, H.; Matyjaszewski, K. Synthesis of High Molecular Weight Poly(styrene-Co-Acrylonitrile) Copolymers with Controlled Architecture. *Macromolecules* **2006**, *39*, 6384–6390.
- (43) Matyjaszewski, K.; Jakubowski, W.; Min, K.; Tang, W.; Huang, J.; Braunecker, W. A.; Tsarevsky, N. V. Diminishing Catalyst Concentration in Atom Transfer Radical Polymerization with Reducing Agents. *Proc. Natl. Acad. Sci.* **2006**, *103*, 15309–15314.
- (44) Moad, G.; Chiefari, J.; Chong, B. Y. K.; Krstina, J.; Mayadunne, R. T. A.; Postma, A.; Rizzardo, E.; Thang, S. H. Living Free Radical Polymerization with Reversible Addition – Fragmentation Chain Transfer ( the Life of RAFT ). **2000**, *1001*, 993–1001.
- (45) Moad, G. The Emergence of RAFT Polymerization. *Aust. J. Chem.* **2006**, *59*, 661.
- (46) Barner-kowollik, C. *Handbook of RAFT Polymerization*; Barner-Kowollik, C., Ed.; Wiley-VCH Verlag GmbH & Co. KGaA: Weinheim, Germany, 2008.
- (47) Moad, G.; Rizzardo, E.; Thang, S. H. Radical Addition–fragmentation Chemistry in Polymer Synthesis. *Polymer* **2008**, *49*, 1079–1131.
- (48) Perrier, S. 50th Anniversary Perspective: RAFT Polymerization - A User Guide. *Macromolecules* **2017**, *50*, 7433–7447.
- (49) Moad, G.; Rizzardo, E.; Thang, S. H. Living Radical Polymerization by the RAFT Process—A First Update. *Aust. J. Chem.* **2006**, *59*, 669–692.
- (50) Moad, G.; Rizzardo, E.; Thang, S. H. Living Radical Polymerization by the RAFT Process-A Second Update. *Aust. J. Chem.* **2009**, *62*, 1402–1472.
- (51) Keddie, D. J. A Guide to the Synthesis of Block Copolymers Using Reversible-Addition Fragmentation Chain Transfer (RAFT) Polymerization. *Chem. Soc. Rev.* **2014**, *43*, 496–505.
- (52) Chiefari, J.; Mayadunne, R. T. A.; Moad, C. L.; Moad, G.; Rizzardo, E.; Postma, A.; Skidmore, M. A.; Thang, S. H. Thiocarbonylthio Compounds ( S D C ( Z ) S - R ) in Free Radical Polymerization with Reversible Addition-Fragmentation Chain Transfer ( RAFT Polymerization ). Effect of the Activating Group Z. *Macromolecules* **2003**, *36*, 2273–2283.
- (53) Chong, B. Y. K.; Krstina, J.; Le, T. P. T.; Moad, G.; Postma, A.; Rizzardo, E.; Thang, S. H. Thiocarbonylthio Compounds [ S D C ( Ph ) S - R ] in Free Radical Polymerization with Reversible Addition-Fragmentation Chain Transfer ( RAFT Polymerization ). Role of the Free-Radical Leaving Group ( R ). **2003**, *60*, 2256–2272.
- (54) Benaglia, M.; Chiefari, J.; Chong, Y. K.; Moad, G.; Rizzardo, E.; Thang, S. H. Universal (Switchable) RAFT Agents. *J. Am. Chem. Soc.* **2009**, *131*, 6914–6915.
- (55) Moad, G. Mechanism and Kinetics of Dithiobenzoate-Mediated RAFT Polymerization - Status of the Dilemma. *Macromol. Chem. Phys.* **2014**, *215*, 9–26.
- (56) Hawthorne, D. G.; Moad, G.; Rizzardo, E.; Thang, S. H. Living Radical Polymerization with Reversible Addition–Fragmentation Chain Transfer (RAFT): Direct ESR Observation of Intermediate Radicals. *Macromolecules* **1999**, *32*, 5457–5459.
- (57) Meiser, W.; Barth, J.; Buback, M.; Kattner, H.; Vana, P. EPR Measurement of Fragmentation Kinetics in Dithiobenzoate-Mediated RAFT Polymerization. *Macromolecules* **2011**, *44*, 2474–2480.
- (58) Kwak, Y.; Goto, A.; Komatsu, K.; Sugiura, Y.; Fukuda, T. Characterization of Low-Mass Model 3-Arm Stars Produced in Reversible Addition-Fragmentation Chain Transfer (RAFT) Process. *Macromolecules* **2004**, *37*, 4434–4440.

- (59) Kwak, Y.; Goto, A.; Fukuda, T. Rate Retardation in Reversible Addition - Fragmentation Chain Transfer (RAFT) Polymerization: Further Evidence for Cross-Termination Producing 3-Arm Star Chain. *Macromolecules* **2004**, *37*, 1219–1225.
- (60) Willcock, H.; O'Reilly, R. K. End Group Removal and Modification of RAFT Polymers. *Polym. Chem.* **2010**, *1*, 149–157.
- (61) Wang, Z.; He, J.; Tao, Y.; Yang, L.; Jiang, H.; Yang, Y. Controlled Chain Branching by RAFT-Based Radical Polymerization. *Macromolecules* **2003**, *36*, 7446–7452.
- (62) Llauro, M. F.; Loiseau, J.; Boisson, F.; Delolme, F.; Ladavière, C.; Claverie, J. Unexpected End-Groups of Poly(acrylic Acid) Prepared by RAFT Polymerization. *J. Polym. Sci. Part A Polym. Chem.* **2004**, *42*, 5439–5462.
- (63) Perrier, S.; Takolpuckdee, P.; Mars, C. A. Reversible Addition-Fragmentation Chain Transfer Polymerization: End Group Modification for Functionalized Polymers and Chain Transfer Agent Recovery. *Macromolecules* **2005**, *38*, 2033–2036.
- (64) Chen, M.; Moad, G.; Rizzardo, E. Thiocarbonylthio End Group Removal from RAFT-Synthesized Polymers by a Radical-Induced Process. *J. Polym. Sci. Part A Polym. Chem.* **2009**, *47*, 6704–6714.
- (65) Inglis, A. J.; Sinnwell, S.; Davis, T. P.; Barner-Kowollik, C.; Stenzel, M. H. Reversible Addition Fragmentation Chain Transfer (RAFT) and Hetero-Diels-Alder Chemistry as a Convenient Conjugation Tool for Access to Complex Macromolecular Designs. *Macromolecules* **2008**, *41*, 4120–4126.
- (66) Sinnwell, S.; Inglis, A. J.; Davis, T. P.; Stenzel, M. H.; Barner-Kowollik, C. An Atom-Efficient Conjugation Approach to Well-Defined Block Copolymers Using RAFT Chemistry and Hetero Diels-Alder Cycloaddition. *Chem. Commun.* **2008**, *2*, 2052–2054.
- (67) Jesson, C. P.; Pearce, C. M.; Simon, H.; Werner, A.; Cunningham, V. J.; Lovett, J. R.; Smallridge, M. J.; Warren, N. J.; Armes, S. P. H<sub>2</sub>O<sub>2</sub> Enables Convenient Removal of RAFT End-Groups from Block Copolymer Nano-Objects Prepared via Polymerization-Induced Self-Assembly in Water. *Macromolecules* **2017**, *50*, 182–191.
- (68) Postma, A.; Davis, T. P.; Moad, G.; O'Shea, M. S. Thermolysis of RAFT-Synthesized Polymers. A Convenient Method for Trithiocarbonate Group Elimination. *Macromolecules* **2005**, *38*, 5371–5374.
- (69) Osmond, D. J. W.; Thompson, H. H. Dispersion Polymerisation GB Patent. No. 893429 **1958**.
- (70) Van Herk, A. M.; Monteiro, M. Heterogeneous Systems. In *Handbook of Radical Polymerization*; John Wiley & Sons, Inc.: Hoboken, NJ, USA; pp 301–331.
- (71) Ugelstad, J.; Berge, A.; Ellingsen, T.; Schmid, R.; Nilsen, T. N.; Mørk, P. C.; Stenstad, P.; Hornes, E.; Olsvik. Preparation and Application of New Monosized Polymer Particles. *Prog. Polym. Sci.* **1992**, *17*, 87–161.
- (72) Barrett, K. E. J. Dispersion Polymerisation in Organic Media. *Br. Polym. J.* **1973**, *5*, 259–271.
- (73) Ali, A. M. I.; Pareek, P.; Sewell, L.; Schmid, A.; Fujii, S.; Armes, S. P.; Shirley, I. M. Synthesis of poly(2-Hydroxypropyl Methacrylate) Latex Particles via Aqueous Dispersion Polymerization. *Soft Matter* **2007**, *3*, 1003–1013.
- (74) Almog, Y.; Reich, S.; Levy, M. Monodisperse Polymeric Spheres in the Micron Size Range by a Single Step Process. *Br. Polym. J.* **1982**, *14*, 131–136.
- (75) Baines, F. L.; Dionisio, S.; Billingham, N. C.; Armes, S. P. Use of Block Copolymer Stabilizers for the Dispersion Polymerization of Styrene in Alcoholic Media. *Macromolecules* **1996**, *29*, 3096–3102.
- (76) Paine, A. J.; Luymes, W.; McNulty, J. Dispersion Polymerization of Styrene in Polar Solvents. 6. Influence of Reaction Parameters on Particle Size and Molecular Weight in poly(N-Vinylpyrrolidone)-Stabilized Reactions. *Macromolecules* **1990**, *23*, 3104–3109.
- (77) Richez, A. P.; Yow, H. N.; Biggs, S.; Cayre, O. J. Dispersion Polymerization in Non-Polar Solvent: Evolution toward Emerging Applications. *Prog. Polym. Sci.* **2013**, *38*, 897–931.
- (78) Paine, A. J. Dispersion Polymerization of Styrene in Polar Solvents. 7. A Simple

- Mechanistic Model to Predict Particle Size. *Macromolecules* **1990**, *23*, 3109–3117.
- (79) Shen, S.; Sudol, E. D.; El-Aasser, M. S. Control of Particle Size in Dispersion Polymerization of Methyl Methacrylate. *J. Polym. Sci. Part A Polym. Chem.* **2003**, *31*, 1393–1402.
- (80) Lok, K. P.; Ober, C. K. Particle Size Control in Dispersion Polymerization of Polystyrene. *Can. J. Chem.* **1985**, *63*, 209–216.
- (81) Q. Wang; S. Fu; T. Yu. Emulsion Polymerization. *Prog. Polym. Sci.* **1994**, *19*, 703–753.
- (82) Asua, J. M. Emulsion Polymerization: From Fundamental Mechanisms to Prozess Development. *J. Polym. Sci.* **2004**, *42*, 1025–1041.
- (83) Hansen, F. K.; Ugelstad, J. Particle Nucleation in Emulsion Polymerization. I. A Theory for Homogeneous Nucleation. *J. Polym. Sci. Polym. Chem. Ed.* **1978**, *16*, 1953–1979.
- (84) Ugelstad, J.; Mörk, P. C.; Aasen, J. O. Kinetics of Emulsion Polymerization. *J. Polym. Sci. Part A-1 Polym. Chem.* **1967**, *5*, 2281–2288.
- (85) Chern, C. S. Emulsion Polymerization Mechanisms and Kinetics. *Prog. Polym. Sci.* **2006**, *31*, 443–486.
- (86) Israelachvili, J. *Intermolecular & Surface Forces*, 2nd ed.; Academic Press: London, 1991.
- (87) Israelachvili, J. N.; Mitchell, D. J.; Ninham, B. W. Theory of Self-Assembly of Hydrocarbon Amphiphiles into Micelles and Bilayers. *J. Chem. Soc. Faraday Trans. 2* **1976**, *72*, 1525–1568.
- (88) Atkins, P.; De Paula, J. *Physical Chemistry*, 9th ed.; Oxford University Press: Oxford, 2009.
- (89) Bates, F. S.; Fredrickson, G. H. Block Copolymers-Designer Soft Materials. *Phys. Today* **1999**, *52*, 32–38.
- (90) Wellinghoff, S. T.; Koenig, J. L.; Baer, E. Spectroscopic Examination of Chain Conformation and Bonding in Poly (Phenylene Oxide)-Polystyrene. *J. Polym. Sci. Polym. Phys. Ed.* **1977**, *15*, 1913–1925.
- (91) Matsen, M. W.; Bates, F. S. Origins of Complex Self-Assembly in Block Copolymers. *Macromolecules* **1996**, *29*, 7641–7644.
- (92) Matsen, M. W.; Schick, M. Stable and Unstable Phases of a Linear Multiblock Copolymer Melt. *Macromolecules* **1994**, *27*, 7157–7163.
- (93) Matsen, M. W.; Schick, M. Microphase Separation in Starblock Copolymer Melts. *Macromolecules* **1994**, *27*, 6761–6767.
- (94) Matsen, M. W.; Schick, M. Stable and Unstable Phases of a Diblock Copolymer Melt. *Phys. Rev. Lett.* **1994**, *72*, 2660–2663.
- (95) Mai, Y.; Eisenberg, A. Self-Assembly of Block Copolymers. *Chem. Soc. Rev.* **2012**, *41*, 5969–5985.
- (96) Bates, F. S.; Fredrickson, G. H. Conformational Asymmetry and Polymer-Polymer Thermodynamics. *Macromolecules* **1994**, *27*, 1065–1067.
- (97) Khandpur, A. K.; Förster, S.; Bates, F. S.; Hamley, I. W.; Ryan, A. J.; Bras, W.; Almdal, K.; Mortensen, K. Polyisoprene-Polystyrene Diblock Copolymer Phase Diagram near the Order-Disorder Transition. *Macromolecules* **1995**, *28*, 8796–8806.
- (98) Blanazs, A.; Armes, S. P.; Ryan, A. J. Self-Assembled Block Copolymer Aggregates: From Micelles to Vesicles and Their Biological Applications. *Macromol. Rapid Commun.* **2009**, *30*, 267–277.
- (99) Won, Y.-Y.; Davis, H. T.; Bates, F. S. Giant Wormlike Rubber Micelles. *Science* **1999**, *283*, 960–963.
- (100) Jain, S.; Bates, F. S. On the Origins of Morphological Complexity in Block Copolymer Surfactants. *Science* **2003**, *300*, 460–464.
- (101) Discher, D. E.; Eisenberg, A. Polymer Vesicles. *Science* **2002**, *297*, 967–973.
- (102) Zhang, L.; Eisenberg, A. Multiple Morphologies and Characteristics of “Crew-Cut” Micelle-like Aggregates of Polystyrene-B-Poly(acrylic Acid) Diblock Copolymers in Aqueous Solutions. *J. Am. Chem. Soc.* **1996**, *118*, 3168–3181.

- (103) Zhang, L.; Eisenberg, A. Multiple Morphologies of “Crew-Cut” Aggregates of Polystyrene-B-Poly(acrylic Acid) Block Copolymers. *Science* **1995**, *268*, 1728–1731.
- (104) Zhang, L.; Yu, K.; Eisenberg, A. Ion-Induced Morphological Changes in “Crew-Cut” Aggregates of Amphiphilic Block Copolymers. *Science* **1996**, *272*, 1777–1779.
- (105) Antonietti, M.; Förster, S. Vesicles and Liposomes: A Self-Assembly Principle Beyond Lipids. *Adv. Mater.* **2003**, *15*, 1323–1333.
- (106) Canning, S. L.; Smith, G. N.; Armes, S. P. A Critical Appraisal of RAFT-Mediated Polymerization-Induced Self-Assembly. *Macromolecules* **2016**, *49*, 1985–2001.
- (107) Rymaruk, M. J.; Thompson, K. L.; Derry, M. J.; Warren, N. J.; Ratcliffe, L. P. D.; Williams, C. N.; Brown, S. L.; Armes, S. P. Bespoke Contrast-Matched Diblock Copolymer Nanoparticles Enable the Rational Design of Highly Transparent Pickering Double Emulsions. *Nanoscale* **2016**, *8*, 14497–14506.
- (108) Penfold, N. J. W.; Ning, Y.; Verstraete, P.; Smets, J.; Armes, S. P. Cross-Linked Cationic Diblock Copolymer Worms Are Superfloculants for Micrometer-Sized Silica Particles. *Chem. Sci.* **2016**, *7*, 6894–6904.
- (109) Ratcliffe, L. P. D.; Ryan, a. J.; Armes, S. P. From a Water-Immiscible Monomer to Block Copolymer Nano-Objects via a One-Pot RAFT Aqueous Dispersion Polymerization Formulation. *Macromolecules* **2013**, *46*, 769–777.
- (110) Derry, M. J.; Fielding, L. A.; Armes, S. P. Industrially-Relevant Polymerization-Induced Self-Assembly Formulations in Non-Polar Solvents: RAFT Dispersion Polymerization of Benzyl Methacrylate. *Polym. Chem.* **2015**, *6*, 3054–3062.
- (111) Warren, N. J.; Armes, S. P. Polymerization-Induced Self-Assembly of Block Copolymer Nano-Objects via RAFT Aqueous Dispersion Polymerization. *J. Am. Chem. Soc.* **2014**, *136*, 10174–10185.
- (112) Charleux, B.; Delaittre, G.; Rieger, J.; D’Agosto, F. Polymerization-Induced Self-Assembly: From Soluble Macromolecules to Block Copolymer Nano-Objects in One Step. *Macromolecules* **2012**, *45*, 6753–6765.
- (113) Obeng, M.; Milani, A. H.; Musa, M. S.; Cui, Z.; Fielding, L. A.; Farrand, L.; Goulding, M.; Saunders, B. R. Self-Assembly of Poly(lauryl Methacrylate)-B-Poly(benzyl Methacrylate) Nano-Objects Synthesised by ATRP and Their Temperature-Responsive Dispersion Properties. *Soft Matter* **2017**, *13*, 2228–2238.
- (114) Delaittre, G.; Nicolas, J.; Lefay, C.; Save, M.; Charleux, B. Aqueous Suspension of Amphiphilic Diblock Copolymer Nanoparticles Prepared in Situ from a Water-Soluble Poly(sodium Acrylate) Alkoxyamine Macroinitiator. *Soft Matter* **2006**, *2*, 223–231.
- (115) Groison, E.; Brusseau, S.; D’Agosto, F.; Magnet, S.; Inoubli, R.; Couvreur, L.; Charleux, B. Well-Defined Amphiphilic Block Copolymer Nanoobjects via Nitroxide-Mediated Emulsion Polymerization. *ACS Macro Lett.* **2012**, *1*, 47–51.
- (116) Kim, K. H.; Kim, J.; Jo, W. H. Preparation of Hydrogel Nanoparticles by Atom Transfer Radical Polymerization of N-Isopropylacrylamide in Aqueous Media Using PEG Macro-Initiator. *Polymer* **2005**, *46*, 2836–2840.
- (117) Li, Y.; Armes, S. P. RAFT Synthesis of Sterically Stabilized Methacrylic Nanolatexes and Vesicles by Aqueous Dispersion Polymerization. *Angew. Chemie* **2010**, *49*, 4042–4046.
- (118) Warren, N. J.; Mykhaylyk, O. O.; Mahmood, D.; Ryan, A. J.; Armes, S. P. RAFT Aqueous Dispersion Polymerization Yields Poly(ethylene Glycol)-Based Diblock Copolymer Nano-Objects with Predictable Single Phase Morphologies. *J. Am. Chem. Soc.* **2014**, *136*, 1023–1033.
- (119) Semsarilar, M.; Ladmiral, V.; Blanazs, A.; Armes, S. P. Anionic Polyelectrolyte-Stabilized Nanoparticles via RAFT Aqueous Dispersion Polymerization. **2012**, 914–922.
- (120) Doncom, K. E. B.; Warren, N. J.; Armes, S. P. Polysulfobetaine-Based Diblock Copolymer Nano-Objects via Polymerization-Induced Self-Assembly. *Polym. Chem.* **2015**, *6*, 7264–7273.
- (121) Blanazs, A.; Madsen, J.; Battaglia, G.; Ryan, A. J.; Armes, S. P. Mechanistic Insights for Block Copolymer Morphologies: How Do Worms Form Vesicles? *J. Am. Chem. Soc.*
-

- 2011, *133*, 16581–16587.
- (122) Derry, M. J.; Fielding, L. A.; Warren, N. J.; Mable, C. J.; Smith, A. J.; Mykhaylyk, O. O.; Armes, S. P. In Situ Small-Angle X-Ray Scattering Studies of Sterically-Stabilized Diblock Copolymer Nanoparticles Formed during Polymerization-Induced Self-Assembly in Non-Polar Media. *Chem. Sci.* **2016**, *7*, 5078–5090.
- (123) Blanazs, A.; Ryan, A. J.; Armes, S. P. Predictive Phase Diagrams for RAFT Aqueous Dispersion Polymerization: Effect of Block Copolymer Composition, Molecular Weight, and Copolymer Concentration. *Macromolecules* **2012**, *45*, 5099–5107.
- (124) Derry, M. J.; Fielding, L. A.; Armes, S. P. Polymerization-Induced Self-Assembly of Block Copolymer Nanoparticles via RAFT Non-Aqueous Dispersion Polymerization. *Prog. Polym. Sci.* **2016**, *52*, 1–18.
- (125) Houillot, L.; Bui, C.; Save, M.; Charleux, B.; Farcet, C.; Moire, C.; Raust, J. A.; Rodriguez, I. Synthesis of Well-Defined Polyacrylate Particle Dispersions in Organic Medium Using Simultaneous RAFT Polymerization and Self-Assembly of Block Copolymers. A Strong Influence of the Selected Thiocarbonylthio Chain Transfer Agent. *Macromolecules* **2007**, *40*, 6500–6509.
- (126) Raust, J. A.; Houillot, L.; Save, M.; Charleux, B.; Moire, C.; Farcet, C.; Pasch, H. Two Dimensional Chromatographic Characterization of Block Copolymers of 2-Ethylhexyl Acrylate and Methyl Acrylate, P2EHA-B-PMA, Produced via RAFT-Mediated Polymerization in Organic Dispersion. *Macromolecules* **2010**, *43*, 8755–8765.
- (127) Houillot, L.; Bui, C.; Farcet, C.; Moire, C.; Raust, J. A.; Pasch, H.; Save, M.; Charleux, B. Dispersion Polymerization of Methyl Acrylate in Nonpolar Solvent Stabilized by Block Copolymers Formed in Situ via the RAFT Process. *ACS Appl. Mater. Interfaces* **2010**, *2*, 434–442.
- (128) Fielding, L. A.; Derry, M. J.; Ladmiral, V.; Rosselgong, J.; Rodrigues, A. M.; Ratcliffe, L. P. D.; Sugihara, S.; Armes, S. P. RAFT Dispersion Polymerization in Non-Polar Solvents: Facile Production of Block Copolymer Spheres, Worms and Vesicles in N-Alkanes. *Chem. Sci.* **2013**, *4*, 2081–2087.
- (129) Fielding, L. A.; Lane, J. A.; Derry, M. J.; Mykhaylyk, O. O.; Armes, S. P. Thermo-Responsive Diblock Copolymer Worm Gels in Non-Polar Solvents. *J. Am. Chem. Soc.* **2014**, *136*, 5790–5798.
- (130) Lovett, J. R.; Derry, M. J.; Yang, P.; Hatton, F. L.; Warren, N. J.; Fowler, P. W.; Armes, S. P. Can Percolation Theory Explain the Gelation Behavior of Diblock Copolymer Worms? *Chem. Sci.* **2018**, *9*, 7138–7144.
- (131) Zheng, R.; Liu, G.; Devlin, M.; Hux, K.; Jao, T. C. Friction Reduction of Lubricant Base Oil by Micelles and Crosslinked Micelles of Block Copolymers. *Tribol. Trans.* **2010**, *53*, 97–107.
- (132) Pei, Y.; Thurairajah, L.; Sugita, O. R.; Lowe, A. B. RAFT Dispersion Polymerization in Nonpolar Media: Polymerization of 3-Phenylpropyl Methacrylate in N-Tetradecane with Poly(stearyl Methacrylate) Homopolymers as Macro Chain Transfer Agents. *Macromolecules* **2015**, *48*, 236–244.
- (133) Pei, Y.; Sugita, O. R.; Thurairajah, L.; Lowe, A. B. Synthesis of Poly(stearyl Methacrylate-B-3-Phenylpropyl Methacrylate) Nanoparticles in N-Octane and Associated Thermoreversible Polymorphism. *RSC Adv.* **2015**, *5*, 17636–17646.
- (134) Warren, N. J.; Mykhaylyk, O. O.; Ryan, A. J.; Williams, M.; Doussineau, T.; Dugourd, P.; Antoine, R.; Portale, G.; Armes, S. P. Testing the Vesicular Morphology to Destruction: Birth and Death of Diblock Copolymer Vesicles Prepared via Polymerization-Induced Self-Assembly. *J. Am. Chem. Soc.* **2015**, *137*, 1929–1937.
- (135) Derry, M. J.; Mykhaylyk, O. O.; Armes, S. P. A Vesicle-to-Worm Transition Provides a New High-Temperature Oil Thickening Mechanism. *Angew. Chemie* **2017**, *129*, 1772–1776.
- (136) Lopez-Oliva, A. P.; Warren, N. J.; Rajkumar, A.; Mykhaylyk, O. O.; Derry, M. J.; Doncom, K. E. B.; Rymaruk, M. J.; Armes, S. P. Polydimethylsiloxane-Based Diblock

- Copolymer Nano-Objects Prepared in Nonpolar Media via RAFT-Mediated Polymerization-Induced Self-Assembly. *Macromolecules* **2015**, *48*, 3547–3555.
- (137) Ferguson, C. J.; Hughes, R. J.; Nguyen, D.; Pham, B. T. T.; Gilbert, R. G.; Serelis, A. K.; Such, C. H.; Hawket, B. S. Ab Initio Emulsion Polymerization by RAFT-Controlled Self-Assembly <sup>§</sup>. *Macromolecules* **2005**, *38*, 2191–2204.
- (138) Chaduc, I.; Girod, M.; Antoine, R.; Charleux, B.; D'Agosto, F.; Lansalot, M. Batch Emulsion Polymerization Mediated by Poly(methacrylic Acid) macroRAFT Agents: One-Pot Synthesis of Self-Stabilized Particles. *Macromolecules* **2012**, *45*, 5881–5893.
- (139) Chaduc, I.; Crepet, A.; Boyron, O.; Charleux, B.; D'Agosto, F.; Lansalot, M. Effect of the Ph on the Raft Polymerization of Acrylic Acid in Water. Application to the Synthesis of Poly(acrylic Acid)-Stabilized Polystyrene Particles by RAFT Emulsion Polymerization. *Macromolecules* **2013**, *46*, 6013–6023.
- (140) Rieger, J.; Zhang, W.; Stoffelbach, F.; Charleux, B. Surfactant-Free RAFT Emulsion Polymerization Using poly(N,N -Dimethylacrylamide) Trithiocarbonate Macromolecular Chain Transfer Agents. *Macromolecules* **2010**, *43*, 6302–6310.
- (141) Rieger, J.; Stoffelbach, F.; Bui, C.; Alaimo, D.; Jérôme, C.; Charleux, B. Amphiphilic Poly(ethylene Oxide) Macromolecular RAFT Agent as a Stabilizer and Control Agent in Ab Initio Batch Emulsion Polymerization. *Macromolecules* **2008**, *41*, 4065–4068.
- (142) Zhang, X.; Rieger, J.; Charleux, B. Effect of the Solvent Composition on the Morphology of Nano-Objects Synthesized via RAFT Polymerization of Benzyl Methacrylate in Dispersed Systems. *Polym. Chem.* **2012**, *3*, 1502–1509.
- (143) Zhang, W.; D'Agosto, F.; Dugas, P. Y.; Rieger, J.; Charleux, B. RAFT-Mediated One-Pot Aqueous Emulsion Polymerization of Methyl Methacrylate in Presence of Poly(methacrylic Acid-Co-Poly(ethylene Oxide) Methacrylate) Trithiocarbonate Macromolecular Chain Transfer Agent. *Polym. (United Kingdom)* **2013**, *54*, 2011–2019.
- (144) Zhang, W.; D'Agosto, F.; Boyron, O.; Rieger, J.; Charleux, B. Toward a Better Understanding of the Parameters That Lead to the Formation of Nonspherical Polystyrene Particles via RAFT-Mediated One-Pot Aqueous Emulsion Polymerization. *Macromolecules* **2012**, *45*, 4075–4084.
- (145) Cunningham, V. J.; Alswieleh, A. M.; Thompson, K. L.; Williams, M.; Leggett, G. J.; Armes, S. P.; Musa, O. M. Poly(glycerol monomethacrylate)–Poly(benzyl Methacrylate) Diblock Copolymer Nanoparticles via RAFT Emulsion Polymerization: Synthesis, Characterization, and Interfacial Activity. *Macromolecules* **2014**, *47*, 5613–5623.
- (146) Cockram, A. A.; Neal, T. J.; Derry, M. J.; Mykhaylyk, O. O.; Williams, N. S. J.; Murray, M. W.; Emmett, S. N.; Armes, S. P. Effect of Monomer Solubility on the Evolution of Copolymer Morphology during Polymerization-Induced Self-Assembly in Aqueous Solution. *Macromolecules* **2017**, *50*, 796–802.
- (147) Banchio, A. J.; Nägele, G.; Bergenholtz, J. Viscoelasticity and Generalized Stokes–Einstein Relations of Colloidal Dispersions. *J. Chem. Phys.* **1999**, *111*, 8721–8740.
- (148) Frisken, B. J. Revisiting the Method of Cumulants for the Analysis of Dynamic Light-Scattering Data. *Appl. Opt.* **2001**, *40*, 4087.
- (149) Barnes, H. A. *A Handbook of Elementary Rheology*; The University of Wales: Aberystwyth, 2000.
- (150) Barnes, H. A.; Hutton, J. F.; Walters, K. *An Introduction to Rheology*; Elsevier: Amsterdam, 1993; Vol. 3.
- (151) Shaw, M. T.; MacKnight, W. J. *Introduction to Polymer Viscoelasticity*, 4th ed.; Wiley: Hoboken, NJ, USA, 2018.
- (152) Hecht, E. *Optics*, 5th ed.; Pearson: Harlow, 2017.
- (153) Mykhaylyk, O. O.; Warren, N. J.; Parnell, A. J.; Pfeifer, G.; Laeuger, J. Applications of Shear-Induced Polarized Light Imaging (SIPLI) Technique for Mechano-Optical Rheology of Polymers and Soft Matter Materials. *J. Polym. Sci. Part B Polym. Phys.* **2016**, *54*, 2151–2170.
- (154) Mykhaylyk, O. O. Time-Resolved Polarized Light Imaging of Sheared Materials:

- Application to Polymer Crystallization. *Soft Matter* **2010**, 6, 4430–4440.
- (155) Schnablegger, H.; Singh, Y. *The SAXS Guide: Getting Acquainted with the Principles*, 2nd ed.; Anton Paar GmbH: Gratz, 2011.
- (156) Glatter, O.; Kratky, O. *Small-Angle X-Ray Scattering*; Academic Press: London, 1982.
- (157) Kikhney, A. G.; Svergun, D. I. A Practical Guide to Small Angle X-Ray Scattering (SAXS) of Flexible and Intrinsically Disordered Proteins. *FEBS Lett.* **2015**, 589, 2570–2577.

# **Chapter 2 : Synthesis of Diblock Copolymer Nanoparticles in Silicone Oils**

### 2.1 Introduction

The self-assembly behaviour of diblock copolymers in solution has been of considerable academic interest for a number of years.<sup>1-5</sup> However, such self-assembly protocols require two steps: (i) the preparation of the diblock copolymer in a good solvent for both blocks and (ii) replacing the good solvent for one that is selective for only one of the two blocks. A number of techniques exist for doing this, but the most common are thin-film rehydration and solvent switches.<sup>4</sup> However, all of these methods suffer from one major drawback; they must be conducted at very high dilution, on the order of 1 % w/w. This places limitations on the applications of the resulting nanoparticles.

Over the past decade or so, polymerisation-induced self-assembly (PISA) has emerged as a robust strategy for the convenient synthesis of a range of diblock copolymer nanoparticles directly in the form of concentrated dispersions.<sup>6-9</sup> Typically, a controlled radical polymerisation technique such as reversible addition-fragmentation chain transfer (RAFT) polymerisation<sup>10-13</sup> is used to prepare the precursor block, which is dissolved in a good solvent. The second block is selected such that it is insoluble in this solvent. Thus, as the second stage of the polymerisation proceeds, the growing second block eventually becomes insoluble when it reaches a critical DP, which drives *in situ* self-assembly to form sterically-stabilised nanoparticles. Such PISA syntheses eliminate the requirement for any post-polymerisation processing steps and can be conducted at up to 50 % w/w solids.<sup>14</sup>

Thus far, PISA syntheses have been performed in various solvents, including water,<sup>15-19</sup> alcohol,<sup>20-25</sup> ionic liquids,<sup>26</sup> chloroform,<sup>27,28</sup> and various non-polar solvents, including *n*-alkanes,<sup>25,29,30</sup> supercritical CO<sub>2</sub>,<sup>31,32</sup> mineral oil and poly( $\alpha$ -olefins).<sup>14</sup> However, there are currently no reports of PISA syntheses being conducted in silicone oil. Silicones comprise a unique class of liquid polymers, oligomers or small molecules, whose highly flexible backbones are composed of inorganic Si-O-Si bonds. The most common silicone oil is polydimethylsiloxane (PDMS). Silicone oils are non-toxic, chemically inert and non-flammable.<sup>33</sup> They are used as anti-foaming agents,<sup>34</sup> in medical devices,<sup>33</sup> as hydraulic fluids,<sup>35</sup> as standards for NMR, and in various cosmetic formulations.<sup>36</sup> In addition, cyclic silicones such as decamethylcyclopentasiloxane (D5) or dodecamethylcyclohexasiloxane (D6) exhibit relatively low viscosity and high volatility, enabling their widespread use as lubricious carrier fluids in personal care products such as deodorants and antiperspirants.<sup>36,37</sup> Some of the most commonly encountered silicones are depicted in **Figure 2.1**.

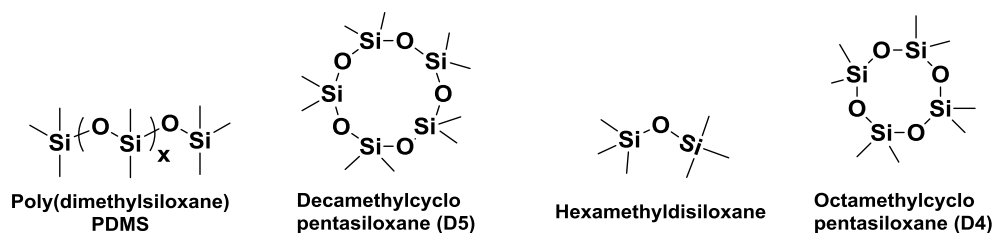


**Figure 2.1:** Some of the most commonly encountered silicone-based materials.

Recently, Lopez-Oliva et al reported the use of a PDMS<sub>66</sub> macro-CTA as a steric stabiliser in the dispersion polymerisation of benzyl methacrylate in *n*-heptane.<sup>38</sup> In principle, such a macro-CTA would be an ideal stabiliser for use with silicone oils. In this chapter, the chain extension of a PDMS<sub>66</sub> macro-CTA with a range of methacrylic monomers in D5 silicone oil is described. Perhaps surprisingly, only one of the nine monomers used allowed access to the full range of copolymer morphologies. As such, a phase diagram was constructed to facilitate the reproducible targeting of pure spheres, worms and vesicles for this particular PISA formulation. It is also demonstrated that PDMS-based diblock copolymer worms can be prepared in hexamethyldisiloxane, D4, and also *n*-dodecane. Finally, a potential application for such worm gels as a bespoke thickener for silicone oils is briefly explored.

## 2.2 Experimental Section

### 2.2.1 Materials

Polydimethylsiloxane (PDMS<sub>66</sub>-OH; moncarbinol terminated,  $M_n = 5,000 \text{ g mol}^{-1}$ , mean degree of polymerisation = 66) was purchased from Fluorochem (UK) and used as received. Decamethylpentacyclosiloxane (D5) and octamethyltetrasiloxane (D4) were donated by Scott Bader Company Ltd. (UK). Trigonox 21s (T21s) was purchased from AkzoNobel (The Netherlands). 2-(Dimethylamino)ethyl methacrylate (DMA), hexamethyldisiloxane (HMDS), *n*-dodecane, dichloromethane (DCM), triethyl amine (TEA), butylated hydroxytoluene (BHT), *N,N'*-dicyclohexylcarbodiimide (DCC), 4-dimethylamino pyridine (DMAP), benzyl methacrylate (BzMA), 2,2,2-trifluoroethyl methacrylate (TFEMA), 2-hydroxyethyl methacrylate (HEMA), methacrylic acid (MAA), 2-phenylethanethiol, sodium hydride (60 % in mineral oil), diethyl ether, carbon disulfide, iodine, sodium thiosulfate, sodium sulfate, ethyl acetate, *n*-hexane, 4,4'-azobis(4-cyanovaleric acid) (ACVA) and ethylene glycol methyl ether methacrylate were purchased from Sigma Aldrich (UK). Glycerol monomethacrylate (GMA) was kindly donated by GEO Specialty Chemicals (UK) and 2-hydroxypropyl methacrylate (HPMA) was purchased from Alfa Aesar (UK). Chloroform-*d*, dichloromethane-*d*<sub>2</sub>, methanol-*d*<sub>4</sub> and acetone-*d*<sub>6</sub> were obtained from Goss Scientific (UK). DMA was passed through basic alumina prior to use to remove its inhibitor. All other reagents were used as received unless otherwise stated.

### 2.2.2 Methods

#### Synthesis of 4-cyano-4-(2-phenylethane sulfanylthiocarbonyl)sulfanylpentanoic acid (PETTC)

2-Phenylethanethiol (21 g, 152 mmol) was added dropwise to a stirred suspension of sodium hydride (60 % in oil, 6.3 g, 158 mmol) in diethyl ether (250 ml) at 0 °C. The evolution of hydrogen was observed and the gray suspension turned to a white slurry of sodium phenylethanethiolate over 45 min. Carbon disulfide (12.0 g, 158 mmol) was added dropwise and a yellow precipitate of sodium 2-phenylethanetrithiocarbonate formed over 30 min., which was collected *via* filtration and used without further purification. To a suspension of sodium 2-phenylethanetrithiocarbonate (23.2 g, 98 mmol) in diethyl ether (150 ml), solid iodine (12.6 g, 50 mmol) was added. The reaction mixture was stirred for 60 min. at room temperature, and the resulting precipitate of sodium iodide was removed *via* filtration. The brown filtrate was washed with a saturated solution of sodium thiosulfate (2 x 150 ml), dried over sodium sulfate and placed under reduced pressure to leave bis-(2-phenylethane sulfanylthiocarbonyl) disulfide as an orange solid (~ 100 % yield). A solution of bis-(2-phenylethane sulfanylthiocarbonyl) disulfide (10 g, 23 mmol) and ACVA (9.67 g, 34.5 mmol) in ethyl acetate (250 ml) was purged with nitrogen for 30 min. at 20 °C before being heated to reflux under a dry nitrogen atmosphere for 18 h. The resulting solution was washed with water (5 x 200 ml), dried over sodium sulfate and placed under reduced pressure to remove the volatiles. The remaining orange residue was recrystallised from ethyl acetate: hexane (4:1 v/v) to yield 4-cyano-4-(2-phenylethane sulfanylthiocarbonyl) sulfanylpentanoic acid (PETTC) as a yellow solid (yield 74 %): <sup>1</sup>H NMR (400.13 MHz, CD<sub>2</sub>Cl<sub>2</sub>, 298 K): δ 1.91 (3H, CH<sub>3</sub>), 2.41-2.62 (m, 2H, CH<sub>2</sub>), 2.72 (t, 2H, CH<sub>2</sub>), 3.04 (t, 2H, CH<sub>2</sub>), 3.63 (t, 2H, CH<sub>2</sub>), 7.3-7.4 (m, 5H, aromatic). <sup>13</sup>C NMR (400.13 MHz, CD<sub>2</sub>Cl<sub>2</sub>, 298 K): δ 24.4 (CH<sub>3</sub>), 29.6 (CH<sub>2</sub>CH<sub>2</sub>COOH), 30.2 (CH<sub>2</sub>Ph), 33.2 (CH<sub>2</sub>CH<sub>2</sub>COOH), 40.0 (SCH<sub>2</sub>-CH<sub>2</sub>Ph), 45.7 (SCCH<sub>2</sub>), 118.7 (CN), 127.3, 128.9, 129.2, 144.2 (Ph), 177.5 (C=O), 222.2 (C=S).

#### Synthesis of the PDMS<sub>66</sub>-PETTC macro-CTA

A flame dried 100 ml round-bottomed flask, equipped with a magnetic follower, was charged with monocarbinol terminated PDMS<sub>66</sub> (9.83 g, 1.97 mmol). The monocarbinol terminated PDMS<sub>66</sub> was then stirred for one hour under high vacuum, in order to remove any traces of water and volatile compounds. PETTC (1.00 g, 2.95 mmol), DMAP (0.04 g, 0.29 mmol) and dry DCM (50 ml) were then added to the monocarbinol terminated PDMS<sub>66</sub> and the resulting mixture was cooled to 0 °C (ice bath), before being purged with nitrogen gas for 30 min. An ice cold DCC solution in anhydrous DCM (1.22 g, 5.90 mmol in 10 ml DCM) was then added dropwise over 20 min. to the cold mixture. After a further hour at 0 °C, the mixture was allowed to warm to room temperature gradually before being heated at 35 °C for 16 h. The reaction was then quenched

*via* exposure to air, filtered to remove the N,N'-dicyclohexylurea precipitate, and purified *via* column chromatography (*n*-hexane as eluent). The mixture was then washed with methanol (3 x 100 ml) and placed under reduced pressure to remove the solvent. <sup>1</sup>H NMR indicated an end-group functionality of 92 %, similarly, UV/ Vis indicated a mean functionality of 94 %.

### **Synthesis of PDMS<sub>66</sub>-PDMA<sub>x</sub> diblock copolymer nanoparticles in D5 silicone oil**

RAFT dispersion polymerisation of DMA in D5 silicone oil was conducted using the PDMS<sub>66</sub>-PETTC precursor block as follows. A round-bottomed flask was charged with the PDMS<sub>66</sub>-PETTC precursor (0.10 g, 0.019 mmol) and DMA monomer [from 0.089 g (0.56 mmol) to 0.74 g (4.7 mmol)], depending on the desired target DP for the PDMA block. T21s initiator was then added (1.30 mg, 6.30 μmol; added as 15 μl of a 10 % v/v stock solution in D5) along with an appropriate mass of D5 silicone oil depending on the desired final copolymer concentration (ranging from 10 to 30 % w/w copolymer concentration). The resulting reaction mixture was purged with nitrogen for 20 min, then sealed and placed in a preheated oil bath set at 90 °C for 8 h. Depending on the final diblock copolymer composition and solids content, the product was obtained as either a free-flowing dispersion or as a free-standing gel.

### **Synthesis of other PDMS<sub>66</sub>-stabilised diblock copolymer nanoparticles in D5 silicone oil**

A typical RAFT polymerisation (conducted under either dispersion or emulsion conditions, depending on the monomer solubility) was conducted as follows. A round-bottomed flask was charged with the PDMS<sub>66</sub>-PETTC precursor (0.10 g, 0.019 mmol), an appropriate mass of a methacrylic monomer to afford a target DP of 200 [e.g. benzyl methacrylate (0.33 g, 0.19 mmol)], an appropriate mass of D5 silicone oil for a final copolymer concentration of 25 % w/w solids and T21s initiator (1.30 mg, 6.30 μmol; added as 15 μl of a 10 % v/v stock solution in D5 silicone oil). The resulting solution (or emulsion, depending on the monomer solubility) was then purged with nitrogen, sealed and placed in a preheated oil bath set at 90 °C for 16 h.

## **2.2.3 Characterisation**

### **<sup>1</sup>H NMR spectroscopy**

<sup>1</sup>H NMR spectra were recorded in either d<sub>6</sub>-acetone, chloroform-d or dichloromethane-d<sub>2</sub> using a Bruker AV1-400 MHz spectrometer. Typically, 64 scans were averaged per spectrum.

### **Gel permeation chromatography**

Molecular weight distributions were determined using a GPC instrument operating at 30 °C that comprised two Polymer Laboratories PL gel 5 μm Mixed C columns, a LC20AD ramped isocratic pump, THF eluent and a WellChrom K-2301 refractive index detector operating at 950 ± 30 nm.

The mobile phase contained 2.0 % v/v triethylamine and 0.05 % w/v 3,5-di-tert-4-butylhydroxytoluene (BHT); the flow rate was fixed at 1.0 ml min<sup>-1</sup> and toluene was used as a flow rate marker. A series of ten near-monodisperse poly(methyl methacrylate) standards ( $M_p = 1,280$  to 330,000 g mol<sup>-1</sup>) were used for calibration. Chromatograms were analysed using Varian Cirrus GPC software.

### Dynamic light scattering

DLS studies were performed using a Zetasizer Nano-ZS instrument (Malvern Instruments, UK) at 25 °C at a fixed scattering angle of 173°. Copolymer dispersions were diluted in the solvent in which they were synthesised (typically D5) to a final copolymer concentration of 0.10 % w/w. The intensity-average diameter and polydispersity (PDI) of the diblock copolymer particles were calculated by cumulants analysis of the experimental correlation function using Dispersion Technology Software version 6.20. Data were averaged over ten runs each of thirty seconds duration.

### Transmission electron microscopy

Transmission electron microscopy (TEM) studies were conducted using a FEI Tecnai G2 spirit instrument operating at 80 kV and equipped with a Gatan 1k CCD camera. Copper TEM grids were surface-coated in-house to yield a thin film of amorphous carbon. The grids were then loaded with dilute copolymer dispersions (0.20 % w/w) at 7 °C. Prior to imaging, each grid was exposed to ruthenium(IV) vapour for 7 min. at ambient temperature, in order to improve contrast. The ruthenium oxide stain was prepared by adding ruthenium(II) oxide (0.3 g) to water (50 g), to form a slurry. Then, sodium periodate (2.0 g) was added whilst stirring to form a yellow solution of ruthenium(IV) oxide within 1 minute.<sup>39</sup>

### Rheology studies

An AR-G2 rheometer equipped with a 40 mm 2° aluminum cone was used for all measurements. The storage and loss moduli were determined, *via* oscillatory rheometry, either as a function of strain at a fixed angular frequency of 1.0 rad s<sup>-1</sup> or as a function of angular frequency at a fixed strain of 1.0 %. Viscosities were measured *via* rotational rheometry at a fixed shear rate of 10 s<sup>-1</sup>. In all cases, the gap between the cone and plate was 58 µm.

### UV/Vis spectroscopy.

UV/Vis absorption spectra were recorded between 200 and 800 nm using a PC-controlled UV-1800 spectrophotometer at 25 °C using a 1 cm quartz cell. A Beer–Lambert calibration curve was constructed using a series of twelve PETTC solutions in dichloromethane. The absorption

maximum at 298 nm assigned to the trithiocarbonate group was used for this calibration plot, with PETTC concentrations ranging from  $1.2 \times 10^{-5} \text{ mol dm}^{-3}$  to  $1.0 \times 10^{-4} \text{ mol dm}^{-3}$ . The mean DP for the PDMS<sub>66</sub>-PETTC macro-CTA was determined using the molar extinction coefficient of  $10,153 \pm 66 \text{ mol}^{-1} \text{ dm}^3 \text{ cm}^{-1}$  determined for PETTC.

## 2.3 Results and discussion

A monocarbinol PDMS<sub>66</sub>-OH precursor was esterified with a carboxylic acid-functionalised trithiocarbonate RAFT agent (PETTC), *via* DCC/DMAP coupling in dichloromethane, according to a previously reported protocol.<sup>38</sup> <sup>1</sup>H NMR and UV/Vis spectroscopy were each used to characterise the resulting PDMS<sub>66</sub>-PETTC macro-CTA. In the former case, the five aromatic protons assigned to the phenyl group of the PETTC RAFT agent were compared to the integrated PDMS<sub>66</sub> backbone signal, indicating a mean degree of esterification of  $92 \pm 4 \%$  (see **Figure 2.2**).

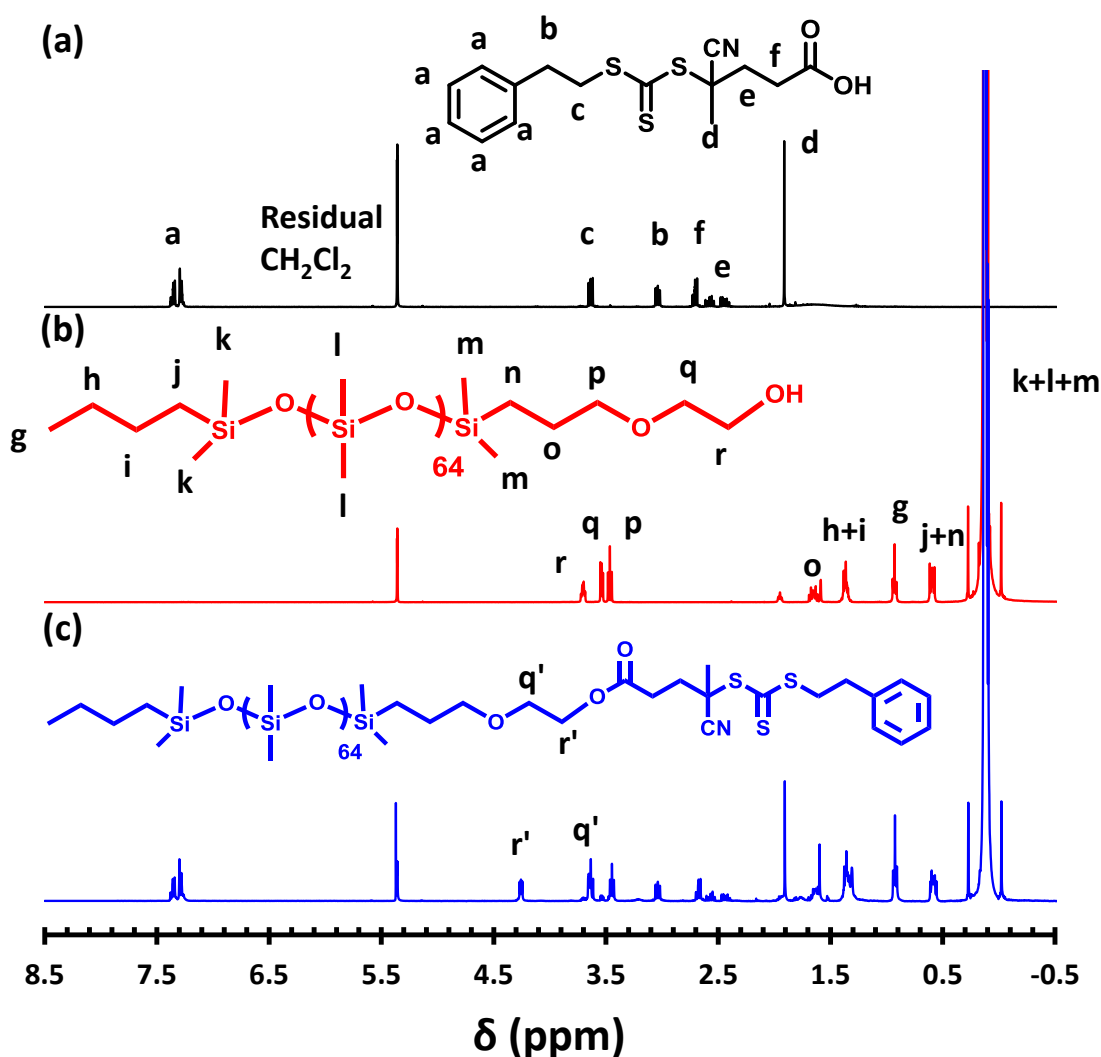


**Figure 2.2:** <sup>1</sup>H NMR spectra recorded in CD<sub>2</sub>Cl<sub>2</sub> for: (a) the PETTC chain-transfer agent (CTA), (b) the monocarbinol-terminated PDMS<sub>66</sub>-OH precursor, and (c) the final PDMS<sub>66</sub>-PETTC macro-CTA.

In the case of UV/Vis spectroscopy, a linear Beer-Lambert calibration curve recorded at a maximum wavelength of 298 nm indicated a mean degree of esterification of  $94 \pm 5 \%$  (see Figure 2.3).

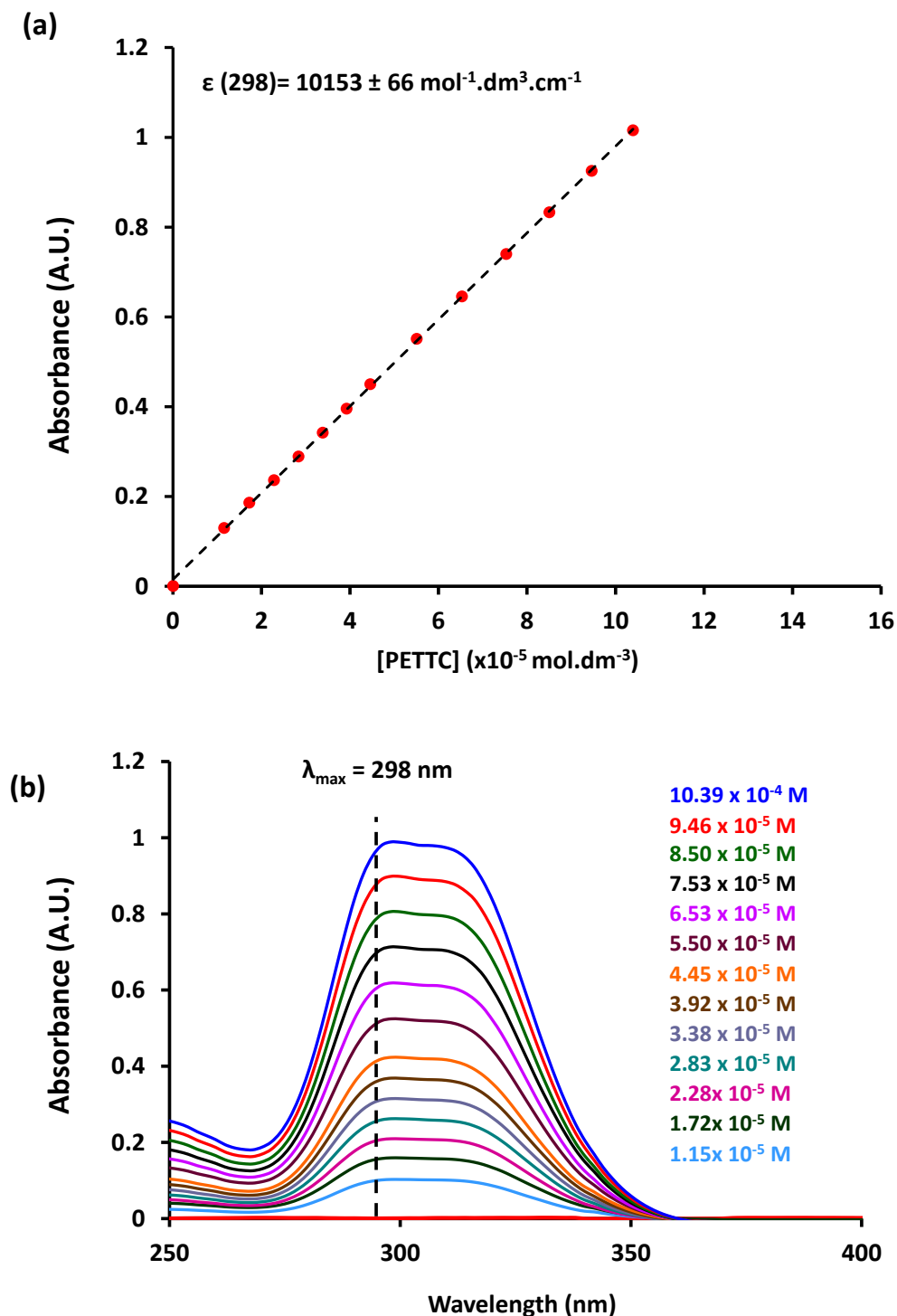


**Figure 2.3:** (a) Beer-Lambert calibration curve constructed for 4-cyano-4-(2-phenylethanesulfanylthiocarbonyl)sulfanylpentanoic acid in dichloromethane ( $\epsilon = 10,153 \pm 66 \text{ mol}^{-1} \text{ dm}^3 \text{ cm}^{-1}$ ) using UV/Vis spectroscopy at a  $\lambda_{\text{max}}$  of 298 nm. (b) Corresponding UV/Vis spectra for the different PETTC concentrations used to construct the calibration curve.

## 2.3.1 Synthesis of diblock copolymers in D5 silicone oil

The PDMS<sub>66</sub>-PETTC precursor was chain-extended in D5 silicone oil using a range of methacrylic monomers, according to **Figure 2.4**, and summarised in **Table 2.1**.

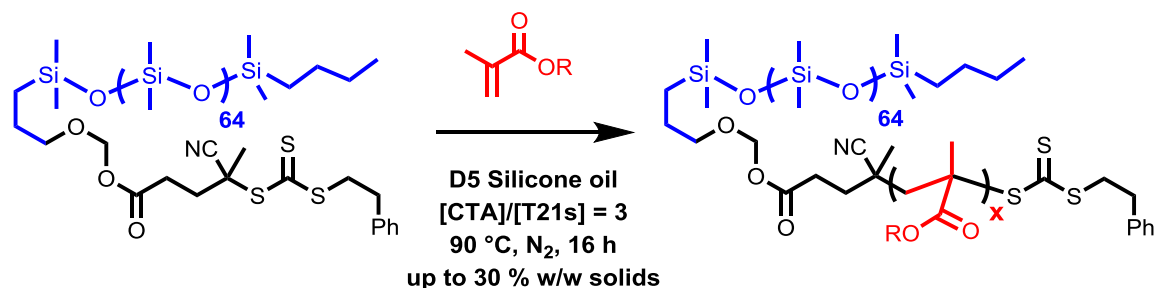


**Figure 2.4:** RAFT polymerisation of a generic methacrylic monomer in D5 silicone oil, using a PDMS<sub>66</sub> macromolecular chain transfer agent.

For each PISA synthesis, the target DP for the structure-directing methacrylic block and the copolymer concentration were fixed at 200 and 25 % w/w solids, respectively. These conditions were selected because it was previously reported that PDMS<sub>66</sub>-PBzMA<sub>200</sub> diblock copolymers prepared at 25 % w/w in another non-polar solvent (*n*-heptane) occupy vesicle phase space. Thus, in principle this target DP should be sufficient to also produce vesicular morphologies in D5 silicone oil. In each case, the final copolymer morphology was determined *via* post-mortem TEM studies (see **Figure 2.5**).

Inspection of **Table 2.1** reveals that the only methacrylic monomer that enables access to copolymer morphologies other than spheres in these initial scouting experiments is 2-(dimethylamino)ethyl methacrylate (DMA). In view of the relevant PISA literature,<sup>38</sup> it is rather surprising that the PISA synthesis of PDMS<sub>66</sub>-PBzMA<sub>200</sub> is restricted to spherical nanoparticles. These unexpected observations indicate that simply switching the continuous phase from *n*-heptane to D5 silicone oil is sufficient to produce solely kinetically-trapped morphologies. Such morphological restrictions are well-documented for RAFT aqueous emulsion polymerisation syntheses,<sup>17,19,40,41</sup> but typically do not apply to RAFT dispersion polymerisation formulations unless the mean degree of polymerisation of the stabiliser block is sufficiently high to prevent efficient sphere-sphere fusion.<sup>42</sup> However, in the present case it has already been established that the PDMS<sub>66</sub>-PETTC precursor is *not* so long as to prevent the formation of either worms or vesicles for RAFT dispersion polymerisation syntheses conducted in *n*-heptane.<sup>38</sup> Clearly, the observations described herein illustrate that our current understanding of PISA remains frustratingly incomplete.

Monomer	Target DP	Conversion ( <sup>1</sup> H NMR) / %	Actual DP	Polymerisation conditions	M <sub>n</sub> / g mol <sup>-1</sup>	M <sub>w</sub> / M <sub>n</sub>	DLS diameter (PDI) / nm	TEM morphology
Dimethylaminoethyl methacrylate	200	97	194	Dispersion	34,000	1.36	364 (0.13)	Vesicles
Benzyl methacrylate	200	98	196	Dispersion	36,300	1.22	51 (0.02)	Spheres
2,2,2,-trifluoroethyl methacrylate	200	98	196	Dispersion	32,000	1.47	65 (0.25)	Spheres
Methyl methacrylate	200	85	170	Dispersion	26,100	1.10	32 (0.4)	Spheres
Ethylene glycol methyl ether methacrylate	200	99	198	Dispersion	34,000	1.34	42 (0.05)	Spheres
Methacrylic acid	200	98	196	Dispersion	42,200**	1.78	277 (0.25)	Ill-defined
2-Hydroxyethyl methacrylate	200	99	198	Emulsion	X	X	245 (0.04)	Spheres
2-Hydroxypropyl methacrylate	200	91	182	Dispersion*	65,000	1.50	202 (0.04)	Spheres
Glycerol monomethacrylate	200	98	196	Emulsion	X	X	99 (0.02)	Spheres

**Table 2.1:** Summary of the various methacrylic monomers examined as structure-directing blocks for RAFT dispersion polymerisation syntheses conducted in D5 silicone oil at 90 °C using a PDMS<sub>66</sub>-PETTC precursor block. In all cases, the copolymer concentration was fixed at 25 % w/w solids and the [macro-CTA]/[T21s] molar ratio = 3.0. An 'X' in the M<sub>n</sub> and M<sub>w</sub>/M<sub>n</sub> columns denotes that GPC analysis was not performed because no common solvent could be identified for the specific diblock copolymer. \*HPMA monomer was immiscible with D5 silicone oil at 25 °C, but miscible at reaction temperature (90 °C). \*\*THF GPC analysis was performed after methylation with trimethylsilyldiazomethane.

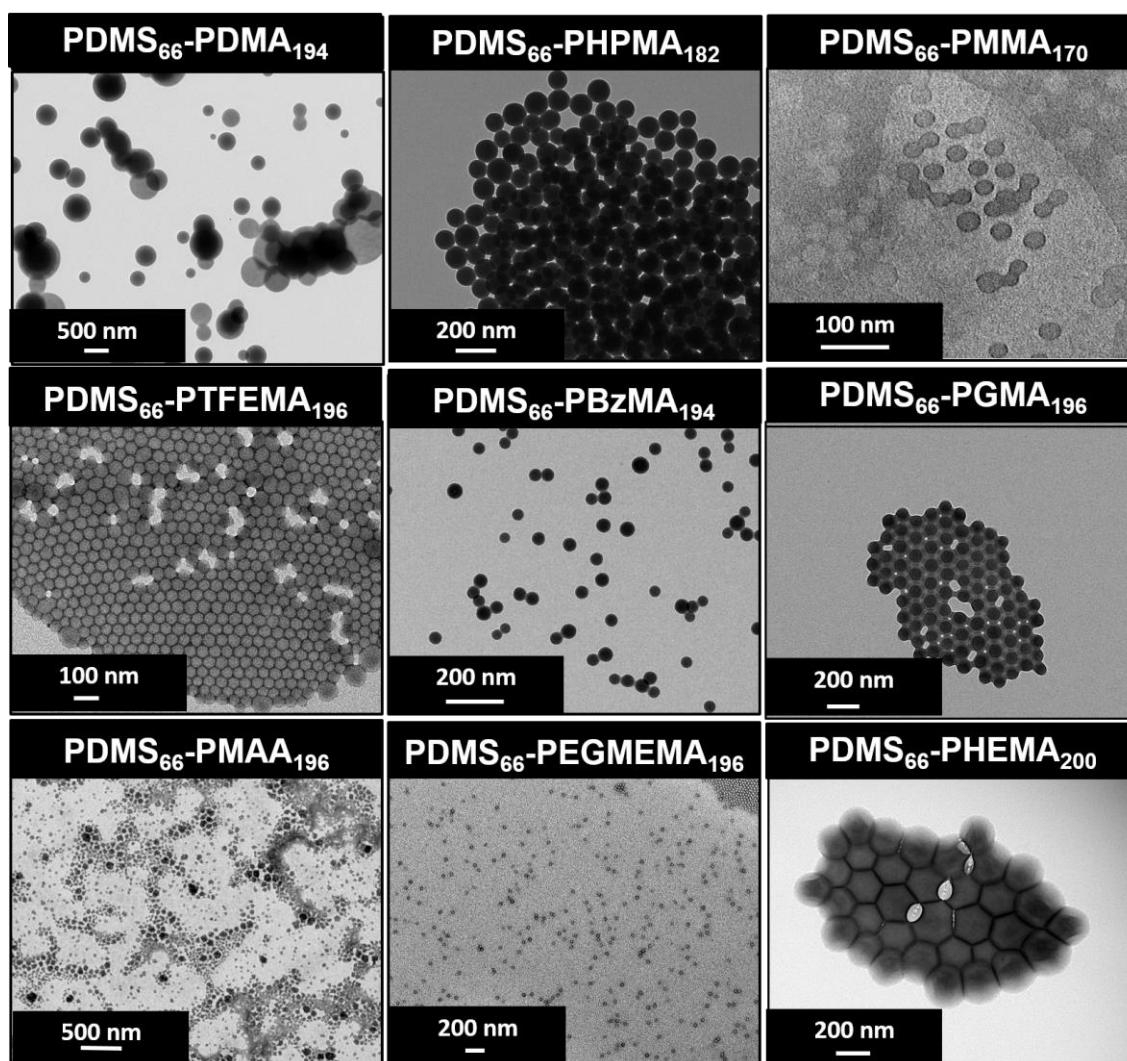


**Figure 2.5** Post-mortem TEM images obtained for the chain extension of a polydimethylsiloxane<sub>66</sub> (PDMS<sub>66</sub>) macromolecular chain transfer agent with a range of methacrylic monomers in D5 silicone oil. PDMA = poly(2-(dimethylamino)ethyl methacrylate), PHPMA = poly(2-hydroxypropylmethacrylate), PMMA = poly(methyl methacrylate), PTFEMA = poly(2,2,2-trifluoroethyl methacrylate), PBzMA = poly(benzyl methacrylate), PGMA = poly(glycerol monomethacrylate), PMAA = poly(methacrylic acid), PEGMEMA = poly(ethyleneglycol methylether methacrylate) and PHEMA = poly(2-hydroxyethyl methacrylate).

It is perhaps also worth emphasising here that this PDMS<sub>66</sub>-PDMA<sub>200</sub> formulation is a relatively rare example of a PISA synthesis involving a structure-directing block based on a tertiary amine methacrylate. In unpublished work, attempts to use tertiary amine methacrylates as the core-forming block have almost invariably resulted in substantially incomplete polymerisations and are often accompanied by a significant discolouration. These lower monomer conversions seem to be associated with the premature loss of RAFT chain-ends, with dithiobenzoates in particular being susceptible to attack by aliphatic amines to form thiols.<sup>43,44</sup>

A kinetic study was performed targeting a diblock copolymer composition of PDMS<sub>66</sub>-PDMA<sub>200</sub> vesicles at 25 % w/w solids using a PDMS<sub>66</sub>-PETTC/initiator molar ratio of 3.0. This was achieved by removing small aliquots from the polymerising reaction mixture at regular time intervals. <sup>1</sup>H NMR studies of the declining vinyl monomer signals (relative to the methacrylic backbone signals) revealed that 87 % DMA conversion was attained within 4 h at 90 °C. According to the semi-logarithmic plot displayed in **Figure 2.6a**, a three-fold increase in the rate of DMA polymerisation was observed after 2 h, which corresponds to a DMA conversion of 60 % (and hence an intermediate diblock copolymer composition of PDMS<sub>66</sub>-PDMA<sub>120</sub>). In the PISA literature, such a rate enhancement normally corresponds to the onset of micellar nucleation.<sup>45–47</sup> However, in this case the rate acceleration appears to occur *after* the nucleation event. This interpretation is based on the observation that aliquots abstracted after 2 h formed physical gels 20 °C, indicating the presence of weakly interacting worms (which are believed to be formed *via* multiple 1D fusion of the initial spherical micelles). It is currently not understood why the rate of polymerisation occurs much later than expected, but similar observations have been reported for at least two other PISA formulations.<sup>38,48</sup>

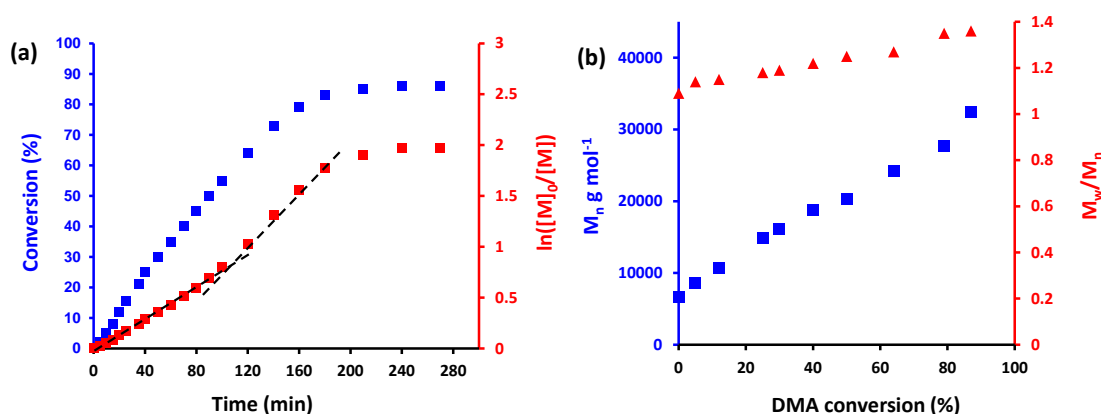


**Figure 2.6:** (a) Conversion vs. time curve (blue squares) and the corresponding semi-logarithmic plot (red squares) for the RAFT dispersion polymerisation of DMA in D5 at 90 °C using a PDMS<sub>66</sub> macro-CTA at 25 % w/w solids when targeting a PDMA block DP of 200. (b) Evolution of  $M_n$  (blue squares) and  $M_w/M_n$  (red triangles) with DMA conversion as determined by gel permeation chromatography (THF eluent; calibration against a series of near-monodisperse poly(methyl methacrylate) standards).

Each aliquot removed for these kinetic studies was also analysed *via* GPC to assess the evolution of  $M_n$  and  $M_w/M_n$  during the DMA polymerisation (see **Figure 2.6b**). A linear evolution of  $M_n$  with conversion was observed, as expected for a RAFT polymerisation. However, the dispersity ( $M_w/M_n$ ) gradually increased with conversion, although it remained below 1.40 throughout the

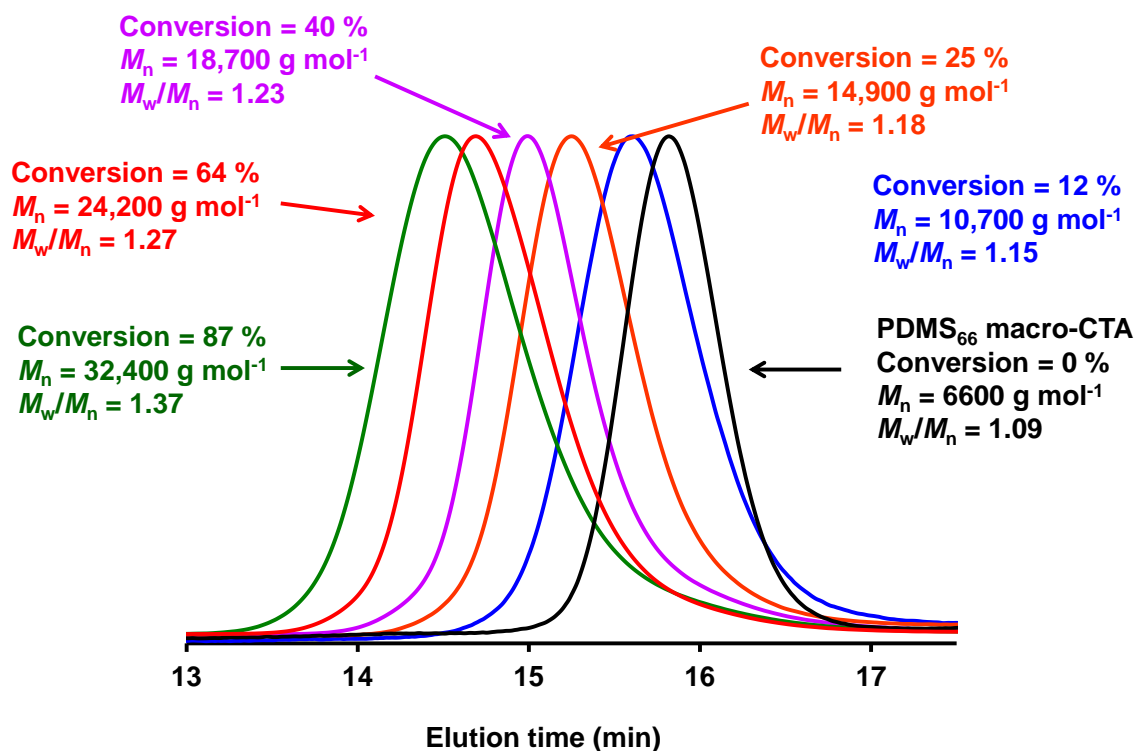


**Figure 2.7:** Normalised THF GPC chromatograms obtained by removing aliquots at regular time intervals from a dispersion polymerisation of DMA in D5 silicone oil at 25 % w/w. A PDMA core-forming DP of 200 was targeted, at a PDMS<sub>66</sub> macro-CTA/initiator ratio of 3.0. The DMA conversion of each aliquot, as determined by <sup>1</sup>H NMR, was also obtained.

polymerisation. Moreover, the blocking efficiency is relatively high and each GPC trace is unimodal (see **Figure 2.7**). Several further series of PDMS<sub>66</sub>-PDMA<sub>x</sub> diblock copolymers were prepared by systematically varying the target PDMA DP and the copolymer concentration. In each case, the final copolymer morphology was assessed by TEM in order to construct a phase diagram (see **Figure 2.8**). Below a PDMA DP of 30, no nanoparticles were obtained because the PDMA blocks were too short to induce micellar nucleation. At relatively low copolymer concentrations (e.g. 10 or 15 % w/w), spherical micelles were obtained when targeting PDMA DPs below 100, whereas mixed phases were typically produced for target DPs above 100. In contrast, the full range of copolymer morphologies (spheres, worms or vesicles) could be obtained when PISA syntheses were conducted at 25 % w/w solids or above. Spheres had mean core diameters ranging from 23 nm to 46 nm, depending on the DP of the core-forming block and the copolymer concentration at which the synthesis was conducted. Well-defined worms with a mean cross-sectional diameter of around 21 nm were obtained for PDMA DPs ranging between 99 and 109, while polydisperse vesicles were obtained when targeting DPs of 180 or higher. Representative TEM images for spheres, worms and vesicles are shown in **Figure 2.8b-d**.

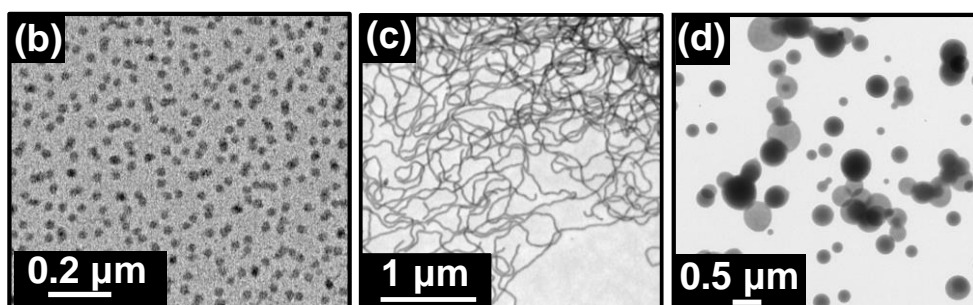
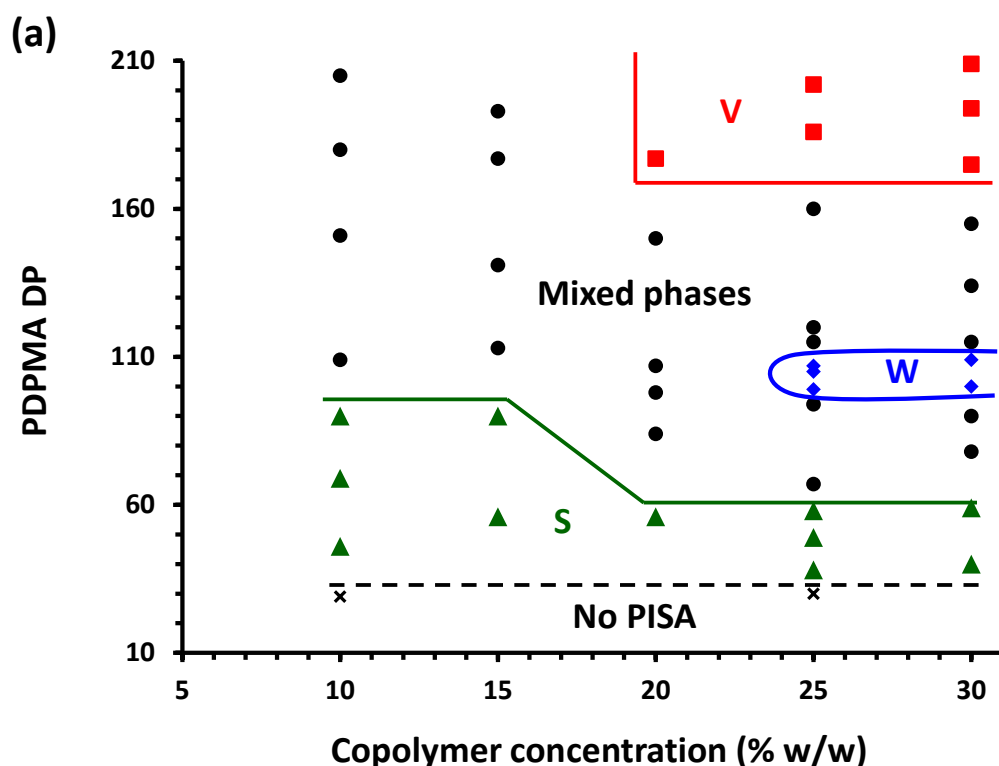


**Figure 2.8:** (a) Phase diagram constructed for PDMS<sub>66</sub>-PDMA<sub>x</sub> diblock copolymer nanoparticles prepared by RAFT dispersion polymerisation of DMA in D5 using a PDMS<sub>66</sub>-PETTC RAFT agent and T21s as an initiator ([PDMS<sub>66</sub>-PETTC]/[T21s] molar ratio = 3.0). Spheres, worms, vesicles and mixed phases are denoted by S, W, V and M, respectively. A representative TEM image for each pure copolymer morphology is also shown: (b) PDMS<sub>66</sub>-PDMA<sub>49</sub> spheres synthesised at 25 % w/w solids, (c) PDMS<sub>66</sub>-PDMA<sub>100</sub> worms synthesised at 25 % w/w solids and (d) PDMS<sub>66</sub>-PDMA<sub>186</sub> vesicles synthesised at 25 % w/w solids.

The series of PDMS<sub>66</sub>-PDMA<sub>x</sub> diblock copolymer used to construct the phase diagram shown in **Figure 2.8** are summarised in **Table 2.2**

Target Composition	Conc. / % w/w	DMA Conv / % <sup>a</sup>	Actual PDMA DP	GPC		DLS		Morphology (TEM)
				M <sub>n</sub> / kg mol <sup>-1</sup>	M <sub>w</sub> /M <sub>n</sub>	Z-Avg. Diam. / nm	PDI	
PDMS <sub>66</sub> -PDMA <sub>40</sub>	30	99	40	14.2	1.17	23	0.01	Spheres
PDMS <sub>66</sub> -PDMA <sub>60</sub>	30	99	59	16.6	1.19	33	0.01	Spheres
PDMS <sub>66</sub> -PDMA <sub>80</sub>	30	97	78	18.4	1.26	89	0.15	Mixed
PDMS <sub>66</sub> -PDMA <sub>95</sub>	30	95	90	19.6	1.23	99	0.17	Mixed

PDMS <sub>66</sub> -PDMA <sub>105</sub>	30	95	100	19.5	1.26	181	0.37	Worms
PDMS <sub>66</sub> -PDMA <sub>115</sub>	30	95	109	23.2	1.24	229	0.43	Worms
PDMS <sub>66</sub> -PDMA <sub>120</sub>	30	96	115	21.6	1.32	228	0.21	Mixed
PDMS <sub>66</sub> -PDMA <sub>140</sub>	30	96	134	27.40	1.28	264	0.32	Mixed
PDMS <sub>66</sub> -PDMA <sub>160</sub>	30	97	155	29.1	1.30	231	0.23	Mixed
PDMS <sub>66</sub> -PDMA <sub>180</sub>	30	97	175	33.1	1.37	321	0.15	Vesicles
PDMS <sub>66</sub> -PDMA <sub>200</sub>	30	95	190	34.7	1.37	309	0.12	Vesicles
PDMS <sub>66</sub> -PDMA <sub>230</sub>	30	91	209	34.9	1.36	346	0.15	Vesicles
PDMS <sub>66</sub> -PDMA <sub>30</sub>	25	>99	30	10.7	1.18	X	X	No PISA
PDMS <sub>66</sub> -PDMA <sub>40</sub>	25	96	38	13.9	1.23	25	0.03	Spheres
PDMS <sub>66</sub> -PDMA <sub>50</sub>	25	97	49	14.4	1.21	28	0.01	Spheres
PDMS <sub>66</sub> -PDMA <sub>60</sub>	25	97	58	16.2	1.13	35	0.02	Spheres
PDMS <sub>66</sub> -PDMA <sub>70</sub>	25	96	67	17.7	1.21	134	0.34	Mixed
PDMS <sub>66</sub> -PDMA <sub>100</sub>	25	94	94	22.8	1.23	197	0.27	Mixed
PDMS <sub>66</sub> -PDMA <sub>105</sub>	25	94	99	22.4	1.22	187	0.19	Worms
PDMS <sub>66</sub> -PDMA <sub>110</sub>	25	95	105	23.1	1.21	161	0.24	Worms
PDMS <sub>66</sub> -PDMA <sub>115</sub>	25	93	107	23.8	1.24	286	0.39	Worms
PDMS <sub>66</sub> -PDMA <sub>125</sub>	25	92	115	23.3	1.25	148	0.19	Mixed
PDMS <sub>66</sub> -PDMA <sub>130</sub>	25	92	120	20.7	1.25	137	0.20	Mixed
PDMS <sub>66</sub> -PDMA <sub>170</sub>	25	94	160	27.0	1.30	266	0.27	Mixed
PDMS <sub>66</sub> -PDMA <sub>200</sub>	25	93	186	34.0	1.36	276	0.13	Vesicles
PDMS <sub>66</sub> -PDMA <sub>220</sub>	25	92	202	36.2	1.33	288	0.09	Vesicles
PDMS <sub>66</sub> -PDMA <sub>60</sub>	20	94	56	16.0	1.14	33	0.02	Spheres
PDMS <sub>66</sub> -PDMA <sub>90</sub>	20	93	84	17.6	1.14	98	0.14	Mixed
PDMS <sub>66</sub> -PDMA <sub>105</sub>	20	93	98	20.5	1.17	189	0.27	Mixed
PDMS <sub>66</sub> -PDMA <sub>120</sub>	20	89	107	24.7	1.23	226	0.34	Mixed
PDMS <sub>66</sub> -PDMA <sub>160</sub>	20	94	150	27.2	1.27	244	0.21	Mixed
PDMS <sub>66</sub> -PDMA <sub>190</sub>	20	93	177	29.2	1.29	332	0.15	Vesicles
PDMS <sub>66</sub> -PDMA <sub>60</sub>	15	94	56	13.5	1.14	32	0.04	Spheres
PDMS <sub>66</sub> -PDMA <sub>100</sub>	15	90	90	18.0	1.19	45	0.02	Spheres
PDMS <sub>66</sub> -PDMA <sub>120</sub>	15	94	113	21.4	1.24	63	0.10	Mixed
PDMS <sub>66</sub> -PDMA <sub>150</sub>	15	94	141	25.1	1.31	66	0.14	Mixed
PDMS <sub>66</sub> -PDMA <sub>190</sub>	15	93	177	28.3	1.28	126	0.16	Mixed
PDMS <sub>66</sub> -PDMA <sub>210</sub>	15	92	193	28.3	1.28	126	0.16	Mixed
PDMS <sub>66</sub> -PDMA <sub>30</sub>	10	98	29	9.3	1.18	X	X	No PISA
PDMS <sub>66</sub> -PDMA <sub>50</sub>	10	91	46	15.3	1.26	28	0.01	Spheres
PDMS <sub>66</sub> -PDMA <sub>80</sub>	10	86	69	15.7	1.20	34	0.01	Spheres
PDMS <sub>66</sub> -PDMA <sub>100</sub>	10	90	90	18.4	1.22	47	0.02	Spheres
PDMS <sub>66</sub> -PDMA <sub>120</sub>	10	91	109	23.9	1.22	65	0.04	Mixed
PDMS <sub>66</sub> -PDMA <sub>170</sub>	10	89	151	32.1	1.27	87	0.09	Mixed
PDMS <sub>66</sub> -PDMA <sub>220</sub>	10	82	180	33.2	1.35	146	0.14	Mixed
PDMS <sub>66</sub> -PDMA <sub>260</sub>	10	79	205	36.3	1.38	278	0.21	Mixed

a <sup>1</sup>H NMR in chloroform-d

Table 2.2: Summary of the PDMS<sub>66</sub>-PDMA<sub>x</sub> diblock copolymers used to construct the phase diagram described in (Figure 2.8).

To assess the evolution of molecular weight on varying the PDMA DP at a fixed copolymer concentration of 25 % w/w solids, selected samples were analysed by GPC (see **Figure 2.9**). Each GPC curve displayed no evidence of unreacted macro-CTA, indicating a high blocking efficiency. Furthermore,  $M_w/M_n$  values remained below 1.40 for target PDMA DPs up to 200, indicating that these additional DMA polymerisations were also reasonably well-controlled.

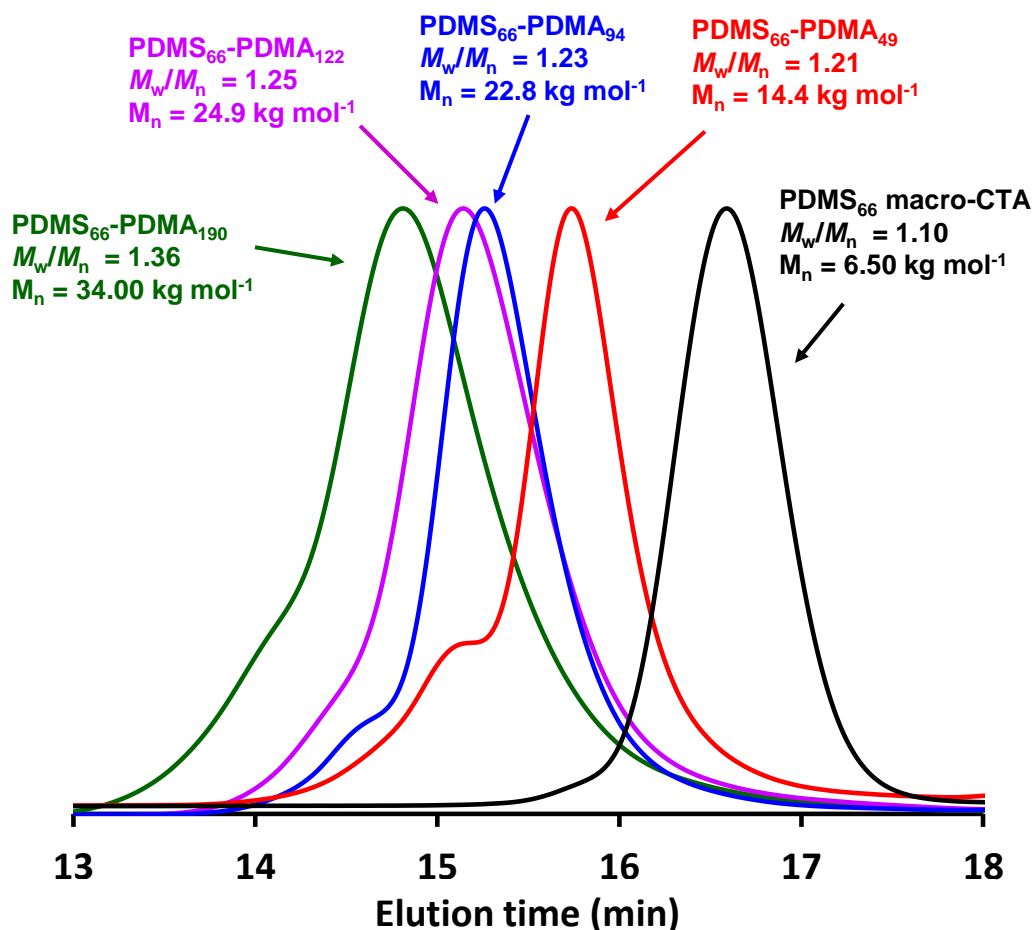


**Figure 2.9:** Gel permeation chromatograms (THF eluent; calibrated using a series of near-monodisperse poly(methyl methacrylate) standards) recorded for the PDMS<sub>66</sub>-PETTC precursor (black curve) and a series of PDMS<sub>66</sub>-PDMA<sub>x</sub> diblock copolymers prepared at 25 % w/w solids in D5 silicone oil while targeting an increasing degree of polymerisation for the PDMA block.

The PDMS<sub>66</sub>-PDMA<sub>99-109</sub> diblock copolymer worms prepared at 25 – 30 % w/w solids formed soft, free-standing gels on cooling to ambient temperature. To examine the physical properties of such worm gels, a 30 % w/w PDMS<sub>66</sub>-PDMA<sub>100</sub> worm dispersion in D5 silicone oil was analysed *via* oscillatory rheology. First, the effect of varying the applied strain on the storage ( $G'$ ) and loss ( $G''$ ) moduli was determined (**Figure 2.10**). The plateau region observed for  $G'$  and  $G''$  below 10 % strain confirmed the viscoelastic nature of this worm gel. For strains exceeding 10 %, the magnitude of  $G'$  falls below  $G''$ , indicating the yield stress.<sup>49</sup> For a truly viscoelastic material,  $G'$  should be independent of the applied frequency. Hence, the effect of varying the applied

frequency between 0.1 and 100  $\text{rad s}^{-1}$  on the gel properties was also assessed. However, for PDMS<sub>66</sub>-PDMA<sub>100</sub> worms prepared in D5 silicone oil, a modest increase in both  $G'$  and  $G''$  was observed on increasing the applied frequency. This has been observed for other worm gels prepared *via* PISA and suggests some mild deviation from ideal viscoelastic behavior.<sup>18,50</sup>

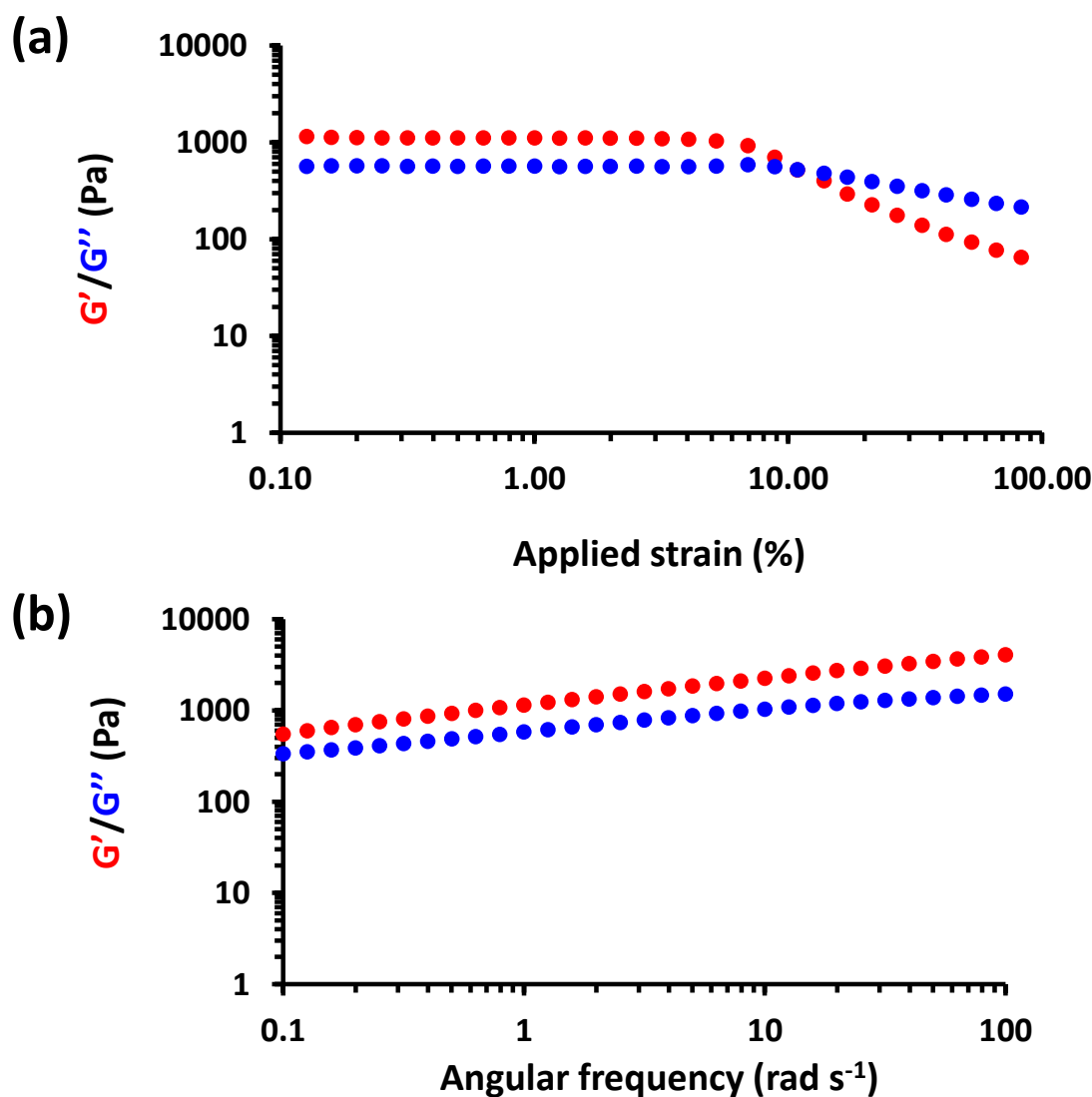


**Figure 2.10:** Effect of varying the applied strain on the storage moduli ( $G'$ ; red circles) and loss moduli ( $G''$ ; blue circles) of a PDMS<sub>66</sub>-PDMA<sub>100</sub> worm-gel at 30 % w/w (b) Effect of varying the angular frequency on the storage moduli ( $G'$ ; red circles) and loss moduli ( $G''$ ; blue circles) on a PDMS<sub>66</sub>-PDMA<sub>100</sub> worm-gel at 30 % w/w.

To assess the critical gelation concentration (CGC) of the PDMS<sub>66</sub>-PDMA<sub>100</sub> worms, a larger scale batch was prepared at 30 % w/w solids. Aliquots were diluted using D5 silicone oil *via* gentle stirring overnight to achieve copolymer concentrations ranging from 5 to 30 % w/w solids. The resulting dispersions were then assessed *via* oscillatory rheology at a fixed strain of 1.0 % and an angular frequency of 1  $\text{rad s}^{-1}$  in order to determine  $G'$  and  $G''$  in each case. Inspecting **Figure 2.11**,  $G'$  exceeds  $G''$  for copolymer concentrations equal to or greater than 12 % w/w,

indicating that these worm dispersions are physical gels. On the other hand,  $G'$  is less than  $G''$  for copolymer concentrations below 10 % w/w, indicating free-flowing fluids in this case. Hence, the CGC for PDMS<sub>66</sub>-PDMA<sub>100</sub> worm-gels is estimated to lie between 10 and 12 % w/w solids. This is consistent with CGC values reported for related PISA syntheses of diblock copolymer worms in non-polar media.<sup>14</sup>

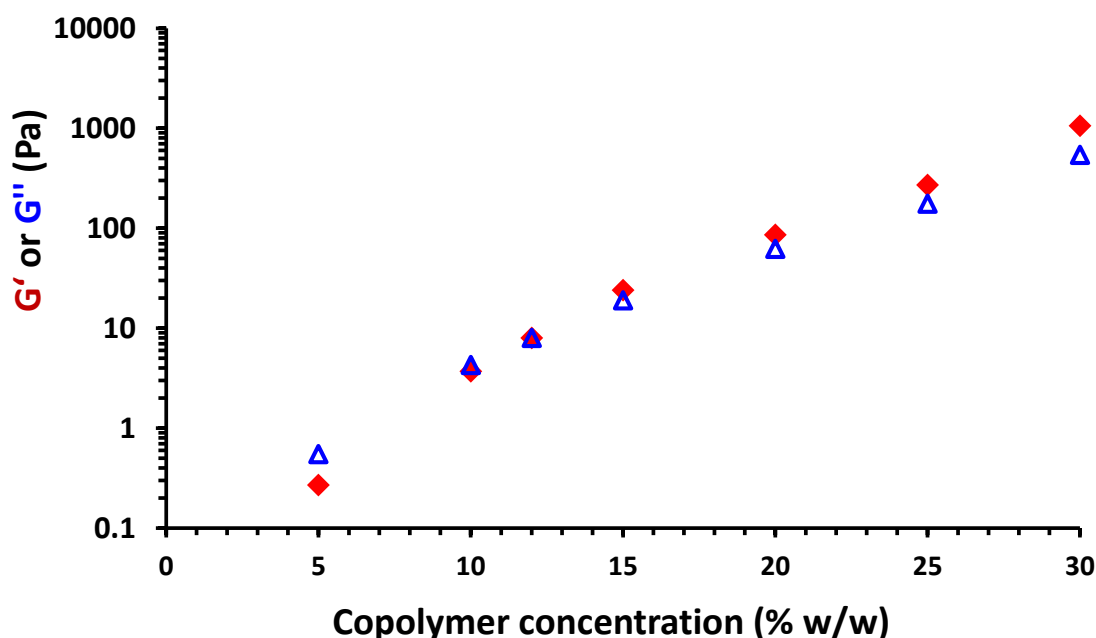


**Figure 2.11:** Concentration dependence of the storage moduli ( $G'$ ; filled red diamonds) and loss moduli ( $G''$ ; open blue triangles) determined for a series of PDMS<sub>66</sub>-PDMA<sub>100</sub> worm dispersions at a fixed angular frequency of 1 rad s<sup>-1</sup> and a fixed strain of 1 %.

In addition to D5 silicone oil, PDMS<sub>66</sub>-PDMA<sub>x</sub> worm-gels were also synthesised at 30 % w/w solids in three other non-polar solvents, namely D4 silicone oil, hexamethyldisiloxane and *n*-dodecane. The critical DP required for the PDMA block to obtain worms in each solvent differed slightly, but not by more than ten units. A summary of these various PISA formulations is provided in **Table 2.3**, along with the storage moduli ( $G'$ ) and CGC observed for each copolymer-solvent pair.

Solvent	Copolymer composition	$G'$ at 20 °C / Pa s	CGC / % w/w
D5	PDMS <sub>66</sub> -PDMA <sub>100</sub>	1057	12
D4	PDMS <sub>66</sub> -PDMA <sub>104</sub>	677	12
<i>n</i> -dodecane	PDMS <sub>66</sub> -PDMA <sub>90</sub>	845	10
Hexamethyldisiloxane	PDMS <sub>66</sub> -PDMA <sub>106</sub>	450	14

**Table 2.3.** Summary of the gel modulus ( $G'$ ) and critical gelation concentration (CGC) for four PDMS<sub>66</sub>-PDMA<sub>x</sub> worm gels prepared *via* RAFT dispersion polymerisation of DMA at 30 % w/w solids in various solvents.

The corresponding TEM images for worms prepared in D4, hexamethyldisiloxane and *n*-dodecane can be seen in **Figure 2.12**.

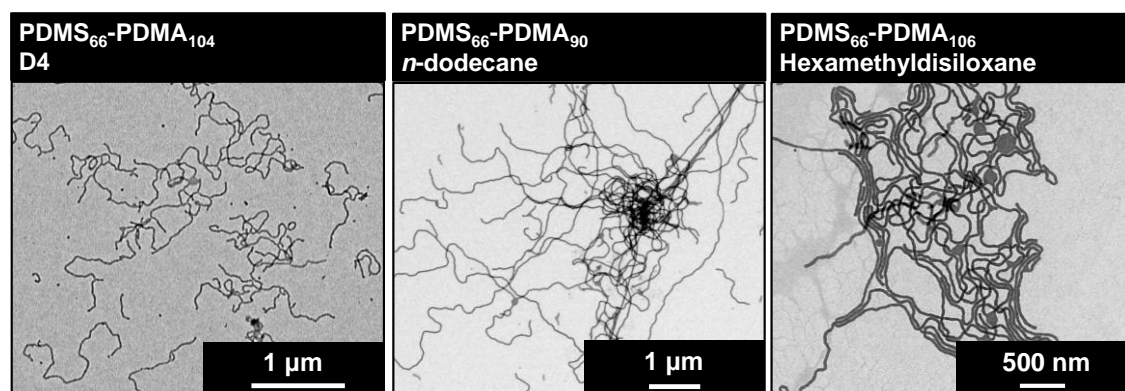


**Figure 2.12:** TEM images obtained for PDMS<sub>66</sub>-PDMA<sub>x</sub> worms synthesised in either D4, *n*-dodecane or hexamethyldisiloxane. The precise diblock copolymer composition is indicated above each image.

Finally, the viscosity-modifying performance of PDMS<sub>66</sub>-PDMA<sub>x</sub> worms was investigated in each of these four solvents over a copolymer concentration range of 5 to 25 % w/w solids.

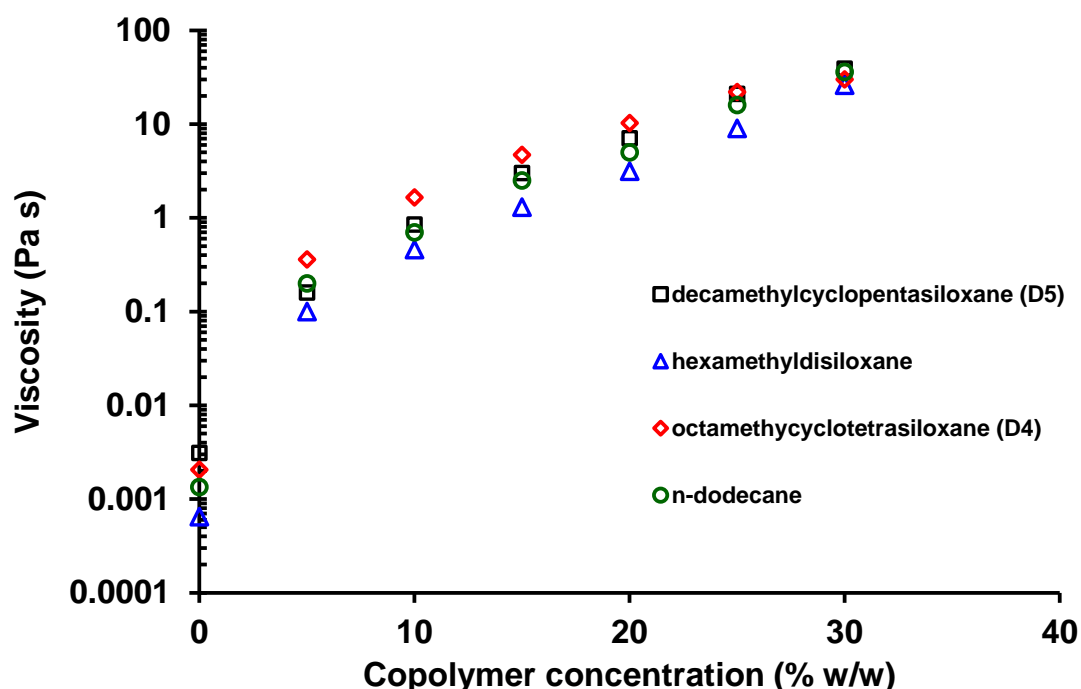


**Figure 2.13.** Concentration dependence of the solution viscosity (determined at a fixed shear rate of 10 s<sup>-1</sup>) determined for PDMS<sub>66</sub>-PDMA<sub>x</sub> diblock copolymer worms prepared in either D5 silicone oil (open black squares), D4 (open green diamonds), hexamethyldisiloxane (open blue triangles) or *n*-dodecane (open red circles), where *x* = 90 to 106 depending on the solvent type. In each case, worms were prepared at an initial copolymer concentration of 30 % w/w solids and then sequentially diluted using the same solvent for viscosity measurements. The precise PDMA target DP required to produce a pure worm phase varied slightly according to the solvent: the actual diblock compositions in each case are shown in **Table 2.3**.

The viscosity for each dispersion was determined *via* rotational rheometry at a fixed shear rate of  $10 \text{ s}^{-1}$  (see **Figure 2.13**). Clearly, only a relatively low concentration ( $\sim 5 \text{ \% w/w}$ ) of PDMS<sub>66</sub>-PDMA<sub>x</sub> worms is required to produce a sixty-fold increase in solution viscosity relative to the corresponding pure solvent. Higher copolymer concentrations lead to a viscosity enhancement by well over four orders of magnitude. Such observations suggest that PDMS<sub>66</sub>-PDMA<sub>x</sub> worms may be useful as viscosity modifiers for non-polar oils, especially silicones.

## 2.4 Conclusions

A well-defined PDMS<sub>66</sub>-PETTC precursor was prepared with a high degree of end-group functionality using a previously reported esterification protocol.<sup>38</sup> Chain extension was examined with a range of methacrylic monomers *via* PISA formulations conducted in D5 silicone oil. Surprisingly, only 2-(dimethylamino)ethyl methacrylate (DMA) provided access to the full range of copolymer morphologies (spheres, worms or vesicles). All other methacrylic monomers led to the formation of kinetically-trapped spherical morphologies. This unexpected restriction is particularly perplexing in the case of benzyl methacrylate, for which the full range of copolymer morphologies has been previously reported for PISA syntheses conducted using the same PDMS-PETTC precursor block in another non-polar solvent (*n*-heptane).<sup>38</sup>

The RAFT dispersion polymerisation of DMA in D5 silicone oil exhibited similar kinetics to previously reported PISA formulations conducted in non-polar solvents. Initially, the relatively slow solution polymerisation of DMA was observed. Once a critical degree of polymerisation was obtained for the growing PDMA block, micellar nucleation occurred - as indicated by the onset of turbidity in the reaction solution. This led to a significantly faster rate of polymerisation because the heterogeneous polymerisation henceforth proceeded within monomer-swollen nascent nanoparticles. This relatively high local DMA concentration led to a three-fold rate enhancement, which enabled more than 95 % conversion to be achieved within 4 h at 90 °C. GPC analysis confirmed a linear evolution of  $M_n$  with conversion while the dispersity ( $M_w/M_n$ ) remained below 1.40 throughout the polymerisation, as expected for a well-controlled RAFT polymerisation.

A phase diagram was constructed to enable the reproducible targeting of pure spheres, worms or vesicles. Samples of pure worms formed free-standing gels at room temperature, which is consistent with the behaviour of concentrated dispersions of worm-like micelles reported in the literature. The worm gels formed by PDMS<sub>66</sub>-PDMA<sub>100</sub> were characterised *via* oscillatory

rheology. Such gels have a  $G'$  of 1,057 Pa at 30 % w/w and a relatively high critical gelation concentration of approximately 10 – 12 % w/w.

Finally, PDMS<sub>66</sub>-PDMA<sub>90-100</sub> worms were also prepared in hexamethyldisiloxane, *n*-dodecane and D4. Such worms can increase the solution viscosity by a factor of up to sixty at copolymer concentrations as low as 5.0 % w/w. Hence, these new PISA formulations offer potential applications as viscosity modifiers for non-polar solvents, particularly silicone oils.

## 2.5 References

- (1) Zhang, L.; Yu, K.; Eisenberg, A. Ion-Induced Morphological Changes in “Crew-Cut” Aggregates of Amphiphilic Block Copolymers. *Science* **1996**, *272*, 1777–1779.
- (2) Zhang, L.; Eisenberg, A. Multiple Morphologies and Characteristics of “Crew-Cut” Micelle-like Aggregates of Polystyrene-B-Poly(acrylic Acid) Diblock Copolymers in Aqueous Solutions. *J. Am. Chem. Soc.* **1996**, *118*, 3168–3181.
- (3) Zhang, L.; Eisenberg, A. Multiple Morphologies of “Crew-Cut” Aggregates of Polystyrene-B-Poly(acrylic Acid) Block Copolymers. *Science* **1995**, *268*, 1728–1731.
- (4) Mai, Y.; Eisenberg, A. Self-Assembly of Block Copolymers. *Chem. Soc. Rev.* **2012**, *41*, 5969–5985.
- (5) Bates, F. S.; Fredrickson, G. H. Block Copolymers-Designer Soft Materials. *Phys. Today* **1999**, *52*, 32–38.
- (6) Charleux, B.; Delaittre, G.; Rieger, J.; D’Agosto, F. Polymerization-Induced Self-Assembly: From Soluble Macromolecules to Block Copolymer Nano-Objects in One Step. *Macromolecules* **2012**, *45*, 6753–6765.
- (7) Canning, S. L.; Smith, G. N.; Armes, S. P. A Critical Appraisal of RAFT-Mediated Polymerization-Induced Self-Assembly. *Macromolecules* **2016**, *49*, 1985–2001.
- (8) Derry, M. J.; Fielding, L. A.; Armes, S. P. Polymerization-Induced Self-Assembly of Block Copolymer Nanoparticles via RAFT Non-Aqueous Dispersion Polymerization. *Prog. Polym. Sci.* **2016**, *52*, 1–18.
- (9) Warren, N. J.; Armes, S. P. Polymerization-Induced Self-Assembly of Block Copolymer Nano-Objects via RAFT Aqueous Dispersion Polymerization. *J. Am. Chem. Soc.* **2014**, *136*, 10174–10185.
- (10) Moad, G.; Rizzardo, E.; Thang, S. H. Living Radical Polymerization by the RAFT Process. *Aust. J. Chem.* **2005**, *58*, 379–410.
- (11) Chiefari, J.; Chong, Y. K. B.; Ercole, F.; Krstina, J.; Jeffery, J.; Le, T. P. T.; Mayadunne, R. T. A.; Meijs, G. F.; Moad, C. L.; Moad, G.; et al. Living Free-Radical Polymerization by Reversible Addition–Fragmentation Chain Transfer: The RAFT Process. *Macromolecules* **1998**, *31*, 5559–5562.
- (12) Keddie, D. J. A Guide to the Synthesis of Block Copolymers Using Reversible-Addition Fragmentation Chain Transfer (RAFT) Polymerization. *Chem. Soc. Rev.* **2014**, *43*, 496–505.
- (13) Perrier, S. 50th Anniversary Perspective: RAFT Polymerization - A User Guide. *Macromolecules* **2017**, *50*, 7433–7447.
- (14) Derry, M. J.; Fielding, L. A.; Armes, S. P. Industrially-Relevant Polymerization-Induced Self-Assembly Formulations in Non-Polar Solvents: RAFT Dispersion Polymerization of Benzyl Methacrylate. *Polym. Chem.* **2015**, *6*, 3054–3062.
- (15) Grazon, C.; Rieger, J.; Sanson, N.; Charleux, B. Study of poly(N,N-Diethylacrylamide) Nanogel Formation by Aqueous Dispersion Polymerization of N,N-Diethylacrylamide in the Presence of Poly(ethylene Oxide)-B-poly(N,N-Dimethylacrylamide) Amphiphilic

- Macromolecular RAFT Agents. *Soft Matter* **2011**, *7*, 3482.
- (16) Boissé, S.; Rieger, J.; Belal, K.; Di-Cicco, A.; Beaunier, P.; Li, M.-H.; Charleux, B. Amphiphilic Block Copolymer Nano-Fibers via RAFT-Mediated Polymerization in Aqueous Dispersed System. *Chem. Commun.* **2010**, *46*, 1950–1952.
- (17) Zhang, X.; Boissé, S.; Zhang, W.; Beaunier, P.; D'Agosto, F.; Rieger, J.; Charleux, B. Well-Defined Amphiphilic Block Copolymers and Nano-Objects Formed in Situ via RAFT-Mediated Aqueous Emulsion Polymerization. *Macromolecules* **2011**, *44*, 4149–4158.
- (18) Warren, N. J.; Mykhaylyk, O. O.; Mahmood, D.; Ryan, A. J.; Armes, S. P. RAFT Aqueous Dispersion Polymerization Yields Poly(ethylene Glycol)-Based Diblock Copolymer Nano-Objects with Predictable Single Phase Morphologies. *J. Am. Chem. Soc.* **2014**, *136*, 1023–1033.
- (19) Cunningham, V. J.; Alswieleh, A. M.; Thompson, K. L.; Williams, M.; Leggett, G. J.; Armes, S. P.; Musa, O. M. Poly(glycerol monomethacrylate)–Poly(benzyl Methacrylate) Diblock Copolymer Nanoparticles via RAFT Emulsion Polymerization: Synthesis, Characterization, and Interfacial Activity. *Macromolecules* **2014**, *47*, 5613–5623.
- (20) Sun, J.-T.; Hong, C.-Y.; Pan, C.-Y. Recent Advances in RAFT Dispersion Polymerization for Preparation of Block Copolymer Aggregates. *Polym. Chem.* **2013**, 873–881.
- (21) Wan, W.-M.; Hong, C.-Y.; Pan, C.-Y. One-Pot Synthesis of Nanomaterials via RAFT Polymerization Induced Self-Assembly and Morphology Transition. *Chem. Commun.* **2009**, No. 39, 5883–5885.
- (22) Wan, W.-M.; Pan, C.-Y. One-Pot Synthesis of Polymeric Nanomaterials via RAFT Dispersion Polymerization Induced Self-Assembly and Re-Organization. *Polym. Chem.* **2010**, *1*, 1475.
- (23) Semsarilar, M.; Jones, E. R.; Blanazs, A.; Armes, S. P. Efficient Synthesis of Sterically-Stabilized Nano-Objects via RAFT Dispersion Polymerization of Benzyl Methacrylate in Alcoholic Media. *Adv. Mater.* **2012**, *24*, 3378–3382.
- (24) Wan, W.-M.; Sun, X.-L.; Pan, C.-Y. Morphology Transition in RAFT Polymerization for Formation of Vesicular Morphologies in One Pot. *Macromolecules* **2009**, *42*, 4950–4952.
- (25) Pei, Y.; Dharsana, N. C.; van Hensbergen, J. A.; Burford, R. P.; Roth, P. J.; Lowe, A. B. RAFT Dispersion Polymerization of 3-Phenylpropyl Methacrylate with poly[2-(Dimethylamino)ethyl Methacrylate] Macro-CTAs in Ethanol and Associated Thermoreversible Polymorphism. *Soft Matter* **2014**, *10*, 5787–5796.
- (26) Zhang, Q.; Zhu, S. Ionic Liquids: Versatile Media for Preparation of Vesicles from Polymerization-Induced Self-Assembly. *ACS Macro Lett.* **2015**, *4*, 755–758.
- (27) Kang, Y.; Pitto-Barry, A.; Willcock, H.; Quan, W.-D.; Kirby, N.; Sanchez, A. M.; O'Reilly, R. K. Exploiting Nucleobase-Containing Materials – from Monomers to Complex Morphologies Using RAFT Dispersion Polymerization. *Polym. Chem.* **2015**, *6*, 106–117.
- (28) Kang, Y.; Pitto-Barry, A.; Maitland, A.; O'Reilly, R. K. RAFT Dispersion Polymerization: A Method to Tune the Morphology of Thymine-Containing Self-Assemblies. *Polym. Chem.* **2015**, *6*, 4984–4992.
- (29) Pei, Y.; Sugita, O. R.; Thurairajah, L.; Lowe, A. B. Synthesis of Poly(stearyl Methacrylate-B-3-Phenylpropyl Methacrylate) Nanoparticles in N-Octane and Associated Thermoreversible Polymorphism. *RSC Adv.* **2015**, *5*, 17636–17646.
- (30) Fielding, L. A.; Derry, M. J.; Ladmiral, V.; Rosselgong, J.; Rodrigues, A. M.; Ratcliffe, L. P. D.; Sugihara, S.; Armes, S. P. RAFT Dispersion Polymerization in Non-Polar Solvents: Facile Production of Block Copolymer Spheres, Worms and Vesicles in N-Alkanes. *Chem. Sci.* **2013**, *4*, 2081–2087.
- (31) Zong, M.; Thurecht, K. J.; Howdle, S. M. Dispersion Polymerisation in Supercritical CO<sub>2</sub> Using Macro-RAFT Agents. *Chem. Commun.* **2008**, No. 45, 5942.
- (32) Thurecht, K. J.; Gregory, A. M.; Wang, W.; Howdle, S. M. “Living” polymer Beads in Supercritical CO<sub>2</sub>. *Macromolecules* **2007**, *40*, 2965–2967.
-

- (33) Mata, A.; Fleischman, A. J.; Roy, S. Characterization of Polydimethylsiloxane (PDMS) Properties for Biomedical Micro/nanosystems. *Biomed. Microdevices* **2005**, *7*, 281–293.
- (34) Bergeron, V.; Cooper, P.; Fischer, C.; Giermanska-Kahn, J.; Langevin, D.; Pouchelon, A. Polydimethylsiloxane (PDMS)-Based Antifoams. *Colloids Surfaces A Physicochem. Eng. Asp.* **1997**, *122*, 103–120.
- (35) Jakobsen, J.; Sanborn, D. M.; Winer, W. O. Pressure Viscosity Characteristics of a Series of Siloxane Fluids. *J. Lubr. Technol.* **1974**, *96*, 410.
- (36) Horii, Y.; Kannan, K. Survey of Organosilicone Compounds, Including Cyclic and Linear Siloxanes, in Personal-Care and Household Products. *Arch. Environ. Contam. Toxicol.* **2008**, *55*, 701–710.
- (37) Wang, R.; Moody, R. P.; Koniecki, D.; Zhu, J. Low Molecular Weight Cyclic Volatile Methylsiloxanes in Cosmetic Products Sold in Canada: Implication for Dermal Exposure. *Environ. Int.* **2009**, *35*, 900–904.
- (38) Lopez-Oliva, A. P.; Warren, N. J.; Rajkumar, A.; Mykhaylyk, O. O.; Derry, M. J.; Doncom, K. E. B.; Rymaruk, M. J.; Armes, S. P. Polydimethylsiloxane-Based Diblock Copolymer Nano-Objects Prepared in Nonpolar Media via RAFT-Mediated Polymerization-Induced Self-Assembly. *Macromolecules* **2015**, *48*, 3547–3555.
- (39) Trent, J. S.; Scheinbeim, J. I.; Couchman, P. R. Ruthenium Tetraoxide Staining of Polymers for Electron Microscopy. *Macromolecules* **1983**, *16*, 589–598.
- (40) Zhang, X.; Rieger, J.; Charleux, B. Effect of the Solvent Composition on the Morphology of Nano-Objects Synthesized via RAFT Polymerization of Benzyl Methacrylate in Dispersed Systems. *Polym. Chem.* **2012**, *3*, 1502–1509.
- (41) Rieger, J.; Stoffelbach, F.; Bui, C.; Alaimo, D.; Jérôme, C.; Charleux, B. Amphiphilic Poly(ethylene Oxide) Macromolecular RAFT Agent as a Stabilizer and Control Agent in Ab Initio Batch Emulsion Polymerization. *Macromolecules* **2008**, *41*, 4065–4068.
- (42) Blanazs, A.; Ryan, A. J.; Armes, S. P. Predictive Phase Diagrams for RAFT Aqueous Dispersion Polymerization: Effect of Block Copolymer Composition, Molecular Weight, and Copolymer Concentration. *Macromolecules* **2012**, *45*, 5099–5107.
- (43) Willcock, H.; O'Reilly, R. K. End Group Removal and Modification of RAFT Polymers. *Polym. Chem.* **2010**, *1*, 149–157.
- (44) Deletre, M.; Levesque, G. Kinetics and Mechanism of Polythioamidation in Solution. 1. Reaction of Mono- and Bis(dithioester)s with Excess Amine. *Macromolecules* **1990**, *23*, 4733–4741.
- (45) Tan, J.; Sun, H.; Yu, M.; Sumerlin, B. S.; Zhang, L. Photo-PISA: Shedding Light on Polymerization-Induced Self-Assembly. *ACS Macro Lett.* **2015**, *4*, 1249–1253.
- (46) Figg, C. A.; Simula, A.; Gebre, K. A.; Tucker, B. S.; Haddleton, D. M.; Sumerlin, B. S. Polymerization-Induced Thermal Self-Assembly (PITSA). *Chem. Sci.* **2015**, *6*, 1230–1236.
- (47) Blanazs, A.; Madsen, J.; Battaglia, G.; Ryan, A. J.; Armes, S. P. Mechanistic Insights for Block Copolymer Morphologies: How Do Worms Form Vesicles? *J. Am. Chem. Soc.* **2011**, *133*, 16581–16587.
- (48) Cunningham, V. J.; Armes, S. P.; Musa, O. M. Synthesis, Characterisation and Pickering Emulsifier Performance of Poly(stearyl methacrylate)–poly(N-2-(Methacryloyloxy)ethyl Pyrrolidone) Diblock Copolymer Nano-Objects via RAFT Dispersion Polymerisation in N-Dodecane. *Polym. Chem.* **2016**, *7*, 1882–1891.
- (49) Dzuy, N. Q.; Boger, D. V. Yield Stress Measurement for Concentrated Suspensions. *J. Rheol.* **1983**, *27*, 321–349.
- (50) Penfold, N. J. W.; Lovett, J. R.; Verstraete, P.; Smets, J.; Armes, S. P. Stimulus-Responsive Non-Ionic Diblock Copolymers: Protonation of a Tertiary Amine End-Group Induces Vesicle-to-Worm or Vesicle-to-Sphere Transitions. *Polym. Chem.* **2017**, *8*, 272–282.

**Chapter 3: Effect of Cross-linking on the  
Thermoresponsive Behaviour of PDMS-  
PDMA Nanoparticles in Silicone Oil**

### 3.1 Introduction

Since the discovery of block copolymer self-assembly around 50 years ago,<sup>1</sup> there has been significant interest in the potential applications of diblock copolymer nano-objects.<sup>2-4</sup> For example, block copolymer vesicles have been investigated for the controlled release of an active payload, and block copolymer spheres have been investigated as engine-oil additives.<sup>5-10</sup> Perhaps surprisingly, worm-like micelles have received relatively little attention compared to vesicles or spherical micelles. This may be due in part to the difficulties associated with synthesising worm-like micelles, which occupy much narrower phase space than spheres or vesicles.<sup>11-14</sup> Nevertheless, worm-like micelles have been recently examined for a number of applications. Discher and co-workers reported that poly(ethylene oxide)-b-poly( $\epsilon$ -caprolactone) (PEO-PCL) worms offered more efficient encapsulation and delivery of a hydrophobic drug than the corresponding spherical micelles.<sup>15</sup> Furthermore, Discher and co-workers also demonstrated that circulation times for worm-like micelles in rodents are almost an order of magnitude longer than for spherical micelles.<sup>16</sup>

In the last decade or so, the invention of PISA has facilitated the synthesis of diblock copolymer nanoparticles, at copolymer concentrations up to 50 % w/w.<sup>17-20</sup> This has alleviated many of the issues traditionally associated with block copolymer self-assembly, which typically requires dilute copolymer concentrations and post-polymerisation processing steps.<sup>3</sup> PISA syntheses are highly reproducible and enable the reliable targeting of spheres, worms, and vesicles.<sup>21,22</sup> In this context, worms have received considerable recent attention. For example, Canton *et al.* demonstrated that PGMA-PHPMA diblock copolymer worm gels can be used as storage media for human pluripotent stem cells.<sup>23</sup> Blanazs and co-workers exploited the worm-to-sphere transition of PGMA-PHPMA worms, that occurs upon cooling, to produce highly sterile, biocompatible hydrogels.<sup>24</sup>

A number of attempts have been made in recent years to improve the physical properties and functionality of nanoparticles prepared by PISA, either *in situ* or by a post-polymerisation modification step.<sup>25-28</sup> For example, Warren *et al.* synthesised PGMA-PHPMA worm gels with a disulfide bond incorporated within the PGMA stabiliser chains.<sup>26</sup> The intra-worm disulfide bonds were then cleaved and reformed to form inter-worm disulphide bonds, resulting in inter-worm cross-linking. Such worms formed significantly stronger gels. In related work, Ratcliffe and co-workers incorporated a disulfide bond into the core of PGMA-PHPMA worms.<sup>27</sup> When this

disulfide was cleaved, the volume fraction of the core-forming block was reduced, and a worm-to-sphere transition was observed.

Cross-linking is a commonly reported method by which to improve the properties of block copolymer micelles.<sup>29</sup> Typically, this can be achieved by either (i) shell cross-linking<sup>30</sup> or (ii) core cross-linking.<sup>29</sup> Shell cross-linked micelles are produced by cross-linking the corona layer.<sup>31–37</sup> However, these reactions are generally limited to dilute solution so as to avoid inter-particle cross-linking. Core cross-linking, on the other hand, usually avoids the issue of inter-particle cross-linking, because the reaction is compartmentalised within the micelle core.<sup>38,39</sup> This concept was first demonstrated almost 40 years ago, when polystyrene-stabilised polybutadiene micelles were cross-linked upon exposure to UV radiation.<sup>40</sup> More recently, a similar approach has been utilised by both Bates and co-workers.<sup>13</sup> and Antonietti and co-workers.<sup>41</sup>

For particles prepared *via* PISA, there are a number of different methods by which to produce core cross-linked micelles. Perhaps the most reported involves the copolymerisation of a small quantity of bifunctional monomer, such as ethylene glycol dimethacrylate (EGDMA) towards the end of the PISA synthesis.<sup>42–44</sup> This works very well for spherical micelles and vesicles, because they each occupy relatively broad phase space. As such, the change in block composition due to the cross-linking monomer does not normally lead to a change in morphology. However, for worms, which can occupy exceptionally narrow phase space,<sup>45</sup> cross-linking can shift the morphology across a phase boundary into a mixed phase.<sup>45</sup> One way to avoid this problem is through the use of more traditional organic chemistry. If the core-forming block contains appropriate functionality, then suitable reactants can be added to induce cross-linking. This was demonstrated by both Lovett *et al.*<sup>45</sup> and Penfold *et al.*,<sup>46</sup> who prepared worms with epoxy-functional cores *via* statistical copolymerisation of HPMA and GlyMA. By adding 3-aminopropyltriethoxysilane to such worms, the epoxide group on the GlyMA residues was ring-opened by the primary amine. Cross-linking then occurred *via* hydrolysis/condensation reactions between the trialkoxysilanes and the secondary hydroxyl groups on the HPMA residues. A slightly different strategy was utilised by Byard *et al.*, who prepared diblock copolymer spheres, worms and vesicles with poly(diacetone acrylamide) (PDAAM) cores.<sup>47</sup> The introduction of a bifunctional amine, adipic acid dihydrazide, to such nanoparticles resulted in imine formation within the core and cross-linking. A similar strategy was also employed by Hatton *et al.*, for the cross-linking of PGMA-stabilised PGlyMA spherical nanoparticles using diamines.<sup>48</sup>

The majority of the published literature describes the cross-linking of particles in polar media, usually water. There are relatively few reports of cross-linking block copolymer nanoparticles in non-polar media.<sup>49</sup> In Chapter 2, PDMS-PDMA block copolymer spheres, worms or vesicles were prepared in D5 silicone oil. Moreover, the core-forming block of such nano-objects contained many tertiary amine residues. In this Chapter, the possibility of cross-linking these nanoparticles with a bifunctional reagent, 1,2-bis(2-iodoethoxy)ethane (BIEE) is explored (**Figure 3.1**). Particular attention is paid to cross-linking worms and the effect on their physical properties, namely their gel strength, CGC and thermoresponsive behaviour.

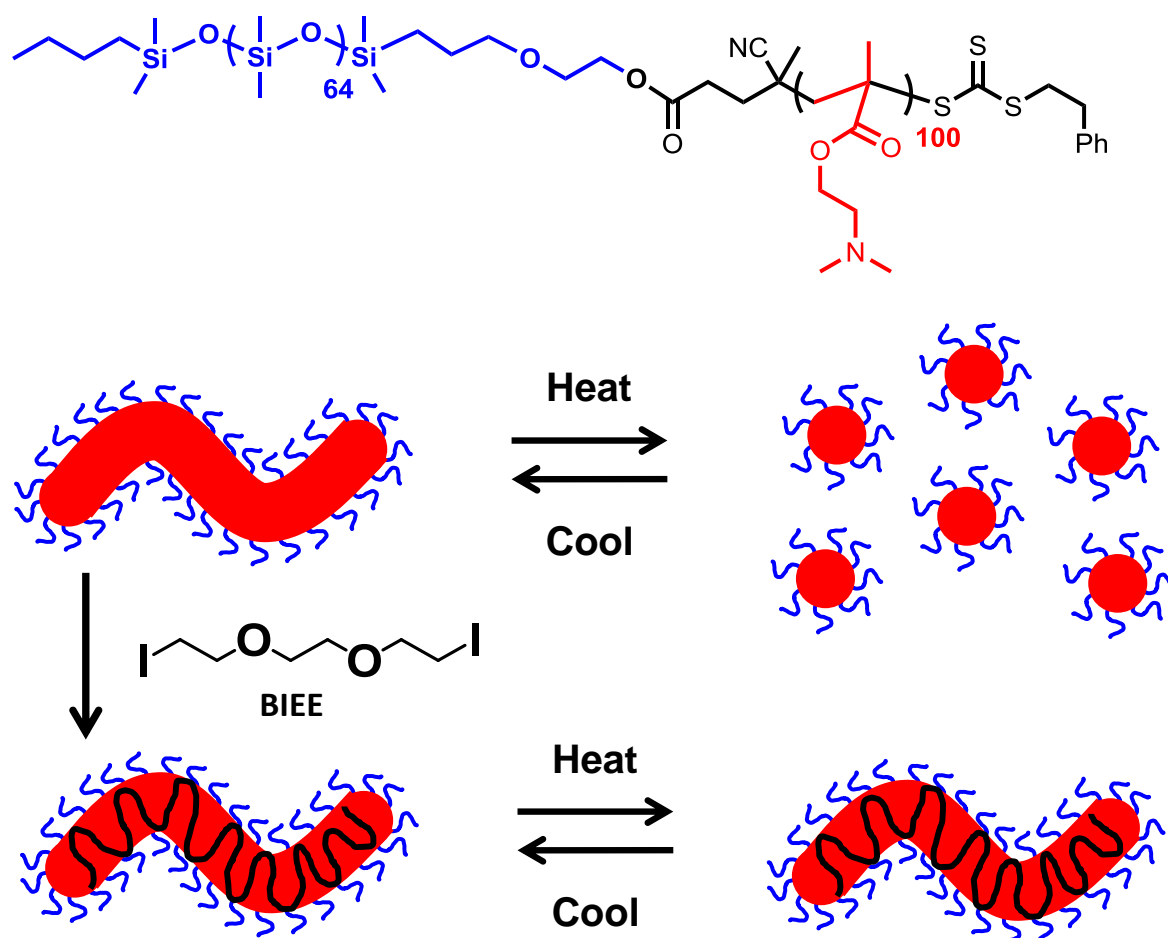


**Figure 3.1:** Chemical structure of a PDMS<sub>66</sub>-PDMA<sub>100</sub> diblock copolymer and a schematic representation of PDMS<sub>66</sub>-PDMA<sub>100</sub> worm cross-linked using BIEE. The precursor linear worms are thermoresponsive, whereas the cross-linked worms are not thermoresponsive.

## 3.2 Experimental

### 3.2.1 Materials

Polydimethylsiloxane (PDMS<sub>66</sub>-OH; monocabrbinol terminated,  $M_n = 5,000 \text{ g mol}^{-1}$ , mean degree of polymerisation = 66) was purchased from Fluorochem (UK) and used as received. D5 was provided by Scott Bader Company Ltd (UK). Trigonox 21s (T21s) was purchased from AkzoNobel (The Netherlands). 2-(Dimethylamino)ethyl methacrylate (DMA), dichloromethane (DCM), triethylamine (TEA), butylated hydroxytoluene (BHT), N,N'-dicyclohexylcarbodiimide (DCC), and 4-dimethylaminopyridine (DMAP) were purchased from Sigma Aldrich (UK). Toluene-d<sub>8</sub>, chloroform-d<sub>2</sub>, and chloroform-d were obtained from Goss Scientific (UK). 4-Cyano-4-(2-phenylethanesulfanylthiocarbonyl)sulfanylpentanoic acid (PETTC) was synthesised according to the protocol described in Chapter 2. DMA was passed through basic alumina prior to use to remove its inhibitor. All other reagents were used as received unless otherwise stated.

### 3.2.2 Methods

#### Synthesis of PDMS<sub>66</sub>-PDMA<sub>x</sub> diblock copolymer nanoparticles in D5 silicone oil

PDMS<sub>66</sub>-PDMA<sub>x</sub> nanoparticles were synthesised in D5 silicone oil at 25 % w/w, according to the protocol described in Chapter 2. In this Chapter, spheres, worms and vesicles were synthesised, where  $x = 49, 100$  and  $176$  respectively.

#### Cross-linking protocol

A typical cross-linking protocol was carried out as follows: PDMS<sub>66</sub>-PDMA<sub>49</sub> spherical nanoparticles, prepared at 25 % w/w in D5 silicone oil, were weighed into a vial (1.00 g, 19  $\mu\text{mol}$  polymer). To the nanoparticle dispersion, BIEE was added (26  $\mu\text{l}$ , 0.15 mmol, BIEE/PDMA molar ratio = 0.15) For spheres and vesicles, BIEE was added with gentle magnetic stirring. For worms, gentle stirring with a spatula was required to aid dissolution within the gel. Targeted degrees of cross-linking ranged from 5 mol % to 15 mol % relative to the DMA residues.

### 3.2.3 Characterisation

#### Gel permeation chromatography

The THF GPC set-up comprised an Agilent Infinity series degasser and pump, two Agilent PLgel 5  $\mu\text{m}$  MIXED-C columns in series and a refractive index detector. The flow rate was fixed at 1.0  $\text{ml min}^{-1}$  and the temperature fixed at 30 ° C. The THF eluent contained trimethylamine (2.0 % w/w) and butylated hydroxytoluene (0.05 % w/v). The GPC was calibrated with twelve near-

monodisperse poly(methyl methacrylate) standards, ranging from 800 g mol<sup>-1</sup> up to 2,200,000 g mol<sup>-1</sup>.

#### **<sup>1</sup>H NMR spectroscopy**

To determine the DMA monomer conversions, spectra were recorded at 20 °C in chloroform-d using a Bruker Avance III HD 400 spectrometer operating at 400 MHz. Typically, 64 scans were averaged per spectrum. For the kinetic study of vesicle cross-linking, aliquots were removed from the reaction at 25 % w/w and diluted to 2.5 % w/w in chloroform. A coaxial insert, which contained toluene-d<sub>8</sub> as a lock solvent, and 0.1 M pyridine as a calibrant, was added to each NMR tube prior to analysis. Variable temperature <sup>1</sup>H NMR experiments were performed using a Bruker Avance 111 HD spectrometer operating at 500 MHz. Samples were equilibrated for 15 minutes at each temperature prior to spectra acquisition. For each experiment, a coaxial insert, which contained toluene-d<sub>8</sub> as a lock solvent, and 0.25 M pyridine as a calibrant was added to the NMR tube. In addition, the copolymer concentration was fixed at 5 % w/w in D<sub>5</sub>.

#### **Transmission electron microscopy**

Transmission electron microscopy (TEM) studies were conducted using a FEI Tecnai G2 spirit instrument operating at 80 kV and equipped with a Gatan 1k CCD camera. Copper TEM grids were surface-coated in-house to yield a thin film of amorphous carbon. The grids were then loaded with dilute copolymer dispersions (0.05 - 0.25 % w/w). Prior to imaging, each grid was exposed to ruthenium(IV) vapour for 7 minutes at ambient temperature, in order to improve contrast. The ruthenium oxide stain was prepared by adding ruthenium(II) oxide (0.30 g) to water (50 g), to form a slurry. Then, sodium periodate (2.0 g) was added while stirring to form a yellow solution of ruthenium(IV) oxide within 1 minute.<sup>50</sup>

#### **Dynamic light scattering**

DLS studies were performed using a Zetasizer Nano-ZS instrument (Malvern Instruments, UK) at 25 °C at a fixed scattering angle of 173°. Typically, copolymer dispersions were diluted to a concentration of 0.25 % w/w prior to analysis. The intensity-average diameter and polydispersity (PDI) of the diblock copolymer particles were calculated by cumulants analysis of the experimental correlation function using Dispersion Technology Software version 6.20. Data were averaged over ten runs each of thirty seconds duration. A heating rate of 2 °C min<sup>-1</sup> was used for variable temperature DLS measurements.

### **Oscillatory rheology**

An AR-G2 rheometer equipped with a 40 mm 2° aluminium cone was used for all measurements. The storage and loss moduli were determined, *via* oscillatory rheometry, as a function of temperature at a fixed angular frequency of 1.0 rad s<sup>-1</sup> and a fixed angular frequency of 1.0 %. In all cases, the gap between the cone and plate was 58 μm, and the heating rate of heating was 2 °C min<sup>-1</sup>.

### **Shear-induced polarised light imaging**

Shear alignment experiments were conducted using a mechano-optical rheometer (Anton Paar Physica MCR301 with SIPLI attachment). Measurements were performed using a plate–plate geometry composed of a 25 mm polished steel plate and a fused quartz plate connected to a variable temperature Peltier system. The gap between plates was set at 1 mm for all experiments and the shear rate fixed at 10 s<sup>-1</sup>. An additional Peltier hood was used to ensure good control of the sample temperature. Sample illumination was achieved using an Edmund Optics 150 W MI-150 high-intensity fiberoptic white light source. The polariser and analyser axes were crossed at 90° in order to obtain polarized light images (PLIs), which were recorded using a colour CCD camera (Lumenera Lu165c). A heating rate of 2 °C min<sup>-1</sup> was used in all cases.

### **Small-angle X-ray scattering**

SAXS patterns were recorded at a synchrotron source (ESRF, station ID02, Grenoble, France) using monochromatic X-ray radiation (wavelength  $\lambda = 0.0995$  nm, with  $q$  ranging from 0.004 to 2.5 nm<sup>-1</sup>, where  $q = 4\pi \sin \theta/\lambda$  is the length of the scattering vector and  $\theta$  is one-half of the scattering angle) and a Rayonix MX-170HS Kodak CCD detector. Measurements were conducted on 1.0% w/w dispersions. A heating rate of 30 °C min<sup>-1</sup> was utilised for each experiment. X-ray scattering data were reduced and normalised using standard routines by the beamline.

## **3.3 Results and discussion**

### **3.3.1 Synthesis of PDMS<sub>66</sub>-PDMA<sub>x</sub> diblock copolymer nanoparticles in D5**

A PDMS<sub>66</sub> macro-CTA was prepared by the DCC/DMAP mediated esterification of monocarbinol-terminated PDMS<sub>66</sub> using PETTC, as described in Chapter 2. <sup>1</sup>H NMR and UV/Vis spectroscopy indicated a mean degree of esterification of 92 ± 4 % and 94 ± 5 % respectively. The resulting macro-CTA was then chain-extended with DMA in D5 at 25 % w/w solids, targeting a PDMA DP of 50, 105 or 190. The resulting three different diblock copolymers are summarised in **Table 3.1**.

### Chapter 3: Effect of Cross-linking on the Thermoresponsive Behaviour of PDMS-PDMA Nanoparticles in Silicone Oil

Target composition	Conv. <sup>a</sup>	Actual DMA DP	GPC <sup>b</sup>		TEM morphology	Z-Average diameter. <sup>c</sup> /nm (PDI)
			M <sub>n</sub> / g mol <sup>-1</sup>	Đ		
PDMS <sub>66</sub> -PDMA <sub>50</sub>	98	49	14,400	1.21	Spheres	28 (0.01)
PDMS <sub>66</sub> -PDMA <sub>105</sub>	95	100	22,400	1.22	Worms	187 (0.19)
PDMS <sub>66</sub> -PDMA <sub>190</sub>	93	176	33,300	1.36	Vesicles	436 (0.17)

<sup>a</sup><sup>1</sup>H NMR in chloroform-d, <sup>b</sup>THF GPC, <sup>c</sup>DLS

**Table 3.1:** Summary of conversions, GPC, TEM morphology and DLS data obtained for a series of PDMS<sub>66</sub>-PDMA<sub>x</sub> diblock copolymer nanoparticles, prepared *via* RAFT dispersion polymerisation of DMA in D5 at 25 % w/w and 90 °C.

#### 3.3.2 Thermoresponsive behaviour of PDMS<sub>66</sub>-PDMA<sub>100</sub> worms

The thermoresponsive nature of many diblock copolymer nanoparticles prepared *via* PISA is well-documented. Typically, such a transition arises from surface plasticisation of the core-forming block upon a change in temperature, *via* ingress of solvent. As a result, the effective stabiliser volume fraction increases and a morphological transition, typically from worms to spheres, is observed. For aqueous PISA formulations, the nanoparticle core typically comprises a polymer with LCST-like behaviour.<sup>51</sup> Therefore, a worm-to-sphere transition is observed on cooling. The opposite behaviour is usually observed for particles prepared in non-aqueous media, since the core-forming block exhibits UCST. Hence, a worm-to-sphere transition is observed on heating.<sup>52</sup> To investigate whether PDMS<sub>66</sub>-PDMA<sub>100</sub> worms in D5 exhibited thermoresponsive behaviour, a 25 % w/w dispersion was heated to 100 °C for 30 min. At ambient temperature, this concentrated worm dispersion formed a free-standing gel, owing to multiple inter-worm contacts.<sup>53</sup> However, a free-flowing fluid was obtained at 100 °C. Moreover, this thermal transition proved to be reversible, with regelation being observed within 1 h on cooling back to 25 °C. TEM studies performed on 0.1 % w/w dispersions of PDMS<sub>66</sub>-PDMA<sub>100</sub> worms confirmed that this degelation behaviour was the result of a worm-to-sphere transition. For TEM studies at high temperature, a portion of the gel was first heated to 100 °C to induce degelation. The resulting fluid was then diluted to 0.1 % w/w with D5 also at 100 °C. Typically, dilution to such a low copolymer concentration serves to kinetically trap the morphology that is present at high temperature,<sup>52</sup> thus preventing a sphere-to-worm transition from occurring on cooling. The resulting dilute dispersion was then cooled to approximately 7 °C, in order to prepare the TEM grids. Ideally, the dilute would be loaded onto the TEM grid at 100 °C to image the high-temperature morphology directly. However, given that the T<sub>g</sub> of the PDMA core-forming block

lies close to ambient temperature,<sup>54</sup> attempts to image the samples by this alternative protocol were always unsuccessful.

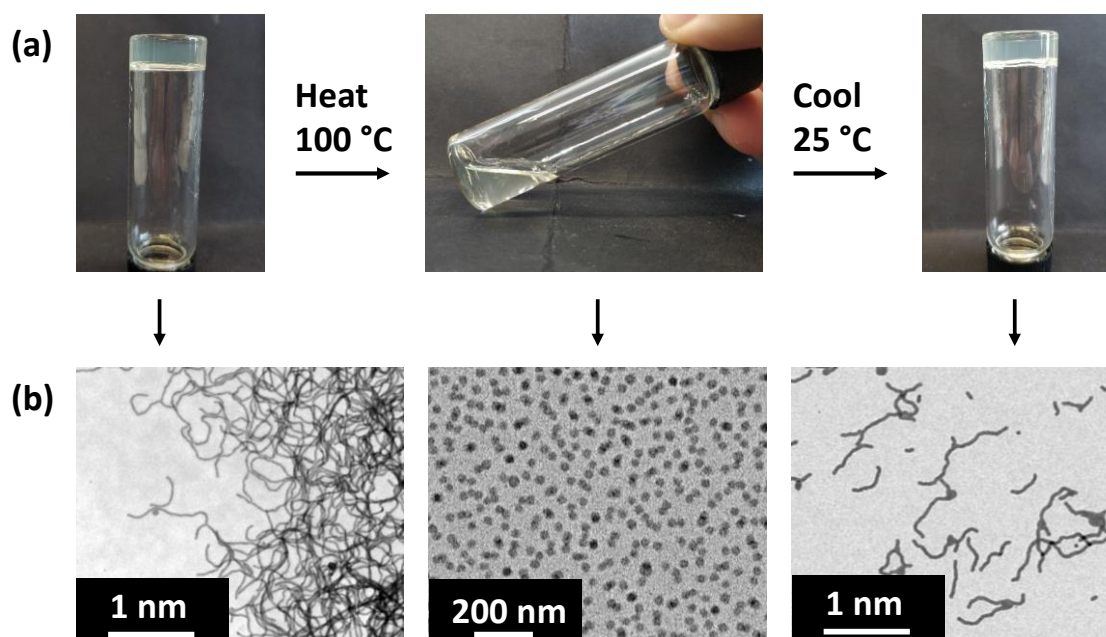


**Figure 3.2:** (a) Reversible (de)gelation observed on heating a 25 % w/w dispersion of PDMS<sub>66</sub>-PDMA<sub>100</sub> worms in D5 silicone oil at 100 °C for 30 min, followed by cooling back to 25 °C. (b) Accompanying TEM images for the thermal transitions shown in (a).

Variable temperature <sup>1</sup>H NMR experiments were performed to investigate this thermoresponsive behaviour further. In this experiment, a 5 % w/w dispersion of PDMS<sub>66</sub>-PDMA<sub>100</sub> worms was heated from 20 °C to 100 °C, and the solvation of the PDMA core-forming block was monitored relative to a pyridine standard contained within a coaxial insert (**Figure 3.3**). At temperatures above 80 °C, the signal due to the six dimethylamino protons at around 2.5 ppm (labelled b in **Figure 3.3**) become significantly more intense relative to the pyridine signals observed at 8.5 ppm. This indicates that the PDMA core-forming block becomes increasingly solvated by D5 at elevated temperatures. Moreover, this change in solvation was reversible, with desolvation of the PDMA core-forming block being observed upon cooling back to 20 °C. Similar behaviour was observed by Fielding *et al.* upon heating block copolymer worms comprising PBzMA cores in deuterated *n*-dodecane.<sup>52</sup> It was hypothesised that the reversible surface plasticisation of the PBzMA core-forming block in hot *n*-dodecane was the driving force behind the worm-to-sphere transition. This shifted the relative volume fractions of the core and stabiliser such that spherical micelles became the preferred morphology. Solvation of the PDMA block in D5 is directly analogous, suggesting that the surface plasticisation of the PDMA core by hot D5 is the driving force for the observed worm-to-sphere transition.

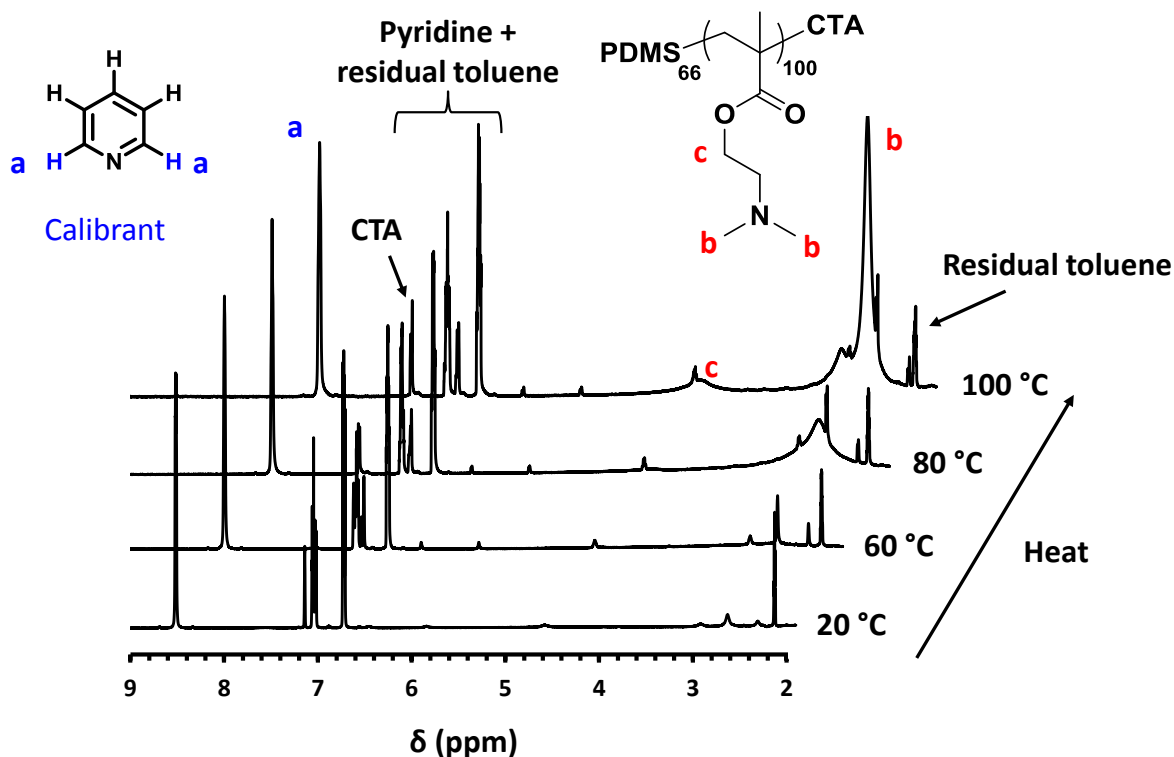


**Figure 3.3:** <sup>1</sup>H NMR spectra recorded at various temperatures for a 5.0 % w/w dispersion of PDMS<sub>66</sub>-PDMA<sub>100</sub> diblock copolymer worms in D<sub>5</sub>. A coaxial insert was also present in the tube, which contained toluene-d<sub>8</sub> as a lock solvent, and pyridine as a calibrant.

### 3.3.3 Cross-linking PDMS<sub>66</sub>-PDMA<sub>100</sub> worms with BIEE

Almost 20 years ago, Armes and co-workers demonstrated that BIEE could be used to prepare *shell* cross-linked PDMA-stabilised micelles, according to the Menshutkin reaction, in both water and *n*-hexane.<sup>49,55–58</sup> In this protocol, the BIEE quaternises the tertiary amine functional groups present on the DMA residues. When this reaction occurs inter-chain rather than intra-chain, the micelles become cross-linked. To examine whether the same strategy could be used to prepare core cross-linked micelles in this case, BIEE was added to PDMS<sub>66</sub>-PDMA<sub>100</sub> worm-gels directly at 25 % w/w. In this initial scoping experiment, 15 mol % BIEE was added relative to the DMA residues in the core. The gel was stirred with a spatula to incorporate all of the BIEE and allowed to stand at ambient temperature for 3 days. On heating this gel to 100 °C, no degelation was observed (**Figure 3.4a**), which suggested that the worm-to-sphere transition has been prevented. This was confirmed by TEM studies which indicated that worms are present at room temperature and remained intact at 100 °C (**Figure 3.4b**).

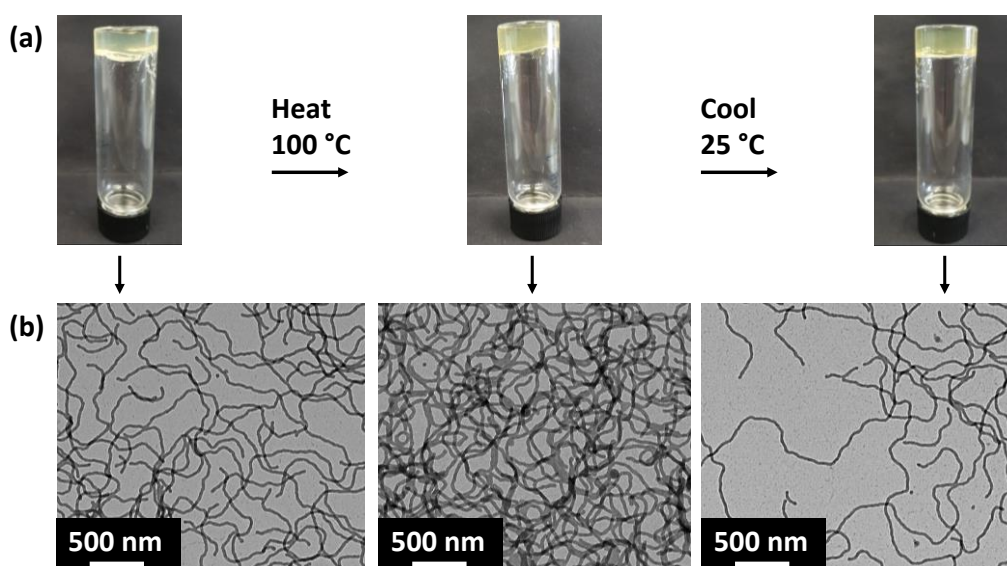


**Figure 3.4:** (a) Digital photographs of vials containing 25 % w/w PDMS<sub>66</sub>-PDMA<sub>100</sub> worm gels w/w cross-linked using 15 mol % BIEE relative to the DMA residues (left) ambient temperature, (middle) 100 °C and (right) cooled to 25 °C. (b) Corresponding TEM images obtained for the cross-linked PDMS<sub>66</sub>-PDMA<sub>100</sub> worms at each temperature, indicating the lack of a worm-to-sphere transition.

Next, a 5.0 % w/w dispersion of the cross-linked PDMS<sub>66</sub>-PDMA<sub>100</sub> worms in D<sub>5</sub>, was heated from 20 °C to 100 °C and analysed by variable temperature <sup>1</sup>H NMR spectroscopy (**Figure 3.5**).

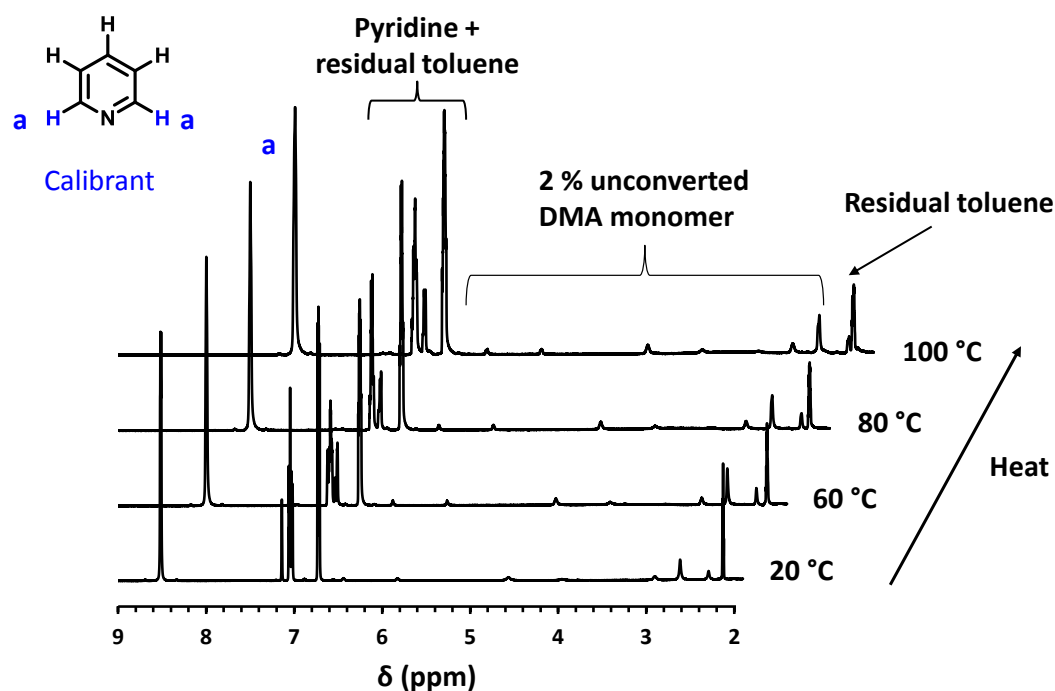


**Figure 3.5:** <sup>1</sup>H NMR spectra recorded at different temperatures upon a 5 % w/w dispersion of PDMS<sub>66</sub>-PDMA<sub>100</sub> diblock copolymer worms in D<sub>5</sub>, cross-linked at 5 % w/w using 15 mol % BIEE, relative to the DMA residues. A coaxial insert was also present in the NMR tube, which contained toluene-d<sub>8</sub> as a lock solvent, and pyridine as a calibrant.

Perhaps surprisingly, the cross-linked PDMA core-forming block displays no observable solvation by the D5 solvent, even at temperatures up to 100 °C. Therefore, the cross-linked worms remain essentially unswollen at elevated temperatures. This suggests that cross-linking is extensive. Moreover, as cross-linking proceeds and quaternary amines are formed in the worm core, a build-up of cationic charge must occur. Due to the low relative permittivity of silicones (~ 2) they are very poor solvents for such cationic polymers.

### 3.3.4 Kinetics of cross-linking

To determine the minimum time taken for the cross-linking to become sufficient to covalently stabilise the copolymer morphology, a kinetic study was performed using  $^1\text{H}$  NMR spectroscopy (Figure 3.6).

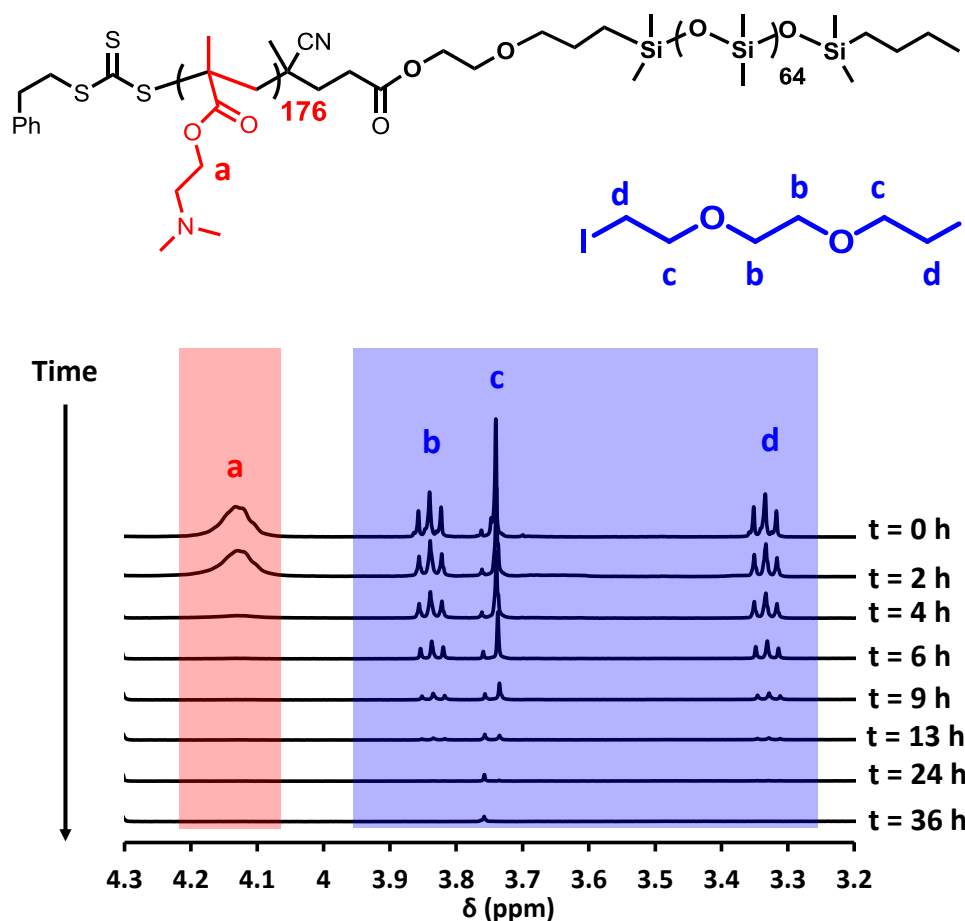


**Figure 3.6:**  $^1\text{H}$  NMR spectra recorded after various intervals at 20 °C for the reaction of PDMS<sub>66</sub>-PDMA<sub>176</sub> diblock copolymer vesicles with BIEE cross-linker, 15 mol % relative to the DMA residues. The reaction was performed at 25 % w/w in D5 silicone oil and diluted to 2.50 % w/w in chloroform for  $^1\text{H}$  NMR analysis. A coaxial tube was inserted containing toluene-d<sub>8</sub> as a lock solvent and 0.1 M pyridine as a calibrant. The gradual disappearance of the core-forming block and the BIEE signals indicated the onset of cross-linking.

In this experiment, a 25 % w/w dispersion of PDMS<sub>66</sub>-PDMA<sub>175</sub> vesicles was cross-linked using 15 mol % BIEE in D5. Vesicles were selected instead of worms because their free-flowing nature facilitated thorough mixing of the BIEE reagent and convenient dissolution/dispersion in the chloroform, required for <sup>1</sup>H NMR analysis. Aliquots were removed at regular intervals from the reaction mixture and diluted 10-fold to 2.5 % w/w in chloroform, i.e. a good solvent for both blocks.

Prior to the onset of cross-linking, the PDMS<sub>66</sub>-PDMA<sub>175</sub> vesicles were fully dissolved when diluted with chloroform. This was expected given this is a good solvent for both the PDMS<sub>66</sub> stabiliser and the PDMA<sub>176</sub> core-forming block. Hence, the oxymethylene signal at ~ 4.15 ppm, assigned to the PDMA<sub>176</sub> (labelled a, **Figure 3.6**) can be seen in the <sup>1</sup>H NMR spectrum. However, as cross-linking proceeded the vesicular morphology became more resistant to dissolution after dilution with chloroform. Thus, progressive attenuation of the core-forming PDMA signal at 4.15 ppm was observed over 36 h. The gradual loss of the BIEE signals was also observed as the BIEE became incorporated within the vesicle membrane. The integrated signals at 4.15 ppm, and the signals at 3.9 – 3.3 ppm due to the PDMA core-forming block and the BIEE respectively (labelled a and b-d **Figure 3.6**), are shown as a function of reaction time in **Figure 3.7**. Each spectrum was calibrated against a pyridine standard contained within a coaxial insert.

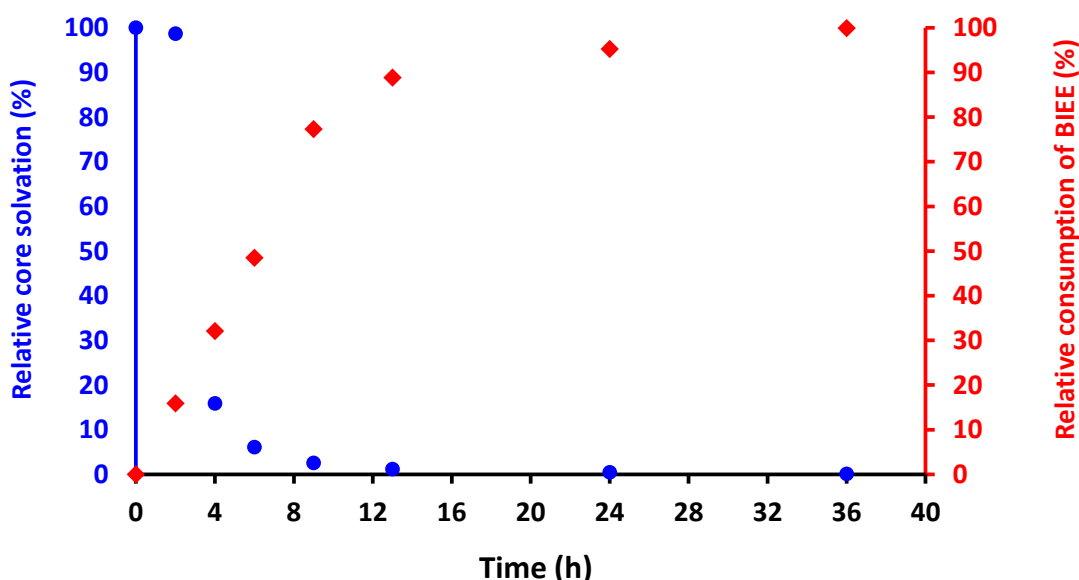


**Figure 3.7:** Kinetics of cross-linking PDMS<sub>66</sub>-PDMA<sub>176</sub> diblock copolymer vesicles with BIEE cross-linker, 15 mol % relative to the DMA residues. The solvation of the core was determined using the signal at 4.15 ppm in the <sup>1</sup>H NMR spectrum, due to the two protons next to the ester group in DMA. The consumption of BIEE was monitored using the signal at 3.3 ppm due to the protons adjacent to the iodine. Each signal was calibrated relative to 0.1 M pyridine in a toluene-d<sub>8</sub> lock solvent, contained within a coaxial NMR tube insert.

Almost no change in core solvation was observed after 2 h, despite almost 16 % of the BIEE being consumed during this time period. This could indicate that at low levels of cross-linking; the copolymer morphology is not sufficiently robust to withstand dispersion in a good solvent for both blocks. Or, it could be that during this time period, the BIEE has only reacted once and therefore no actual cross-linking has occurred. Regardless, after 4 h there is a dramatic reduction in the degree of core solvation which corresponds to 32 % BIEE consumption, indicating cross-linking. Approximately 13 h is required for all of the PDMA core signals to completely disappear from the  $^1\text{H}$  NMR spectra, and 36 h for all of the BIEE to react.

In addition to  $^1\text{H}$  NMR spectroscopy, these kinetic samples were also analysed by DLS after further dilution to 0.25 % w/w in chloroform. Two parameters were monitored (i) the derived count rate and (ii) the Z-average diameter. Each of these is shown plotted vs. reaction time in **Figure 3.8**

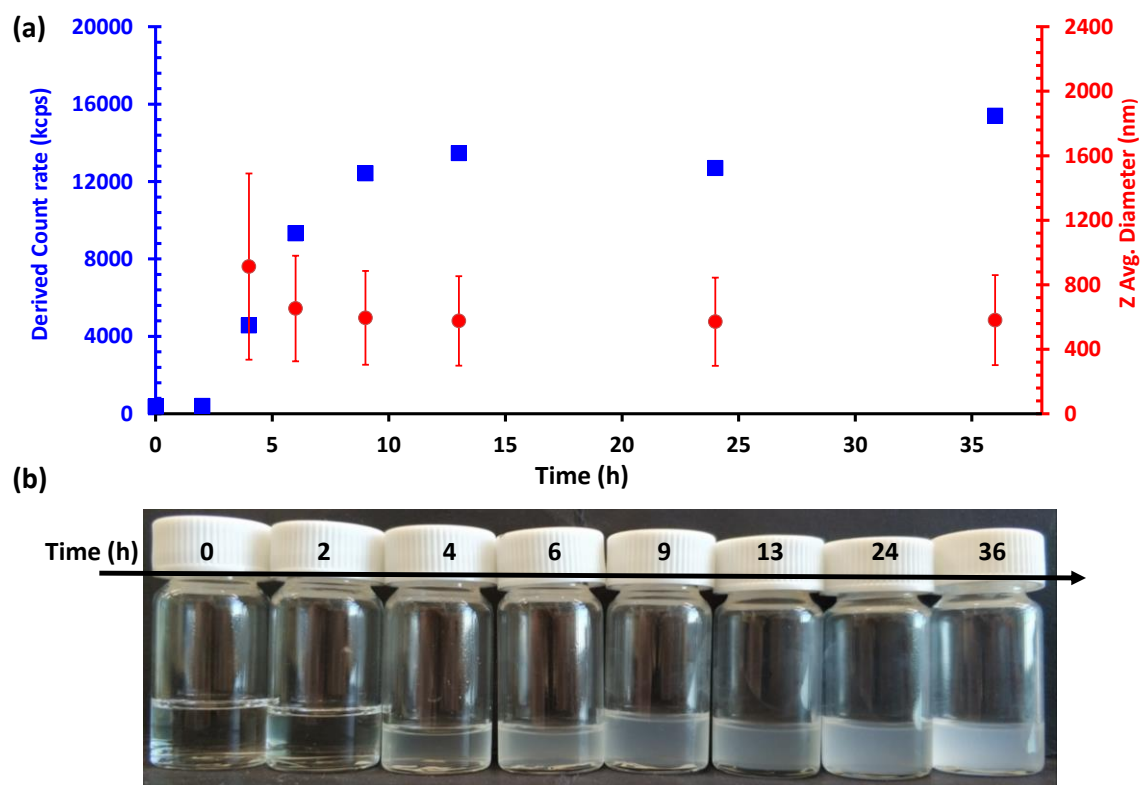


**Figure 3.8:** (a) DLS analysis of the extent of cross-linking of PDMS<sub>66</sub>-PDMA<sub>176</sub> vesicles at 25 % w/w in D5 using BIEE (15 mol % relative to the DMA residues) at 20 °C. Aliquots were removed at regular intervals, diluted 100-fold to 0.25 % w/w in chloroform and analysed *via* DLS. The derived count rate and Z-average diameter are shown against time. (b) Digital photographs of each 0.25 % w/w aliquot used for DLS analysis

### Chapter 3: Effect of Cross-linking on the Thermoresponsive Behaviour of PDMS-PDMA Nanoparticles in Silicone Oil

In a DLS experiment, the derived count rate is an indication of the scattered light intensity. As such, it typically increases with particle concentration and/or particle diameter. At short cross-linking reaction times (< 2 h), a relatively low derived count rate was observed (~ 400 kcps), suggestive of dissolved chains. This is consistent with the <sup>1</sup>H NMR experiment which indicates that despite partial consumption of the BIEE, the vesicles remain fully soluble in chloroform. After 4 h, the derived count rate increases by an order of magnitude, which indicates the presence of particles. The mean vesicle diameter at this stage is relatively large (~ 900 nm). Presumably, this is because they are only lightly cross-linked and therefore highly swollen. As the reaction time increases, the derived count rate plateaus at ~ 15,000 kcps, while the Z-average diameter stabilises at 580 nm. Perhaps surprisingly, the large reduction in particle diameter observed between 4 and 9 h seems to be correlated with a higher derived count rate. This is most likely because the refractive index of the lightly cross-linked, highly-swollen vesicles is more similar to that of the chloroform solvent than the less swollen, highly cross-linked smaller vesicles. As a result, they scatter less incident light despite their larger size. Following this kinetic study both PDMS<sub>66</sub>-PDMA<sub>49</sub> spheres and PDMS<sub>66</sub>-PDMA<sub>100</sub> worms were cross-linked with 15 mol % BIEE. After 36 h, the resulting cross-linked particles were diluted to 0.25 % w/w and analysed *via* DLS in either D5 or chloroform, the results are summarised in **Table 3.2**.

Copolymer (morphology)	Before cross-linking				After cross-linking			
	D5		Chloroform		D5		Chloroform	
	Diam. / nm (PDI)	Derived Counts / kcps	Diam. / nm	Derived Counts / kcps	Diam. / nm (PDI)	Derived Counts / kcps	Diam. / nm (PDI)	Derived Counts / kcps
PDMS <sub>66</sub> - PDMA <sub>49</sub> (spheres)	28 (0.03)	1,728	14	386	29 (0.02)	3,460	32 (0.03)	1,458
PDMS <sub>66</sub> - PDMA <sub>100</sub> (worms)	448 (0.34)	12,800	65	82	543 (0.37)	32,000	564 (0.47)	12,296
PDMS <sub>66</sub> - PDMA <sub>176</sub> (vesicles)	436 (0.17)	10,980	89	376	441 (0.19)	23,332	581 (0.23)	13,465

**Table 3.2:** Summary of DLS data obtained both before and after BIEE cross-linking for PDMS<sub>66</sub>-PDMA<sub>x</sub> nanoparticles (where x = 49, 100 or 176 respectively) in either D5 or chloroform. In all cases the copolymer concentration was fixed at 0.25 % w/w.

Inspecting **Table 3.2**, low derived count rates always result when dispersing non-cross-linked particles in chloroform. This indicates minimal scattering from each solution, which is consistent with dissolved copolymer chains. Conversely, much higher count rates are observed when dispersing cross-linked particles in chloroform, suggesting that such particles are remaining intact. Similarly, larger diameters are obtained for each type of cross-linked particle when dispersed in chloroform vs. D5, which may indicate some slight swelling of the PDMA core-forming block by chloroform. Finally, each dispersion reported in **Table 3.2** was also analysed *via* TEM (see **Figure 3.9**).

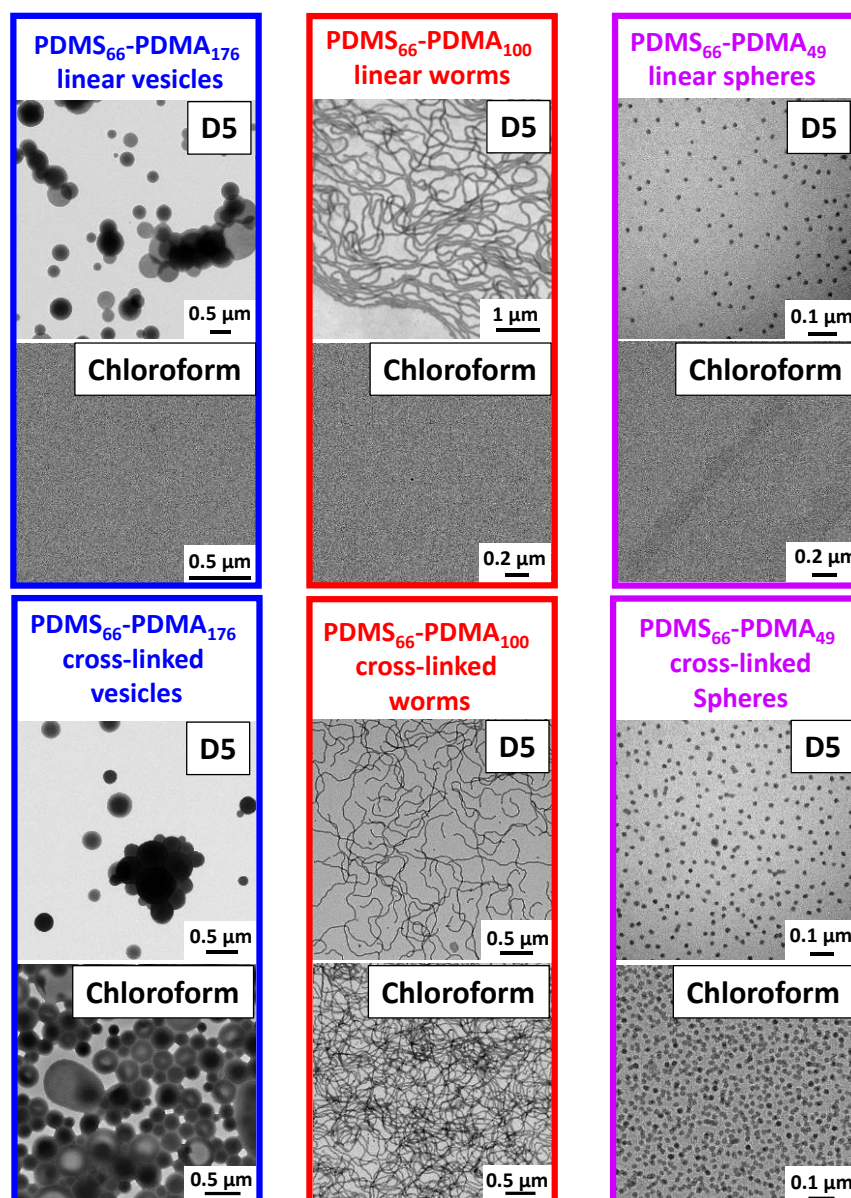


**Figure 3.9:** TEM images obtained for dilute dispersions of PDMS<sub>66</sub>-PDMA<sub>x</sub> diblock copolymer nanoparticles (where x = 49, 100 or 176, corresponding to spheres, worms or vesicles respectively). The upper six images represent non cross-linked nanoparticles. The lower six images represent nanoparticles cross-linked with 15 mol % BIEE, relative to the PDMA core-forming block at 20 °C for 36 h.

---

Inspecting **Figure 3.9**, it is clear that the cross-linked nanoparticles are sufficiently robust to retain their morphology when diluted in chloroform. Conversely, when the non cross-linked samples are imaged in chloroform, no particles can be observed. This confirms complete particle dissolution upon dilution with chloroform.

### 3.3.5 Variable temperature DLS

In addition to TEM, variable temperature DLS is a useful technique for monitoring morphological transitions, or the lack thereof, at dilute concentrations. In this study, DLS was used to probe the effect of heating a 0.25 % w/w dispersion of PDMS<sub>66</sub>-PDMA<sub>100</sub> diblock copolymer worms (**Figure 3.10**), and the corresponding cross-linked worms (**Figure 3.11**), to 90 °C (the limit of the instrument) in D5 silicone oil.

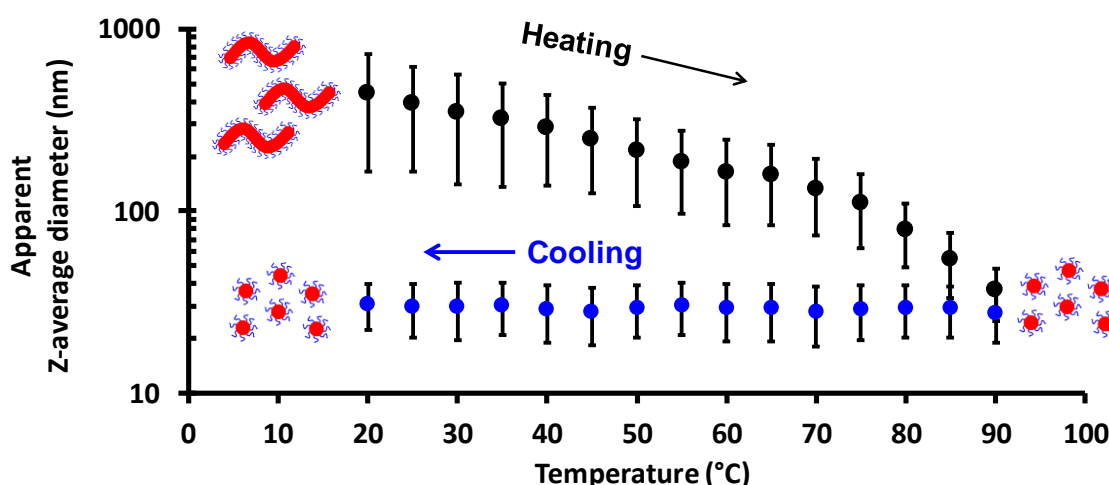


**Figure 3.10:** Variable temperature DLS experiment conducted on a 0.25 % w/w dispersion of PDMS<sub>66</sub>-PDMA<sub>100</sub> worms, subject to a 20 °C – 90 °C – 20 °C thermal cycle. The inset schematic cartoons represent the copolymer morphology at each temperature. The error bars represent one standard deviation of the apparent Z-average diameter, rather than experimental error.

At this point, it is important to emphasise that the Stokes-Einstein equation (equation (1.16)), used for DLS, is only strictly valid for spherical particles. If a non-spherical object such as a worm-like micelle is analysed by DLS, then a spherical-equivalent diameter is reported. In other words, the diameter of a sphere that possesses the same diffusion coefficient as the anisotropic particles being analysed. Nevertheless, this information still provides a useful measure of the change in overall size. At 20 °C, the worms possess an apparent Z-average diameter of  $480 \pm 280$  nm. As this dispersion is heated to 90 °C, the Z-average diameter gradually decreases to  $37 \pm 11$  nm which is consistent with a worm-to-sphere transition. On cooling back to 20 °C, the Z-average diameter remains roughly constant at  $\sim 40$  nm, indicating that the worms do not reform. This

observation is consistent with reported PISA literature, which suggests that the worm-to-sphere transition is irreversible for methacrylic diblock copolymer worms in non-polar media, when conducted at sufficiently dilute concentration.<sup>52</sup> A similar experiment was performed upon a 0.25 % w/w dispersion of PDMS<sub>66</sub>-PDMA<sub>100</sub> worms cross-linked with 15 mol % BIEE relative to the DMA residues.

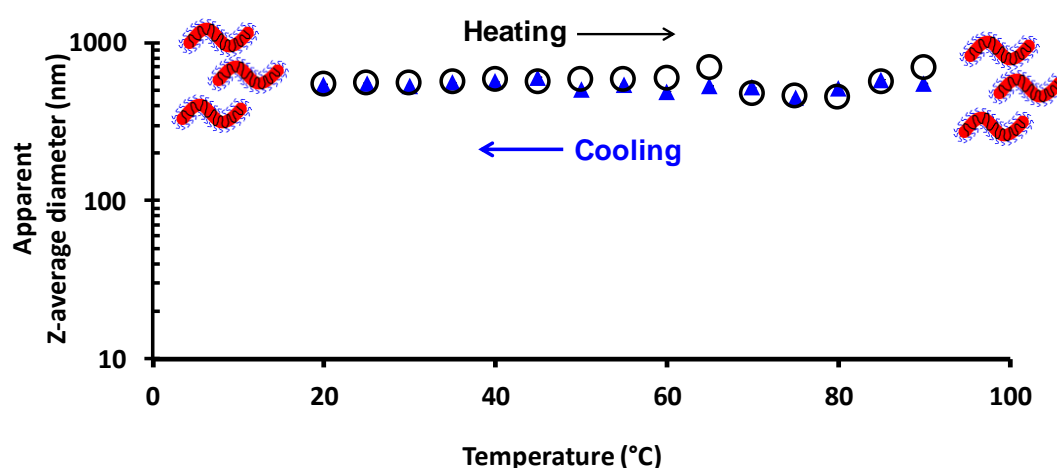


**Figure 3.11:** Variable temperature DLS experiment performed upon a dispersion of PDMS<sub>66</sub>-PDMA<sub>100</sub> worms cross-linked using BIEE (15 mol % relative to the DMA residues). The worms were prepared at 25 % w/w before being diluted to 2.5 % w/w for cross-linking experiments, and then diluted further to 0.25 % w/w for DLS studies. The lack of change in the apparent Z-average diameter indicates that these cross-linked worms do not possess the thermoresponsive behaviour exhibited by the linear precursor worms.

At 20 °C, the cross-linked worms are relatively large, with an apparent Z-average diameter of 540 nm ± 380 nm. This is somewhat larger than that for the non-cross-linked worms, perhaps indicating greater worm stiffness and hence a longer persistence length.<sup>53</sup> On heating to 90 °C and back to 20 °C, the apparent Z-average diameter remains roughly constant. This was expected as the cross-linked worms are now incapable of undergoing a worm-to-sphere transition.

### 3.3.6 Rheology of cross-linked worm gels

To evaluate the physical properties of PDMS<sub>66</sub>-PDMA<sub>100</sub> worm gels cross-linked using various amounts of BIEE, variable temperature oscillatory rheology was used. First, linear PDMS<sub>66</sub>-PDMA<sub>100</sub> worms were analysed at 20 °C. The  $G'$  and  $G''$  were 94 Pa and 64 Pa, respectively (**Figure 3.12**), indicating the presence of a gel. At 33 °C, the magnitude of  $G'$  fell below  $G''$ , confirming the presence of a fluid and indicating that the critical gelation temperature (CGT) has been reached.

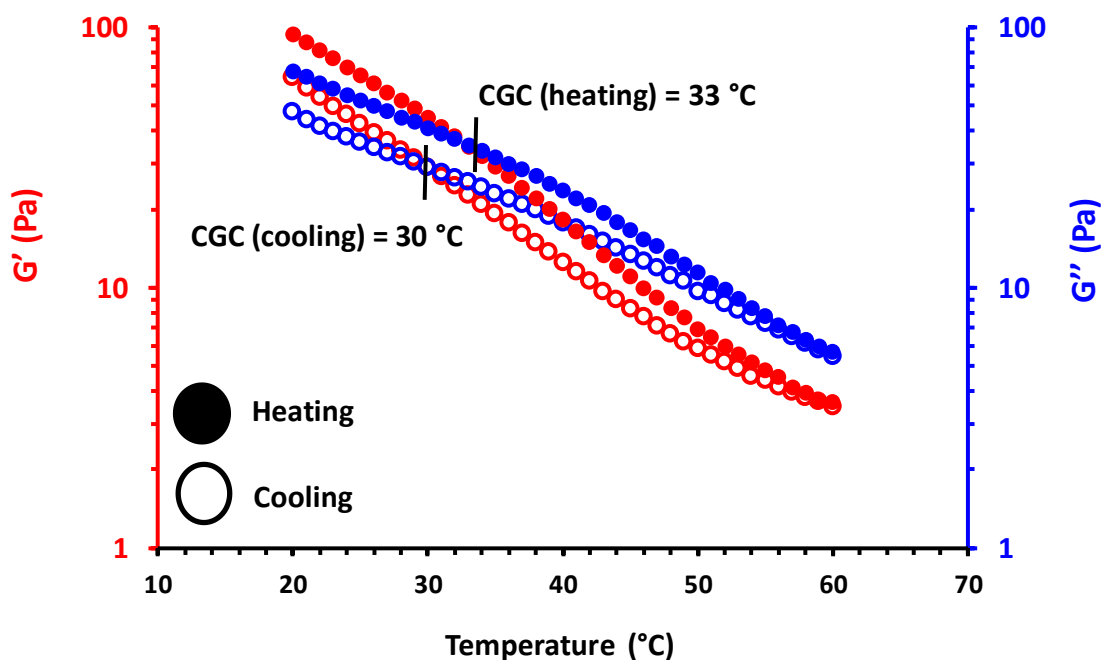


**Figure 3.12:** Variable temperature rheology measurements performed on 25 % w/w PDMS<sub>66</sub>-PDMA<sub>100</sub> worms at 25 % w/w in D5 silicone oil. Filled circles represent heating, open circles represent cooling.  $G'$  is shown in red and  $G''$  is shown in blue. The point at which  $G''$  exceeds  $G'$  is marked on the graph and indicates the critical gelation temperature (CGT).

The sample then remained a free-flowing fluid up to 60°C, after which it was cooled back down to 20 °C. During the cooling cycle, regelation was observed at 30 °C, i.e. some hysteresis in the CGT was observed. Such behaviour is fairly typical of diblock copolymer worms prepared via PISA.<sup>52</sup> In addition, it is worth emphasising that the  $G'$  value at the end of the experiment (68 Pa) is lower than at the start (94 Pa). One plausible explanation for this difference is that the sphere-to-worm transition results in shorter worms, which form fewer inter-worm contacts *per worm*, and therefore weaker gels.<sup>53</sup>

Next, a series of PDMS<sub>66</sub>-PDMA<sub>100</sub> worm gels cross-linked using 5- 15 mol % BIEE were analysed *via* variable temperature rheology. Surprisingly, even the addition of 5 mol % BIEE was sufficient to suppress degelation. Moreover, increasing the cross-linker concentration resulted in dramatically stronger gels. At 15 mol % BIEE, a  $G'$  of 7855 Pa was observed, i.e. almost two orders of magnitude greater than the non-cross-linked worm gel. Interestingly, attempts to cross-link worm gels with 20 % or greater BIEE resulted in loss of colloidal stability

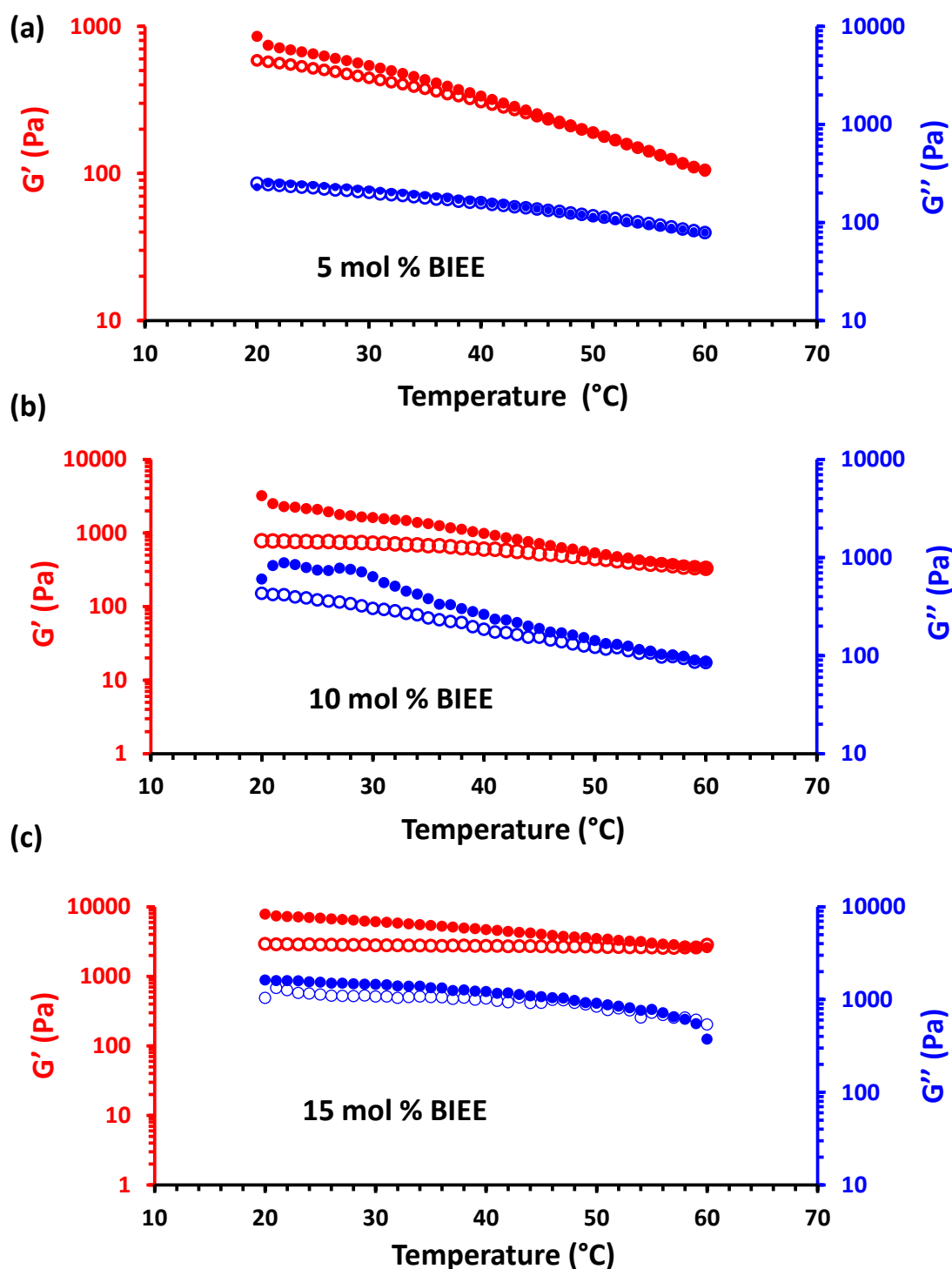


**Figure 3.13:** Variable temperature oscillatory rheology measurements recorded for PDMS<sub>66</sub>-PDMA<sub>100</sub> worm gels cross-linked with varying concentrations of BIEE, relative to the DMA core-forming block: (a) 5 mol % BIEE, (B) 10 mol % BIEE and (c) 15 mol % BIEE. In all cases, filled circles represent heating, open circles represent cooling, red indicates  $G'$  and blue indicates  $G''$ .

### 3.3.7 Shear-induced polarised light imaging

Thus far, a range of different techniques has been used to characterise the worm-to-sphere transition. However, based solely on these experiments it is difficult to pin-point the precise temperature at which all worms have been converted to spheres. TEM, for example, is a number average technique and is likely to be insensitive to the presence of a small fraction of worms. Similarly, nanoparticle morphology can only be inferred from DLS because a spherical morphology is assumed for the analysis. To address this issue, a technique known as shear-induced polarised-light imaging (SIPLI) was utilised.<sup>59</sup> SIPLI combines rotational rheology and polarised imaging, to characterise materials under shear.<sup>59,60</sup> When anisotropic particles are subject to shear forces, alignment occurs and a phenomenon known as birefringence can arise. A material is said to be birefringent if it possesses different indices of refraction, each depending on the polarisation and direction of propagation of the incident light.<sup>59</sup> If polarised light passes through a birefringent material, a rotation of the plane of polarisation is observed. In a SIPLI experiment, plane-polarised light is directed through a sample under shear, and analysed at 90 °C to the plane of polarisation using a CCD camera.<sup>59,60</sup> As the polariser and the camera are aligned orthogonally, only rotated light (due to birefringence) is observed. This leads to the observation of a characteristic ‘Maltese cross’ pattern.

First, the non-cross-linked PDMS<sub>66</sub>-PDMA<sub>100</sub> worms were analysed at 25 % w/w. At 20 °C, the viscosity of this dispersion was relatively high at 4.7 Pa s (**Figure 3.14**), which is typical for worm-like micelles.<sup>61</sup> Moreover, a distinct Maltese cross is observed in the polarised light image (PLI). This confirms the presence of anisotropic particles which become aligned under shear. At higher temperatures, the viscosity of the dispersion gradually decreases, owing to the formation of a population of spherical micelles. However, a Maltese cross is still clearly visible at both 40 °C and 80 °C, indicating there is at least *some* worms still present. At 110 °C, the Maltese cross disappears from the PLI, confirming the complete loss of anisotropic particles. Furthermore, the viscosity of the dispersion is reduced to 0.3 Pa s at 110 °C. This is consistent with that expected for a concentrated dispersion (25 % w/w) of spherical micelles. The TEM studies reported in **Figure 3.2** suggest that 100 °C is sufficient for a complete worm-to-sphere transition. However, TEM is a number-average technique and is insensitive to a relatively small population of worms. Conversely, SIPLI is extremely sensitive to the presence of anisotropic nano-objects. As such, it seems likely that the temperature required for a complete worm-to-sphere transition is in the region of 110 °C. It is worth noting here that only the heating cycle was performed during this experiment because the volatility of the D5 silicone oil led to significant drying, at 110 °C which prevented further imaging.

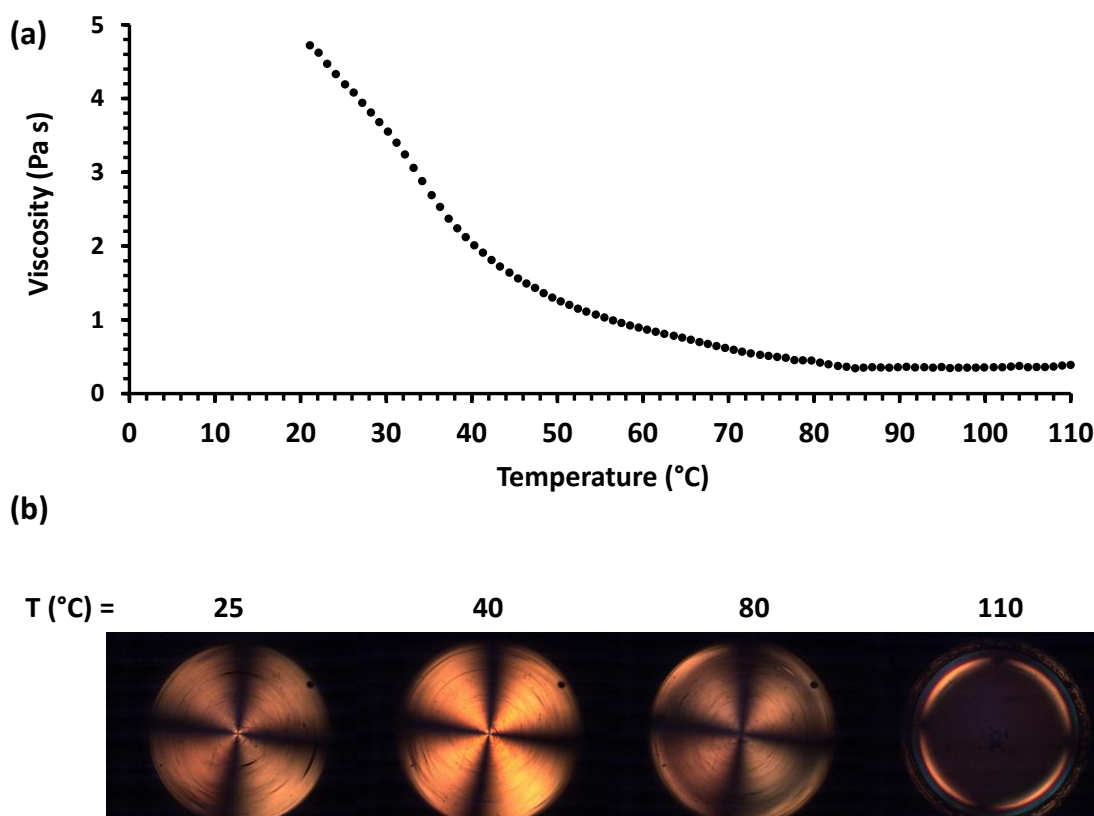


**Figure 3.14:** (a) Viscosity vs. temperature plot obtained, via rotational rheometry studies at a fixed shear rate of  $1.0 \text{ s}^{-1}$  and a heating rate of  $2 \text{ }^\circ\text{C min}^{-1}$ , of 25 % w/w PDMS<sub>66</sub>-PDMA<sub>100</sub> diblock copolymer worms in D5. (b) Polarised light images obtained from the same experiment at a range of different temperatures. A Maltese cross can be observed between 25 °C and 80 °C, indicating the alignment of anisotropic objects, but this characteristic motif is lost at 110 °C.

A similar SIPLI experiment was performed upon PDMS<sub>66</sub>-PDMA<sub>100</sub> worms cross-linked with 15 mol % BIEE (**Figure 3.15**). At 20 °C, the dispersion viscosity was 7.18 Pa s, i.e. more viscous than the non-cross-linked worms. This suggests stiffening of the worms during cross-linking. Furthermore, as the worms are heated to 110 °C, a Maltese cross is still clearly visible in the polarised light images, confirming the continued presence of aligned anisotropic objects, i.e. the covalently stabilised worms.

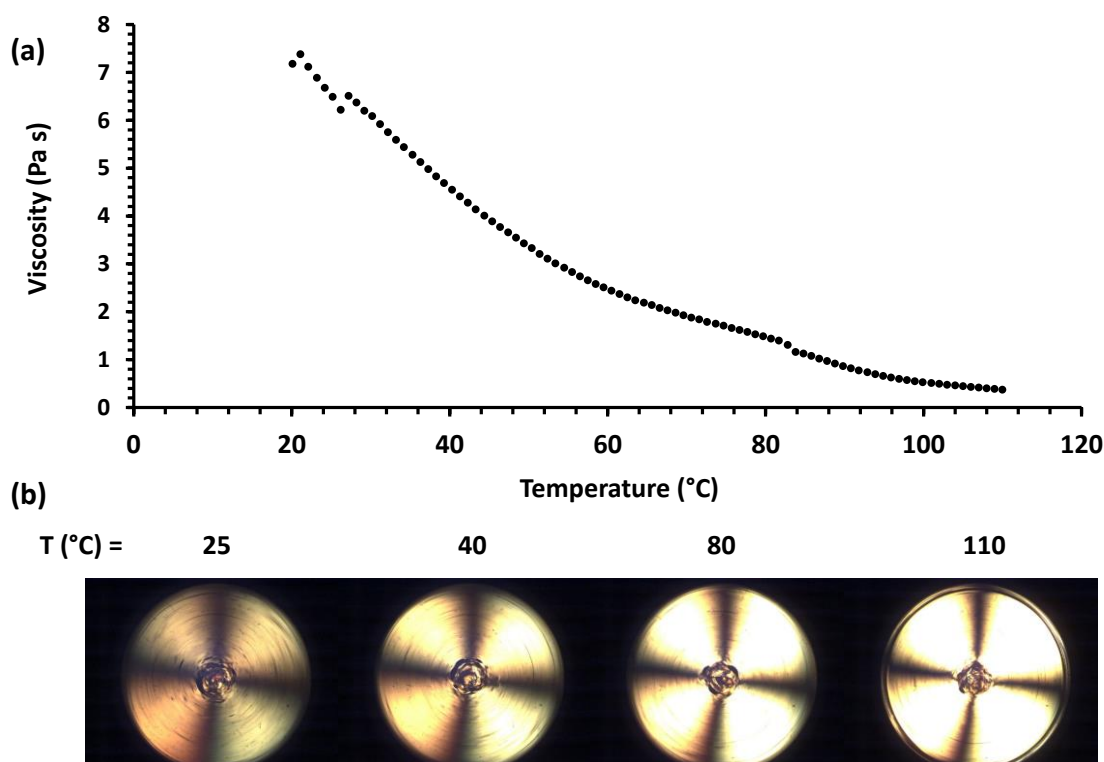


**Figure 3.15:** (a) Viscosity vs. temperature plot obtained, *via* rotational rheometry at a fixed shear rate of  $1.0 \text{ s}^{-1}$  and heating rate of  $2 \text{ }^\circ\text{C min}^{-1}$ , of 25 % w/w PDMS<sub>66</sub>-PDMA<sub>100</sub> diblock copolymer worms cross-linked with 15 mol % BIEE. (b) Select polarised light images obtained from the same experiment at various temperatures. A Maltese cross can be observed between 25 °C and 110 °C, indicating the alignment of anisotropic objects under shear over the entire temperature range.

### 3.3.8 Small-angle x-ray scattering

The PDMS<sub>66</sub>-PDMA<sub>100</sub> worms, both linear and cross-linked, were subject to further characterisation by synchrotron SAXS experiments at the ESRF in Grenoble. Compared to TEM, SAXS provides robust structural information, because X-ray scattering is averaged over many millions of nanoparticles. It is well-known that the dominant copolymer morphology can be inferred by inspecting the gradient of an  $I(q)$  vs.  $q$  plot outside of the Porod region, where  $q$  is the scattering vector ( $q = 4\pi\sin\theta/\lambda$ ) and  $I(q)$  is the X-ray scattering intensity.<sup>52,62–64</sup> At low  $q$ , a gradient of 0 is indicative of spherical particles, whereas a gradient of -1 is indicative of rods (or worms).

First, a sample of PDMS<sub>66</sub>-PDMA<sub>100</sub> worms at 25 % w/w were diluted to 1 % w/w in D5 silicone oil. This low copolymer concentration was selected in order to avoid the presence of a structure factor in the SAXS pattern. The resulting dilute dispersion was then analysed during a heating and cooling cycle from 25 °C – 110 °C – 25 °C. The unmodelled patterns are shown in (Figure 3.16).

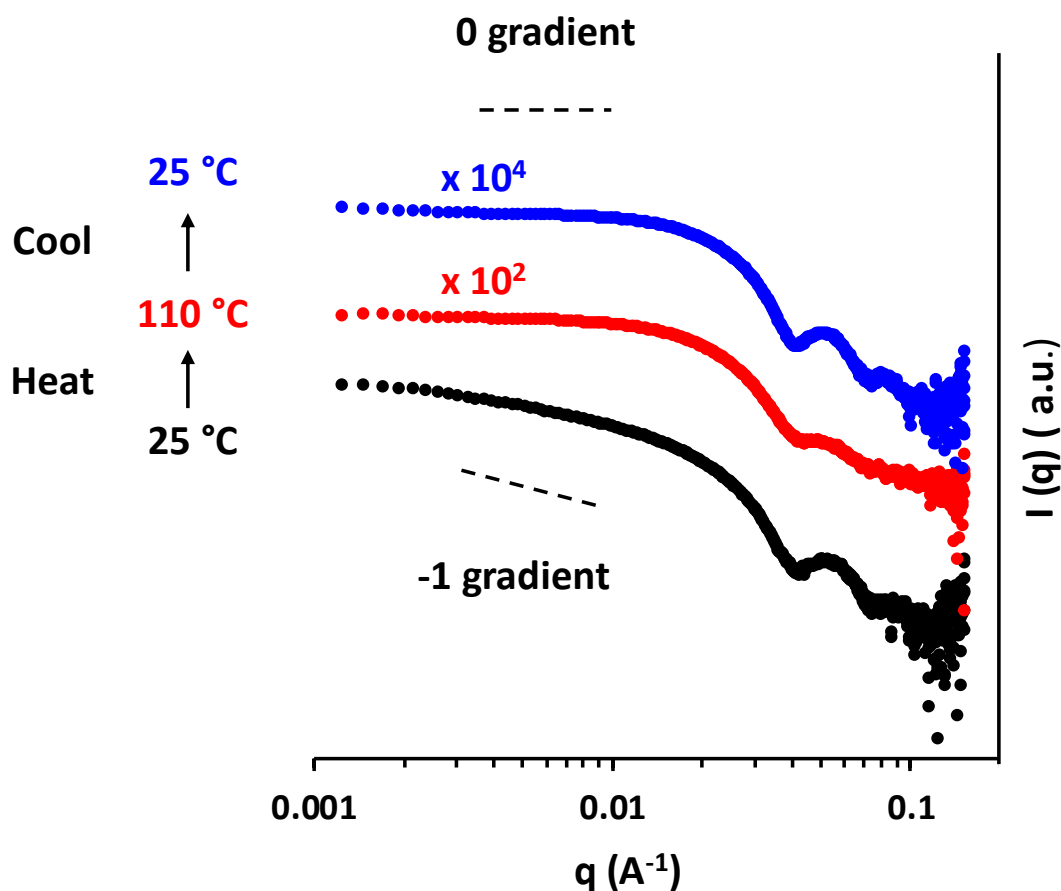


**Figure 3.16:** SAXS data for 1.0 % w/w dispersions of PDMS<sub>66</sub>-PDMA<sub>100</sub> worms during a thermal cycle from 25 °C (black trace) to 110 °C (red trace) and back to 25 °C (blue trace). The black dashed lines indicate a gradient of either 0 or -1 for guidance.

At 25 °C, the gradient of the SAXS pattern is approximately -1, which indicates the presence of worm-like micelles. This gradient shifts to 0 at 110 °C, indicating that a worm-to-sphere transition has occurred. On cooling, the gradient of the curve remains at zero, which suggests the worms are not being reformed. This is expected given that the SAXS analysis is conducted at low copolymer concentration (1 % w/w).

Next, PDMS<sub>66</sub>-PDMA<sub>100</sub> worms cross-linked with 15 mol % BIEE were subject to the same SAXS analysis (**Figure 3.17**). At 25 °C, a gradient of -1 is observed in the SAXS pattern, indicating worm-like micelles. Unsurprisingly, the SAXS patterns do not change significantly on heating to 110 °C, confirming that the cross-linked worms are still present at elevated temperature. This corroborates the observations made by TEM, DLS and SIPLI, which indicate that PDMS<sub>66</sub>-PDMA<sub>100</sub> worms, cross-linked with 15 mol % BIEE relative to the DMA residues, cannot undergo a worm-to-sphere transition.

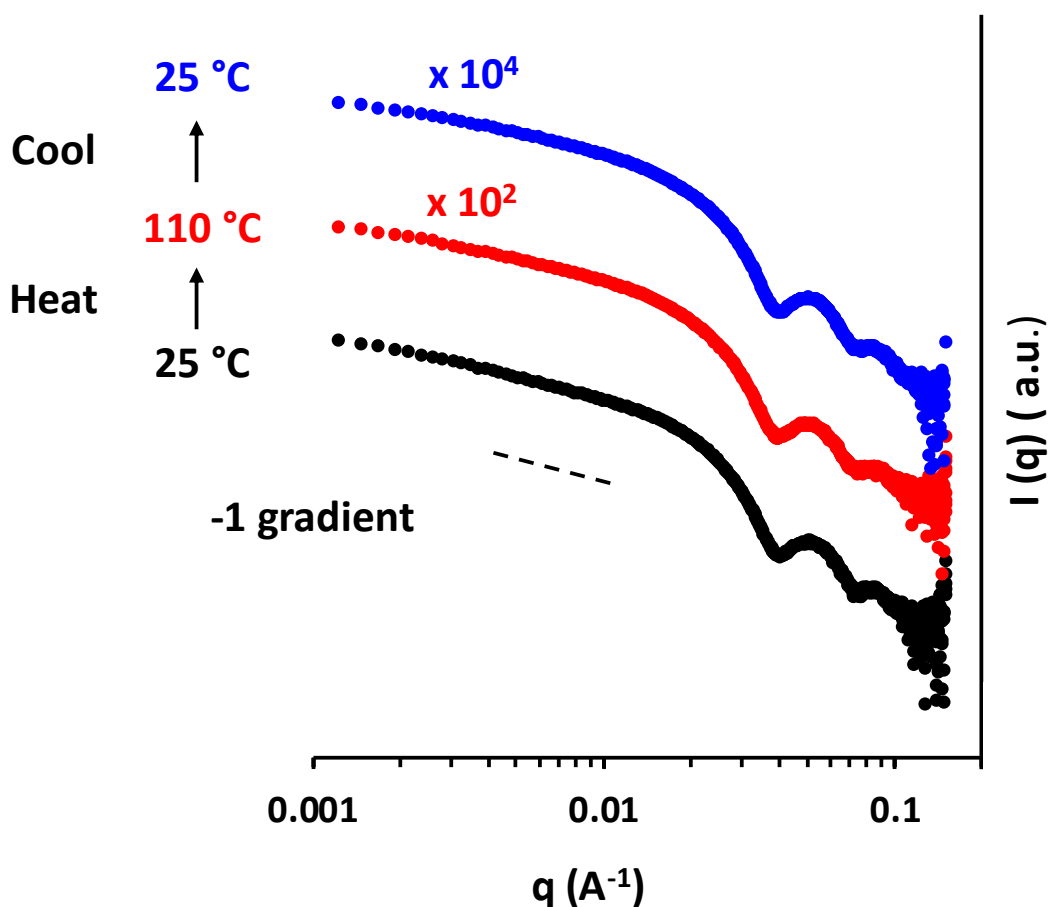


**Figure 3.17:** SAXS data for 1.0 % w/w dispersions of PDMS<sub>66</sub>-PDMA<sub>100</sub> worms (cross-linked using 15 mol % BIEE relative to the DMA residues) during a thermal cycle from 25 °C (black trace) to 110 °C (red trace) and back to 25 °C (blue trace). The black dashed line indicates a gradient of -1 for guidance.

### 3.3.9 Influence of cross-linking on CGC

According to the literature, covalent cross-linking of worms prepared by traditional dilute self-assembly can have a profound effect on their properties. For example, Bates and co-workers reported that cross-linked PEO-PB worms are more stiff than their linear analogues.<sup>13</sup> Moreover, such worms exhibit a dynamic elastic modulus,  $G'$ , over two orders of magnitude greater than the equivalent non cross-linked worms. Recently, developments in percolation theory suggest that worm-stiffness is an important parameter which influences the CGC. Thus, the influence of core cross-linking on the CGC of PDMS<sub>66</sub>-PDMA<sub>100</sub> worms was investigated (**Figure 3.18**). In Chapter 2, the CGC of non-cross-linked PDMS<sub>66</sub>-PDMA<sub>100</sub> worms was determined to lie between 10 and 12.5 % w/w copolymer concentration. In this study, linear PDMS<sub>66</sub>-PDMA<sub>100</sub> worms were prepared at various copolymer concentrations ranging between 3 and 10 % w/w (see **Figure 3.18a**). As expected, each dispersion formed a free-flowing fluid, as indicated by the tube-inversion test.

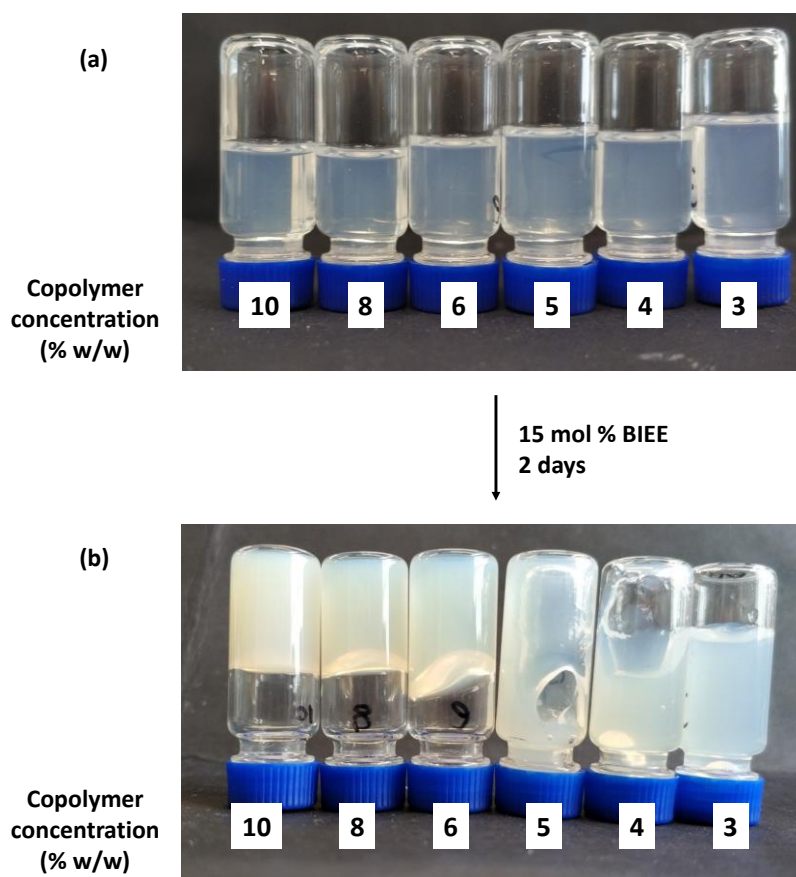


**Figure 3.18:** (a) Series of PDMS<sub>66</sub>-PDMA<sub>100</sub> worm dispersion in D5, at various copolymer concentrations. (b) The same dispersions shown in (a), each cross-linked with 15 mol % BIEE for 2 days. In each case, tubes were inverted and left for 5 minutes before a digital photograph was taken.

Next, 15 mol % BIEE was added to each dispersion and they were allowed to stand at 20 °C for 3 days. The resulting cross-linked worm dispersions were then subject to the same tube-inversion test. From **Figure 3.18b** it is clear that these cross-linked worms exhibit a significantly lower CGC of approximately 6 % w/w.

### 3.4 Conclusions

In summary, PDMS<sub>66</sub>-PDMA<sub>100</sub> worms prepared at 25 % w/w in D5 silicone oil exhibit a reversible worm-to-sphere transition upon heating to 100 °C. Variable temperature <sup>1</sup>H NMR provides evidence that this thermal transition arises from the reversible surface plasticisation of the PDMA core-forming block. This transition was also monitored by variable temperature DLS, SAXS and SIPLI. The latter techniques indicated that heating to 110 °C is required for full conversion of worms into spheres.

Addition of a bifunctional iodine-containing reagent, BIEE, facilitates cross-linking of the PDMA cores. This is thought to occur *via* a Menshutkin reaction, whereby the tertiary amine residues of the PDMA displace the iodine on the BIEE, resulting in quaternisation. When cross-linked, PDMS<sub>66</sub>-PDMA<sub>100</sub> worms exhibit no worm-to-sphere transition and remain as worms at 110 °C. Furthermore, variable temperature <sup>1</sup>H NMR spectroscopy studies indicates no observable core solvation, even at 100 °C.

The kinetics of cross-linking PDMS<sub>66</sub>-PDMA<sub>175</sub> vesicles at 25 % w/w, using 15 mol % BIEE, was monitored *via* <sup>1</sup>H NMR spectroscopy. It was determined that it takes 36 h for all of the BIEE molecules to react *at least once*. However, the vesicles become sufficiently robust as to withstand dispersion in a good solvent for both blocks after approximately 6 h. In addition to worms and vesicles, spherical nanoparticles were also cross-linked with 15 mol % BIEE. For all three cross-linked morphologies, TEM analysis confirmed that well-defined particles were still present when dispersed in a good solvent for both blocks, i.e. chloroform. Control experiments performed on non-cross-linked particles confirm immediate particle dissolution in a good solvent for both blocks, as expected.

Finally, the influence of cross-linking on the worm CGC was investigated. It was shown that the cross-linked PDMS<sub>66</sub>-PDMA<sub>100</sub> worms have a CGC in the region of 5 – 6 % w/w, compared to a CGC of 10 – 12.5 % w/w for the corresponding linear worms. This is believed to be the result of an increase in worm stiffness upon cross-linking.

### 3.5 References

- (1) Tuzar, Z.; Kratochvíl, P. Block and Graft Copolymer Micelles in Solution. *Adv. Colloid Interface Sci.* **1976**, *6*, 201–232.
- (2) Blanazs, A.; Armes, S. P.; Ryan, A. J. Self-Assembled Block Copolymer Aggregates: From Micelles to Vesicles and Their Biological Applications. *Macromol. Rapid Commun.* **2009**, *30*, 267–277.
- (3) Mai, Y.; Eisenberg, A. Self-Assembly of Block Copolymers. *Chem. Soc. Rev.* **2012**, *41*, 5969–5985.
- (4) Bates, F. S.; Fredrickson, G. H. Block Copolymers-Designer Soft Materials. *Phys. Today* **1999**, *52*, 32–38.
- (5) Ahmed, F.; Discher, D. E. Self-Porting Polymersomes of PEG–PLA and PEG–PCL: Hydrolysis-Triggered Controlled Release Vesicles. *J. Control. Release* **2004**, *96*, 37–53.
- (6) Ghoroghchian, P. P.; Li, G.; Levine, D. H.; Davis, K. P.; Bates, F. S.; Hammer, D. A.; Therien, M. J. Bioresorbable Vesicles Formed through Spontaneous Self-Assembly of Amphiphilic Poly(ethylene Oxide)- Block -Polycaprolactone. *Macromolecules* **2006**, *39*, 1673–1675.
- (7) Ahmed, F.; Pakunlu, R. I.; Brannan, A.; Bates, F.; Minko, T.; Discher, D. E. Biodegradable

- Polymersomes Loaded with Both Paclitaxel and Doxorubicin Permeate and Shrink Tumors, Inducing Apoptosis in Proportion to Accumulated Drug. *J. Control. Release* **2006**, *116*, 150–158.
- (8) Deng, R.; Derry, M. J.; Mable, C. J.; Ning, Y.; Armes, S. P. Using Dynamic Covalent Chemistry to Drive Morphological Transitions: Controlled Release of Encapsulated Nanoparticles from Block Copolymer Vesicles. *J. Am. Chem. Soc.* **2017**, *139*, 7616–7623.
- (9) Mable, C. J.; Gibson, R. R.; Prevost, S.; McKenzie, B. E.; Mykhaylyk, O. O.; Armes, S. P. Loading of Silica Nanoparticles in Block Copolymer Vesicles during Polymerization-Induced Self-Assembly: Encapsulation Efficiency and Thermally Triggered Release. *J. Am. Chem. Soc.* **2015**, *137*, 16098–16108.
- (10) Zheng, R.; Liu, G.; Devlin, M.; Hux, K.; Jao, T. C. Friction Reduction of Lubricant Base Oil by Micelles and Crosslinked Micelles of Block Copolymers. *Tribol. Trans.* **2010**, *53*, 97–107.
- (11) Zhang, L.; Eisenberg, A. Multiple Morphologies and Characteristics of “Crew-Cut” Micelle-like Aggregates of Polystyrene-B-Poly(acrylic Acid) Diblock Copolymers in Aqueous Solutions. *J. Am. Chem. Soc.* **1996**, *118*, 3168–3181.
- (12) Zhang, L.; Eisenberg, A. Multiple Morphologies of “Crew-Cut” Aggregates of Polystyrene-B-Poly(acrylic Acid) Block Copolymers. *Science* **1995**, *268*, 1728–1731.
- (13) Won, Y.-Y.; Davis, H. T.; Bates, F. S. Giant Wormlike Rubber Micelles. *Science* **1999**, *283*, 960–963.
- (14) Jain, S.; Bates, F. S. On the Origins of Morphological Complexity in Block Copolymer Surfactants. *Science* **2003**, *300*, 460–464.
- (15) Cai, S.; Vijayan, K.; Cheng, D.; Lima, E. M.; Discher, D. E. Micelles of Different Morphologies - Advantages of Worm-like Filomicelles of PEO-PCL in Paclitaxel Delivery. *Pharm. Res.* **2007**, *24*, 2099–2109.
- (16) Geng, Y.; Dalhaimer, P.; Cai, S.; Tsai, R.; Tewari, M.; Minko, T.; Discher, D. E. Shape Effects of Filaments versus Spherical Particles in Flow and Drug Delivery. *Nat. Nanotechnol.* **2007**, *2*, 249–255.
- (17) Derry, M. J.; Fielding, L. A.; Armes, S. P. Polymerization-Induced Self-Assembly of Block Copolymer Nanoparticles via RAFT Non-Aqueous Dispersion Polymerization. *Prog. Polym. Sci.* **2016**, *52*, 1–18.
- (18) Canning, S. L.; Smith, G. N.; Armes, S. P. A Critical Appraisal of RAFT-Mediated Polymerization-Induced Self-Assembly. *Macromolecules* **2016**, *49*, 1985–2001.
- (19) Warren, N. J.; Armes, S. P. Polymerization-Induced Self-Assembly of Block Copolymer Nano-Objects via RAFT Aqueous Dispersion Polymerization. *J. Am. Chem. Soc.* **2014**, *136*, 10174–10185.
- (20) Charleux, B.; Delaittre, G.; Rieger, J.; D’Agosto, F. Polymerization-Induced Self-Assembly: From Soluble Macromolecules to Block Copolymer Nano-Objects in One Step. *Macromolecules* **2012**, *45*, 6753–6765.
- (21) Blanazs, A.; Ryan, A. J.; Armes, S. P. Predictive Phase Diagrams for RAFT Aqueous Dispersion Polymerization: Effect of Block Copolymer Composition, Molecular Weight, and Copolymer Concentration. *Macromolecules* **2012**, *45*, 5099–5107.
- (22) Sugihara, S.; Blanazs, A.; Armes, S. P.; Ryan, A. J.; Lewis, A. L. Aqueous Dispersion Polymerization: A New Paradigm for in Situ Block Copolymer Self-Assembly in Concentrated Solution. *J. Am. Chem. Soc.* **2011**, *133*, 15707–15713.
- (23) Canton, I.; Warren, N. J.; Chahal, A.; Amps, K.; Wood, A.; Weightman, R.; Wang, E.; Moore, H.; Armes, S. P. Mucin-Inspired Thermo-responsive Synthetic Hydrogels Induce Stasis in Human Pluripotent Stem Cells and Human Embryos. *ACS Cent. Sci.* **2016**, *2*, 65–74.
- (24) Blanazs, A.; Verber, R.; Mykhaylyk, O. O.; Ryan, A. J.; Heath, J. Z.; Douglas, C. W. I.; Armes, S. P. Sterilizable Gels from Thermo-responsive Block Copolymer Worms. *J. Am. Chem. Soc.* **2012**, *134*, 9741–9748.

- (25) Zhou, W.; Qu, Q.; Xu, Y.; An, Z. Aqueous Polymerization-Induced Self-Assembly for the Synthesis of Ketone-Functionalized Nano-Objects with Low Polydispersity. *ACS Macro Lett.* **2015**, *4*, 495–499.
- (26) Warren, N. J.; Rosselgong, J.; Madsen, J.; Armes, S. P. Disulfide-Functionalized Diblock Copolymer Worm Gels. *Biomacromolecules* **2015**, *16*, 2514–2521.
- (27) Ratcliffe, L. P. D.; Couchon, C.; Armes, S. P.; Paulusse, J. M. J. Inducing an Order–Order Morphological Transition via Chemical Degradation of Amphiphilic Diblock Copolymer Nano-Objects. *Biomacromolecules* **2016**, *17*, 2277–2283.
- (28) Rosselgong, J.; Blanazs, A.; Chambon, P.; Williams, M.; Semsarilar, M.; Madsen, J.; Battaglia, G.; Armes, S. P. Thiol-Functionalized Block Copolymer Vesicles. *ACS Macro Lett.* **2012**, *1*, 1041–1045.
- (29) O'Reilly, R. K.; Hawker, C. J.; Wooley, K. L. Cross-Linked Block Copolymer Micelles: Functional Nanostructures of Great Potential and Versatility. *Chem. Soc. Rev.* **2006**, *35*, 1068–1083.
- (30) Read, E. S.; Armes, S. P. Recent Advances in Shell Cross-Linked Micelles. *Chem. Commun.* **2007**, No. 29, 3021.
- (31) Thurmond, K. B.; Kowalewski, T.; Wooley, K. L. Water-Soluble Knedel-like Structures: The Preparation of Shell-Cross-Linked Small Particles. *J. Am. Chem. Soc.* **1996**, *118*, 7239–7240.
- (32) Thurmond, K. B.; Huang, H.; Clark, C. G.; Kowalewski, T.; Wooley, K. L. Shell Cross-Linked Polymer Micelles: Stabilized Assemblies with Great Versatility and Potential. *Colloids Surfaces B Biointerfaces* **1999**, *16*, 45–54.
- (33) Joralemon, M. J.; O'Reilly, R. K.; Hawker, C. J.; Wooley, K. L. Shell Click-Crosslinked (SCC) Nanoparticles: A New Methodology for Synthesis and Orthogonal Functionalization. *J. Am. Chem. Soc.* **2005**, *127*, 16892–16899.
- (34) Ding, J.; Liu, G. Polystyrene- B Lock -poly(2-Cinnamoyl ethyl Methacrylate) Nanospheres with Cross-Linked Shells. *Macromolecules* **1998**, *31*, 6554–6558.
- (35) Weaver, J. V. M.; Tang, Y.; Liu, S.; Iddon, P. D.; Grigg, R.; Billingham, N. C.; Armes, S. P.; Hunter, R.; Rannard, S. P. Preparation of Shell Cross-Linked Micelles by Polyelectrolyte Complexation. *Angew. Chemie - Int. Ed.* **2004**, *43*, 1389–1392.
- (36) Fujii, S.; Cai, Y.; Weaver, J. V. M.; Armes, S. P. Syntheses of Shell Cross-Linked Micelles Using Acidic ABC Triblock Copolymers and Their Application as pH-Responsive Particulate Emulsifiers. *J. Am. Chem. Soc.* **2005**, *127*, 7304–7305.
- (37) Lokitz, B. S.; Convertine, A. J.; Ezell, R. G.; Heidenreich, A.; Li, Y.; McCormick, C. L. Responsive Nanoassemblies via Interpolyelectrolyte Complexation of Amphiphilic Block Copolymer Micelles. *Macromolecules* **2006**, *39*, 8594–8602.
- (38) Guo, A.; Liu, G.; Tao, J. Star Polymers and Nanospheres from Cross-Linkable Diblock Copolymers. *Macromolecules* **1996**, *29*, 2487–2493.
- (39) Henselwood, F.; Liu, G. Water-Soluble Porous Nanospheres. *Macromolecules* **1998**, *31*, 4213–4217.
- (40) Procházka, K.; Baloch, M. K.; Tuzar, Z. Photochemical Stabilization of Block Copolymer Micelles. *Die Makromol. Chemie* **1979**, *180*, 2521–2523.
- (41) Hentze, H.-P.; Krämer, E.; Berton, B.; Förster, S.; Antonietti, M.; Dreja, M. Lyotropic Mesophases of Poly(ethylene Oxide)- B -Poly(butadiene) Diblock Copolymers and Their Cross-Linking To Generate Ordered Gels. *Macromolecules* **1999**, *32*, 5803–5809.
- (42) Li, Y.; Armes, S. P. RAFT Synthesis of Sterically Stabilized Methacrylic Nanolatexes and Vesicles by Aqueous Dispersion Polymerization. *Angew. Chemie* **2010**, *49*, 4042–4046.
- (43) Liu, G.; Qiu, Q.; Shen, W.; An, Z. Aqueous Dispersion Polymerization of 2-Methoxyethyl Acrylate for the Synthesis of Biocompatible Nanoparticles Using a Hydrophilic RAFT Polymer and a Redox Initiator. *Macromolecules* **2011**, *44*, 5237–5245.
- (44) Liu, G.; Qiu, Q.; An, Z. Development of Thermosensitive Copolymers of poly(2-Methoxyethyl Acrylate-Co-Poly(ethylene Glycol) Methyl Ether Acrylate) and Their

- Nanogels Synthesized by RAFT Dispersion Polymerization in Water. *Polym. Chem.* **2012**, *3*, 504–513.
- (45) Lovett, J. R.; Ratcliffe, L. P. D.; Warren, N. J.; Armes, S. P.; Smallridge, M. J.; Cracknell, R. B.; Saunders, B. R. A Robust Cross-Linking Strategy for Block Copolymer Worms Prepared via Polymerization-Induced Self-Assembly. *Macromolecules* **2016**, *49*, 2928–2941.
- (46) Penfold, N. J. W.; Ning, Y.; Verstraete, P.; Smets, J.; Armes, S. P. Cross-Linked Cationic Diblock Copolymer Worms Are Superfloculants for Micrometer-Sized Silica Particles. *Chem. Sci.* **2016**, *7*, 6894–6904.
- (47) Byard, S. J.; Williams, M.; McKenzie, B. E.; Blanazs, A.; Armes, S. P. Preparation and Cross-Linking of All-Acrylamide Diblock Copolymer Nano-Objects via Polymerization-Induced Self-Assembly in Aqueous Solution. *Macromolecules* **2017**, *50*, 1482–1493.
- (48) Hatton, F. L.; Lovett, J. R.; Armes, S. P. Synthesis of Well-Defined Epoxy-Functional Spherical Nanoparticles by RAFT Aqueous Emulsion Polymerization. *Polym. Chem.* **2017**, *8*, 4856–4868.
- (49) Bütün, V.; Top, R. B.; Ufuklar, S. Synthesis and Characterization of Novel “Schizophrenic” Water-Soluble Triblock Copolymers and Shell Cross-Linked Micelles. *Macromolecules* **2006**, *39*, 1216–1225.
- (50) Trent, J. S.; Scheinbeim, J. I.; Couchman, P. R. Ruthenium Tetraoxide Staining of Polymers for Electron Microscopy. *Macromolecules* **1983**, *16*, 589–598.
- (51) Warren, N. J.; Armes, S. P. Polymerization-Induced Self-Assembly of Block Copolymer Nano-Objects via RAFT Aqueous Dispersion Polymerization. *J. Am. Chem. Soc.* **2014**, *136*, 10174–10185.
- (52) Fielding, L. A.; Lane, J. A.; Derry, M. J.; Mykhaylyk, O. O.; Armes, S. P. Thermo-Responsive Diblock Copolymer Worm Gels in Non-Polar Solvents. *J. Am. Chem. Soc.* **2014**, *136*, 5790–5798.
- (53) Lovett, J. R.; Derry, M. J.; Yang, P.; Hatton, F. L.; Warren, N. J.; Fowler, P. W.; Armes, S. P. Can Percolation Theory Explain the Gelation Behavior of Diblock Copolymer Worms? *Chem. Sci.* **2018**, *9*, 7138–7144.
- (54) Pal, S.; Ghosh Roy, S.; De, P. Synthesis via RAFT Polymerization of Thermo- and pH-Responsive Random Copolymers Containing Cholic Acid Moieties and Their Self-Assembly in Water. *Polym. Chem.* **2014**, *5*, 1275–1284.
- (55) Bütün, V.; Billingham, N. C.; Armes, S. P. Synthesis of Shell Cross-Linked Micelles with Tunable Hydrophilic/Hydrophobic Cores. *J. Am. Chem. Soc.* **1998**, *120*, 12135–12136.
- (56) Bütün, V.; Wang, X. S.; De Paz Báñez, M. V.; Robinson, K. L.; Billingham, N. C.; Armes, S. P.; Tuzar, Z. Synthesis of Shell Cross-Linked Micelles at High Solids in Aqueous Media. *Macromolecules* **2000**, *33*, 1–3.
- (57) Liu, S.; Weaver, J. V. M.; Tang, Y.; Billingham, N. C.; Armes, S. P.; Tribe, K. Synthesis of Shell Cross-Linked Micelles with pH-Responsive Cores Using ABC Triblock Copolymers. *Macromolecules* **2002**, *35*, 6121–6131.
- (58) Sola, M.; Lledos, A.; Duran, M.; Bertran, J.; Abboud, J. L. M. Analysis of Solvent Effects on the Menshutkin Reaction. *J. Am. Chem. Soc.* **1991**, *113*, 2873–2879.
- (59) Mykhaylyk, O. O.; Warren, N. J.; Parnell, A. J.; Pfeifer, G.; Laeuger, J. Applications of Shear-Induced Polarized Light Imaging (SIPLI) Technique for Mechano-Optical Rheology of Polymers and Soft Matter Materials. *J. Polym. Sci. Part B Polym. Phys.* **2016**, *54*, 2151–2170.
- (60) Mykhaylyk, O. O. Time-Resolved Polarized Light Imaging of Sheared Materials: Application to Polymer Crystallization. *Soft Matter* **2010**, *6*, 4430–4440.
- (61) Lopez-Oliva, A. P.; Warren, N. J.; Rajkumar, A.; Mykhaylyk, O. O.; Derry, M. J.; Doncom, K. E. B.; Rymaruk, M. J.; Armes, S. P. Polydimethylsiloxane-Based Diblock Copolymer Nano-Objects Prepared in Nonpolar Media via RAFT-Mediated Polymerization-Induced Self-Assembly. *Macromolecules* **2015**, *48*, 3547–3555.

- (62) Derry, M. J.; Fielding, L. A.; Warren, N. J.; Mable, C. J.; Smith, A. J.; Mykhaylyk, O. O.; Armes, S. P. In Situ Small-Angle X-Ray Scattering Studies of Sterically-Stabilized Diblock Copolymer Nanoparticles Formed during Polymerization-Induced Self-Assembly in Non-Polar Media. *Chem. Sci.* **2016**, *7*, 5078–5090.
- (63) Warren, N. J.; Mykhaylyk, O. O.; Mahmood, D.; Ryan, A. J.; Armes, S. P. RAFT Aqueous Dispersion Polymerization Yields Poly(ethylene Glycol)-Based Diblock Copolymer Nano-Objects with Predictable Single Phase Morphologies. *J. Am. Chem. Soc.* **2014**, *136*, 1023–1033.
- (64) Schnablegger, H.; Singh, Y. *The SAXS Guide: Getting Acquainted with the Principles*, 2nd ed.; Anton Paar GmbH: Gratz, 2011.

**Chapter 4: RAFT Dispersion  
Polymerisation in Silicone Oil Using a  
Silicone-Based Methacrylic Stabiliser**

## 4.1 Introduction

Since the discovery of diblock copolymer self-assembly *via* PISA, many different polymers have been evaluated for use as core-forming and stabiliser blocks.<sup>1-7</sup> As such, PISA has been successfully conducted in a range of solvents, such as water,<sup>8-11</sup> alcohols,<sup>12-15</sup> haloalkanes<sup>16</sup> and alkanes.<sup>15,17-20</sup> Despite the broad range of monomers available, some feature far more frequently in PISA formulations than others. BzMA, for example, features in a wide range of PISA formulations involving many different solvents. Cunningham *et al.* demonstrated that PBzMA is a suitable core-forming block for RAFT aqueous emulsion polymerisation, using PGMA as a steric-stabiliser block.<sup>21</sup> Like the majority of RAFT emulsion polymerisations, the resulting PGMA-PBzMA nanoparticles were always spherical, i.e. no worms or vesicles were observed. Nevertheless, these spheres proved to be interesting in term of their surface adsorption behaviour and were evaluated as Pickering emulsifiers.

BzMA is also an effective core-forming block when polymerised *via* RAFT alcoholic dispersion polymerisation. This was demonstrated by Semsarilar *et al.*, who prepared a range of macro-CTAs based on either PDMA, PMAA, PGMA and PMPC.<sup>22</sup> Subsequent chain extension of a PMAA<sub>67</sub> macro-CTA with BzMA in ethanol led to the production of spheres, worms and vesicles respectively (**Figure 4.1**). In addition, Zehm *et al.* also demonstrated that PHPMA is an effective steric stabiliser for PBzMA-based nano-objects prepared in either ethanol or isopropanol.<sup>23</sup>

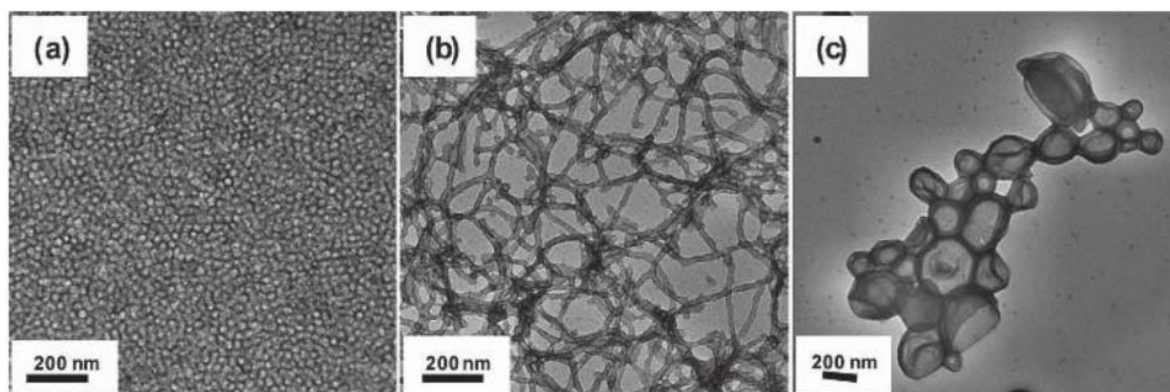


**Figure 4.1:** TEM images of (a) PMAA<sub>67</sub>-PBzMA<sub>50</sub> spheres, (b) PMAA<sub>67</sub>-PBzMA<sub>100</sub> worms and (c) PMAA<sub>67</sub>-PBzMA<sub>200</sub> vesicles obtained via the RAFT dispersion polymerisation of BzMA in ethanol.<sup>22</sup>

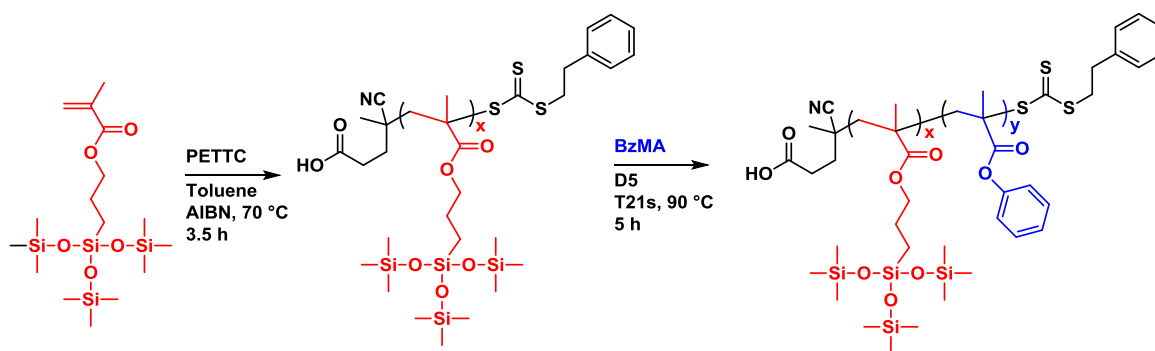
For PISA formulations in non-polar media such as *n*-alkanes,<sup>17,24-26</sup> PBzMA has been extensively used as a core-forming block. In fact, the first report of an entirely methacrylic PISA formulation

## Chapter 4: RAFT Dispersion Polymerisation in Silicone Oil Using a Silicone-Based Methacrylic Stabiliser

comprised PLMA-PBzMA nanoparticles in *n*-heptane.<sup>24</sup> Since this seminal study, this formulation has also been extended to *n*-dodecane,<sup>25</sup> mineral oil<sup>17</sup> and PAO.<sup>17</sup>

In Chapter 2, a PDMS<sub>66</sub> macro-CTA was used to polymerise a range of methacrylic monomers in a silicone oil, more specifically D5. Utilising PDMA as a core-forming block provided access to spheres, worms and vesicles. However, the use of PBzMA as a core-forming block resulted only in kinetically-trapped spheres. This is very surprising, given that the full range of copolymer morphologies are accessible when the same copolymer (PDMS<sub>66</sub>-PBzMA<sub>x</sub>) is prepared in *n*-heptane.<sup>6</sup> Typically, when a RAFT dispersion polymerisation results in kinetically trapped spheres, one strategy to attempt to access worms and vesicles is to reduce the stabiliser DP.<sup>8</sup> This has proven effective in a multitude of different PISA formulations.<sup>7,15,17,22</sup> However, in this case it is not straightforward: the PDMS<sub>66</sub> macro-CTA is prepared by the esterification of a commercially available hydroxyl-terminated PDMS<sub>66</sub>-OH with a carboxylic acid functionalised RAFT agent, and only a few commercially-available PDMS<sub>x</sub>-OH precursors are available.

In this Chapter, new silicone-based methacrylic macro-CTAs prepared *via* RAFT solution polymerisation of 3-[tris(trimethylsiloxy)silyl]propyl methacrylate (SiMA) are evaluated. The resulting PSiMA macro-CTAs are chain-extended with BzMA in silicone oil, *via* RAFT dispersion polymerisation. When the PSiMA DP is 18, only spherical micelles are accessible. However, reducing this DP to 13 leads to the synthesis of spheres, worms or vesicles. Furthermore, two phase diagrams are constructed to enable the reproducible targeting of each of these three diblock copolymer morphologies.



**Scheme 4.1:** Synthesis of a PSiMA macro-CTA and its subsequent chain extension with BzMA in silicone oil (D5) at 90 °C.

## 4.2 Experimental

### 4.2.1 Materials

3-[Tris(trimethylsiloxy)silyl]propyl methacrylate (SiMA), benzyl methacrylate, chloroform-d, dichloromethane-d<sub>2</sub>, methanol, toluene, azobisisobutyronitrile (AIBN) and THF were purchased from Sigma Aldrich (UK) and used as received. PETTC RAFT agent was prepared according to the protocol described in Chapter 2. Trigonox 21s (T21s) initiator was obtained from Akzo Nobel (The Netherlands) and used as received. D5 silicone oil was obtained from Scott Bader Company Ltd. (UK) and used as received.

### 4.2.2 Methods

#### Synthesis of a PSiMA<sub>15</sub> macro-CTA

A typical synthesis of a PSiMA<sub>15</sub> macro-CTA was conducted as follows: PETTC (2.46 g, 7.2 mmol), SiMA monomer (36.73 g, 86.9 mmol) and toluene (59.14 g) were added to a round-bottomed flask, to afford a target PSiMA DP of 12. AIBN was then added (23.77 mg, 1.44 mmol; [PETTC]/[AIBN] = 5). The resulting mixture was then sealed, purged with nitrogen, and placed in a preheated oil bath set at 70 °C for 3.5 h. The polymerisation was then quenched by simultaneously cooling the reaction mixture in an ice bath and exposing it to air. <sup>1</sup>H NMR indicated a SiMA conversion of 70 %. The crude PSiMA was then purified by precipitation into a ten-fold excess of ice cold methanol (three times). <sup>1</sup>H NMR spectroscopy in dichloromethane-d<sub>2</sub> indicated a mean PSiMA DP of 15, by comparing the oxymethylene protons at 3.9 ppm with the five PETTC aromatic protons at 7.3 ppm. THF GPC indicated that M<sub>n</sub> = 4300 g mol<sup>-1</sup> and M<sub>w</sub>/M<sub>n</sub> = 1.14, relative to a series of low-dispersity PMMA standards.

#### Synthesis of PSiMA<sub>15</sub>-PBzMA<sub>x</sub> nanoparticles in silicone oil

PSiMA<sub>y</sub>-PBzMA<sub>x</sub> nanoparticles were synthesised *via* RAFT dispersion polymerisation of BzMA in D5 silicone oil. A typical synthesis targeting PSiMA<sub>15</sub>-PBzMA<sub>200</sub> was conducted as follows: PSiMA<sub>15</sub> macro-CTA was weighed out into a 10 ml vial (0.1 g, 15 μmol). To this, D5 silicone oil (2.51 g) was added, along with benzyl methacrylate (0.53 g, 3.0 mmol) to afford a target PBzMA DP of 200 and a final copolymer concentration of 20 % w/w. Next, T21s initiator was added (3.75 μmol, 9 μl; added as a 10 % v/v solution in D5). The resulting mixture was then sealed, purged with nitrogen gas and placed in a preheated oil bath set at 90 °C for 5 h. <sup>1</sup>H NMR spectroscopy in chloroform-d indicated BzMA conversion between 94 – 99 % in all cases. Furthermore, THF GPC confirmed low dispersities (M<sub>w</sub>/M<sub>n</sub> < 1.25) in all cases. Depending on the target PBzMA

core-forming DP, the final dispersion was obtained as either a free-flowing fluid or a free-standing gel.

#### **4.2.3 Characterisation**

##### **<sup>1</sup>H NMR spectroscopy**

<sup>1</sup>H NMR spectra were recorded in either d<sub>6</sub>-acetone, chloroform-d, or dichloromethane-d<sub>2</sub> using a Bruker AV1-400 MHz spectrometer. Typically, 64 scans were averaged per spectrum.

##### **Gel permeation chromatography**

Molecular weight distributions were determined using a GPC instrument operating at 30 °C that comprised two Polymer Laboratories PL gel 5 µm Mixed C columns, a LC20AD ramped isocratic pump, THF eluent and a WellChrom K-2301 refractive index detector operating at 950 ± 30 nm. The mobile phase contained 2.0 % v/v triethylamine and 0.05 % w/v 3,5-di-tert-4-butylhydroxytoluene (BHT); the flow rate was fixed at 1.0 ml min<sup>-1</sup> and toluene was used as a flow rate marker. A series of ten near-monodisperse poly(methyl methacrylate) standards (M<sub>n</sub> = 1,280 to 330,000 g mol<sup>-1</sup>) were used for calibration. Chromatograms were analysed using Varian Cirrus GPC software.

##### **Dynamic light scattering**

Dynamic light scattering (DLS) studies were performed using a Zetasizer Nano-ZS instrument (Malvern Instruments, UK) at 25 °C at a fixed scattering angle of 173°. Copolymer dispersions were diluted in the solvent in which they were synthesized (typically D5) to a final concentration of 0.10 % w/w. The intensity-average diameter and polydispersity (PDI) of the diblock copolymer particles were calculated by cumulants analysis of the experimental correlation function using Dispersion Technology Software version 6.20. Data were averaged over ten runs each of thirty seconds duration.

##### **Transmission electron microscopy**

Transmission electron microscopy (TEM) studies were conducted using a FEI Tecnai G2 spirit instrument operating at 80 kV and equipped with a Gatan 1k CCD camera. Copper TEM grids were surface-coated in-house to yield a thin film of amorphous carbon. The grids were then loaded with dilute copolymer dispersions (0.20 % w/w). Prior to imaging, each grid was exposed to ruthenium(IV) vapour for 7 minutes at ambient temperature, in order to achieve sufficient contrast. The ruthenium oxide stain was prepared by adding ruthenium(II) oxide (0.3 g) to water

(50 g), to form a slurry. Then, sodium periodate (2.0 g) was added whilst stirring to form a yellow solution of ruthenium(IV) oxide within 1 minute.<sup>27</sup>

### Rheology studies

An AR-G2 rheometer equipped with a 40 mm 2° aluminum cone was used for all measurements. The storage and loss moduli were determined *via* oscillatory rheometry either as a function of strain at a fixed angular frequency of 1.0 rad s<sup>-1</sup> or as a function of angular frequency at a fixed strain of 1.0 %.

## 4.3 Results and discussion

RAFT solution polymerisation of SiMA was conducted in toluene, using PETTC as a RAFT CTA and AIBN as an initiator. The target copolymer concentration was fixed at 40 % w/w, and the PETTC/AIBN molar ratio was fixed at 5. **Figure 4.2** shows typical kinetic data obtained for the RAFT solution polymerisation of SiMA in toluene when conducted at 70 °C and targeting a P*Si*MA DP of 12.

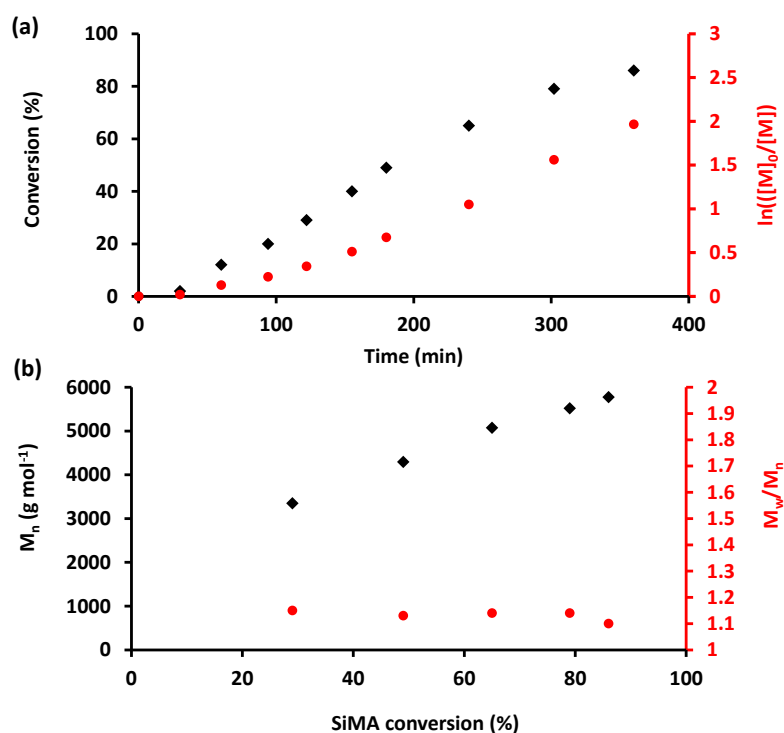


**Figure 4.2:** (a) SiMA monomer conversion vs. time curve obtained for the RAFT solution polymerisation of SiMA in toluene at 70 °C using PETTC as a CTA and AIBN as an initiator ( $[PETTC]/[AIBN] = 5$ ). The P*Si*MA target DP was 12, the target copolymer concentration was 40 % w/w and conversions were determined *via* <sup>1</sup>H NMR spectroscopy by comparing the protons adjacent to the ester group with the two vinyl protons. The corresponding semi-log plot is also shown. (b) Selected THF GPC data obtained for the same polymerisation. The linear evolution of  $M_n$  with SiMA conversion was observed, and  $M_w/M_n$  remained below 1.2 throughout, indicating good pseudo-living character.

This was obtained by removing aliquots from the polymerising mixture at regular time intervals and analysing them via  $^1\text{H}$  NMR spectroscopy and THF GPC. A minor induction period was observed at the beginning of the polymerisation, lasting approximately 30 minutes. Despite this, the polymerisation was relatively quick, reaching 86 % SiMA conversion in 6 h. Moreover, THF GPC confirmed a linear evolution of molecular weight, as expected for a RAFT polymerisation, and dispersities remained below 1.2 throughout.

A representative  $^1\text{H}$  NMR spectrum, removed from the polymerising reaction mixture after 210 minutes, is shown in **Figure 4.3**.

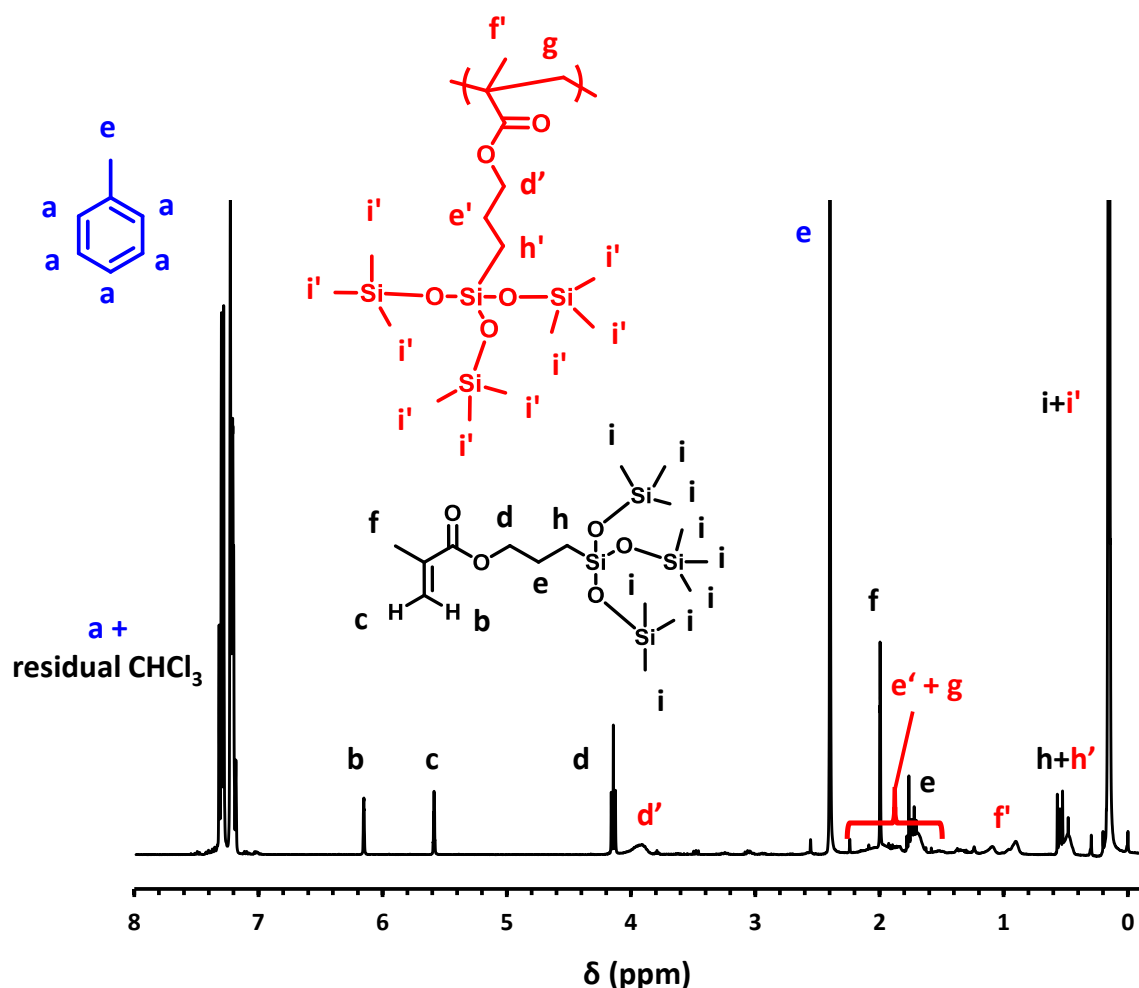


**Figure 4.3:**  $^1\text{H}$  NMR spectrum recorded in chloroform- $d$  of an aliquot removed, after 210 min during the polymerisation of SiMA monomer at 70  $^\circ\text{C}$  and 40 % w/w solids in toluene. PETTC was utilised as a CTA, AIBN as an initiator ( $[\text{PETTC}]/[\text{AIBN}] = 5$ ) and the target PSiMA DP was 12. A SiMA monomer conversion of 66 % can be determined by comparing the integrated intensity of the oxymethylene protons between 3.8 and 4.2 ppm (labelled d and d') for both the polymer and monomer, with that of the vinyl signals at 5.6 and 6.2 ppm (c and b respectively) solely due to the monomer.

To determine the SiMA monomer conversion for each aliquot, the signals between 3.8 and 4.2 ppm assigned to the two oxymethylene protons of the monomer and polymer (labelled d and d') compared to that of the two vinyl monomer protons at 6.2 and 5.6 ppm (labelled b and c, respectively). The monomer conversion consumed in each case was calculated using the following formula:

$$\% \text{ Conversion} = \left( 1 - \frac{\text{integral}(b + c)}{2} \right) \times 100 \quad (4.1)$$

Based on these polymerisation kinetics three PSiMA<sub>x</sub> macro-CTAs were prepared, where x = 13, 15 or 18. In each case, polymerisations were quenched at between 50-80 % conversion, to preserve RAFT chain-ends, and then purified by precipitation into excess ice-cold methanol. A typical <sup>1</sup>H NMR spectrum, obtained for PSiMA<sub>15</sub>-PETTC, is shown in **Figure 4.4**.

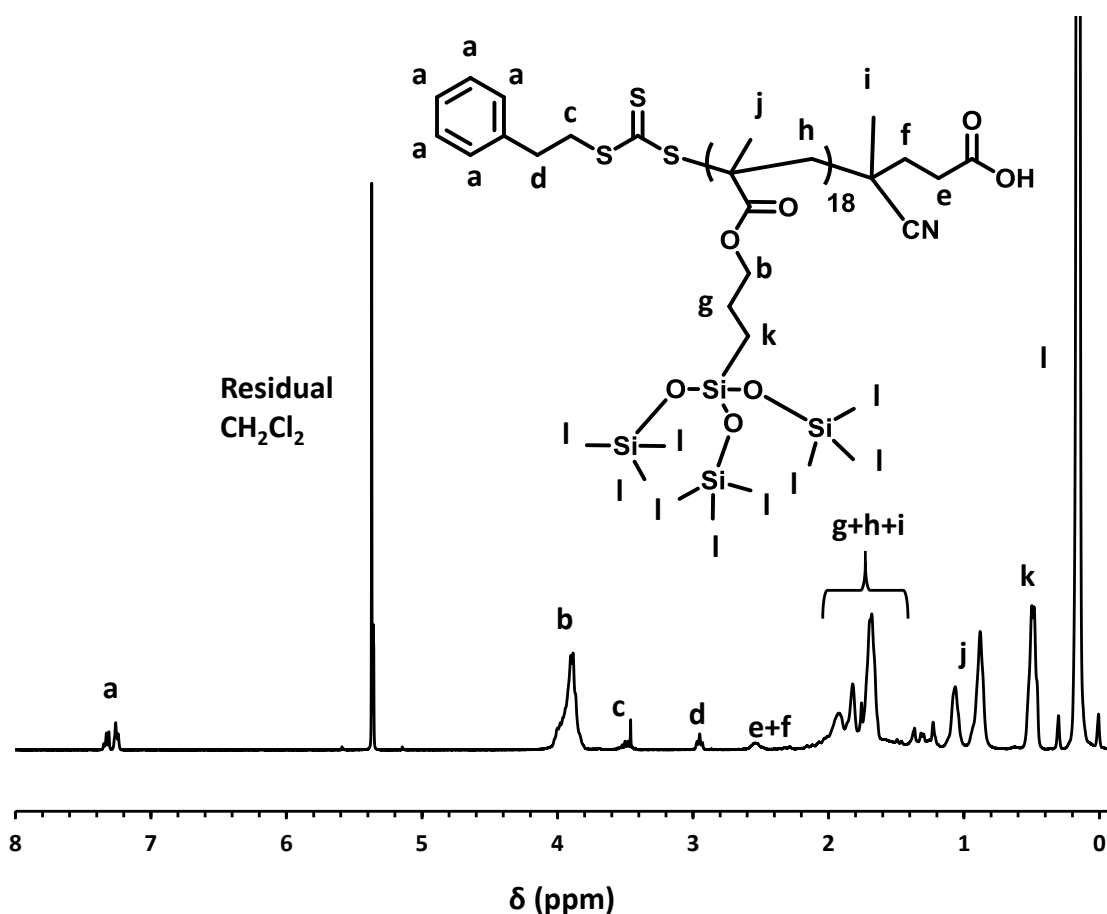


**Figure 4.4:** <sup>1</sup>H NMR spectrum recorded for a PSiMA<sub>14</sub>-macro-CTA recorded in dichlorofom-d<sub>2</sub>. Its mean DP was determined by comparing the integrated intensity of the aromatic protons attached to the PETTC (labelled a) with that of the oxymethylene protons associated with the PSiMA polymer (labelled b).

The mean DP for each macro-CTA was determined by comparing the five aromatic protons at 7.3 ppm assigned to the PETTC CTA (labelled a, **Figure 4.4**) with the oxymethylene protons at ~ 3.9 ppm assigned to the polymer (labelled b, **Figure 4.4**). THF GPC analysis of each macro-CTA was also performed. Each chromatogram was unimodal and analysis indicated low dispersity in each case, as expected for a well-controlled RAFT polymerisation.

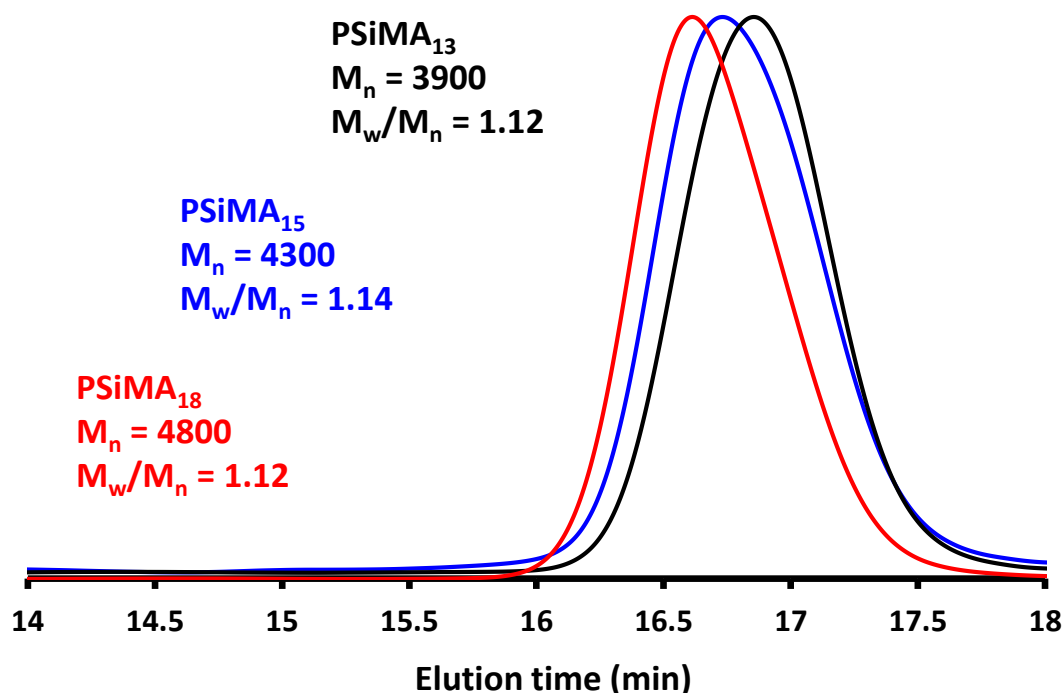


**Figure 4.5:** THF GPC chromatographs obtained for three PSiMA<sub>x</sub> macro-CTAs (x = 13, 15 or 18).

Molecular weight data for each of the three macro-CTAs is summarised in **Table 4.1**

PSiMA target DP	Conversion / % <sup>a</sup>	Actual DP <sup>b</sup>	CTA efficiency / %	M <sub>n</sub> <sup>c</sup> / g mol <sup>-1</sup>	M <sub>w</sub> /M <sub>n</sub> <sup>c</sup>
12	56	13	52	3,900	1.12
12	70	15	60	4,300	1.14
15	74	18	62	4,800	1.12

a. <sup>1</sup>H NMR in chloroform-d b. <sup>1</sup>H NMR in dichloromethane-d<sub>2</sub> c. THF GPC

**Table 4.1:** Summary of conversions, DPs, obtained CTA efficiency, M<sub>n</sub> and M<sub>w</sub>/M<sub>n</sub> values obtained for three PSiMA<sub>x</sub> macro-CTAs (where x = 13, 15, 18).

### 4.3.1 Chain-extension of PSiMA macro-CTAs with BzMA in D5 silicone oil

Next, PSiMA<sub>15</sub> was used to polymerise BzMA via RAFT dispersion polymerisation at 90°C in D5. A PBzMA core-forming DP of 200 was targeted at a final copolymer concentration of 20 % w/w. In addition, the reaction scale was increased in order to facilitate a detailed kinetic study of the polymerisation (Figure 4.6), which required removal of aliquots from the polymerising reaction mixture at regular time intervals, followed by <sup>1</sup>H NMR and THF GPC analysis. The BzMA conversion at each time point was determined in a similar manner to that described for the RAFT solution polymerisation of SiMA monomer. Namely, the oxymethylene protons assigned to the monomer and polymer, at 5.2 and 4.9 ppm respectively, were compared to the integrated signal intensity of the vinyl proton signals at 6.2 and 5.6 ppm.

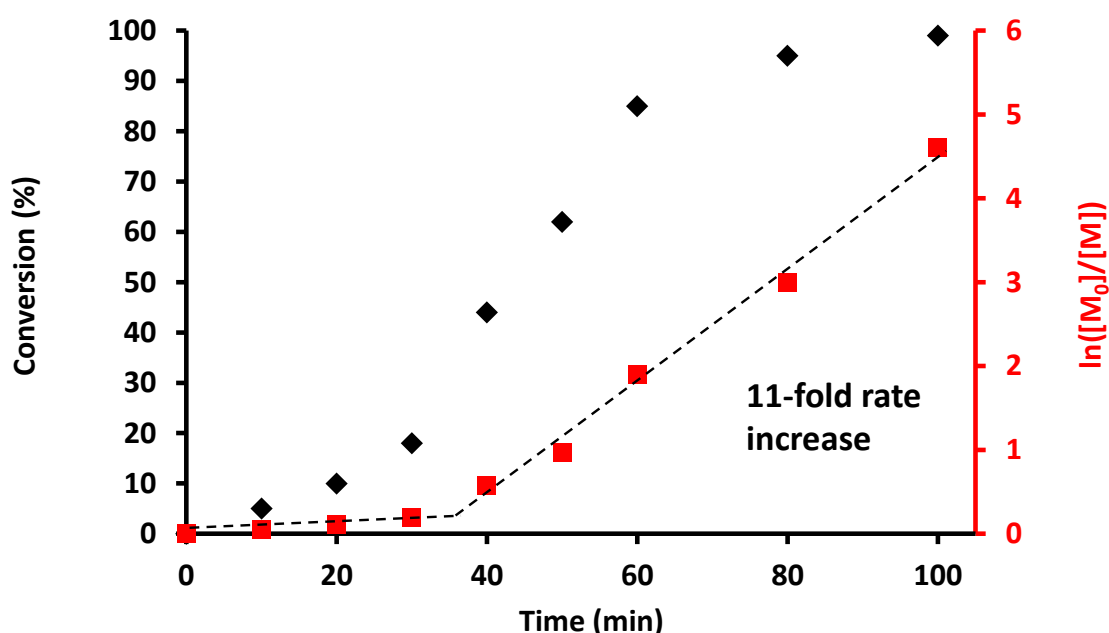


**Figure 4.6:** Conversion vs. time curve obtained for the polymerisation of BzMA in D5 silicone oil at 90 °C utilising a PSiMA<sub>15</sub> macro-CTA and Trigonox 21s (T21s) as an initiator. The copolymer concentration was fixed at 20 % w/w and the [macro-CTA]/[T21s] molar ratio was fixed at 4.

The polymerisation proceeded relatively slowly for the first 30 min, after which an eleven-fold rate enhancement was observed. This is observed for many PISA formulations, and is attributed to the onset of micellar nucleation.<sup>10</sup> Initially, the polymerisation takes place under homogeneous conditions until a critical PBzMA DP is reached, after which this block becomes insoluble in D5 and micellisation occurs. Diffusion of BzMA into the nascent micelle cores results in a higher local monomer concentration and hence a faster rate of reaction.<sup>10</sup> Overall, more than 99 % BzMA conversion was achieved within 100 min. THF GPC analysis confirmed a linear evolution in  $M_n$

with monomer conversion, with  $M_w/M_n$  remaining below 1.22 throughout, as expected for a well-controlled RAFT polymerisation. Furthermore, each chromatogram was unimodal, indicating efficient re-initiation of the  $\text{PSiMA}_{15}$  macro-CTA.

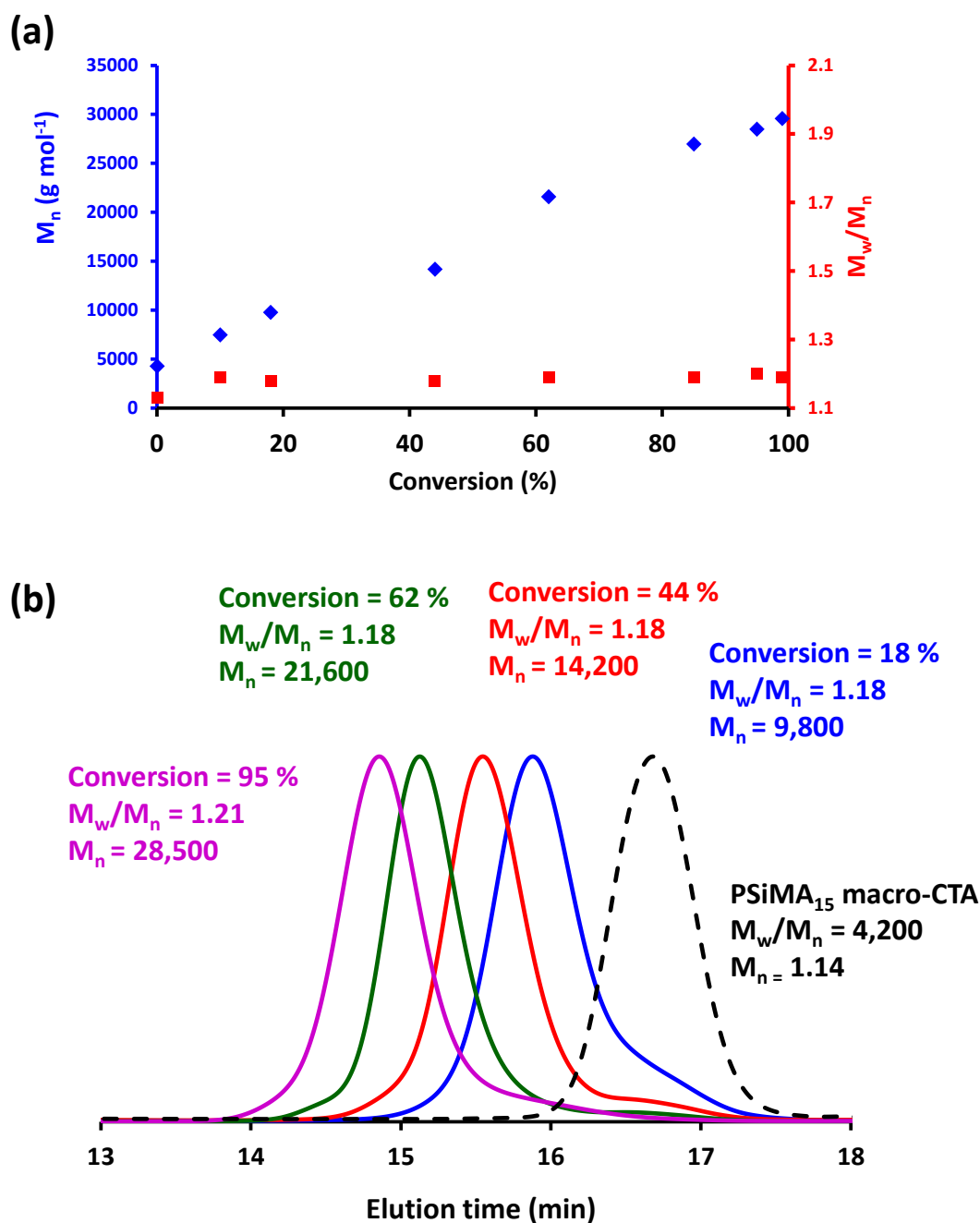


**Figure 4.7:** (a) Evolution of  $M_n$  and  $M_w/M_n$  with BzMA conversion during the RAFT dispersion polymerisation of BzMA at 90 °C and 20 % w/w in D5 silicone oil, targeting a PBzMA DP of 200. In all cases the reported  $M_n$  values are expressed relative to low-dispersity PMMA calibrants. (b) Selected chromatographs for the data shown in (a). In all cases, unimodal traces were obtained, indicating efficient reinitiation of the  $\text{PSiMA}_{15}$  macro-CTA.



averaged diameter, the resulting diameters are skewed towards the larger particles rather than the smaller particles present within the sample. This can be observed as a distinct upturn in a plot of particle diameter vs PBzMA core-forming DP. Below PBzMA DPs of 20, no PISA was observed by TEM.

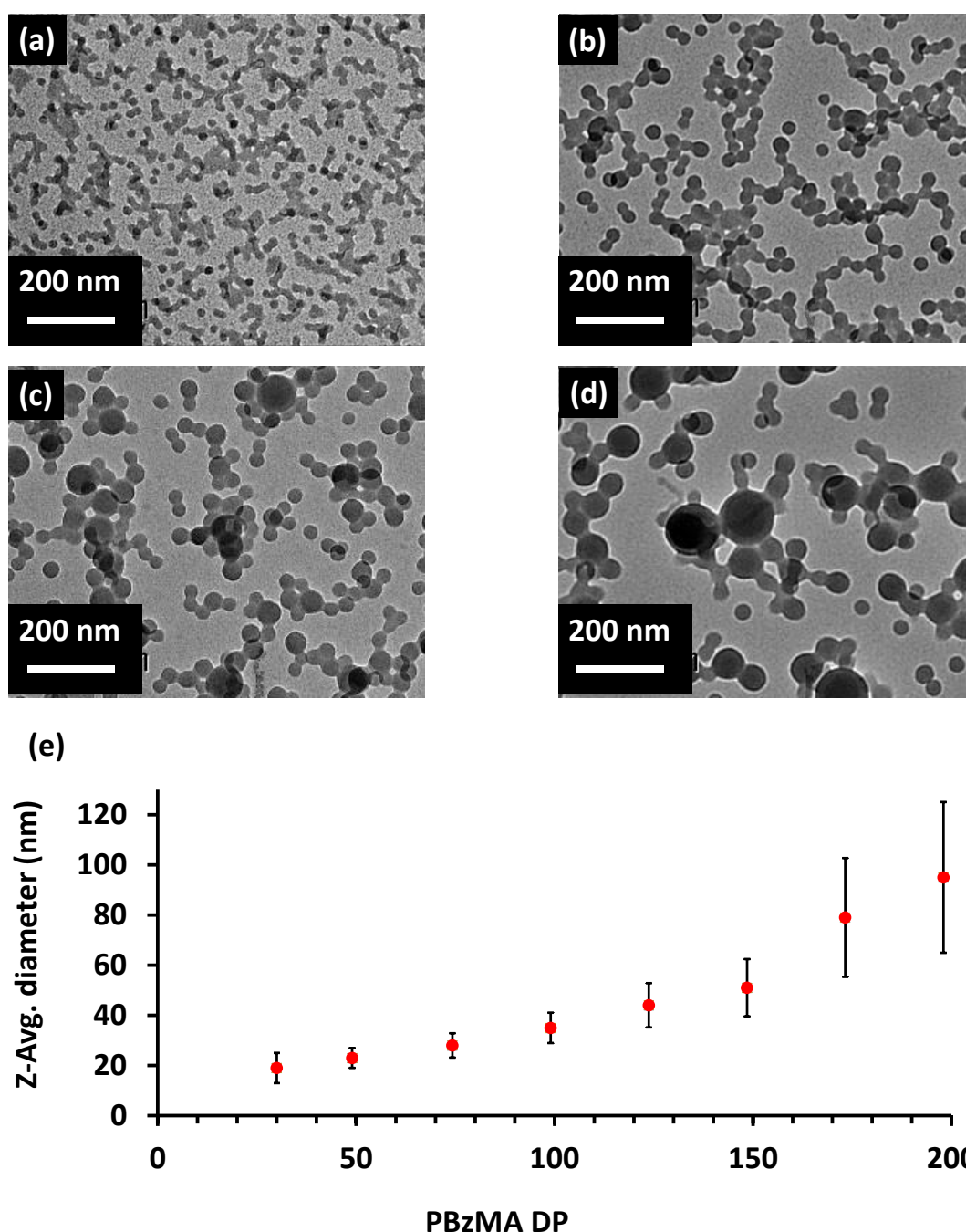


**Figure 4.9:** TEM images obtained for (a) PSiMA<sub>18</sub>-PBzMA<sub>49</sub>, (b) PSiMA<sub>18</sub>-PBzMA<sub>125</sub>, (c) PSiMA<sub>18</sub>-PBzMA<sub>175</sub> and (d) PSiMA<sub>18</sub>-PBzMA<sub>200</sub> (e) Z-average diameter, obtained from DLS, vs. PBzMA core DP for PSiMA<sub>18</sub>-PBzMA<sub>x</sub> spherical nanoparticles. In each case the error bars indicate the standard deviation of the particle size distribution, rather than the experimental error.

## Chapter 4: RAFT Dispersion Polymerisation in Silicone Oil Using a Silicone-Based Methacrylic Stabiliser

Utilising a PSiMA macro-CTA with a mean DP of 13 or 15 enabled the synthesis of vesicles at 20 % w/w, but a pure worm phase was only obtained with the PSiMA<sub>13</sub> macro-CTA. Specifically, pure worms were obtained at a block copolymer composition of PSiMA<sub>13</sub>-PBzMA<sub>54</sub>. Increasing the core-forming DP to 59, i.e. 5 units, resulted in branched worms which were significantly harder to dilute for TEM and DLS studies. The full series of copolymers used to construct the phase diagram in **Figure 4.8** are shown in **Table 4.2**.

Block Composition	Target PBzMA Dp	Conv. / %	Actual PBzMA DP	M <sub>n</sub> / g mol <sup>-1</sup>	$\frac{M_w}{M_n}$	Z-Avg. Diameter / nm	PDI	Assigned Morphology
S <sub>18</sub> -B <sub>20</sub>	20	99	20	9200	1.12	X	X	No PISA
S <sub>18</sub> -B <sub>30</sub>	30	99	30	10800	1.20	19	0.10	Spheres
S <sub>18</sub> -B <sub>49</sub>	50	98	49	11500	1.10	23	0.03	Spheres
S <sub>18</sub> -B <sub>74</sub>	75	99	74	16500	1.08	28	0.03	Spheres
S <sub>18</sub> -B <sub>99</sub>	100	99	99	18000	1.09	35	0.03	Spheres
S <sub>18</sub> -B <sub>124</sub>	125	99	124	22500	1.13	44	0.04	Spheres
S <sub>18</sub> -B <sub>149</sub>	150	99	149	25100	1.14	51	0.05	Spheres
S <sub>18</sub> -B <sub>173</sub>	175	99	173	29200	1.17	79	0.09	Spheres
S <sub>18</sub> -B <sub>198</sub>	200	99	198	32600	1.14	95	0.10	Spheres
S <sub>15</sub> -B <sub>39</sub>	40	97	39	11200	1.10	23	0.03	Spheres
S <sub>15</sub> -B <sub>54</sub>	55	98	54	13900	1.10	24	0.02	Spheres
S <sub>15</sub> -B <sub>58</sub>	60	97	58	14500	1.12	Did not disperse		Mixed
S <sub>15</sub> -B <sub>64</sub>	65	98	64	15600	1.09	Did not disperse		Mixed
S <sub>15</sub> -B <sub>69</sub>	70	98	69	16800	1.09	Did not disperse		Mixed
S <sub>15</sub> -B <sub>78</sub>	80	98	78	18500	1.14	Did not disperse		Mixed
S <sub>15</sub> -B <sub>98</sub>	100	98	98	22000	1.13	Did not disperse		Mixed
S <sub>15</sub> -B <sub>116</sub>	120	97	116	25100	1.20	Did not disperse		Mixed
S <sub>15</sub> -B <sub>139</sub>	140	99	139	27100	1.21	Did not disperse		Mixed
S <sub>15</sub> -B <sub>158</sub>	160	99	158	32000	1.22	Did not disperse		Mixed
S <sub>15</sub> -B <sub>178</sub>	180	99	178	35800	1.22	309	0.47	Vesicles
S <sub>13</sub> -B <sub>20</sub>	20	98	20	8500	1.14	X	X	No PISA
S <sub>13</sub> -B <sub>30</sub>	30	99	30	9800	1.13	22	0.04	Spheres
S <sub>13</sub> -B <sub>40</sub>	40	97	39	9200	1.19	24	0.02	Spheres
S <sub>13</sub> -B <sub>50</sub>	50	97	49	10400	1.14	27	0.03	Spheres
S <sub>13</sub> -B <sub>55</sub>	55	98	54	11600	1.12	121	0.16	Worms
S <sub>13</sub> -B <sub>60</sub>	60	99	59	11500	1.11	543	0.42	Branched W
S <sub>13</sub> -B <sub>80</sub>	80	99	79	13500	1.12	Did not disperse		Mixed
S <sub>13</sub> -B <sub>98</sub>	100	98	98	16300	1.13	Did not disperse		Mixed
S <sub>13</sub> -B <sub>137</sub>	140	98	137	21100	1.13	Did not disperse		Mixed
S <sub>13</sub> -B <sub>158</sub>	160	99	158	22500	1.18	Did not disperse		Mixed
S <sub>13</sub> -B <sub>176</sub>	180	98	176	29800	1.27	319	0.28	Vesicles
S <sub>13</sub> -B <sub>198</sub>	200	99	198	30300	1.27	287	0.36	Vesicles

**Table 4.2:** Summary of the diblock copolymers used to construct the phase diagram shown in **Figure 4.8**. The M<sub>n</sub> data was obtained by THF GPC and the monomer conversions by <sup>1</sup>H NMR in chloroform-d

In addition to the narrow molecular weight distributions obtained for each sample, the GPC curves were always unimodal, indicating high blocking efficiencies. Selected chromatograms obtained for P*SiMA*<sub>15</sub>-P*BzMA*<sub>x</sub> diblock are shown in **Figure 4.10**.

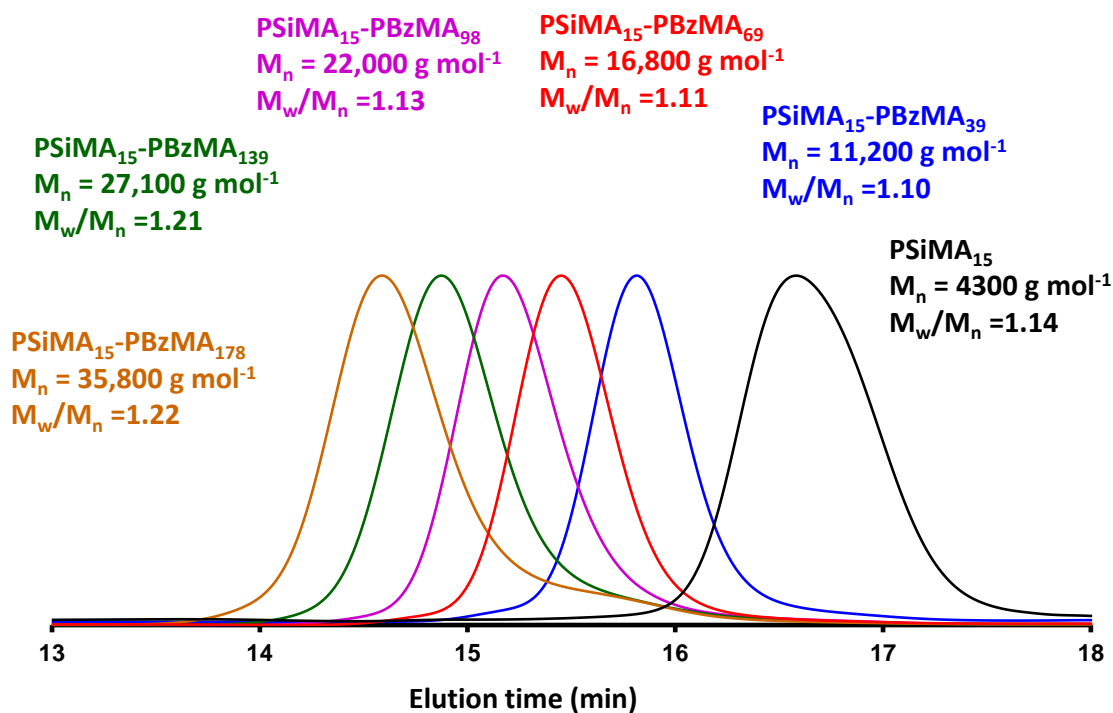


**Figure 4.10:** THF GPC curves obtained for the final P*SiMA*<sub>15</sub>-P*BzMA*<sub>x</sub> diblock copolymers prepared via RAFT dispersion polymerisation of *BzMA* in D5 silicone oil at 20 % w/w.

### 4.3.3 Influence of concentration upon copolymer morphology

To investigate the influence of the polymerisation concentration on the final copolymer morphology, the P*SiMA*<sub>13</sub> macro-CTA was chain extended with *BzMA* for copolymer concentrations ranging between 5 and 15 % w/w in D5 silicone oil. These results, along with the 20 % w/w series, were used to construct a second phase diagram (**Figure 4.11**).

Perhaps surprisingly, worm-like micelles were obtained at concentrations as low as 5 % w/w. This is somewhat unusual for PISA formulations in non-polar systems, which often require concentrations in excess of 10 % w/w to form worm-like micelles.<sup>24</sup> There are some exceptions to this generalisation, P*SiMA*-P*BzMA* worms when prepared in mineral oil, for example.<sup>18</sup> However, such examples are relatively rare in the PISA literature. In addition to worm-like micelles, vesicles were obtained at concentrations ranging between 10 and 20 % w/w.

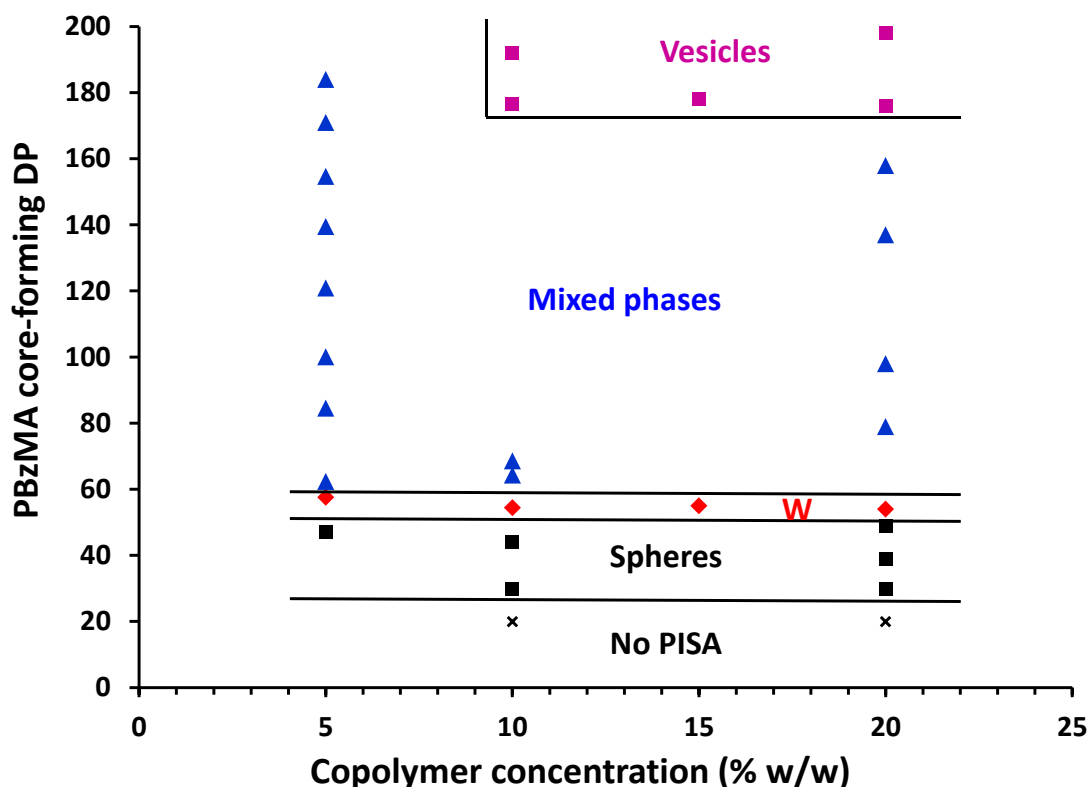


**Figure 4.11:** Phase diagram constructed for PSiMA<sub>13</sub>-PBzMA<sub>x</sub> nanoparticles prepared at various concentrations in D5 silicone oil and accompanying TEMs for selected samples.

However, when prepared at 5 % w/w, a pure vesicle phase could not be isolated. Instead, mixed sphere / vesicle phases were observed.

In all cases worm-like micelles synthesised between 5 and 20 % w/w formed free-standing gels. To investigate the physical nature of such gels, a PSiMA<sub>13</sub>-PBzMA<sub>57</sub> worm-gel was analysed *via* oscillatory rheology. It is perhaps worth noting here that worms prepared at 5 % w/w were chosen because worm gels prepared at 10, 15 and 20 % w/w became increasingly brittle. **Figure 4.12a** shows the variation in  $G'$  and  $G''$  vs. percentage strain, at a fixed angular frequency. As expected for a gel, the magnitude of  $G'$  (~ 90 Pa) is greater than for  $G''$  (20 Pa). Moreover, these two parameters are more or less independent of the applied strain (amplitude of oscillation) over an appreciable range, indicating linear viscoelastic behaviour. For strains greater than 100 %,  $G'$  falls below  $G''$ , indicating the presence of a yield point. **Figure 4.12b** shows the variance of  $G'$  and  $G''$  with angular frequency at a fixed strain of 1 %. Again,  $G'$  exceeds  $G''$  confirming that this sample is indeed a gel. In addition, both parameters are relatively independent of applied frequency within a reasonably broad range, indicating linear viscoelastic behaviour.

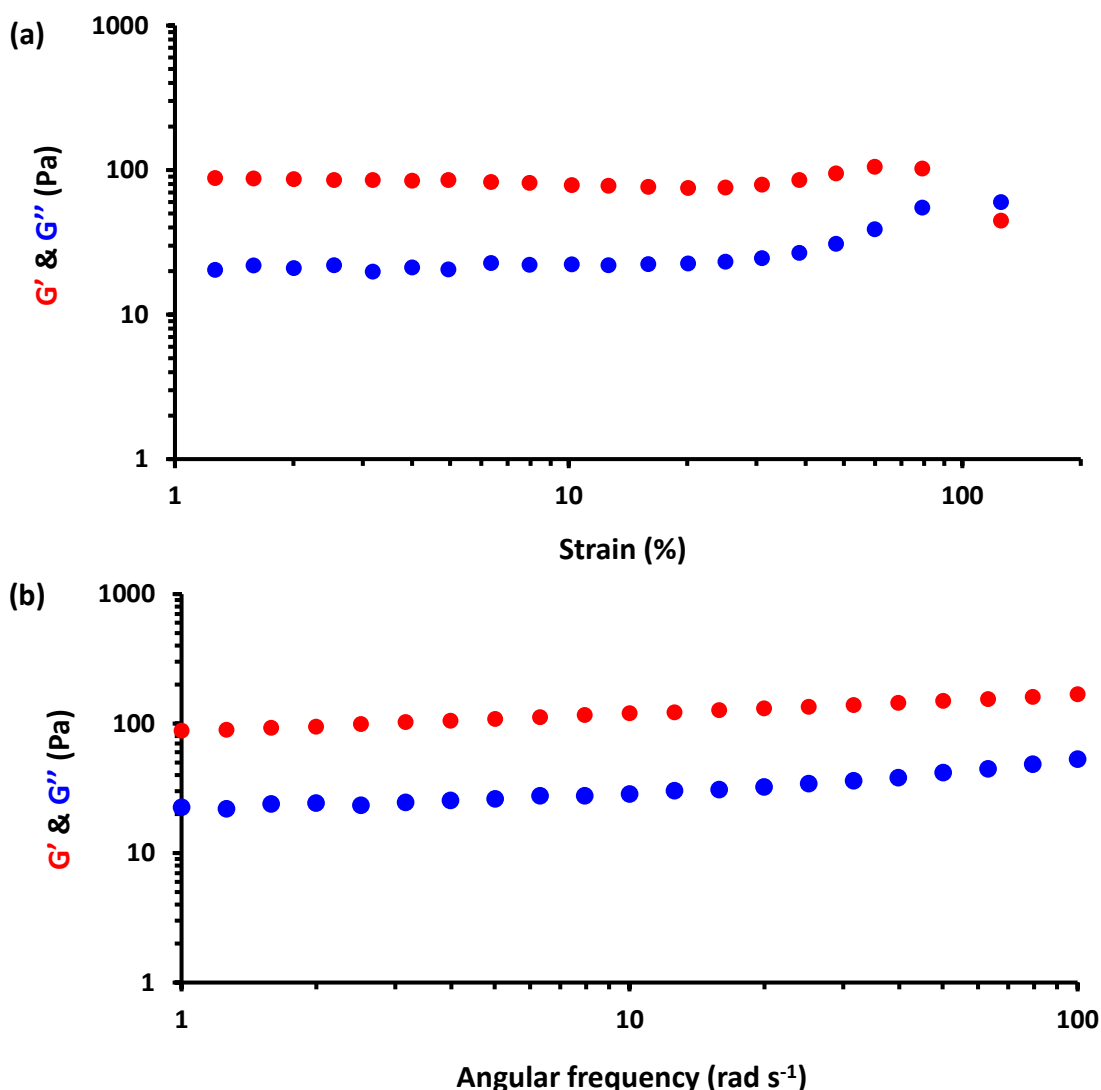


**Figure 4.12:** Oscillatory rheology performed upon a sample of PSiMA<sub>13</sub>-PBzMA<sub>57</sub> worms synthesised at 5 % w/w. (a) The variance of G' and G'' with strain (%) at a fixed angular frequency of 1 rad s<sup>-1</sup>. (b) The variance of G' and G'' with angular frequency at a fixed strain of 1 %.

#### 4.3.4 Spontaneous cross-linking of PSiMA<sub>x</sub>-PBzMA<sub>y</sub> nanoparticles over time

One problem with the PSiMA<sub>x</sub>-PBzMA<sub>y</sub> diblock copolymer nanoparticles described herein is the development of a high molecular weight shoulder, on ageing at 20 °C, as indicated by THF GPC. **Figure 4.13** shows GPC chromatograms obtained for PSiMA<sub>13</sub>-PBzMA<sub>54</sub> worms, synthesised and stored at copolymer concentration of 10 % w/w, over a number of weeks. Initially, the dispersity of the constituent diblock copolymer chains is low (1.12) as expected of diblock copolymers prepared by a well-controlled RAFT polymerisation. After six weeks, a high molecular weight shoulder was observed, and the dispersity increased considerably.

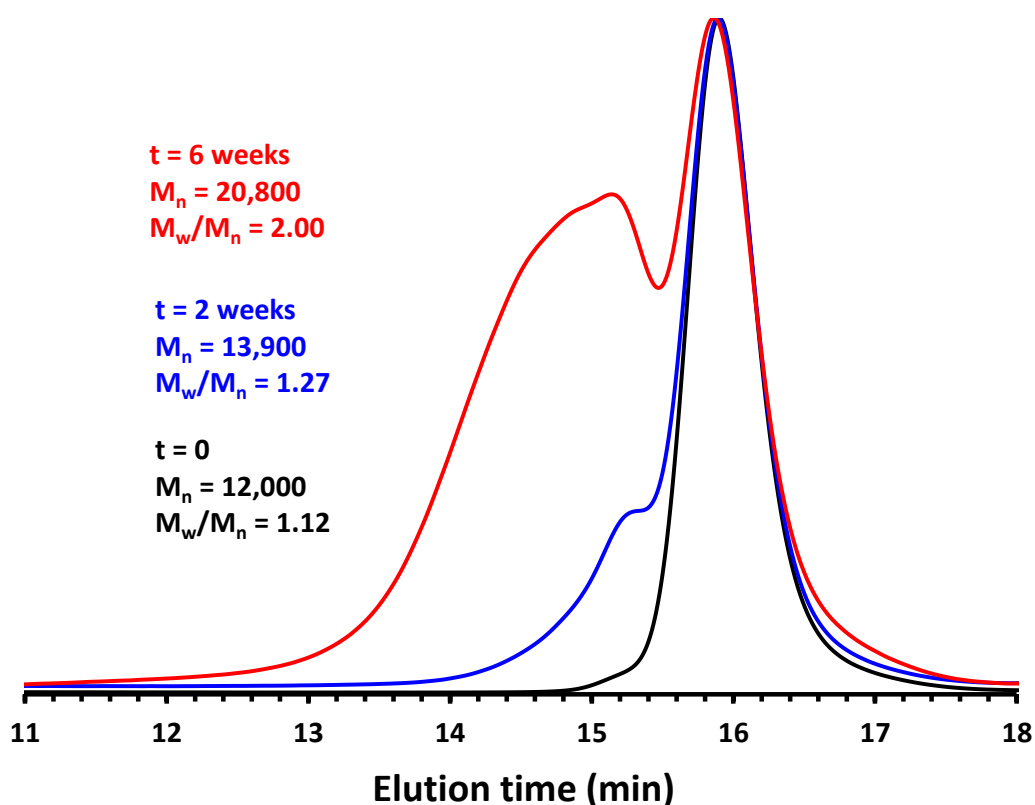
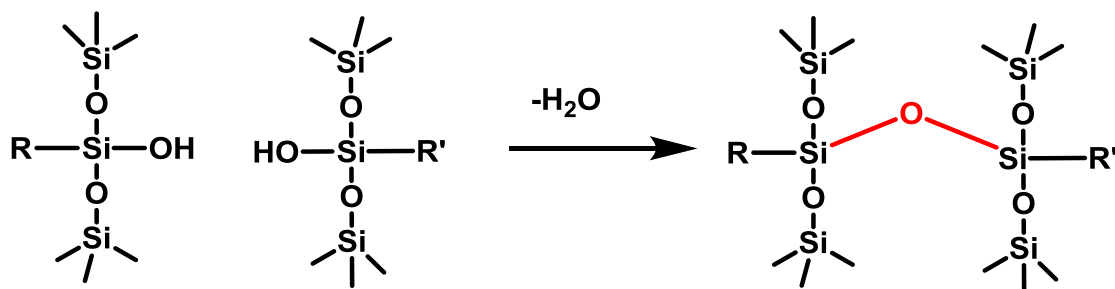


**Figure 4.13:** THF GPC chromatograms obtained over time for PSiMA<sub>13</sub>-PBzMA<sub>54</sub> worms

A plausible explanation for this observation is that these nanoparticles are cross-linking *via* the PSiMA stabilisers over time. Originally, SiMA was selected for the stabiliser-forming monomer because it contains no labile silyl ether or silanol-functional groups, which are known to self-cross-link. However, it is likely that the as-received monomer contains a small fraction unprotected silanol impurity, which, if present could cross-link according to (Scheme 4.2).



**Scheme 4.2:** Potential cross-linking route between two SiMA units containing a silanol impurities.

In an attempt to identify whether this impurity was present, the as-received monomer was analysed by IR and <sup>1</sup>H NMR spectroscopy. However, the IR spectrum exhibits no indication of hydroxyl functionality between 3550 and 3200 cm<sup>-1</sup> and no obvious impurities can be observed in the <sup>1</sup>H NMR spectrum.

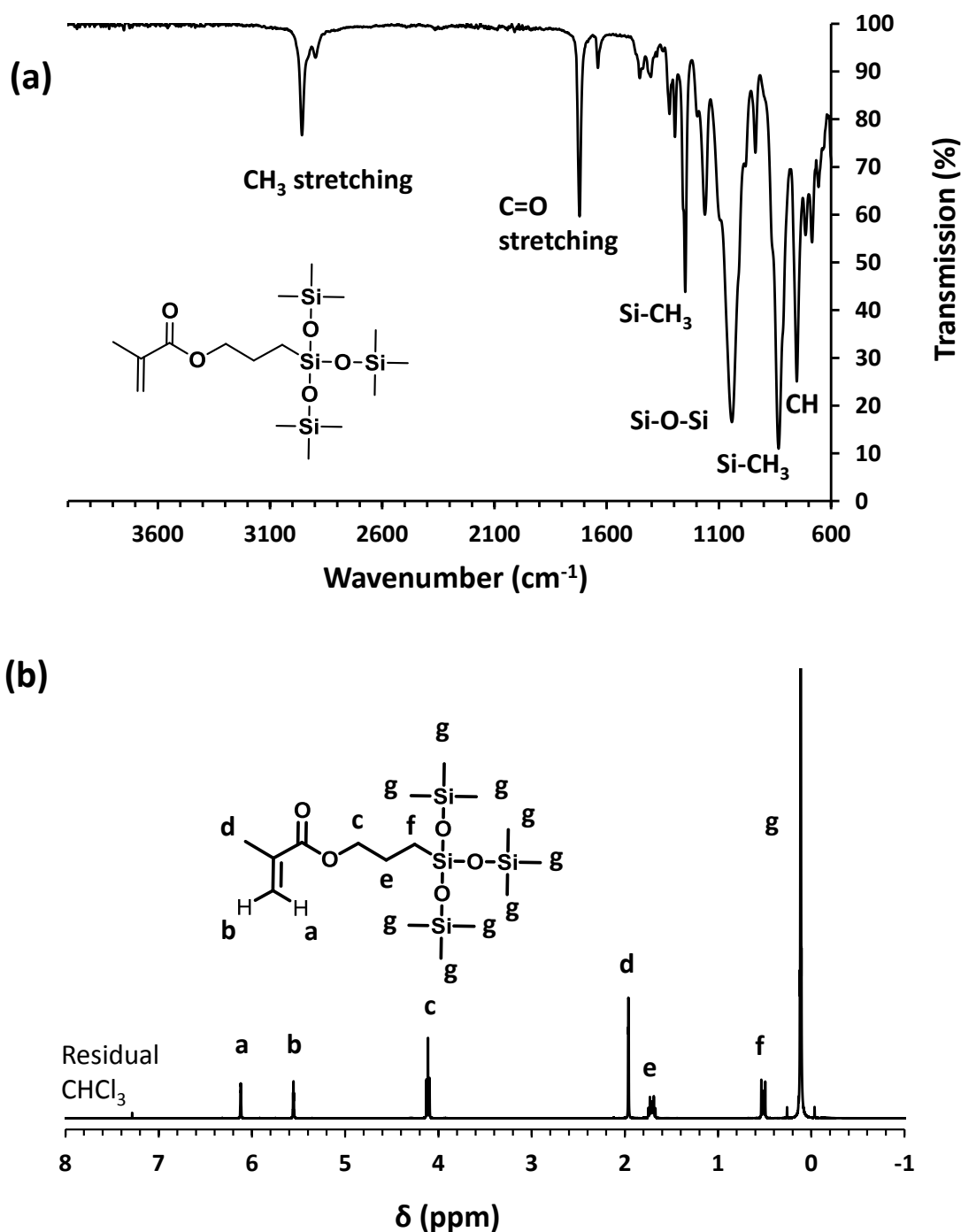


**Figure 14:** (a) IR spectrum of SiMA monomer, recorded in transmission mode between 4000 and 600 cm<sup>-1</sup>. (b) <sup>1</sup>H NMR spectrum recorded of SiMA monomer, recorded in chloroform-d.

Despite this negative result, if the hydroxyl-containing impurity is only present at very low levels it would likely be undetectable in the <sup>1</sup>H NMR and IR spectrum. As such, in future work this monomer will be subject to further, more sensitive, characterisation using gas chromatography mass-spectrometry (GC-MS) and high performance liquid-chromatography.

## 4.4 Conclusions

SiMA monomer was polymerised *via* RAFT solution polymerisation using PETTC in toluene. The kinetics of this polymerisation were determined by  $^1\text{H}$  NMR spectroscopy and the evolution of molecular weight was monitored by THF GPC. The former technique indicated that approximately six hours were required to achieve a SiMA conversion of 80 %. The latter technique indicated that the polymerisation was well-controlled, with a linear evolution of  $M_n$  with monomer conversion and relatively low dispersities ( $\text{Đ} < 1.20$ ) being observed.

Based on these preliminary kinetics three P*Si*MA macro-CTAs were prepared *via* RAFT solution polymerisation in toluene using PETTC RAFT agent. These macro-CTAs were characterised by  $^1\text{H}$  NMR spectroscopy, which indicated a mean DP of either 13, 15 or 18. Furthermore, THF GPC indicated low dispersities in each case. Each of these macro-CTAs was then chain extended with varying amounts of BzMA, in D5, in order to construct phase diagrams. When the stabiliser DP was 18, only spherical micelles were accessible with mean Z-average diameters ranging from 20 nm to 95 nm. In contrast, reducing the stabiliser DP to 13 enabled access to the full range of copolymer morphologies.

In order to investigate the influence of copolymer concentration on the final nanoparticle morphology, the P*Si*MA<sub>13</sub> macro-CTA was chain extended with varying quantities of BzMA at a range of copolymer concentrations ranging between 5 and 20 % w/w. It was demonstrated that a pure worm phase could be obtained at copolymer concentrations as low as 5 % w/w. Moreover, oscillatory rheology studies confirmed that such worms still formed a free-standing gel.

Despite the low dispersities achieved for the polymerisations described herein, a distinct broadening of the molecular weight distribution was observed over time. This is potentially the result of the presence of small quantities of a methacrylic silanol impurities facilitating cross-linking between P*Si*MA chains.

## 4.5 References

- (1) Zhang, X.; Boissé, S.; Zhang, W.; Beaunier, P.; D'Agosto, F.; Rieger, J.; Charleux, B. Well-Defined Amphiphilic Block Copolymers and Nano-Objects Formed in Situ via RAFT-Mediated Aqueous Emulsion Polymerization. *Macromolecules* **2011**, *44*, 4149–4158.
- (2) Zhang, W. J.; Hong, C. Y.; Pan, C. Y. Fabrication of Spaced Concentric Vesicles and Polymerizations in RAFT Dispersion Polymerization. *Macromolecules* **2014**, *47*, 1664–1671.

- (3) Houillot, L.; Bui, C.; Farcet, C.; Moire, C.; Raust, J. A.; Pasch, H.; Save, M.; Charleux, B. Dispersion Polymerization of Methyl Acrylate in Nonpolar Solvent Stabilized by Block Copolymers Formed in Situ via the RAFT Process. *ACS Appl. Mater. Interfaces* **2010**, *2*, 434–442.
- (4) Li, Y.; Armes, S. P. RAFT Synthesis of Sterically Stabilized Methacrylic Nanolatexes and Vesicles by Aqueous Dispersion Polymerization. *Angew. Chemie* **2010**, *49*, 4042–4046.
- (5) Warren, N. J.; Mykhaylyk, O. O.; Mahmood, D.; Ryan, A. J.; Armes, S. P. RAFT Aqueous Dispersion Polymerization Yields Poly(ethylene Glycol)-Based Diblock Copolymer Nano-Objects with Predictable Single Phase Morphologies. *J. Am. Chem. Soc.* **2014**, *136*, 1023–1033.
- (6) Lopez-Oliva, A. P.; Warren, N. J.; Rajkumar, A.; Mykhaylyk, O. O.; Derry, M. J.; Doncom, K. E. B.; Rymaruk, M. J.; Armes, S. P. Polydimethylsiloxane-Based Diblock Copolymer Nano-Objects Prepared in Nonpolar Media via RAFT-Mediated Polymerization-Induced Self-Assembly. *Macromolecules* **2015**, *48*, 3547–3555.
- (7) Canning, S. L.; Smith, G. N.; Armes, S. P. A Critical Appraisal of RAFT-Mediated Polymerization-Induced Self-Assembly. *Macromolecules* **2016**, *49*, 1985–2001.
- (8) Blanazs, A.; Ryan, A. J.; Armes, S. P. Predictive Phase Diagrams for RAFT Aqueous Dispersion Polymerization: Effect of Block Copolymer Composition, Molecular Weight, and Copolymer Concentration. *Macromolecules* **2012**, *45*, 5099–5107.
- (9) Sugihara, S.; Blanazs, A.; Armes, S. P.; Ryan, A. J.; Lewis, A. L. Aqueous Dispersion Polymerization: A New Paradigm for in Situ Block Copolymer Self-Assembly in Concentrated Solution. *J. Am. Chem. Soc.* **2011**, *133*, 15707–15713.
- (10) Blanazs, A.; Madsen, J.; Battaglia, G.; Ryan, A. J.; Armes, S. P. Mechanistic Insights for Block Copolymer Morphologies: How Do Worms Form Vesicles? *J. Am. Chem. Soc.* **2011**, *133*, 16581–16587.
- (11) Warren, N. J.; Armes, S. P. Polymerization-Induced Self-Assembly of Block Copolymer Nano-Objects via RAFT Aqueous Dispersion Polymerization. *J. Am. Chem. Soc.* **2014**, *136*, 10174–10185.
- (12) Jones, E. R.; Semsarilar, M.; Blanazs, A.; Armes, S. P. Efficient Synthesis of Amine-Functional Diblock Copolymer Nanoparticles via RAFT Dispersion Polymerization of Benzyl Methacrylate in Alcoholic Media. *Macromolecules* **2012**, *45*, 5091–5098.
- (13) Gonzato, C.; Semsarilar, M.; Jones, E. R.; Li, F.; Krooshof, G. J. P.; Wyman, P.; Mykhaylyk, O. O.; Tuinier, R.; Armes, S. P. Rational Synthesis of Low-Polydispersity Block Copolymer Vesicles in Concentrated Solution via Polymerization-Induced Self-Assembly. *J. Am. Chem. Soc.* **2014**, *136*, 11100–11106.
- (14) Huang, C. Q.; Pan, C. Y. Direct Preparation of Vesicles from One-Pot RAFT Dispersion Polymerization. *Polymer* **2010**, *51*, 5115–5121.
- (15) Derry, M. J.; Fielding, L. A.; Armes, S. P. Polymerization-Induced Self-Assembly of Block Copolymer Nanoparticles via RAFT Non-Aqueous Dispersion Polymerization. *Prog. Polym. Sci.* **2016**, *52*, 1–18.
- (16) Kang, Y.; Pitto-Barry, A.; Willcock, H.; Quan, W.-D.; Kirby, N.; Sanchez, A. M.; O'Reilly, R. K. Exploiting Nucleobase-Containing Materials – from Monomers to Complex Morphologies Using RAFT Dispersion Polymerization. *Polym. Chem.* **2015**, *6*, 106–117.
- (17) Derry, M. J.; Fielding, L. A.; Armes, S. P. Industrially-Relevant Polymerization-Induced Self-Assembly Formulations in Non-Polar Solvents: RAFT Dispersion Polymerization of Benzyl Methacrylate. *Polym. Chem.* **2015**, *6*, 3054–3062.
- (18) Derry, M. J.; Fielding, L. A.; Warren, N. J.; Mable, C. J.; Smith, A. J.; Mykhaylyk, O. O.; Armes, S. P. In Situ Small-Angle X-Ray Scattering Studies of Sterically-Stabilized Diblock Copolymer Nanoparticles Formed during Polymerization-Induced Self-Assembly in Non-Polar Media. *Chem. Sci.* **2016**, *7*, 5078–5090.
- (19) Pei, Y.; Thurairajah, L.; Sugita, O. R.; Lowe, A. B. RAFT Dispersion Polymerization in

- Nonpolar Media: Polymerization of 3-Phenylpropyl Methacrylate in N -Tetradecane with Poly(stearyl Methacrylate) Homopolymers as Macro Chain Transfer Agents. *Macromolecules* **2015**, *48*, 236–244.
- (20) Pei, Y.; Dharsana, N. C.; van Hensbergen, J. A.; Burford, R. P.; Roth, P. J.; Lowe, A. B. RAFT Dispersion Polymerization of 3-Phenylpropyl Methacrylate with poly[2-(Dimethylamino)ethyl Methacrylate] Macro-CTAs in Ethanol and Associated Thermoreversible Polymorphism. *Soft Matter* **2014**, *10*, 5787–5796.
- (21) Cunningham, V. J.; Alswieleh, A. M.; Thompson, K. L.; Williams, M.; Leggett, G. J.; Armes, S. P.; Musa, O. M. Poly(glycerol monomethacrylate)–Poly(benzyl Methacrylate) Diblock Copolymer Nanoparticles via RAFT Emulsion Polymerization: Synthesis, Characterization, and Interfacial Activity. *Macromolecules* **2014**, *47*, 5613–5623.
- (22) Semsarilar, M.; Jones, E. R.; Blanazs, A.; Armes, S. P. Efficient Synthesis of Sterically-Stabilized Nano-Objects via RAFT Dispersion Polymerization of Benzyl Methacrylate in Alcoholic Media. *Adv. Mater.* **2012**, *24*, 3378–3382.
- (23) Zehm, D.; Ratcliffe, L. P. D.; Armes, S. P. Synthesis of Diblock Copolymer Nanoparticles via RAFT Alcoholic Dispersion Polymerization: Effect of Block Copolymer Composition, Molecular Weight, Copolymer Concentration, and Solvent Type on the Final Particle Morphology. *Macromolecules* **2013**, *46*, 128–139.
- (24) Fielding, L. A.; Derry, M. J.; Admiral, V.; Rosselgong, J.; Rodrigues, A. M.; Ratcliffe, L. P. D.; Sugihara, S.; Armes, S. P. RAFT Dispersion Polymerization in Non-Polar Solvents: Facile Production of Block Copolymer Spheres, Worms and Vesicles in N-Alkanes. *Chem. Sci.* **2013**, *4*, 2081–2087.
- (25) Fielding, L. A.; Lane, J. A.; Derry, M. J.; Mykhaylyk, O. O.; Armes, S. P. Thermo-Responsive Diblock Copolymer Worm Gels in Non-Polar Solvents. *J. Am. Chem. Soc.* **2014**, *136*, 5790–5798.
- (26) Derry, M. J.; Mykhaylyk, O. O.; Armes, S. P. A Vesicle-to-Worm Transition Provides a New High-Temperature Oil Thickening Mechanism. *Angew. Chemie* **2017**, *129*, 1772–1776.
- (27) Trent, J. S.; Scheinbeim, J. I.; Couchman, P. R. Ruthenium Tetraoxide Staining of Polymers for Electron Microscopy. *Macromolecules* **1983**, *16*, 589–598.

**Chapter 5: Oil-in-Oil Pickering  
Emulsions Stabilised by Polymeric  
Nanoparticles**

### 5.1 Introduction

Generally, the interface between two immiscible fluids such as water and oil is unstable.<sup>1</sup> This is because the interaction between water molecules is more favourable than that between water and oil molecules.<sup>2,3</sup> Water molecules in the bulk liquid can interact with the maximum possible number of neighbouring molecules, whereas water molecules at the oil/water interface cannot.<sup>4</sup> As such, water molecules at the interface occupy a higher energy state than those in the bulk. Typically, the system will seek to minimise this energy by reducing the interfacial area of each fluid, giving rise to a phenomenon known as interfacial tension.<sup>4</sup> However, this poses a significant technical challenge for the formation of stable emulsions, which comprise droplets of one liquid dispersed in a second immiscible liquid. This is because they have a very large interfacial area and hence are thermodynamically unstable.<sup>5,6</sup>

This problem can be addressed by the addition of a suitable surfactant.<sup>7–10</sup> Surfactants can stabilise fluid interfaces by adsorbing at the interface and reducing the interfacial energy.<sup>11,12</sup> This enables the formation of oil-in-water emulsions,<sup>13</sup> water-in-oil emulsions<sup>14</sup> and aqueous foams.<sup>15</sup> Around the turn of the twentieth century, Ramsden and Pickering demonstrated that various types of colloidal particles can also stabilise fluid interfaces.<sup>16,17</sup> Furthermore, unlike surfactants, such particles need not be amphiphilic – they simply need to be partially wetted by both fluids.<sup>7,18,19</sup> After decades of relative inactivity, there has been a resurgence of interest in Pickering emulsions over the past two decades or so.<sup>19</sup>

For conventional surfactant-stabilised emulsions, the hydrophile-lipophile balance (HLB) of the surfactant is the most important characteristic in determining whether it resides predominantly in the aqueous or oil phase.<sup>20</sup> The packing parameter of any given surfactant is dictated by its geometry, see equation (1.15)<sup>1,21</sup> This determines whether a close-packed surfactant monolayer curves towards the oil, or aqueous phase, or remains effectively planar.<sup>21</sup> For hydrophilic surfactants, the area occupied per head-group is larger than that of the hydrophobic chain. Therefore, monolayers of hydrophilic surfactants afford oil-in-water (o/w) emulsions i.e. oil droplets dispersed in an aqueous continuous phase. Conversely, for surfactants with more lipophilic character, the area occupied by the hydrophobic chain exceeds that occupied by the head group. This results in curvature towards the water phase, which gives rise to water-in-oil (w/o) emulsions.<sup>7</sup> For colloidal particles, the relevant parameter is the three-phase contact angle,  $\theta$ , (measured through the oil/water interface) which relates to the surface wettability and usually dictates the emulsion type.<sup>7</sup> For hydrophilic particles, for which  $\theta < 90^\circ$ , the majority of each particle resides in the aqueous phase. In contrast,  $\theta > 90^\circ$  for hydrophobic particles, and most of

each particle resides in the oil phase. Like surfactants adsorbed at an interface, monolayers of adsorbed particles will also curve so that the phase that wets the particle the most will be located on the external side.<sup>7,18</sup> As a direct consequence, o/w emulsions are formed when  $\theta < 90^\circ$  and w/o emulsions are formed when  $\theta > 90^\circ$  (**Figure 5.1**).

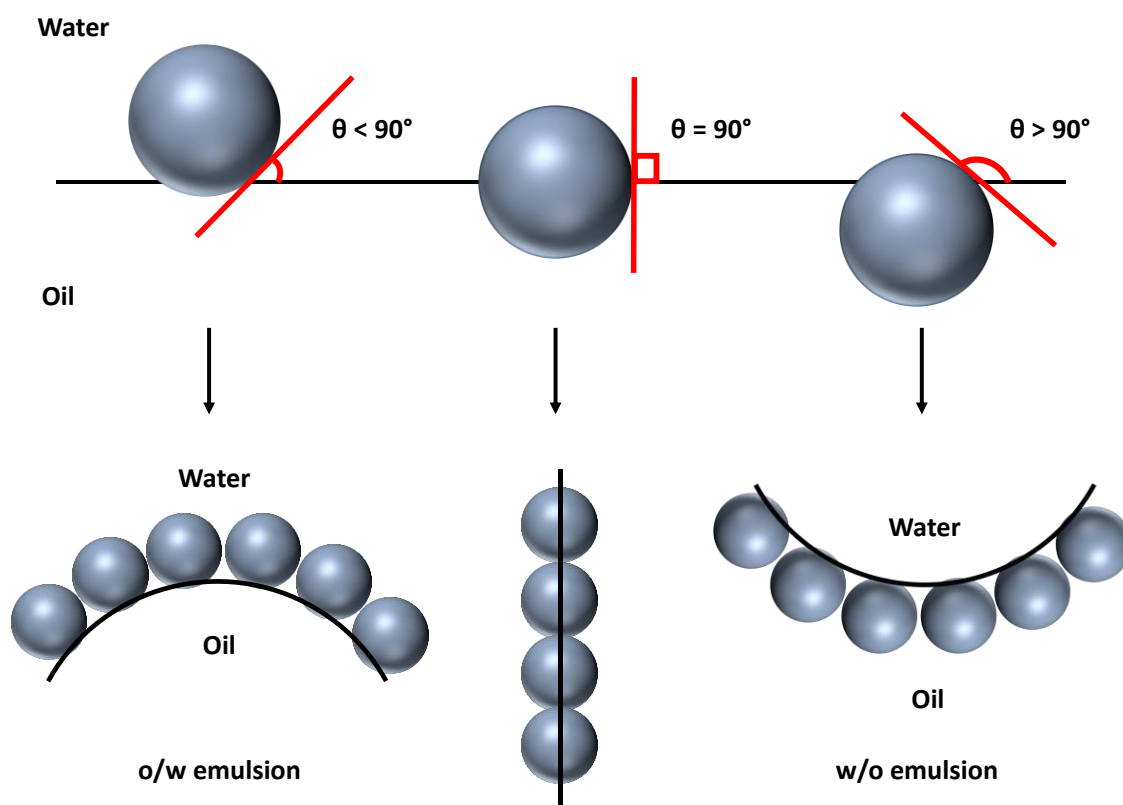


**Figure 5.1:** Consider three types of spherical particles adsorbed at the oil/water interface: a hydrophilic particle with a contact angle less than  $90^\circ$  (left), a particle of intermediate wettability with a contact angle of  $90^\circ$  (centre) and a hydrophobic particle with a contact angle greater than  $90^\circ$  (right). The lower images represent the likely position of each type of particles at an oil/water interface. For the hydrophilic particles (left) an oil-in-water emulsion is formed, for hydrophobic particles (right) a water-in-oil emulsion results.<sup>7</sup>

In addition to the contact angle made by the particle at a given interface, two other parameters must also be considered to describe the strength of its adsorption: (i) the particle diameter, and (ii) the interfacial tension of the interface at which the particle is adsorbed.<sup>7,22,23</sup> When a particle adsorbs at an interface, such as oil/water, it replaces an area of energetically unfavourable oil/water interface with energetically more favourable water/particle and particle/oil interfaces.<sup>24</sup> Therefore, particle adsorption reduces the total interfacial area of the system, and consequently also lowers the interfacial energy. As such, adsorption of a larger particle provides a greater reduction in interfacial area than a smaller particle.<sup>7</sup> Hence, larger particles adsorb more strongly than smaller particles at a particular interface, for a given particle contact angle. Similarly, if the interfacial energy is very high, there is a greater driving force for particle adsorption. This is

because the energy reduction *per particle* is greater when adsorbing at a high-energy interface than at a low-energy interface. Using the three aforementioned parameters, the energy of detachment of a particle at an interface can be calculated using equation (5.1).<sup>7</sup>

$$E = \pi r^2 \gamma_{\alpha\beta} (1 \pm \cos\theta)^2 \quad (5.1)$$

Here,  $E$  is the energy required to remove a particle from an interface,  $r$  is the particle radius,  $\gamma_{\alpha\beta}$  is the interfacial energy,  $\theta$  is the contact angle that the particle makes with the interface,  $\pi$  is the mathematical constant, and the  $\cos$  function within the bracket is negative for removal into the water phase and positive for removal into the oil phase.<sup>7</sup>

Consider the adsorption of a nanoparticle at the water/*n*-dodecane interface ( $\gamma \sim 0.045 \text{ N m}^{-1}$ ), with a radius of  $10^{-7} \text{ m}$ . At a contact angle of  $90^\circ$  the energy of detachment is of the order of  $10^5 k_B T$ , i.e. much greater than the mean thermal energy. This falls off rapidly either side of  $90^\circ$ . A similar effect is observed when varying the nanoparticle diameter. For contact angles ranging from  $60^\circ$  to  $120^\circ$ , nanoparticle diameters greater than 10 nm are adsorbed essentially irreversibly at the interface. This is in stark contrast to surfactant-stabilised interfaces which are in rapid dynamic equilibrium.<sup>7</sup>

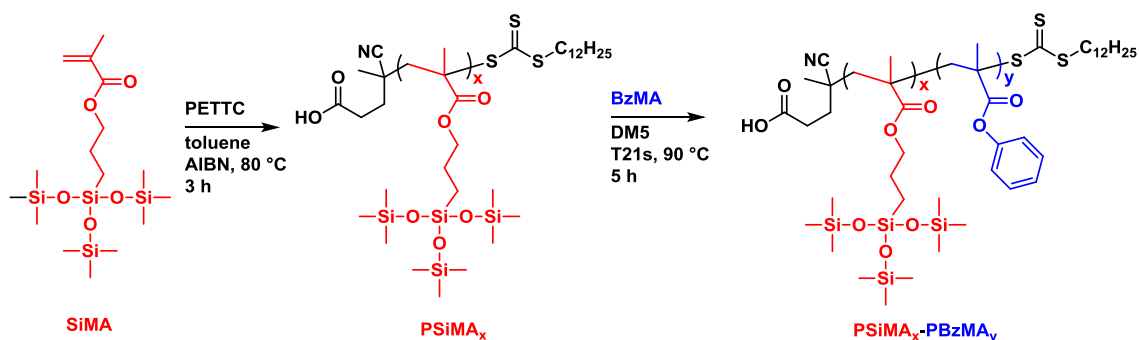
Several conclusions can be drawn from equation (5.1). For example, the interfacial adsorption of particles is at a maximum when the contact angle is  $90^\circ$  and increases with increasing nanoparticle diameter. However, it does not necessarily follow from equation (5.1) that once particles are adsorbed at the interface, stable emulsions/foams will be formed. In fact, from equation (5.1) one may incorrectly predict that maximum emulsion/foam stability should occur at a particle contact angle of  $90^\circ$ , i.e. at the strongest possible particle adsorption. However, Schulman and Leja demonstrated that this is not the case.<sup>25</sup> Furthermore, this has been independently confirmed by other researchers.<sup>26–28</sup> It turns out that equation (5.1) provides an incomplete picture with regards to an emulsion or foam. More specifically it does not take into account that, in order to stabilise emulsions/foams, the thin liquid film present between the large particle-stabilised droplets/bubbles must also be stabilised.<sup>29</sup> This problem was addressed by Kaptay, who devised a model that incorporated both the energy required to remove a particle from an interface, *and* the ability of the same particles to stabilise thin liquid films *via* capillary interactions.<sup>29</sup> Kaptay concluded that for o/w emulsions, maximum stability occurs close to a contact angle of  $70^\circ$ . Conversely, a contact angle of  $110^\circ$  provides maximum stability for w/o emulsions.<sup>29</sup> Therefore, the rational design and synthesis of bespoke nanoparticles with tunable wettability is crucial for

producing effective Pickering emulsifiers. PISA is one such technique by which this goal can be achieved.

There are many reported literature examples of water-in-oil Pickering emulsions.<sup>30-33</sup> These have been obtained using a large range of particles, of varying size,<sup>34,35</sup> and morphology.<sup>36-38</sup> Similarly, oil-in-water Pickering emulsions have also been explored by a number of research groups.<sup>24,39,40</sup> However, there are currently only a few reports of oil-in-oil emulsions stabilised by nanoparticles.<sup>41</sup> In this context, an oil refers to a liquid with a low relative permittivity (typically less than 5). While non-aqueous Pickering emulsions, which comprise polar solvents such as methanol or DMF instead of water, are sometimes referred to as oil-in-oil emulsions,<sup>42</sup> these are not considered herein.

Oil-in-oil Pickering emulsions have been investigated for a range of different applications, such as lubricants and cosmetics.<sup>41</sup> In fact, the majority of reports of oil-in-oil Pickering emulsions appear in the patent literature, dating back as far as the late 1960s.<sup>41</sup> Generally, such systems comprise a silicone oil as one phase and either a mineral oil or a vegetable oil as the other. In addition to the patent literature, there are also a few reports of o/o Pickering emulsions in the peer-reviewed literature. For example, Binks and co-workers demonstrated that hydrophobised fumed silica could act as an effective Pickering emulsifier for emulsions comprising PDMS as one phase, and either olive oil, sunflower oil or rapeseed oil as another.<sup>41</sup> Furthermore, such particles also facilitated the production of oil-in-oil-in-oil double emulsions.<sup>43</sup> More recently, Rozynek and co-workers reported that silicone oil droplets can be stabilised in castor oil using a range of particles, including dyed polyethylene, polystyrene or silica.<sup>44,45</sup> Moreover, applying an electric field to such emulsions enables their coalescence behaviour to be tuned to produce droplets with a narrow size distribution compared to emulsions produced by more conventional techniques.

The work presented in this Chapter is also concerned with oil-in-oil Pickering emulsions, and was conducted during a six-month industrial secondment at Scott Bader Ltd. More specifically, the utility of P*Si*MA-P*Bz*MA spherical nanoparticles as Pickering emulsifiers was investigated. A range of P*Si*MA-P*Bz*MA nanoparticles were prepared directly in a low-viscosity silicone oil, dimethicone 5 (DM5), which is a linear PDMS with a viscosity of 5 cS. The resulting nanoparticles were then evaluated as emulsifiers for a range of non-polar oils. Furthermore, it is shown that statistical copolymerisation of lauryl methacrylate (LMA) into the nanoparticle core can enhance Pickering emulsifier performance significantly.



**Scheme 5.1:** Synthesis of a PSiMA macro-CTA *via* RAFT solution polymerisation in toluene, and its subsequent chain extension using benzyl methacrylate in dimethicone at 90 °C (DM5; 5 cSt)

## 5.2 Experimental section

### 5.2.1 Materials

4-Cyano-4-(((dodecylthio)carbonothioyl)thio)pentanoic acid (CDCP) was purchased from Boron Molecular (Australia). SiMA was obtained from TER (UK). Benzyl methacrylate, 1-pyrenemethanol, 4-dimethylaminopyridine (DMAP), *N,N'*-dicyclohexylcarbodiimide (DCC), dichloromethane, chloroform-*d*, dichloromethane-*d*<sub>2</sub> castor oil, lauryl methacrylate (LMA) and linseed oil were obtained from Sigma Aldrich (UK). Tall oil fatty acid (TOFA 2 %), tall oil fatty acid (TOFA 26 %), azobisisobutyronitrile (AIBN) and trigonox 21s (T21s) were provided by Scott Bader Ltd. (UK). Olive oil and sunflower oil were purchased from Co-Op Food Ltd. (UK). DM5 (5 cSt) was obtained from Bluestar Silicones (USA). Anhydrous dichloromethane was obtained from an in-house Grubbs dry solvent system. Lauryl methacrylate was passed through basic alumina prior to use, while all other reagents were used as received.

### 5.2.2 Methods

#### Synthesis of PSiMA macro-CTA

A typical PSiMA macro-CTA synthesis was conducted as follows: SiMA monomer (20.95 g, 49.55 mmol) and toluene (32.70 g) were weighed into a round-bottomed flask. CDCP CTA (0.80 g, 1.98 mmol) and AIBN (0.10 g, 0.66 mmol) were added, to afford a target PSiMA DP of 25 and a CDCP/AIBN molar ratio of 3.0. The reaction mixture was then sealed, cooled (using an ice-bath) and purged with nitrogen for 30 minutes. The degassed solution was then placed in a pre-heated oil bath at 80 °C. The polymerisation was quenched after 3h by simultaneous cooling to 0 °C and exposure to air. <sup>1</sup>H NMR spectroscopy in chloroform-*d* indicated a SiMA conversion of 80 %. The resulting mixture was purified (precipitation into a 10-fold excess of methanol three times) and dried under high vacuum. UV/vis spectroscopy indicated a PSiMA DP of 19.

### Synthesis of P*SiMA*<sub>19</sub>-P*BzMA*<sub>x</sub> nanoparticles in DM5

A typical synthesis of P*SiMA*<sub>19</sub>-P*BzMA*<sub>x</sub> nanoparticles in DM5 was conducted as follows: P*SiMA* macro-CTA (0.38 g, 45.3  $\mu$ mol), DM5 (7.92 g) and BzMA (1.60 g, 9.0 mmol) (targeting a core-forming DP of 200 in this case) were added to a round-bottomed flask equipped with a magnetic flea. The solution was stirred for 1 h, or until all of the macro-CTA had dissolved. T21s initiator was then added (9.0  $\mu$ mol, added as a 10 % v/v solution in DM5), and the mixture was sealed, purged with nitrogen for 30 min. and finally placed in a pre-heated oil bath at 90 °C for 5 h. The resulting dispersions were obtained as free-flowing fluids, which were either turbid or transparent depending on the target BzMA core-forming DP. <sup>1</sup>H NMR spectroscopy in chloroform-d confirmed that more than 99 % BzMA conversion was achieved in each case.

### Synthesis of P*SiMA*<sub>19</sub>-P(BzMA<sub>x</sub>-stat-LMA<sub>y</sub>) nanoparticles in DM5

A typical synthesis of P*SiMA*<sub>19</sub>-P(BzMA<sub>175</sub>-stat-LMA<sub>25</sub>) nanoparticles in DM5 was conducted as follows: P*SiMA* macro-CTA (0.24 g, 28.45  $\mu$ mol), DM5 (5.19 g), BzMA (0.88 g, 4.98 mmol) and LMA (0.18 g, 0.71 mmol) were added to a round-bottomed flask equipped with a magnetic flea. The solution was stirred for 1 h, or until all of the macro-CTA had dissolved. T21s initiator was then added (5.6  $\mu$ mol, added as a 10 % v/v solution in DM5), and the mixture was sealed, purged with nitrogen for 30 minutes, and finally placed in a pre-heated oil bath at 90 °C for 5 h. The resulting dispersions were obtained as a free-flowing turbid fluid. <sup>1</sup>H NMR spectroscopy confirmed that more than 99 % monomer conversion was achieved in each case.

### Synthesis of a pyrene-labelled P*SiMA*<sub>19</sub> macro-CTA

P*SiMA*<sub>19</sub> macro-CTA (1.00 g, 118  $\mu$ mol) was weighed into a flame-dried round-bottomed flask and placed under an inert nitrogen atmosphere. 1-Hydroxymethylpyrene (55.0 mg, 237  $\mu$ mol) and DMAP (2.10 mg, 17.78  $\mu$ mol) were then dissolved in anhydrous DCM (10 ml) and added *via* syringe. The resulting mixture was then cooled to 0 °C for 30 min and DCC was added (73.25 mg, 355  $\mu$ mol, dissolved in 5 ml DCM prior to addition) dropwise over 30 min. The resulting mixture was allowed to warm up to ambient temperature, before being heated at 35 °C for 18 h. The reaction mixture was then exposed to air and cooled in a freezer at -17 °C overnight. A white precipitate gradually formed, which was removed *via* filtration. The product was then purified (column chromatography with *n*-hexane eluent) and dried under reduced pressure. <sup>1</sup>H NMR spectroscopy indicated a degree of esterification of 30 % by comparing the integrated pyrene signals at ~ 8 ppm to that of the oxymethylene protons of the monomer repeat units at ~ 4.5 ppm.

### Synthesis of pyrene-labelled PSiMA<sub>19</sub>-PBzMA<sub>200</sub> spherical nanoparticles

The preparation of pyrene-labelled PSiMA<sub>19</sub>-PBzMA<sub>200</sub> nanoparticles in DM5 was conducted as follows: pyrene-labelled PSiMA macro-CTA (0.30 g, 34.6  $\mu\text{mol}$ ), with a mean degree of functionality of 30 %, was added to a round-bottomed flask equipped with a magnetic flea. DM5 (6.08 g) and BzMA (1.22 g, 6.92 mmol) were then added to target a PBzMA core-forming DP of 200. The solution was stirred for 1 h, or until all of the macro-CTA had dissolved. T21s initiator was then added (1.5 mg, 7.0  $\mu\text{mol}$ , added as a 10 % v/v solution in DM5), and the mixture was sealed, purged with nitrogen for 30 min and placed in a pre-heated oil bath at 90 °C for 5 h. The resulting dispersion was obtained as a free-flowing fluid. <sup>1</sup>H NMR spectroscopy confirmed that more than 99 % BzMA conversion was achieved and DLS indicated a Z-average diameter of 95 nm.

### Preparation of Pickering emulsions

Pickering emulsions were prepared using a Silverson L4RT high-shear mixer at a fixed homogenisation time of 2 min at 7,500 rpm. Unless otherwise stated, the volume fraction of each oil was 0.50.

### Preparation of fluorescent Pickering emulsions

A typical preparation of a fluorescent Pickering emulsion was conducted as follows: 4.0 ml of DM5 containing 0.75 % w/w PSiMA<sub>19</sub>-PBzMA<sub>200</sub> spherical nanoparticles was added to 4.0 ml of castor oil. The resulting mixture was then homogenised for 2 min at 7500 RPM using a Silverson L4RT high-shear mixer. Over the course of 1 h, droplet sedimentation was observed due to the density difference between the castor oil (dispersed phase) and the DM5 (continuous phase). The DM5 layer containing excess fluorescent particles was removed *via* pipette and replaced with fresh DM5. The emulsion was then gently hand-shaken to redisperse the droplets and the process was repeated a further four times to ensure complete removal of the non-adsorbed fluorescent particles from the continuous phase.

## 5.2.3 Characterisation

### <sup>1</sup>H NMR spectroscopy

<sup>1</sup>H NMR spectra were recorded using a Magnitek Spinsolve bench-top instrument operating at 60 MHz and 25 °C. For characterisation of the pyrene-labelled PSiMA<sub>19</sub> macro-CTA, a Bruker AV1-400 MHz spectrometer was utilised, again operating at 25 °C. Typically, 64 scans were averaged per spectra

### Gel permeation chromatography

Molecular weight distributions were determined using a GPC instrument operating at 30 °C that comprised two Polymer Laboratories PL gel 5 µm Mixed C columns, a LC20AD ramped isocratic pump, THF eluent and a WellChrom K-2301 refractive index detector operating at  $950 \pm 30$  nm. The mobile phase contained 2.0 % v/v triethylamine and 0.05 % w/v 3,5-di-tert-4-butylhydroxytoluene (BHT); the flow rate was fixed at  $1.0 \text{ ml min}^{-1}$  and toluene was used as a flow rate marker. A series of ten near-monodisperse poly(methyl methacrylate) standards ( $M_p = 1,280$  to  $330,000 \text{ g mol}^{-1}$ ) were used for calibration. Chromatograms were analysed using Varian Cirrus GPC software.

### Dynamic light scattering

DLS studies were performed using a Zetasizer Nano-ZS instrument (Malvern Instruments, UK) at 25 °C at a scattering angle of  $173^\circ$  and using a copolymer concentration of  $\sim 0.2$  % w/w. The Z-average diameter and polydispersity (PDI) of the diblock copolymer nanoparticles were calculated by cumulants analysis of the experimental correlation function using Dispersion Technology Software version 6.20. Data were averaged over ten runs each of thirty seconds duration.

### UV/Vis spectroscopy

UV/Vis absorption spectra were recorded between 200 and 800 nm using a PC-controlled UV-1800 spectrophotometer at 25 °C using a 1 cm quartz cell. A Beer–Lambert calibration curve was constructed using a series of twelve CDCP solutions in chloroform. The absorption maximum at 312 nm, assigned to the trithiocarbonate group, was used for this calibration plot, with CDCP concentrations ranging from  $1.2 \times 10^{-5} \text{ mol dm}^{-3}$  to  $1.0 \times 10^{-4} \text{ mol dm}^{-3}$ . The mean DP for each PSiMA<sub>19</sub> macro-CTA was determined using the molar extinction coefficient of  $11,460 \pm 229 \text{ mol}^{-1} \text{ dm}^3 \text{ cm}^{-1}$  determined for CDCP.

### Density measurements

Densities were determined using an Anton Paar DMA 4100 M density meter operating at 25 °C.

### Surface tension measurements

Surface tensions were measured using a KRUSS digital tensiometer K9 equipped with a du Noüy ring

### Transmission electron microscopy

Transmission electron microscopy (TEM) studies were conducted using a FEI Tecnai G2 spirit instrument operating at 80 kV and equipped with a Gatan 1k CCD camera. Copper TEM grids were surface-coated in-house to yield a thin film of amorphous carbon. The grids were then loaded with dilute copolymer dispersions (0.20 % w/w). Prior to imaging, each grid was exposed to ruthenium(IV) vapour for 7 minutes at ambient temperature, in order to improve contrast. The ruthenium oxide stain was prepared by adding ruthenium(II) oxide (0.3 g) to water (50 g), to form a slurry. Then, sodium periodate (2.0 g) was added with stirring to form a yellow solution of ruthenium(IV) oxide within 1 minute.<sup>46</sup>

### Optical microscopy

Optical microscopy images were recorded using a Zeiss Axio Scope A1 microscope and analysed using ArcSoft ShowBiz software - version 3.5.15.67. Droplet diameters were determined *via* image analysis using ImageJ software. At least 100 droplets were imaged in each case.

### Fluorescence microscopy

Fluorescence microscopy images were recorded on a Zeiss Axio Scope A1 microscope fitted with an AxioCam 1Cm1 monochrome camera using Zeiss filter set 43 HE (excitation 550/25 nm and emission 605/70 nm). Images were captured and processed using ZEN lite 2012 software.

## 5.3 Results and discussion

### 5.3.1 Nanoparticle synthesis

Two P*Si*MA macro-CTAs with DPs of 19 and 43 respectively, were prepared *via* RAFT solution polymerisation of *Si*MA in toluene, using the commercially available RAFT agent 4-cyano-4-(((dodecylthio)carbonothioyl)thio)pentanoic acid (CDCP). In each case, the polymerisation was quenched at approximately 80 % *Si*MA conversion, as determined by <sup>1</sup>H NMR, to preserve the RAFT chain ends. Each P*Si*MA homopolymer was further characterised by UV/Vis spectroscopy and THF GPC, the latter of which indicated low dispersities, see **Table 5.1**

Target <i>Si</i> MA DP	Conversion / % <sup>a</sup>	Actual DP (UV/Vis)	M <sub>n</sub> <sup>b</sup> / g mol <sup>-1</sup>	M <sub>w</sub> /M <sub>n</sub> <sup>b</sup>
50	83	43	11,200	1.34
25	79	19	6,200	1.16

<sup>a</sup>Determined by <sup>1</sup>H NMR spectroscopy in chloroform-d. <sup>b</sup>THF GPC vs. PMMA standards

**Table 5.1:** Summary of two P*Si*MA macro-CTAs prepared by RAFT solution polymerisation in toluene at 80 °C. For each polymerisation, the *Si*MA concentration was 40 % w/w and the CTA to initiator ratio ([CDCP]/[AIBN]) was 3.0.

The lack of a convenient  $^1\text{H}$  NMR signal associated with the CDCP meant that UV spectroscopy was required to determine the mean PSiMA DP. Therefore, a linear Beer-Lambert calibration curve was recorded for CDCP at a maximum wavelength of 312 nm in chloroform (**Figure 5.2**).

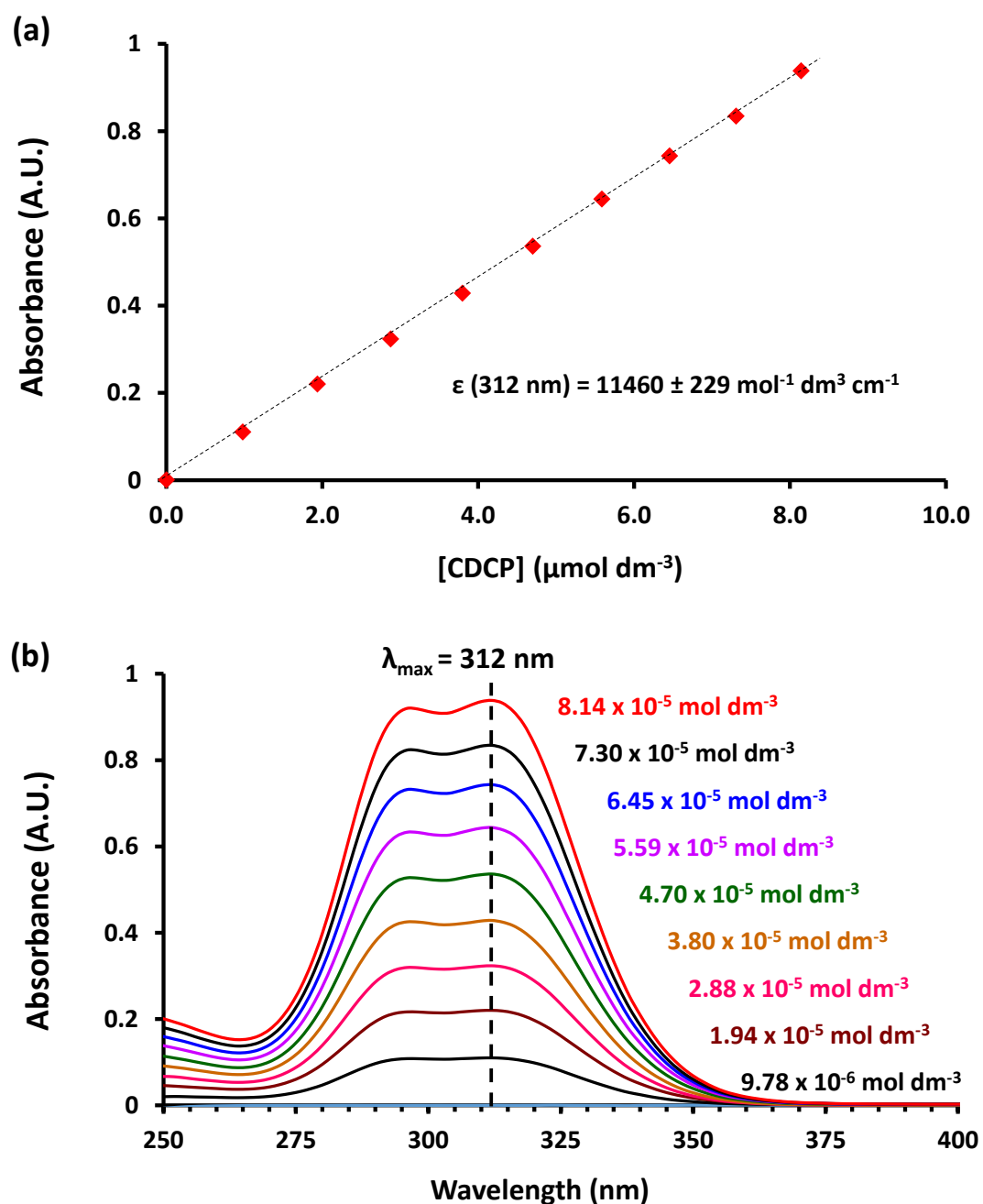


**Figure 5.2:** (a) Beer-Lambert calibration curve constructed for CDCP in chloroform ( $\epsilon = 11460 \pm 229 \text{ mol}^{-1} \text{ dm}^3 \text{ cm}^{-1}$ ) using UV/Vis spectroscopy at a  $\lambda_{\text{max}}$  of 312 nm. (b) Corresponding UV spectra for the different CDCP concentrations used to construct the calibration curve.

**Figure 5.3** shows typical kinetic data obtained for the solution polymerisation of SiMA monomer, in toluene at 80 °C using CDCP. This polymerisation is relatively rapid, reaching an SiMA conversion of 80 % within 5 h. However, a 1 h induction period was observed.

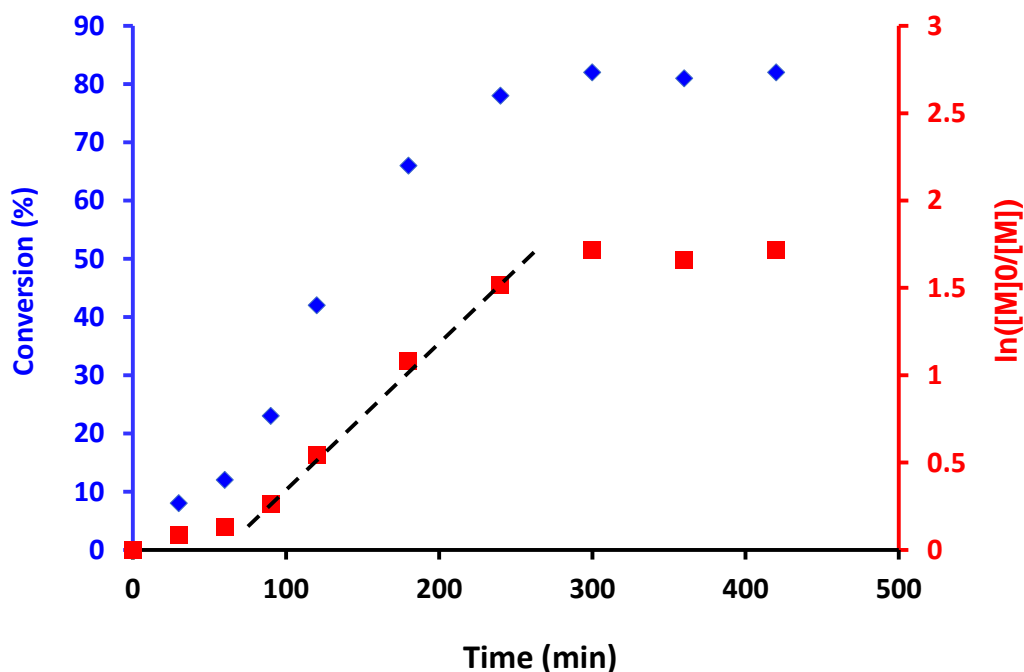


**Figure 5.3:** SiMA monomer conversion vs time curve and corresponding semi logarithmic  $\ln([M]_0/[M])$  plot, obtained for the solution polymerisation of SiMA in toluene at 80 °C and 40 % w/w using CDCP as the RAFT agent and AIBN initiator ( $[CDCP]/[AIBN] = 3$ ).

Each PSiMA macro-CTA was then chain-extended in DM5 with BzMA at 20 % w/w, targeting a PBzMA DP of either 50 or 200. In all, four different diblock compositions were synthesised, which are summarised in **Table 5.2**

PSiMA DP	Target PBzMA DP	Conv. <sup>a</sup> / %	Block Copolymer Composition	THF GPC		DLS	
				$M_n$ / $\text{g mol}^{-1}$	$M_w/M_n$	Diameter / nm	PDI
19	50	> 99	S <sub>19</sub> -B <sub>50</sub>	22,700	1.29	30	0.04
19	200	> 99	S <sub>19</sub> -B <sub>200</sub>	40,500	3.30	123	0.08
43	50	> 99	S <sub>43</sub> -B <sub>50</sub>	11,200	1.49	30	0.03
43	200	> 99	S <sub>43</sub> -B <sub>200</sub>	40,800	3.33	105	0.03

<sup>a</sup><sup>1</sup>H NMR in chloroform-d.

**Table 5.2:** Diblock copolymer composition, BzMA conversions,  $M_n$ ,  $M_w/M_n$  and DLS data obtained for four S<sub>X</sub>-B<sub>Y</sub> nanoparticles. For brevity, S denotes PSiMA and B denotes PBzMA.

TEM studies were performed using dilute nanoparticle dispersions and confirmed that well-defined spheres had been formed in each case (Figure 5.4)

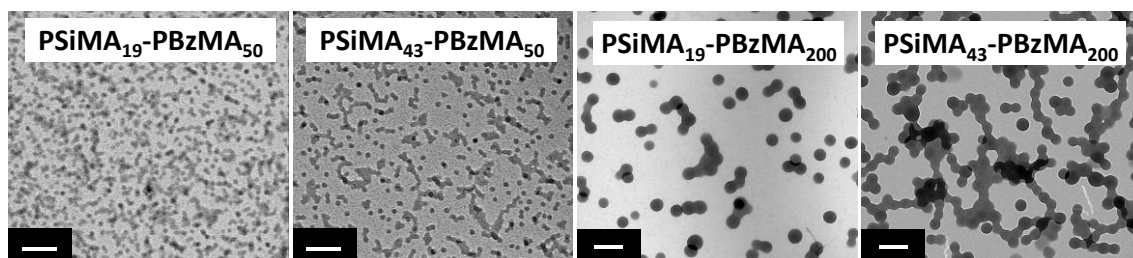


**Figure 5.4:** TEM images obtained for a series of  $\text{PSiMA}_x\text{-PBzMA}_y$  spherical nanoparticles. In each case, the diblock copolymer synthesis was conducted at 20 % w/w and the TEM analysis at  $\sim 0.2$  % w/w. The scale bars correspond to 200 nm in each case

### 5.3.2 Determination and characterisation of immiscible oils.

To form oil-in-DM5 Pickering emulsions, an oil that is immiscible with DM5 is required. To identify suitable candidate oils, a range of different vegetable oils were examined. In each case, 4.0 ml of DM5 and 4.0 ml of the oil of interest were homogenised together, for 2 min, at 7,500 rpm. The resulting emulsions were then allowed to stand for 24 h, prior to visual inspection. The successful candidates, i.e. the oils which were immiscible with DM5, are shown in Figure 5.5.

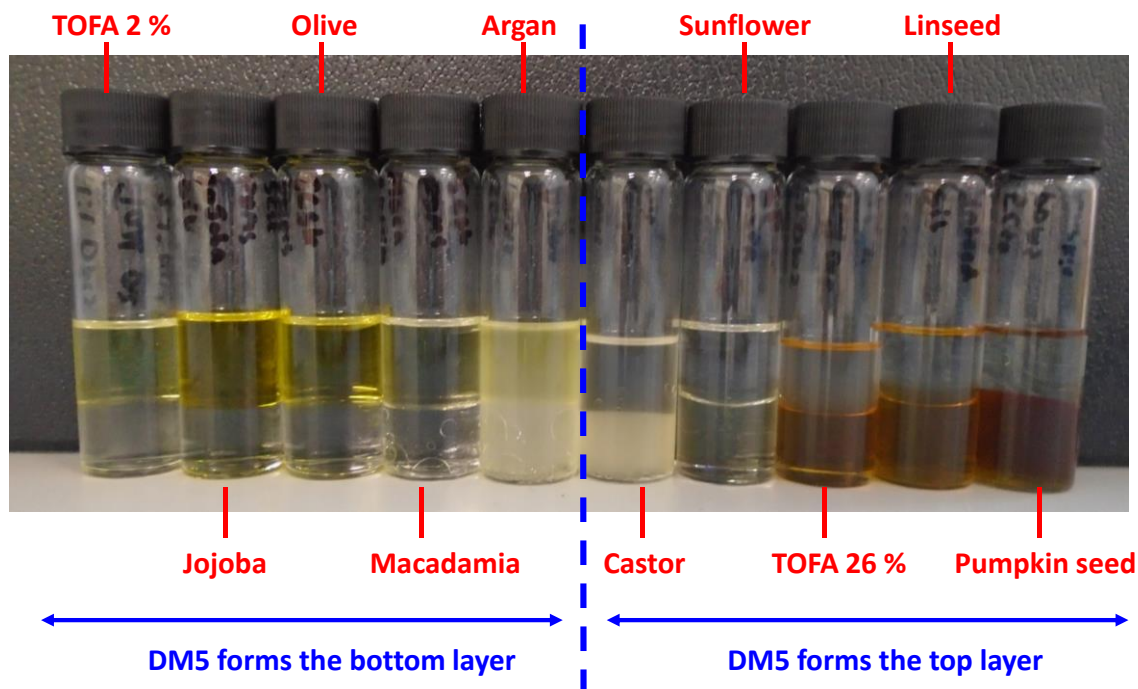


**Figure 5.5:** Digital photograph of vials taken after 24 h after homogenising equal volumes of DM5 (PDMS with a viscosity of 5 cSt) with a range of different vegetable oils (indicated). TOFA denotes tall oil fatty acid, and the % indicates its rosin acid content. For the five vials on the left-hand side, DM5 is the denser oil and forms the bottom layer, for the five vials on the right-hand side, DM5 is the less dense oil and so forms the upper layer.

The density and interfacial tension of each oil/DM5 fluid pair was also measured (**Table 5.3**)

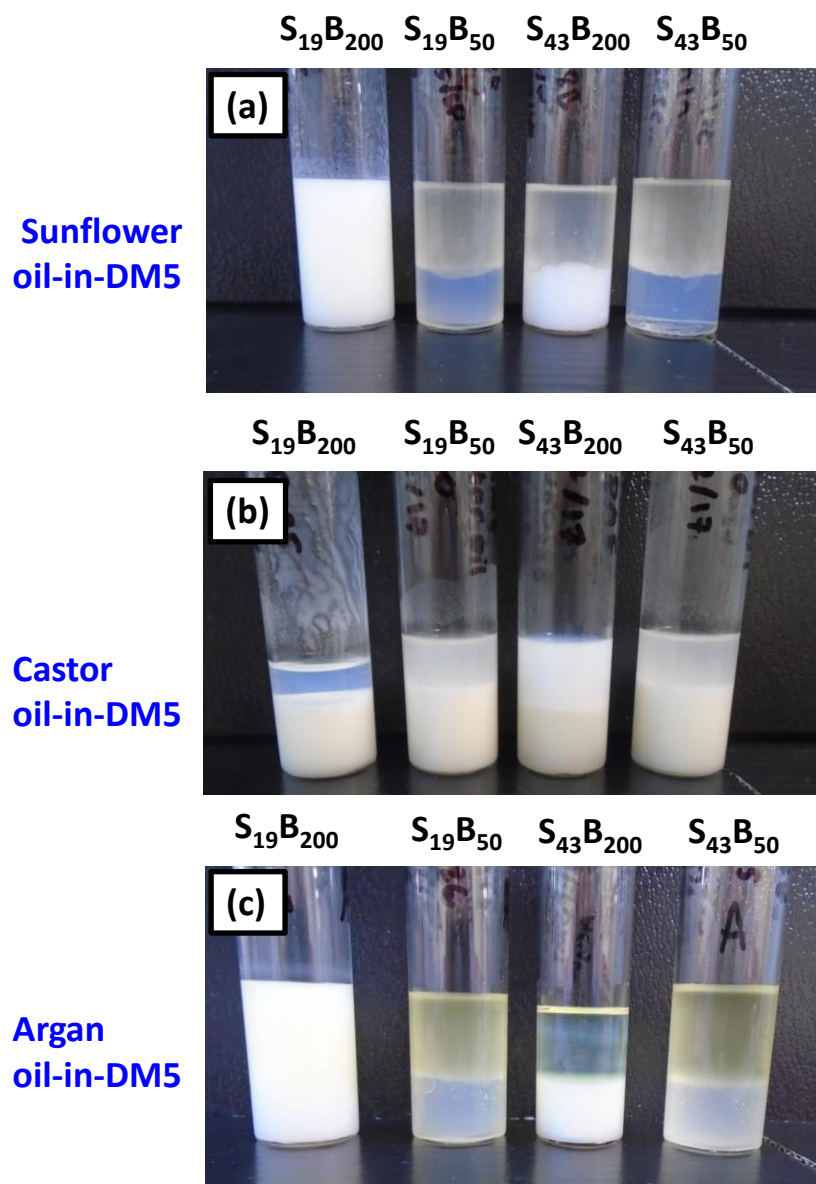
Oil	Interfacial tension with DM5 / $\gamma \pm 0.2 \text{ mN m}^{-1}$	Density / $\text{g cm}^{-3}$
Dimethicone 5 (DM5)	Not applicable	0.9127
Macadamia oil	1.3	0.8401
Jojoba oil	0.9	0.8618
Tall oil fatty acid (2 %)	0.9	0.9091
Olive oil	1.5	0.9094
Argan oil	1.2	0.9121
Pumpkin seed oil	0.8	0.9160
Sunflower oil	1.2	0.9171
Linseed oil	1.6	0.9265
Tall oil fatty acid (26 %)	0.8	0.9499
Castor oil	4.4	0.9569

**Table 5.3:** Oil/DM5 interfacial tensions for the range of oils used in this study. The density of each oil was also measured

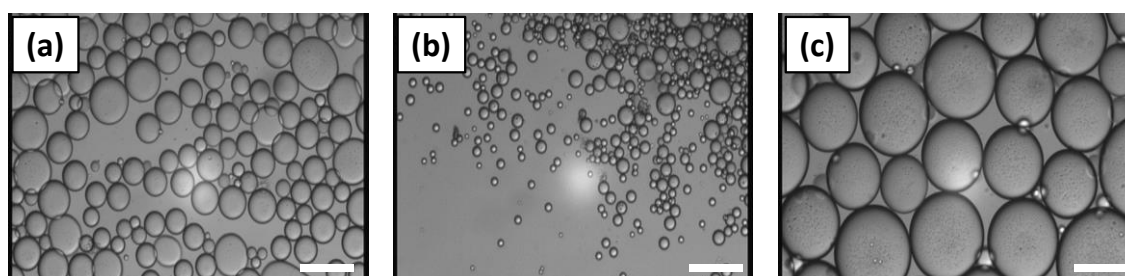
### 5.3.3 PSiMA-PBzMA spherical nanoparticles as Pickering emulsifiers

In preliminary experiments to determine which of the four different PSiMA<sub>x</sub>-PBzMA<sub>y</sub> spherical nanoparticles was the most effective Pickering emulsifier, each was tested with only three of the ten oils described in **Figure 5.5**, specifically argan, sunflower and castor oil. In this scoping experiment, 4.0 ml of the nanoparticle of interest (2 % w/w in DM5) was added to 4.0 ml of each oil, before being homogenised for 2 minutes at 7,500 rpm. The resulting emulsions were then left to stand for two weeks before visual inspection.

**Figure 5.6** indicates that of the four types of PSiMA<sub>x</sub>-PBzMA<sub>y</sub> nanoparticles examined, only PSiMA<sub>19</sub>-PBzMA<sub>200</sub> produced emulsions that remained stable after two weeks with sunflower, argan or castor oil. The stability of each PSiMA<sub>19</sub>-PBzMA<sub>200</sub>-stabilised emulsion was confirmed using optical microscopy, which demonstrated the presence of well-defined spherical droplets in each case (**Figure 5.7**). Furthermore, each emulsion was readily dispersible in excess DM5, indicating that the dispersed phase comprises vegetable oil while DM5 formed the continuous phase, as expected.



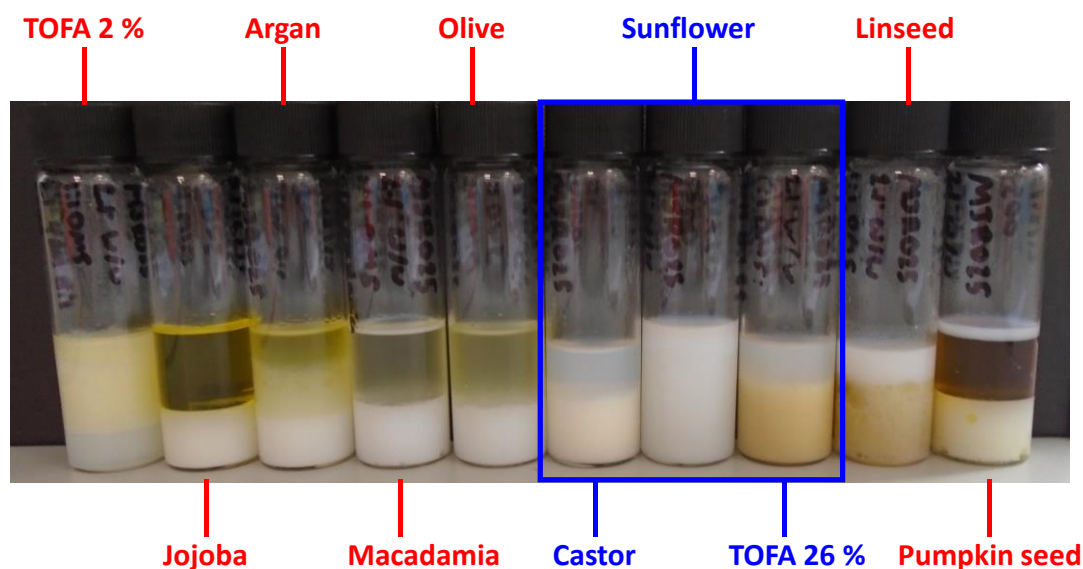
**Figure 5.6:** Digital photographs, taken after two weeks for vials containing (a) sunflower oil-in-DM5, (b) castor oil-in-DM5 or (c) argan oil-in-DM5 emulsions, stabilised by  $S_x-B_y$  spherical nanoparticles (where  $x = 19$  or  $43$  and  $y = 50$  or  $200$ ). Here S denotes the DP of the PSiMA stabiliser and B denotes the DP of the PBzMA core-forming block.



**Figure 5.7:** Corresponding optical microscopy images for the  $S_{19}-B_{200}$ -stabilised emulsions shown in **Figure 5.6** (a) sunflower oil-in-DM5, (b) castor oil-in-DM5 and (c) argan oil-in-DM5. In each case the scale bar corresponds to  $100\ \mu\text{m}$ . For brevity, S denotes PSiMA and B denotes PBzMA.

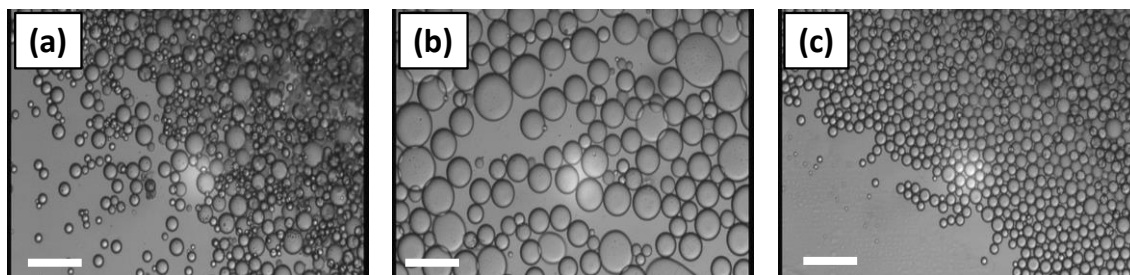
The precise reason for the super performance offered by P*SiMA*<sub>19</sub>-P*BzMA*<sub>200</sub> nanoparticles as oil-in-oil Pickering emulsifiers is not immediately obvious, although it might be due in part to their larger mean diameter when compared to the other three nanoparticles. The energy of detachment of a nanoparticle at a given interface is known to be proportional to the square of the diameter, hence bigger nanoparticles adsorb much more strongly than smaller ones, see equation (5.1). Therefore, based on these initial scoping experiments, only P*SiMA*<sub>19</sub>-P*BzMA*<sub>200</sub> nanoparticles were utilised for further experiments.

Next, Pickering emulsions were prepared using the full range of oils explored in **Figure 5.5**. P*SiMA*<sub>19</sub>-P*BzMA*<sub>200</sub> was used as a stabiliser at a fixed copolymer concentration of 2.0 % w/w in the DM5 continuous phase. The volume fraction of DM5 was fixed at 0.50 in each case, and the emulsions were homogenised for 2 min at 7,500 rpm (**Figure 5.8**). After 2 months, sunflower oil-in-DM5, castor oil-in-DM5 and TOFA 26 %-in-DM5 Pickering emulsions were still stable. Sedimentation was observed for castor oil and TOFA 26 %, because they are denser than DM5, but in each case these emulsions could be easily dispersed by gentle hand shaking. Conversely, no creaming or sedimentation was observed with sunflower oil as a dispersed phase because it is approximately the same density as DM5. Emulsions prepared with TOFA 2 %, argan, macadamia, olive and linseed oil displayed some initial stability, but phase separation was still observed after 2-3 weeks. On the other hand, emulsions prepared with jojoba or pumpkin seed oil displayed no stability and separated almost immediately.



**Figure 5.8:** Digital photograph, taken after 2 months, of vials containing various oil-in-DM5 Pickering emulsions (each specific oil is indicated above or below the relevant vial), prepared with 2.0 % w/w P*SiMA*<sub>19</sub>-P*BzMA*<sub>200</sub> spherical nanoparticles. The emulsions that were still stable after two months after indicated in blue, whereas emulsions that phase-separated or partially separated are shown in red. In each case the volume fraction of the DM5 was fixed at 0.50.

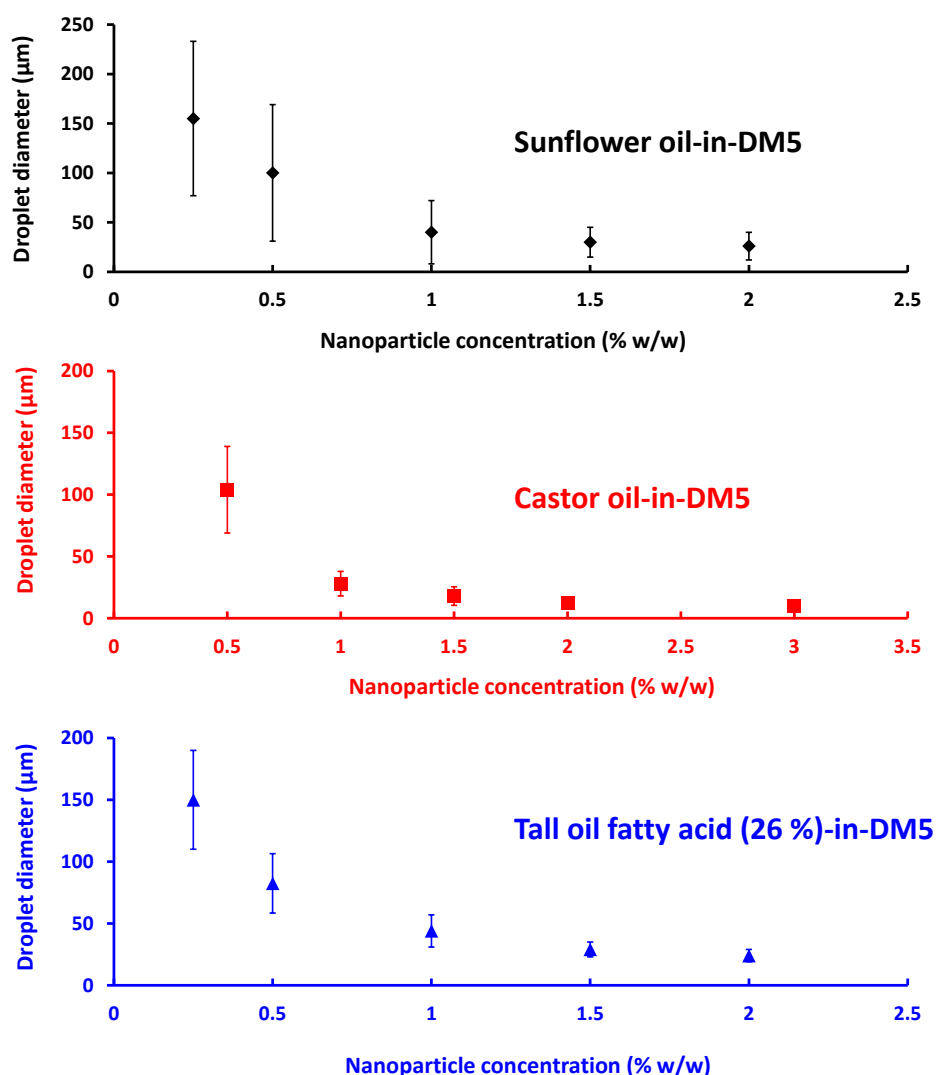
For each of the three stable emulsions, optical microscopy confirmed the presence of well-defined droplets (**Figure 5.9**). Furthermore, each emulsion was readily dispersible in excess DM5, indicating that DM5 was the continuous phase.



**Figure 5.9:** Optical microscopy images for the P*SiMA*<sub>19</sub>-P*BzMA*<sub>200</sub>-stabilised Pickering emulsions shown in **Figure 5.8**. (a) castor oil-in-DM5 (b) sunflower oil-in-DM5 and (c) tall oil fatty acid (26 %)-in-DM5. The DM5 volume fraction is 0.50 in each case, and the P*SiMA*<sub>19</sub>-P*BzMA*<sub>200</sub> concentration in the DM5 prior to homogenisation was 2.0 % w/w. The scale bar corresponds to 100  $\mu$ m.

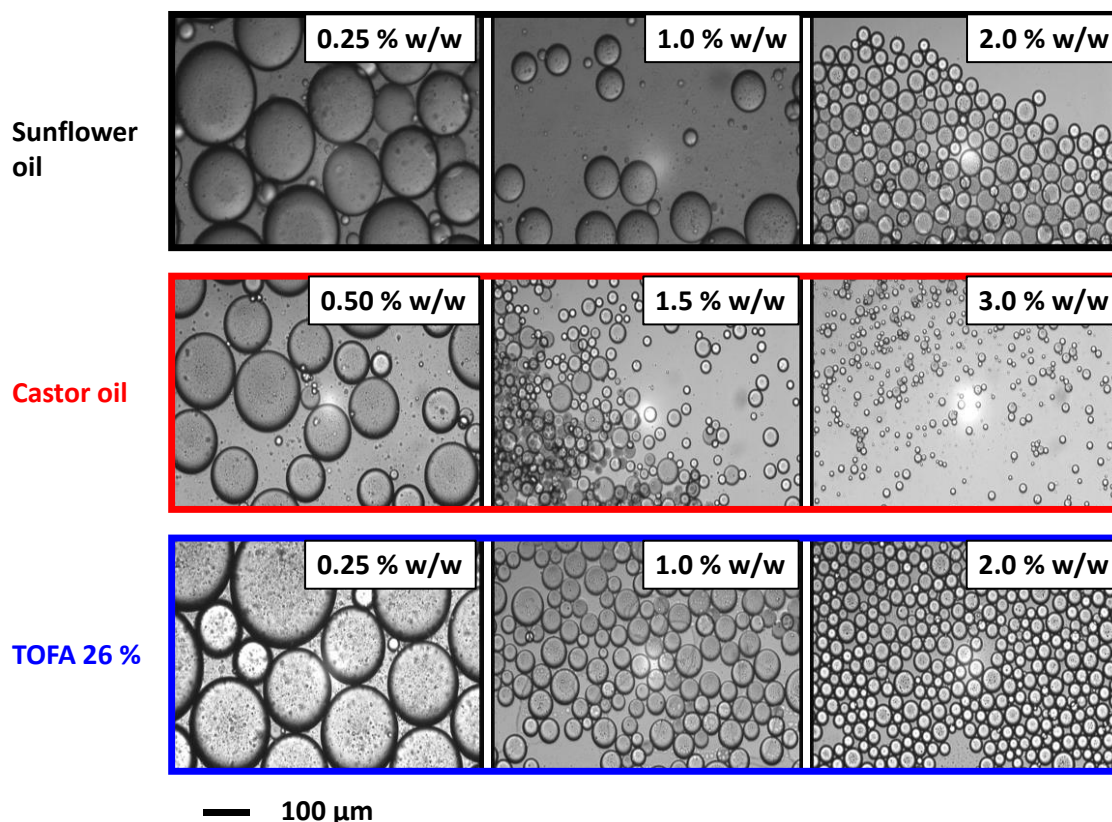
### 5.3.4 Droplet diameter as a function of P*SiMA*<sub>19</sub>-P*BzMA*<sub>200</sub> concentration

One concern when preparing Pickering emulsions with such diblock copolymer nanoparticles is that the nanoparticles might dissociate under high shear, resulting in the adsorption of individual diblock copolymer chains at the interface rather than particles. This has been demonstrated by Thompson and co-workers when attempting to prepare *n*-dodecane-in-water emulsions using linear PGMA-PHPMA latexes.<sup>38</sup> The weakly hydrophobic nature of the PHPMA core-forming block means that these nanoparticles cannot withstand high shear homogenisation conditions. Therefore, during emulsion preparation, the particles break up and adsorb at the oil/water interface as diblock copolymer chains. However, such instability was not observed when the core-forming block was much more solvophobic, e.g. for PGMA-P*BzMA* nanoparticles in water. However, given the possibility of nanoparticle dissociation under shear, the mechanism of stabilisation for the three stable oil-in-oil emulsions (castor oil, sunflower oil or TOFA 26 %-in-DM5) described herein was investigated. This was performed by varying the P*SiMA*<sub>19</sub>-P*BzMA*<sub>200</sub> concentration at which the emulsions were prepared and monitoring the influence of this parameter on the final emulsion droplet diameter (**Figure 5.10**).



**Figure 5.10:** Variation in number-average emulsion droplet diameter as determined by optical microscopy vs. P*SiMA*<sub>19</sub>-P*BzMA*<sub>200</sub> nanoparticle concentration for sunflower oil-in-DM5 (black, top) castor oil-in-DM5 (red, middle) and tall oil fatty acid (26 %)-in-DM5 (blue, bottom). Here, the error bars represent one standard deviation of the mean, rather than the experimental error.

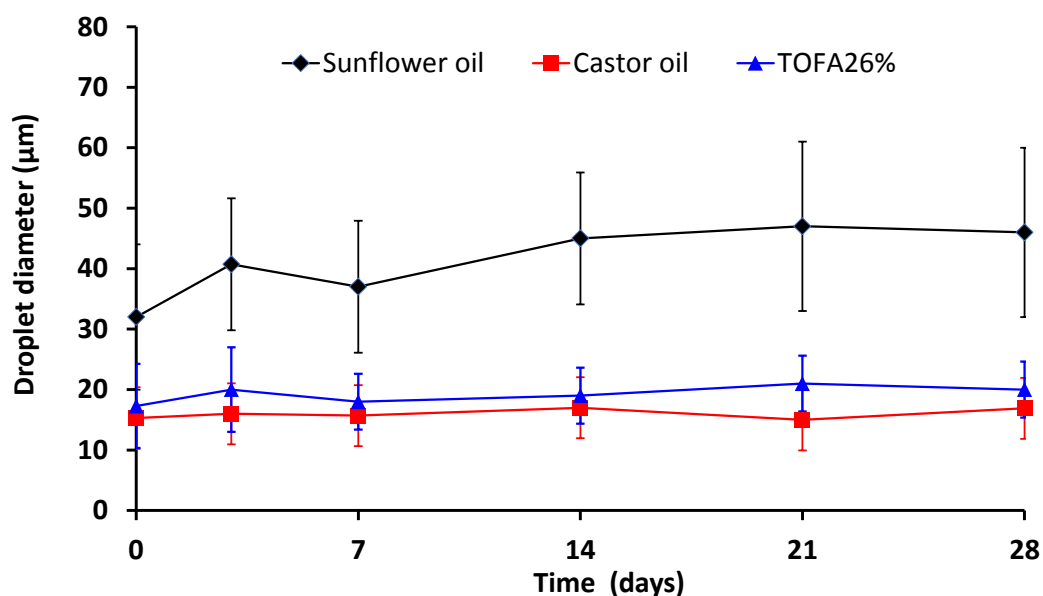
For Pickering emulsions, the total interfacial area that can be stabilised is directly proportional to the nanoparticle concentration. Consequently, as the nanoparticle concentration is reduced, so too does the interfacial area that can be stabilised. For a fixed volume fraction of the droplet phase, this manifests as fewer but larger droplets. This upturn in droplet diameter at lower nanoparticle concentrations can be clearly observed for the three different oil-in-DM5 emulsions stabilised by P*SiMA*<sub>19</sub>-P*BzMA*<sub>200</sub> described in **Figure 5.10**. Thus, this confirms that these nanoparticles survive the high-shear homogenisation conditions of and adsorb intact at the oil-oil interface. The corresponding optical micrographs are shown in **Figure 5.11**.



**Figure 5.11:** Optical microscopy images obtained for a series of oil-in-DM5 Pickering emulsions prepared using various concentrations of PSiMA<sub>19</sub>-PBzMA<sub>200</sub> spherical nanoparticles. (top, black) sunflower oil-in-DM5, (middle, red) castor oil-in-DM5 and (bottom, blue) tall oil fatty acid 26 %-in-DM5. In each case the DM5 volume fraction was 0.50.

### 5.3.5 Droplet diameter as a function of time

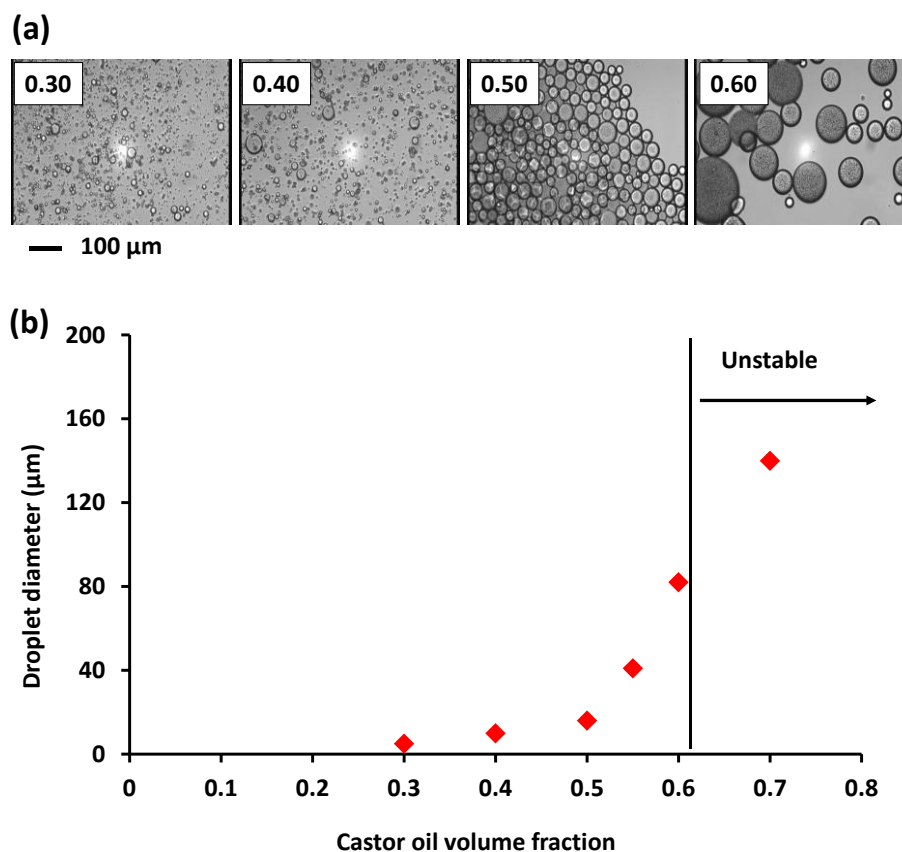
One of the primary mechanisms of emulsion instability is known as Ostwald ripening.<sup>47</sup> This is a thermodynamically-driven spontaneous process whereby larger droplets grow at the expense of smaller ones, because larger droplets are more thermodynamically stable. In emulsions, this occurs by the diffusion of the molecules of the dispersed-phase from smaller droplets into larger ones, *via* the continuous phase. To investigate whether this phenomenon was prevalent for the oil-in-oil Pickering emulsions described herein, the droplet diameter was monitored as a function of time for the castor oil-in-DM5, TOFA (26 %)-in-DM5 and sunflower oil-in-DM5 emulsions, each stabilised using 2.0 % w/w PSiMA<sub>19</sub>-PBzMA<sub>200</sub> spherical nanoparticles (**Figure 5.12**).



**Figure 5.12:** Number-average droplet diameter (as determined by image analysis of optical micrographs) shown vs. time for either sunflower oil-in-DM5 (black diamonds) castor oil-in-DM5 (red squares) or tall oil fatty acid 26%-in-DM5 (blue triangles). Each Pickering emulsion was prepared using 2.0 % w/w P*SiMA*<sub>19</sub>-P*BzMA*<sub>200</sub> at a fixed DM5 volume fraction of 0.50. The error bars correspond to one standard deviation of the droplet diameter, not the experimental error.

According to **Figure 5.12** both castor oil-in-DM5 and TOFA 26 %-in-DM5 emulsions are stable for at least four weeks, as no noticeable increase in mean droplet diameter occurs over this time period. On the other hand, the sunflower oil-in-DM5 does display some Ostwald ripening, with an increase in the mean droplet diameter from  $32 \pm 12 \mu\text{m}$  to  $50 \pm 13 \mu\text{m}$  being observed over four weeks. This suggests that the background solubility of sunflower oil in DM5 compared to that of castor oil or TOFA 26 %. Given that TOFA 26 % contains a significant proportion of rosin acid, and castor oil has some hydroxyl functionality, this is a reasonable explanation.

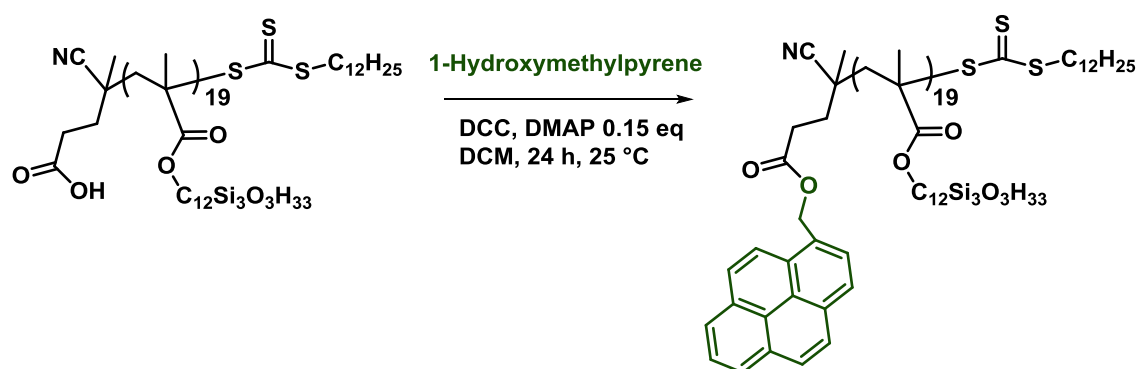
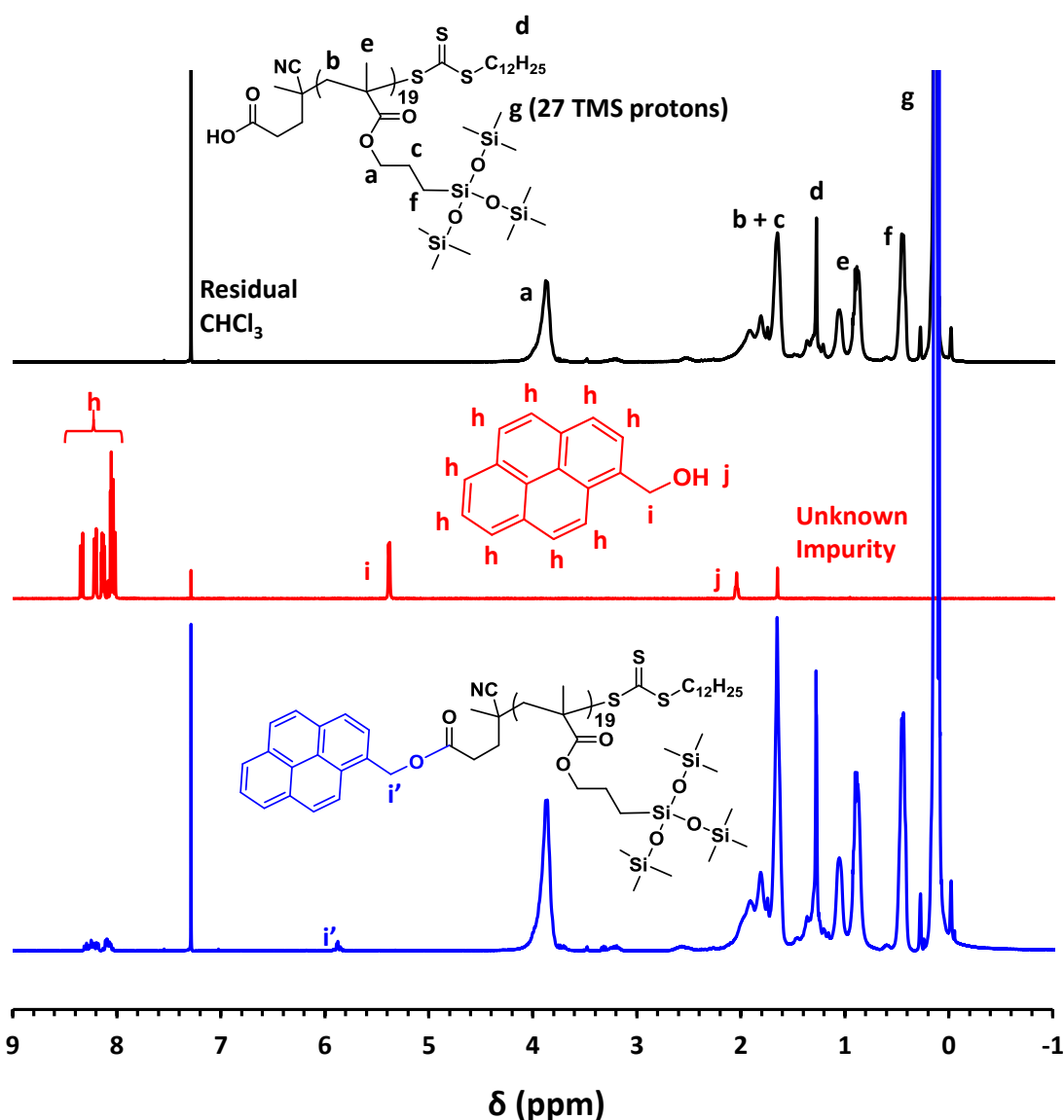
Thus far, the influence of both P*SiMA*<sub>19</sub>-P*BzMA*<sub>200</sub> concentration and aging time on the mean droplet diameter for three different Pickering emulsions has been studied. Next, the influence of oil volume fraction on the final droplet diameter was investigated. Specifically, Pickering emulsions were prepared with castor oil volume fractions ranging from 30 % to 70 %, while the P*SiMA*<sub>19</sub>-P*BzMA*<sub>200</sub> concentration in the DM5 was fixed at 2.0 % w/w (**Figure 5.13**).



**Figure 5.13:** (a) Optical micrographs for a range of castor oil-in-DM5 Pickering emulsions, each prepared with P*Si*MA<sub>19</sub>-P*Bz*MA<sub>200</sub> nanoparticles at a fixed concentration of 2.0 % w/w and using various castor oil volume fractions (indicated by the number in the top left corner of each image). (b) Variation in mean number-average droplet diameter (as determined by optical microscopy) vs. initial nanoparticle concentration, for castor oil-in-DM5 Pickering emulsions stabilised by 2.0 % w/w P*Si*MA<sub>19</sub>-P*Bz*MA<sub>200</sub>.

At castor oil volume fractions below 0.50, the influence on the final droplet diameter is negligible. In this regime, the P*Si*MA<sub>19</sub>-P*Bz*MA<sub>200</sub> nanoparticles are in excess and therefore the droplet diameter remains roughly the same. As the castor oil volume fraction is increased to 0.60, the total interfacial area requiring stabilisation increases. In this regime, the P*Si*MA<sub>19</sub>-P*Bz*MA<sub>200</sub> nanoparticles are no longer in excess and the final droplet diameter increases with increasing volume fraction. For castor oil volume fractions above 0.60, the emulsions became highly aggregated and underwent phase-separation over time scales of days.

To provide further evidence that the P*Si*MA<sub>19</sub>-P*Bz*MA<sub>200</sub> diblock copolymer nanoparticles are indeed present at the oil/oil interface, they were tagged with a fluorescence label (pyrene). This was achieved by esterification of the carboxylic acid on the macro-CTA with 1-hydroxymethylpyrene, according to **Scheme 5.2**. <sup>1</sup>H NMR studies indicated a mean esterification of 30 %, by comparing the nine aromatic protons assigned to the pyrene with the 38 oxymethylene protons assigned to the P*Si*MA<sub>19</sub> macro-CTA (**Figure 5.14**).

Scheme 5.2: Esterification of the terminal COOH group of PSiMA<sub>19</sub> with 1-hydroxymethylpyreneFigure 5.14 <sup>1</sup>H NMR spectra recorded in chloroform-d for the PSiMA<sub>19</sub> macro-CTA (black, top), 1-hydroxymethylpyrene (red, middle) and pyrene-functionalised PSiMA<sub>19</sub> macro-CTA (blue, bottom)

The resulting pyrene-labelled macro-CTA was then chain-extended in DM5 with BzMA, targeting a core-forming PBzMA block DP of 200, to produce fluorescent nanoparticles.  $^1\text{H}$  NMR spectroscopy indicated greater than 99 % BzMA conversion, and DLS indicated well-defined nanoparticles of 95 nm diameter. Castor oil-in-DM5 Pickering emulsions were then prepared, using a nanoparticle concentration of 0.75 % w/w and a fixed DM5 volume fraction of 0.50, and analysed *via* fluorescence microscopy (**Figure 5.15**).

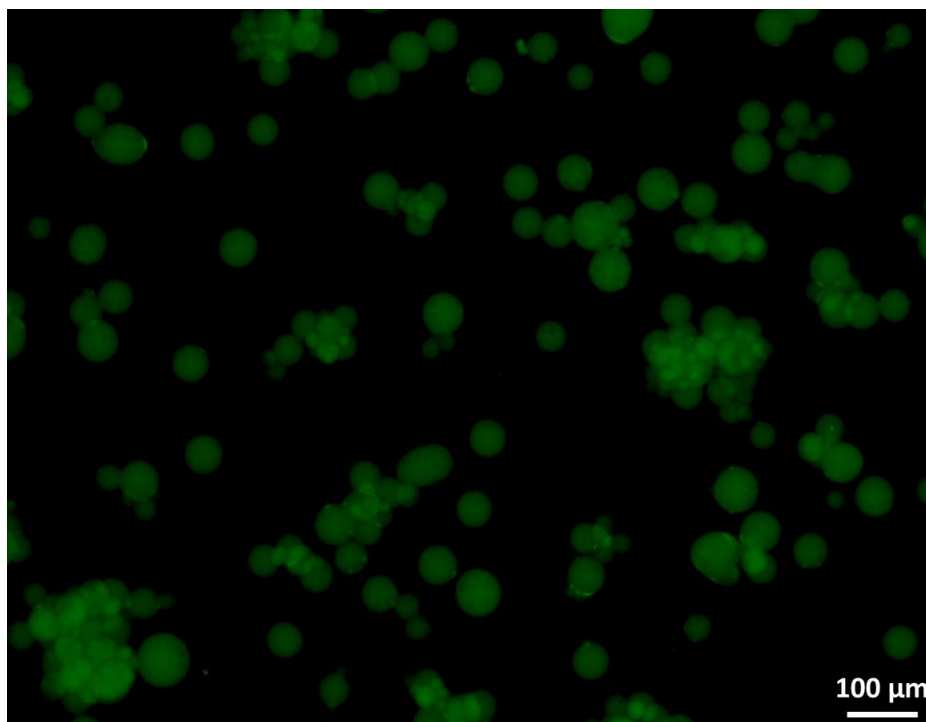


**Figure 5.15:** Fluorescence microscopy image obtained for a castor oil-in-DM5 Pickering emulsion stabilised with pyrene-labelled P*Si*MA<sub>19</sub>-PBzMA<sub>200</sub> spherical nanoparticles. The emulsion was diluted using excess DM5 (the continuous phase) prior to analysis.

### 5.3.6 Tuning the nanoparticle wettability to improve emulsifier performance

Thus far it has been demonstrated that P*Si*MA<sub>19</sub>-PBzMA<sub>200</sub> spherical nanoparticles are effective Pickering emulsifiers for oil-in-DM5 emulsions, when the oil is either castor, sunflower or tall oil fatty acid (26 %). However, seven out of the ten different oils evaluated as the internal phase resulted in unstable emulsions. In an attempt to improve the Pickering emulsifier performance of the P*Si*MA-stabilised nanoparticles, LMA was statistically copolymerised into the core-forming block. Given that LMA is soluble in most of the vegetable oils, this should increase the wettability of the resulting nanoparticles by the dispersed phase. A summary of this nanoparticle series is given in **Table 5.4**. The LMA content was incrementally increased up to 18 mol % relative to the BzMA. However, LMA contents of higher than 18 mol % gave rise to colloidal instability of the resulting nanoparticles.

Composition	Conv. / % <sup>a</sup>	LMA (mol %) of core	DLS		GPC <sup>b</sup>	
			Z-Avg. Diameter / nm	PDI	M <sub>n</sub> / g mol <sup>-1</sup>	M <sub>w</sub> /M <sub>n</sub>
S <sub>19</sub> -B <sub>200</sub>	99	0	123	0.08	40,500	3.30
S <sub>19</sub> -(B <sub>190</sub> -stat-L <sub>10</sub> )	99	5	130	0.07	44,600	2.06
S <sub>19</sub> -(B <sub>175</sub> -stat-L <sub>25</sub> )	99	12.5	147	0.07	55,200	1.58
S <sub>19</sub> -(B <sub>164</sub> -stat-L <sub>36</sub> )	99	18	210	0.10	76,100	2.10

a. <sup>1</sup>H NMR in chloroform-d. b. THF GPC

**Table 5.4:** Summary of block copolymer composition, conversions, M<sub>n</sub>, M<sub>w</sub>/M<sub>n</sub> and DLS data obtained for a series of PSiMA<sub>19</sub>-P(BzMA<sub>x</sub>-stat-LMA<sub>y</sub>) nanoparticles. For brevity, S denotes PSiMA, L denotes LMA and B denotes BzMA residues.

TEM confirmed that spherical nanoparticles were obtained in each case (**Figure 5.16**).

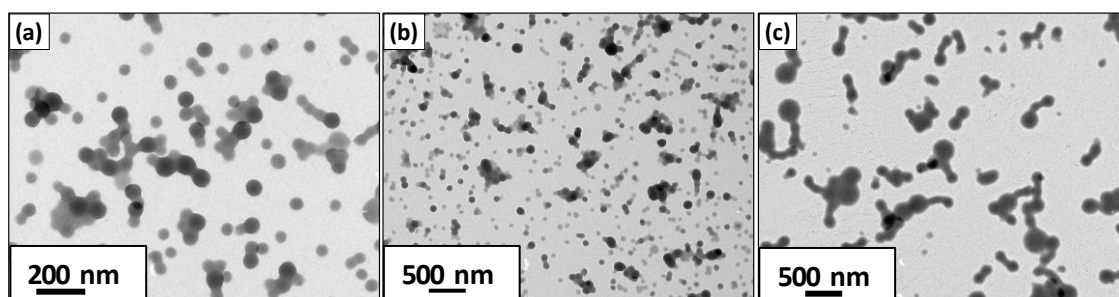


**Figure 5.16:** TEM images obtained for (a) PSiMA<sub>19</sub>-P(BzMA<sub>190</sub>-stat-LMA<sub>10</sub>), (b) PSiMA<sub>19</sub>-P(BzMA<sub>175</sub>-stat-LMA<sub>25</sub>) and (c) PSiMA<sub>19</sub>-P(BzMA<sub>164</sub>-stat-LMA<sub>36</sub>).

In a similar experiment to that described in **Figure 5.8**, oil-in-DM5 Pickering emulsions were prepared with the full range oils, using the LMA-containing nanoparticles described above. For each of the following emulsions, the nanoparticle concentration was fixed at 2 % w/w and the volume fraction of each oil was 0.5. When the nanoparticle core contained 5 mol % LMA, i.e. PSiMA<sub>19</sub>-P(BzMA<sub>190</sub>-s-LMA<sub>10</sub>), five of the ten different emulsions prepared were still stable after 2 months (**Figure 5.17**), compared with just three when using PSiMA<sub>19</sub>-PBzMA<sub>200</sub> nanoparticles. In each case, optical microscopy confirmed the presence of well-defined spherical droplets (**Figure 5.18**), and each emulsion was readily dispersible in excess DM5, confirming that DM5 was the continuous phase. Therefore, this experiment suggests that the incorporation of even small quantities of LMA into the nanoparticle core can increase Pickering emulsifier performance.

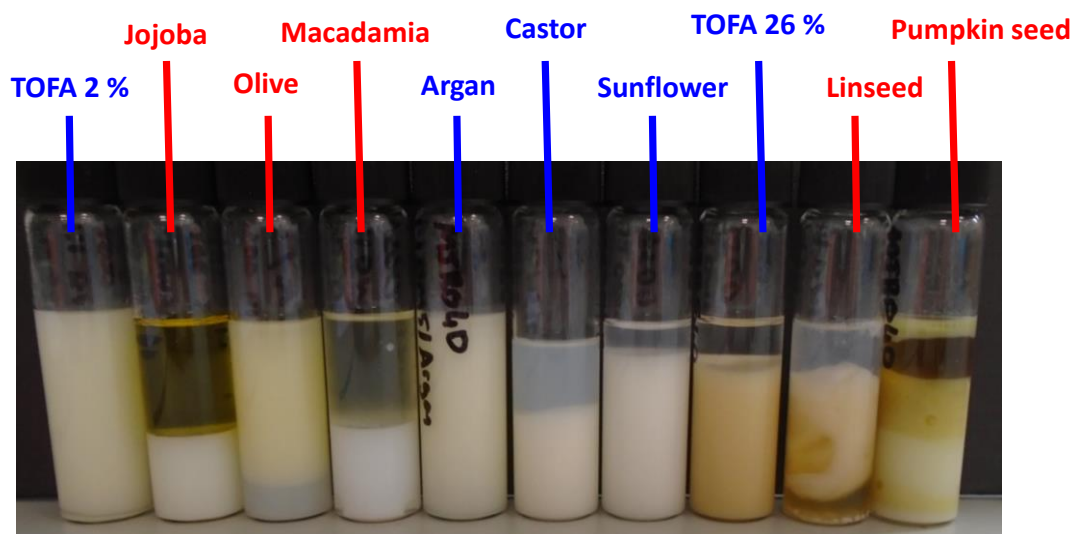


**Figure 5.17:** Digital photograph, taken after two months, of vials containing oil-in-DM5 Pickering emulsions, stabilised by  $\text{PSiMA}_{19}\text{-P}(\text{BzMA}_{190}\text{-stat-LMA}_{10})$  nanoparticles. The volume fraction of DM5 was 0.50 in each case, and the nanoparticle concentration in the DM5 prior to homogenisation was 2.0 % w/w. The oils in blue indicate stable emulsions after two months, the oils depicted in red indicates separated/partially separated emulsions after two months.

It is hypothesised that this increase in performance is owing to greater wettability of the  $\text{PSiMA}_{19}\text{-P}(\text{BzMA}_{190}\text{-stat-LMA}_{10})$  nanoparticles by the various oils. However, the  $\text{PSiMA}_{19}\text{-P}(\text{BzMA}_{190}\text{-stat-LMA}_{10})$  nanoparticles are also marginally larger in diameter than the  $\text{PSiMA}_{19}\text{-PBzMA}_{200}$  control (130 nm vs. 123 nm), and therefore would be expected to adsorb slightly more strongly at the interface. As such, it is difficult to determine precisely which of these two mechanisms is primarily responsible for the enhanced performance.

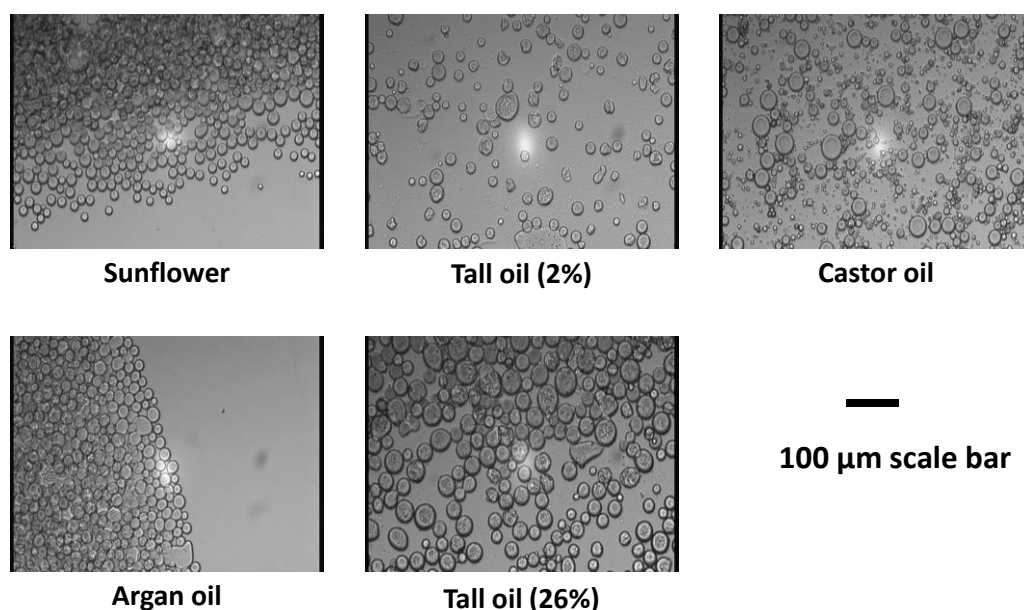


**Figure 5.18:** Optical micrographs recorded for the most stable emulsions shown in **Figure 5.17**.

Next, emulsions were prepared using the P*SiMA*-stabilised nanoparticles containing 12.5 mol % LMA (i.e. P*SiMA*<sub>19</sub>-P(BzMA<sub>174</sub>-stat-LMA<sub>25</sub>)), see **Figure 5.19**. As before, each emulsion was prepared at 7,500 rpm for 2 min, using a fixed DM5 volume fraction of 0.50 and a nanoparticle concentration of 2.0 % w/w (in the DM5 prior to homogenisation).

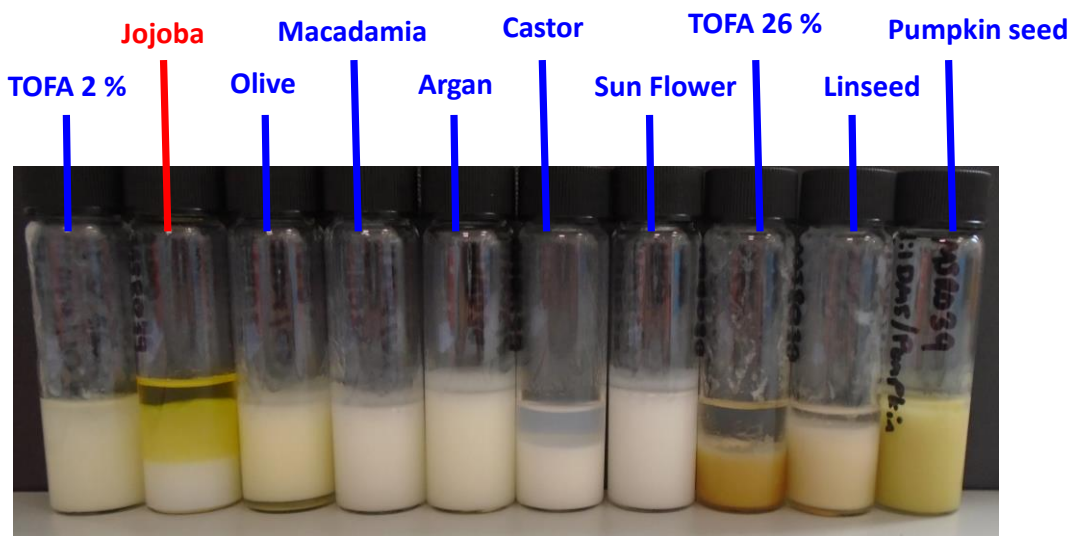


**Figure 5.19:** Digital photographs, taken after 2 months, of oil-in-DM5 Pickering emulsions prepared using P*SiMA*<sub>19</sub>-P(BzMA<sub>174</sub>-stat-LMA<sub>25</sub>) spherical nanoparticles. In each case, the DM5 volume fraction was fixed at 0.50 and the P*SiMA*<sub>19</sub>-P(BzMA<sub>175</sub>-stat-LMA<sub>25</sub>) concentration prior to homogenisation was fixed at 2.0 % w/w. Emulsions labelled in blue indicate stability after two months whereas emulsions labelled in red indicate an unstable emulsion was obtained after 2 months.

Examination of **Figure 5.19** indicates that Pickering emulsions prepared with P*SiMA*<sub>19</sub>-P(BzMA<sub>175</sub>-stat-LMA<sub>25</sub>) spherical nanoparticles are much more stable than those prepared with the P*SiMA*<sub>19</sub>-PBzMA<sub>200</sub> control. More specifically, only one emulsion (jojoba oil-in-DM5) was unstable after two months. Why jojoba oil is more difficult to stabilise in droplet form than the other nine oils is not immediately obvious, as all of the oils utilised in this study are composed of similar compounds, i.e. medium and long-chain triglycerides. One reasonable explanation is that Ostwald ripening is more significant for jojoba oil-in-DM5 emulsions than it is for the other nine oils. This is plausible because jojoba oil is composed primarily of triglycerides of 11-eicosenoic acid, which is a triglyceride containing unsaturated C<sub>20</sub> chains. This is less polar than components from which the other oils are composed (triglycerides with unsaturated C<sub>16-18</sub> chains), and therefore may have a higher background solubility in DM5.

For the other nine emulsions that were still stable after 2 months, optical microscopy was utilised to confirm the presence of well-defined spherical droplets in each case (**Figure 5.20**). In addition, each emulsion was readily dispersible in excess DM5, confirming that DM5 remained the continuous phase.

— Scale bar (100 microns)

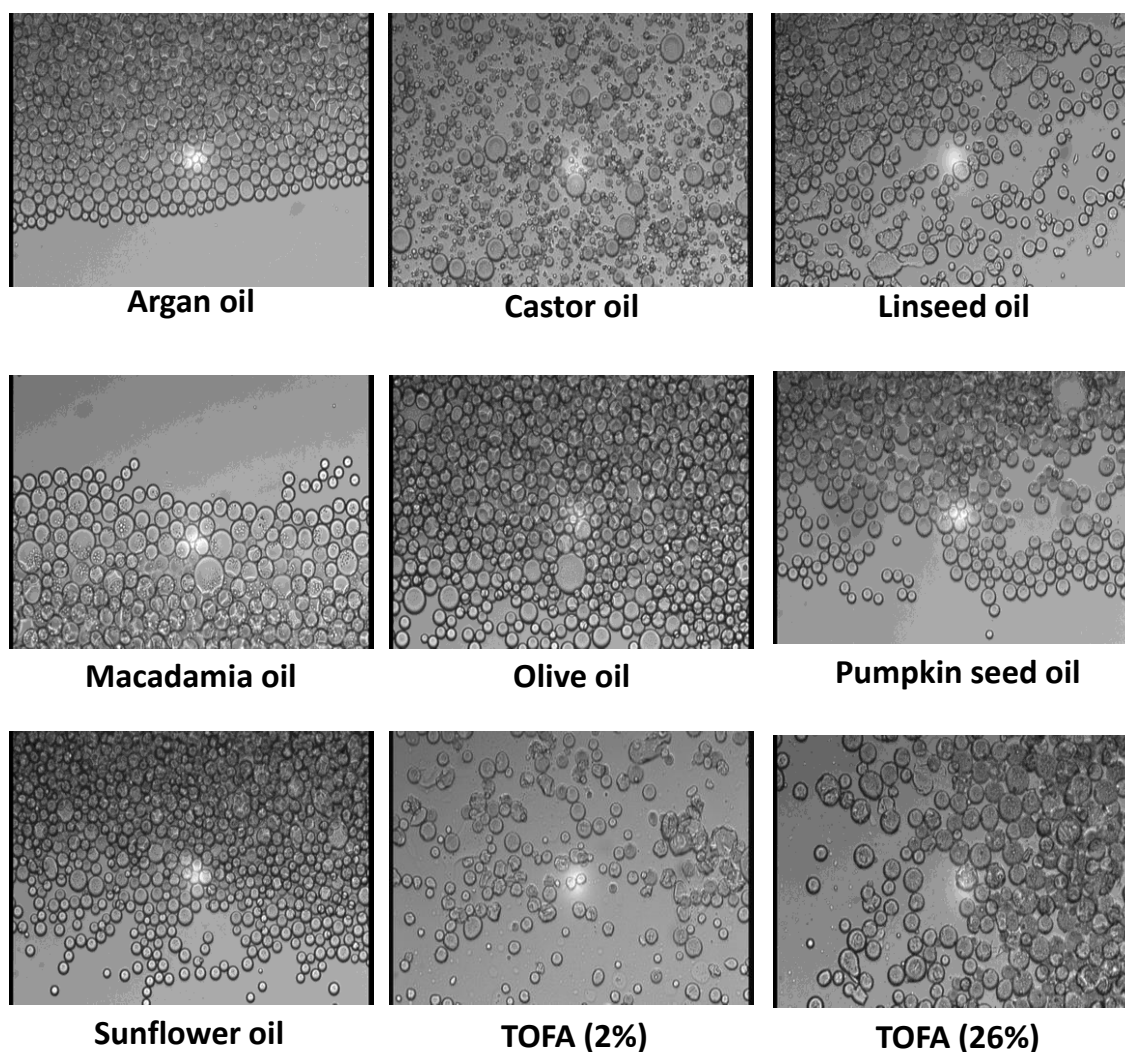


**Figure 5.20:** Optical micrographs obtained for the nine stable Pickering emulsions shown in **Figure 5.19**.

Perhaps surprisingly, increasing the LMA content of the nanoparticle core up to 18 mol % resulted in *reduced* stability for resulting emulsions. This instability manifested in either (i) phase separation, which was observed for TOFA 2 %, jojoba oil and TOFA 26 %, or (ii) aggregation and high viscosity, see **Figure 5.21**. Attempts to disperse each of the aggregated emulsions in excess DM5 failed. However, attempts to disperse each emulsion in the relevant vegetable oil (argan oil for argan oil-in-DM5 emulsions, for example) resulted in dissolution in each case. This confirmed that, despite the aggregation and high viscosity observed for some of the emulsions, DM5 still formed the continuous phase. Where possible, these emulsions were imaged *via* optical microscopy (**Figure 5.22**).

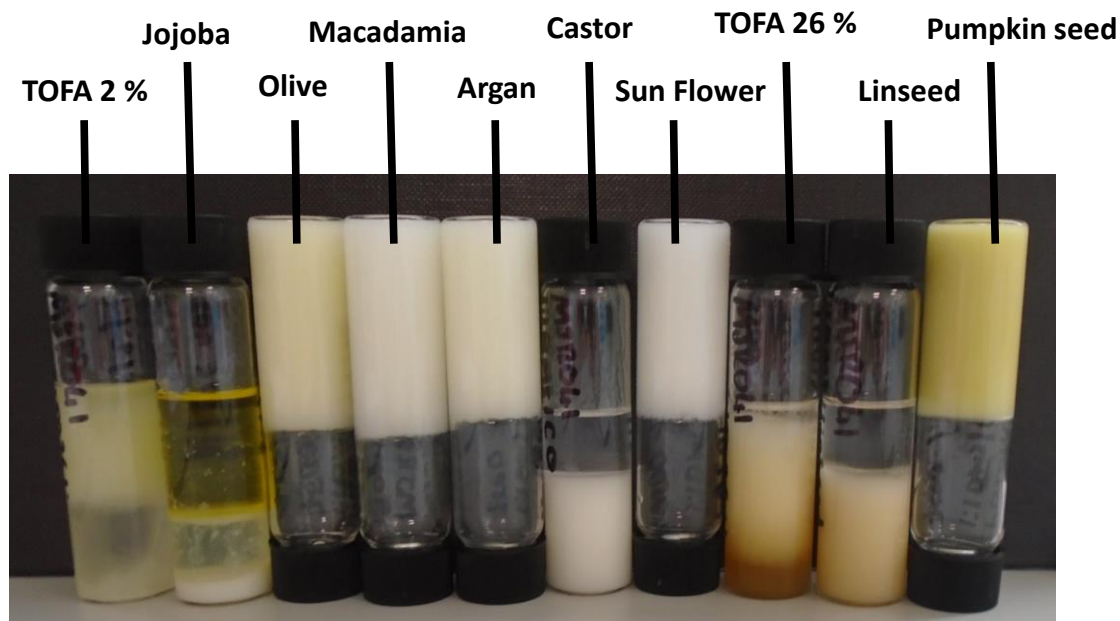


**Figure 5.21:** Digital photographs, taken after 2 months, of oil-in-DM5 Pickering emulsions prepared using P*SiMA*<sub>19</sub>-P(BzMA<sub>164</sub>-*S*-LMA<sub>36</sub>) spherical nanoparticles. In each case, the DM5 volume fraction was fixed at 0.50 and the P*SiMA*<sub>19</sub>-P(BzMA<sub>164</sub>-*S*-LMA<sub>36</sub>) concentration was fixed at 2 % w/w prior to homogenisation.

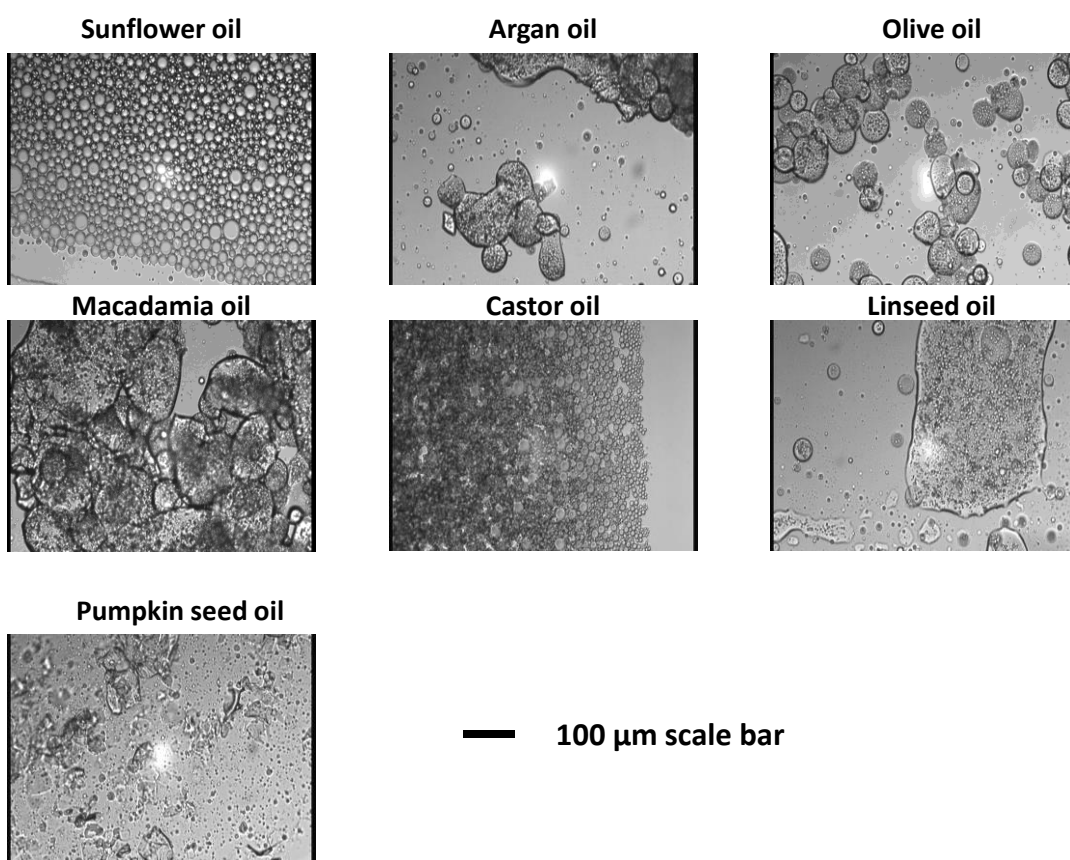


**Figure 5.22:** Corresponding optical micrographs for select emulsions shown in **Figure 5.21**.

### 5.4 Conclusions

PSiMA<sub>19</sub>-PBzMA<sub>200</sub> spherical nanoparticles can be prepared directly in a low-viscosity PDMS solvent, specifically DM5. Moreover, such nanoparticle can act as efficient Pickering stabilisers for oil-in-DM5 emulsions, where the droplet phase is either castor oil, sunflower oil, or TOFA 26 %. When utilised at a concentration of 2.0 % w/w, such nanoparticles can stabilise emulsions for at least two months, as determined by visual inspection and optical microscopy. Furthermore, the carboxylic acid functionality present on the steric-stabiliser block enables fluorescent labelling with pyrene, facilitating fluorescence microscopy to be performed on the resulting particle-stabilised castor oil-in-DM5 emulsions. Such experiments clearly indicate the presence of the PSiMA<sub>19</sub>-PBzMA<sub>200</sub> diblock copolymers at the castor oil/DM5 interface.

By preparing a series of either TOFA 26%, castor oil or sunflower oil-in-DM5 emulsions, over a range of PSiMA<sub>19</sub>-PBzMA<sub>200</sub> spherical nanoparticle concentrations, it was demonstrated that the particles remain intact at the interface during homogenisation and adsorb at the interface as particles rather than individual diblock copolymer chains. The droplet diameter was monitored over time for the three aforementioned emulsions in order to investigate the influence of Ostwald ripening on the droplet diameter. Ostwald ripening did indeed occur for the sunflower-in-DM5 emulsions, which then stabilised after approximately three weeks. In contrast, castor oil and TOFA 26 % -in-DM5 emulsions displayed no Ostwald ripening for at least a month at 20 °C.

Finally, PSiMA<sub>19</sub>-based nanoparticles with a statistical copolymer core, comprising BzMA and LMA, can be used as Pickering emulsifiers, provided that the PLMA content is less than 18 mol %. Moreover, when the LMA content of the core is 12.5 mol %, the resulting nanoparticles can stabilise a broader range of oils as the internal phase. However, when the core comprises 18 mol % LMA, the resulting Pickering emulsions become highly aggregated and unstable. This suggests that there is an optimum LMA content for the copolymer core, between 5 mol % and 18 mol %, for optimal Pickering emulsifier performance.

### 5.5 References

- (1) Israelachvili, J. *Intermolecular & Surface Forces*, 2nd ed.; Academic Press: London, 1991.
- (2) Tanford, C. Interfacial Free Energy and the Hydrophobic Effect. *Proc. Natl. Acad. Sci.* **1979**, *76*, 4175–4176.
- (3) Hildebrand, J. H. Is There A “hydrophobic Effect”? *Proc. Natl. Acad. Sci.* **1979**, *76*, 194–194.
- (4) Glasstone, S.; Lewis, D. *Elements of Physical Chemistry*, 2nd ed.; Macmillan & Co. Ltd: London, 1966.

- (5) Kabalnov, A. Thermodynamic and Theoretical Aspects of Emulsions and Their Stability. *Curr. Opin. Colloid Interface Sci.* **1998**, *3*, 270–275.
- (6) Finkle, P.; Draper, H. D.; Hildebrand, J. H. The Theory of Emulsification. *J. Am. Chem. Soc.* **1923**, *45*, 2780–2788.
- (7) Binks, B. P. Particles as Surfactants—similarities and Differences. *Curr. Opin. Colloid Interface Sci.* **2002**, *7*, 21–41.
- (8) Wilde, P. Interfaces: Their Role in Foam and Emulsion Behaviour. *Curr. Opin. Colloid Interface Sci.* **2000**, *5*, 176–181.
- (9) Bancroft, W. D. The Theory of Emulsification, V. *J. Phys. Chem.* **1913**, *17*, 501–519.
- (10) Bancroft, W. D. The Theory of Emulsification, VI. *J. Phys. Chem.* **1914**, *19*, 275–309.
- (11) Aveyard, R.; Binks, B. P.; Clark, S.; Mead, J. Interfacial Tension Minima in Oil–water–surfactant Systems. Behaviour of Alkane–aqueous NaCl Systems Containing Aerosol OT. *J. Chem. Soc. Faraday Trans. 1 Phys. Chem. Condens. Phases* **1986**, *82*, 125–142.
- (12) Burcik, E. J. The Rate of Surface Tension Lowering and Its Role in Foaming. *J. Colloid Sci.* **1950**, *5*, 421–436.
- (13) Hsu, J. P.; Nacu, A. Behavior of Soybean Oil-in-Water Emulsion Stabilized by Nonionic Surfactant. *J. Colloid Interface Sci.* **2003**, *259*, 374–381.
- (14) Opawale, F.; Burgess, D. Influence of Interfacial Properties of Lipophilic Surfactants on Water-in-Oil Emulsion Stability. *J. Colloid Interface Sci.* **1998**, *197*, 142–150.
- (15) Tamura, T.; Kaneko, Y.; Ohyama, M. Dynamic Surface Tension and Foaming Properties of Aqueous Polyoxyethylene N-Dodecyl Ether Solutions. *J. Colloid Interface Sci.* **1995**, *173*, 493–499.
- (16) Ramsden, W. Separation of Solids in the Surface-Layers of Solutions and “Suspensions” (Observations on Surface-Membranes, Bubbles, Emulsions, and Mechanical Coagulation). -- Preliminary Account. *Proc. R. Soc. London* **1903**, *72*, 156–164.
- (17) Pickering, S. U. CXCVI.—Emulsions. *J. Chem. Soc., Trans.* **1907**, *91*, 2001–2021.
- (18) Aveyard, R.; Binks, B. P.; Clint, J. H. Emulsions Stabilised Solely by Colloidal Particles. *Adv. Colloid Interface Sci.* **2003**, *100–102*, 503–546.
- (19) Binks, B. P. Colloidal Particles at a Range of Fluid–Fluid Interfaces. *Langmuir* **2017**, *33*, 6947–6963.
- (20) Griffin, W. C. Classification of Surface-Active Agents by “HLB.” *J. Soc. Cosmet. Chem.* **1949**, *1*, 311–326.
- (21) Israelachvili, J. N.; Mitchell, D. J.; Ninham, B. W. Theory of Self-Assembly of Hydrocarbon Amphiphiles into Micelles and Bilayers. *J. Chem. Soc. Faraday Trans. 2* **1976**, *72*, 1525–1568.
- (22) Scheludko, A.; Toshev, B. V.; Bojadjev, D. T. Attachment of Particles to a Liquid Surface (Capillary Theory of Flotation). *J. Chem. Soc. Faraday Trans. 1 Phys. Chem. Condens. Phases* **1976**, *72*, 2815–2828.
- (23) Levine, S.; Bowen, B. D.; Partridge, S. J. Stabilization of Emulsions by Fine Particles I. Partitioning of Particles between Continuous Phase and Oil/water Interface. *Colloids and Surfaces* **1989**, *38*, 325–343.
- (24) Sturzenegger, P. N.; Gonzenbach, U. T.; Koltzenburg, S.; Gauckler, L. J. Controlling the Formation of Particle-Stabilized Water-in-Oil Emulsions. *Soft Matter* **2012**, *8*, 7471–7479.
- (25) Schulman, J. H.; Leja, J. Control of Contact Angles at the Oil-Water-Solid Interfaces. Emulsions Stabilized by Solid Particles (BaSO<sub>4</sub>). *Trans. Faraday Soc.* **1954**, *50*, 598–605.
- (26) Yan, N.; Masliyah, J. H. Characterization and Demulsification of Solids-Stabilized Oil-in-Water Emulsions Part 1. Partitioning of Clay Particles and Preparation of Emulsions. *Colloids Surfaces A Physicochem. Eng. Asp.* **1995**, *96*, 229–242.
- (27) Johansson, G.; Pugh, R. J. The Influence of Particle Size and Hydrophobicity on the Stability of Mineralized Froths. *Int. J. Miner. Process.* **1992**, *34*, 1–21.
- (28) Ip, S. W.; Wang, Y.; Toguri, J. M. Aluminum Foam Stabilization by Solid Particles. *Can. Metall. Q.* **1999**, *38*, 81–92.
- (29) Kaptay, G. On the Equation of the Maximum Capillary Pressure Induced by Solid Particles

- to Stabilize Emulsions and Foams and on the Emulsion Stability Diagrams. *Colloids Surfaces A Physicochem. Eng. Asp.* **2006**, 282–283, 387–401.
- (30) Manga, M. S.; Cayre, O. J.; Williams, R. A.; Biggs, S.; York, D. W. Production of Solid-Stabilised Emulsions through Rotational Membrane Emulsification: Influence of Particle Adsorption Kinetics. *Soft Matter* **2012**, 8, 1532–1538.
- (31) Chen, T.; Colver, P. J.; Bon, S. A. F. Organic–Inorganic Hybrid Hollow Spheres Prepared from TiO<sub>2</sub>-Stabilized Pickering Emulsion Polymerization. *Adv. Mater.* **2007**, 19, 2286–2289.
- (32) Williams, M.; Armes, S. P.; York, D. W. Clay-Based Colloidosomes. *Langmuir* **2012**, 28, 1142–1148.
- (33) Cauvin, S.; Colver, P. J.; Bon, S. A. F. Pickering Stabilized Miniemulsion Polymerization: Preparation of Clay Armored Latexes. *Macromolecules* **2005**, 38, 7887–7889.
- (34) Binks, B. P.; Lumsdon, S. O. Pickering Emulsions Stabilized by Monodisperse Latex Particles: Effects of Particle Size. *Langmuir* **2001**, 17, 4540–4547.
- (35) Cunningham, V. J.; Alswieleh, A. M.; Thompson, K. L.; Williams, M.; Leggett, G. J.; Armes, S. P.; Musa, O. M. Poly(glycerol monomethacrylate)–Poly(benzyl Methacrylate) Diblock Copolymer Nanoparticles via RAFT Emulsion Polymerization: Synthesis, Characterization, and Interfacial Activity. *Macromolecules* **2014**, 47, 5613–5623.
- (36) Kalashnikova, I.; Bizot, H.; Bertocini, P.; Cathala, B.; Capron, I. Cellulosic Nanorods of Various Aspect Ratios for Oil in Water Pickering Emulsions. *Soft Matter* **2013**, 9, 952–959.
- (37) Kalashnikova, I.; Bizot, H.; Cathala, B.; Capron, I. New Pickering Emulsions Stabilized by Bacterial Cellulose Nanocrystals. *Langmuir* **2011**, 27, 7471–7479.
- (38) Thompson, K. L.; Mable, C. J.; Cockram, A.; Warren, N. J.; Cunningham, V. J.; Jones, E. R.; Verber, R.; Armes, S. P. Are Block Copolymer Worms More Effective Pickering Emulsifiers than Block Copolymer Spheres? *Soft Matter* **2014**, 10, 8615–8626.
- (39) Thompson, K. L.; Fielding, L. A.; Mykhaylyk, O. O.; Lane, J. A.; Derry, M. J.; Armes, S. P. Vermicious Thermo-Responsive Pickering Emulsifiers. *Chem. Sci.* **2015**, 6, 4207–4214.
- (40) Andresen, M.; Stenius, P. Water-in-oil Emulsions Stabilized by Hydrophobized Microfibrillated Cellulose. *J. Dispers. Sci. Technol.* **2007**, 28, 837–844.
- (41) Binks, B. P.; Tyowua, A. T. Oil-in-Oil Emulsions Stabilised Solely by Solid Particles. *Soft Matter* **2016**, 12, 876–887.
- (42) Rodier, B. J.; de Leon, A.; Hemmingsen, C.; Pentzer, E. Polymerizations in Oil-in-Oil Emulsions Using 2D Nanoparticle Surfactants. *Polym. Chem.* **2018**, 9, 1547–1550.
- (43) Tyowua, A. T.; Yiase, S. G.; Binks, B. P. Double Oil-in-Oil-in-Oil Emulsions Stabilised Solely by Particles. *J. Colloid Interface Sci.* **2017**, 488, 127–134.
- (44) Rozynek, Z.; Bielas, R.; Józefczak, A. Efficient Formation of Oil-in-Oil Pickering Emulsions with Narrow Size Distributions by Using Electric Fields. *Soft Matter* **2018**, 14, 5140–5149.
- (45) Mikkelsen, A.; Khobaib, K.; Eriksen, F. K.; Måløy, K. J.; Rozynek, Z. Particle-Covered Drops in Electric Fields: Drop Deformation and Surface Particle Organization. *Soft Matter* **2018**, 5442–5451.
- (46) Trent, J. S.; Scheinbeim, J. I.; Couchman, P. R. Ruthenium Tetraoxide Staining of Polymers for Electron Microscopy. *Macromolecules* **1983**, 16, 589–598.
- (47) Taylor, P. Ostwald Ripening in Emulsions. *Colloids Surfaces A Physicochem. Eng. Asp.* **1995**, 99, 175–185.

# **Chapter 6: Bespoke Isorefractive Diblock Copolymer Nanoparticles Enable the Rational Design of Highly Transparent Pickering Emulsions**

Reproduced, in part, with permission from “Rymaruk, M. J.; Thompson, K. L.; Derry, M. J.; Warren, N. J.; Ratcliffe, L. P. D.; Williams, C. N.; Brown, S. L.; Armes, S. P. Bespoke Contrast-Matched Diblock Copolymer Nanoparticles Enable the Rational Design of Highly Transparent Pickering Double Emulsions. *Nanoscale* **2016**, *8*, 14497-14506.”

---

## 6.1 Introduction

Ramsden<sup>1</sup> and Pickering<sup>2</sup> demonstrated over a century ago that colloidal particles can stabilise emulsions. After many decades of little or no activity, there has been a resurgence of interest in Pickering emulsions over the last 17 years or so.<sup>3</sup> Many types of particles have now been evaluated in this context, including inorganic materials such as silica,<sup>4–6</sup> iron oxide,<sup>7</sup> calcium carbonate,<sup>8</sup> barium sulfate,<sup>9</sup> titanium dioxide<sup>10</sup> or clays<sup>11–13</sup> and organic materials such as copolymer latexes<sup>14–26</sup> cellulosic particles,<sup>27–30</sup> carbon black,<sup>31</sup> epoxy resins<sup>32</sup> and nanocomposite particles.<sup>33</sup> As we have seen in Chapter 5, the particle contact angle,  $\theta$ , is related to the surface wettability and usually dictates the emulsion type: hydrophilic particles ( $\theta < 90^\circ$ ) normally produce oil-in-water emulsions, whereas hydrophobic particles ( $\theta > 90^\circ$ ) favour the formation of water-in-oil emulsions.<sup>34–39</sup> Compared to conventional surfactant-stabilised emulsions, Pickering emulsions offer enhanced long-term stability, reduced foaming and more reproducible formulations.<sup>40</sup>

According to Snell's law (equation (6.1)), refraction occurs when light travels between two media with different refractive indices.<sup>41</sup>

$$\frac{\sin\theta_2}{\sin\theta_1} = \frac{n_1}{n_2} \quad (6.1)$$

Here,  $n_1$  is the refractive index of medium 1,  $n_2$  is the refractive index of medium 2,  $\theta_1$  is the angle of incidence measured normal to the interface (for light travelling from medium 1 into medium 2) and  $\theta_2$  is the angle of refraction.

Consequently, if the two different media have *the same* refractive index, no refraction occurs. This scenario applies to emulsions when the continuous phase and the droplet phase have equal refractive indices and results in transparency.<sup>41</sup> For *surfactant-stabilised* emulsions, the emulsifier is too small to cause light scattering (or turbidity). Thus, transparent *surfactant-stabilised* emulsions have been reported for various applications.<sup>41–43</sup> However, the design of refractive index-matched *Pickering* emulsions is much more technically challenging. In general, the particles are likely to scatter light, particularly if they are adsorbed at the oil/water interface as aggregates, rather than as primary particles.<sup>44,45</sup> Thus in this case the droplet phase, continuous phase *and* the Pickering emulsifier must be contrast-matched for high transparency.

Recently, Binks and co-workers reported the production of *translucent non-aqueous* Pickering emulsions. This formulation comprised paraffin liquid droplets stabilised by silica nanoparticles, dispersed in a poly(ethylene glycol)<sub>300</sub> continuous phase.<sup>46</sup> The refractive index similarity between the two immiscible liquids (1.475 and 1.464 respectively) gave rise to Pickering emulsions of relatively low turbidity. However, the non-isorefractive silica nanoparticles scattered light sufficiently strongly to limit the transparency of this emulsion. Similarly, Thompson and co-workers reported the preparation of a near-isorefractive *non-aqueous* Pickering emulsions.<sup>47</sup> This formulation comprised *n*-tetradecane, ethylene glycol and poly(lauryl methacrylate)<sub>16</sub>-poly(benzyl methacrylate)<sub>37</sub> (PLMA<sub>16</sub>-PBzMA<sub>37</sub>) diblock copolymer worms<sup>48</sup> as the Pickering emulsifier. However, *n*-tetradecane is relatively expensive, ethylene glycol has significant toxicity and the worms were not contrast-matched, which limited the transmittance to around 70-80% depending on the precise wavelength of visible light. Thus, although of some academic interest, this particular formulation appears to have little or no commercial potential.

In this chapter, the preparation of highly transparent oil-in-water (o/w) emulsions and oil-in-water-in-oil (o/w/o) double emulsions using contrast-matched Pickering emulsifiers is described. This was achieved by designing two new types of sterically-stabilised diblock copolymer nanoparticles each comprising a poly(2,2,2-trifluoroethyl methacrylate) (PTFEMA) core-forming block combined with either (i) a *hydrophilic* poly(glycerol monomethacrylate) (PGMA) stabiliser block or (ii) a *hydrophobic* PLMA stabiliser block. The PTFEMA block was chosen for its relatively low refractive index of 1.42;<sup>49</sup> this almost precisely matches that of *n*-dodecane, which was the model oil used in this study.<sup>50</sup> The PGMA stabiliser was selected for its exceptional tolerance towards high concentrations of sucrose or glycerol, which were judiciously added to an aqueous dispersion of PGMA-PTFEMA nanoparticles to raise the refractive index of this phase in order to achieve a near-perfect contrast match. The PLMA stabiliser was selected to ensure good colloidal stability for the PLMA-PTFEMA nanoparticles, which were prepared directly in *n*-dodecane.<sup>51</sup>

## **6.2 Experimental**

### **6.2.1 Materials**

Glycerol monomethacrylate (GMA, purity 97 %) was obtained from GEO speciality chemicals (UK) and was used as received. 2,2,2-Trifluoroethylmethacrylate (TFEMA, 99 %), lauryl methacrylate (LMA, 96 %), *n*-dodecane (> 99 %), glycerol (> 99 %), sucrose (> 99.5 %), Nile red, methanol-d<sub>4</sub>, tetrahydrofuran (THF), dimethylformamide (DMF), acetone-d<sub>6</sub>, lithium

bromide (LiBr), chloroform-d, dimethyl sulfoxide (DMSO), triethylamine, 3,5-di-tert-4-butylhydroxytoluene (BHT), toluene, benzyl methacrylate (BzMA, 96 %), 4,4'-Azobis(4-cyanovaleric acid) (ACVA, > 97 %), benzophenone (> 99 %), pyrene (> 99 %), 2-cyanopropylidithiobenzoate (CPDB, > 97 %), 2-phenylethanethiol, sodium hydride (60 % in mineral oil), diethyl ether, carbon disulfide, iodine, sodium thiosulfate, sodium sulfate, ethyl acetate and *n*-hexane were purchased from Sigma Aldrich (UK). Trigonox 21S (T21s) initiator was supplied by AkzoNobel (The Netherlands) and sodium dodecylsulfate (SDS) was obtained from BDH Laboratory Supplies (UK). Benzyl methacrylate was passed through basic alumina prior to use; all remaining reagents were used as received unless otherwise stated. Deionised water (pH 6.1 at 20 °C) was used for all experiments described herein. All solvents used were of HPLC grade.

## 6.2.2 Methods

### **Synthesis of 4-cyano-4-(2-phenylethane sulfanylthiocarbonyl) sulfanylpentanoic acid (PETTC)**

2-Phenylethanethiol (21 g, 152 mmol) was added dropwise to a stirred suspension of sodium hydride (60 % in oil, 6.3 g, 158 mmol) in diethyl ether (250 ml) at 0 °C. The evolution of hydrogen was observed and the gray suspension turned to a white slurry of sodium phenylethanethiolate over 45 minutes. Carbon disulfide (12.0 g, 158 mmol) was added dropwise and a yellow precipitate of sodium 2-phenylethanetrithiocarbonate formed over 30 minutes, which was collected *via* filtration and used without further purification. To a suspension of sodium 2-phenylethanetrithiocarbonate (23.2 g, 98 mmol) in diethyl ether (150 ml), solid iodine (12.6 g, 50 mmol) was added. The reaction mixture was stirred for 60 minutes at room temperature, and the resulting precipitate of sodium iodide was removed *via* filtration. The brown filtrate was washed with a saturated solution of sodium thiosulfate (2 x 150 ml), dried over sodium sulfate and placed under reduced pressure to leave bis-(2-phenylethane sulfanylthiocarbonyl) disulfide as an orange solid (~ 100 % yield). A solution of bis-(2-phenylethane sulfanylthiocarbonyl) disulfide (10 g, 23 mmol) and 4,4'-azobis(4-cyanovaleric acid) (9.67 g, 34.5 mmol) in ethyl acetate (250 ml) was purged with nitrogen for 30 minutes at ambient temperature before being heated to reflux under a dry nitrogen atmosphere for 18 h. The resulting solution was washed with water (5 x 200 ml), dried over sodium sulfate and placed under reduced pressure to remove the volatiles. The remaining orange residue was recrystallised from ethyl acetate: hexane (4:1 v/v) to yield 4-cyano-4-(2-phenylethane sulfanylthiocarbonyl) sulfanylpentanoic acid (PETTC) as a yellow solid (yield 74 %): <sup>1</sup>H NMR (400.13 MHz, CD<sub>2</sub>Cl<sub>2</sub>, 298 K): δ 1.91 (3H, CH<sub>3</sub>), 2.41-2.62 (m, 2H, CH<sub>2</sub>), 2.72 (t, 2H, CH<sub>2</sub>), 3.04 (t, 2H, CH<sub>2</sub>), 3.63 (t, 2H, CH<sub>2</sub>), 7.3-7.4 (m, 5H, aromatic). <sup>13</sup>C NMR (400.13

MHz, CD<sub>2</sub>Cl<sub>2</sub>, 298 K):  $\delta$  24.4 (CH<sub>3</sub>), 29.6 (CH<sub>2</sub>CH<sub>2</sub>COOH), 30.2 (CH<sub>2</sub>Ph), 33.2 (CH<sub>2</sub>CH<sub>2</sub>COOH), 40.0 (SCH<sub>2</sub>-CH<sub>2</sub>Ph), 45.7 (SCCH<sub>2</sub>), 118.7 (CN), 127.3, 128.9, 129.2, 144.2 (Ph), 177.5 (C=O), 222.2 (C=S).

#### **Synthesis of poly(glycerol monomethacrylate) macro-chain transfer agent**

A typical synthesis of a PGMA<sub>56</sub> macro-CTA was conducted as follows: a round-bottomed flask was charged with a magnetic follower, CPDB (0.020 mol, 6.03 g), ethanol (156.0 g), GMA monomer (1.268 mol, 203.0 g) and ACVA (4.07 mmol, 1.14 g), to afford a target DP of 63 and a [CPDB]/[ACVA] molar ratio of 5, respectively. The flask was then sealed, purged with nitrogen for 20 minutes and placed in a pre-heated oil bath set at 70 °C for 140 minutes. The reaction was then quenched by the simultaneous exposure to air and cooling to 0 °C (ice bath), <sup>1</sup>H NMR indicated a GMA monomer conversion of 69 %. The crude PGMA homopolymer was then purified by precipitation into excess DCM (twice), before being dissolved in water and freeze-dried. <sup>1</sup>H NMR spectroscopy indicated a mean DP of 56, and DMF GPC indicated that M<sub>n</sub> = 15,000 g mol<sup>-1</sup> and M<sub>w</sub>/M<sub>n</sub> = 1.20.

#### **Synthesis of poly(lauryl methacrylate) macro-CTA**

A typical synthesis of a PLMA<sub>39</sub> macro-CTA was conducted as follows. A 250 ml round-bottomed flask was charged with lauryl methacrylate (LMA; 18.7 g; 73.5 mmol), 4-cyano-4-(2-phenylethane sulfanylthiocarbonyl) sulfanylpentanoic acid (PETTC; 0.50 g; 1.47 mmol; target degree of polymerisation, DP = 50), 2,2'-azobisisobutyronitrile (AIBN; 48.3 mg, 294  $\mu$ mol; [PETTC]/[AIBN] molar ratio = 5.0) and toluene (19.2 g; total solids content = 50% w/w). The sealed reaction vessel was purged with nitrogen and placed in a pre-heated oil bath at 70 °C for 3.5 h. The resulting PLMA<sub>39</sub> (LMA conversion = 63 %; CTA efficiency = 81%; M<sub>n</sub> = 8,200 g mol<sup>-1</sup>, M<sub>w</sub>/M<sub>n</sub> = 1.18) was purified by twice precipitating into excess methanol.

#### **Synthesis of PGMA<sub>56</sub>-PTFEMA<sub>500</sub> diblock copolymer spheres**

A typical RAFT emulsion polymerization of PGMA<sub>56</sub>-PTFEMA<sub>500</sub> at 15% w/w was conducted as follows. PGMA<sub>56</sub> macro-CTA (0.3 g, 0.033 mmol) and ACVA initiator (2.3 mg, 0.0083 mmol) were dissolved in water (15.2 g). The reaction mixture was then sealed in a round-bottomed flask, submerged in an ice bath and purged with nitrogen for 25 minutes. TFEMA monomer was separately purged with nitrogen for 15 minutes before being transferred (2.3 ml, 16.3 mmol) to the reaction mixture. The resulting deoxygenated emulsion was submerged in an oil bath at 70 °C for 8 h (final TFEMA conversion by <sup>19</sup>F NMR = 98 %, M<sub>n</sub> = 72,000 g mol<sup>-1</sup>, M<sub>w</sub>/M<sub>n</sub> = 1.25).

### **Synthesis of PLMA<sub>39</sub>-PTFEMA<sub>800</sub> diblock copolymer spheres**

A typical RAFT dispersion polymerisation of PLMA<sub>39</sub>-PTFEMA<sub>800</sub> at 10% w/w was conducted as follows. PLMA<sub>39</sub> macro-CTA (0.2 g, 0.019 mmol) and T21s initiator (1.0 mg, 0.0048 mmol) were dissolved in *n*-dodecane (25.42 g). The reaction mixture was then sealed in a round-bottomed flask, submerged in an ice bath and purged with nitrogen for 25 minutes. TFEMA monomer was separately purged with nitrogen for 15 minutes before being transferred (2.22 ml, 15.6 mmol) to the reaction mixture. The resulting deoxygenated solution was submerged in an oil bath at 90 °C for 8 h (final TFEMA conversion by <sup>19</sup>F NMR = 99 %,  $M_n = 132,000 \text{ g mol}^{-1}$ ,  $M_w/M_n = 1.64$ ).

### **Synthesis of PGMA<sub>56</sub>-PBzMA<sub>300</sub> diblock copolymer spheres**

PGMA<sub>56</sub>-PBzMA<sub>300</sub> spherical nanoparticles were prepared *via* RAFT aqueous emulsion polymerisation at 10 % w/w according to a previously-reported protocol. Final BzMA conversion by <sup>1</sup>H NMR = 99 %,  $M_n = 59,000 \text{ g mol}^{-1}$ ,  $M_w/M_n = 1.21$ ).

### **Preparation of o/w isorefractive emulsions using glycerol**

The as-prepared 15% w/w PGMA<sub>56</sub>-PTFEMA<sub>500</sub> aqueous dispersion was diluted with glycerol until a 65% w/w glycerol/water mixture was reached. The resulting 5.8% w/w PGMA<sub>56</sub>-PTFEMA<sub>500</sub> dispersion in 65% aqueous glycerol was then serially diluted with pre-prepared 65 % w/w aqueous glycerol to obtain copolymer concentrations ranging from 1.5 to 4.0 wt %. To prepare the contrast-matched Pickering emulsion, a dilute sphere dispersion (2.0 ml) was homogenised with *n*-dodecane (2.0 ml) for 2.0 minutes using a IKA Ultra-Turrax T-18 homogeniser with a 10 mm dispersing tool operating at 9,000 rpm.

### **Preparation of o/w isorefractive emulsions using sucrose**

Sucrose was added to the as-prepared 15% w/w PGMA<sub>56</sub>-PTFEMA<sub>500</sub> aqueous dispersion until a 50.5% w/w sucrose/water mixture was reached. The resulting 7.4% w/w PGMA<sub>56</sub>-PTFEMA<sub>500</sub> dispersion in ~ 50 % aqueous sucrose was then serially diluted with pre-prepared 50 % w/w aqueous sucrose to obtain copolymer concentrations ranging from 1.2 to 3.5 % w/w. To prepare the contrast-matched Pickering emulsion, a dilute dispersion of PGMA<sub>56</sub>-PTFEMA<sub>500</sub> nanoparticles (2.0 ml) was homogenised with *n*-dodecane (2.0 ml) for 2.0 minutes using a IKA Ultra-Turrax T-18 homogeniser with a 10 mm dispersing tool operating at 9,000 rpm.

**Preparation of o/w/o isorefractive Pickering double emulsion.**

A single contrast-matched o/w emulsion stabilised by 2.0 % w/w PGMA<sub>56</sub>-PTFEMA<sub>500</sub> nanoparticles was prepared at 24,000 rpm as above. 2.0 ml of this single o/w emulsion was then homogenised at 20 °C with 2.0 ml of a 2.0 % w/w dispersion of PLMA<sub>39</sub>-PTFEMA<sub>500</sub> in *n*-dodecane, for 2.0 minutes at 7,000 rpm.

**6.2.3 Characterisation**

**<sup>1</sup>H and <sup>19</sup>F NMR spectroscopy**

<sup>1</sup>H and <sup>19</sup>F NMR spectra were recorded in either acetone-d<sub>6</sub>, chloroform-d, dichloromethane-d<sub>2</sub> or methanol-d<sub>4</sub> using a Bruker AV1-400 MHz spectrometer. Typically, 64 scans were averaged per spectrum.

**DMF gel permeation chromatography**

Molecular weight distributions were determined using a DMF gel permeation chromatography (GPC) instrument operating at 60 °C that comprised two Polymer Laboratories PL gel 5 µm Mixed C columns and one PL polar gel 5 µm guard column connected in series to a Varian 390 LC multidetector suite (only the refractive index detector was utilised) and a Varian 290-LC pump injection module. The GPC eluent was HPLC grade DMF containing 10 mM LiBr and was filtered prior to use. The flow rate was 1.0 ml min<sup>-1</sup> and DMSO was used as a flow-rate marker. Calibration was conducted using a series of 10 near-monodisperse poly(methyl methacrylate) standards ( $M_p = 625 - 618,000 \text{ g mol}^{-1}$ ). Chromatograms were analysed using Varian Cirrus GPC software.

**THF gel permeation chromatography**

Molecular weight distributions were determined using a THF GPC instrument operating at 30 °C that comprised two Polymer Laboratories PL gel 5 µm Mixed C columns, a LC20AD ramped isocratic pump and a WellChrom K-2301 refractive index detector operating at 950 ± 30 nm. The THF mobile phase contained 2.0 % v/v triethylamine and 0.05 % w/v 3,5-di-tert-4-butylhydroxytoluene (BHT) and the flow rate was fixed at 1.0 ml min<sup>-1</sup> and toluene was used as a flow-rate marker. A series of ten near-monodisperse poly(methyl methacrylate) standards ( $M_p = 1280 - 330,000 \text{ g mol}^{-1}$ ) were used for calibration. Chromatograms were analysed using Varian Cirrus GPC software.

### **Dynamic light scattering**

DLS studies were performed using a Zetasizer Nano-ZS instrument (Malvern Instruments, UK) at 25 °C at a scattering angle of 173°. Copolymer dispersions were diluted in water, 65% w/w glycerol/water mixtures or 50.5% w/w sucrose/water mixtures prior to light scattering studies. The intensity-average diameter and polydispersity (PDI) of the diblock copolymer particles were calculated by cumulants analysis of the experimental correlation function using Dispersion Technology Software version 6.20. Data were averaged over ten runs each of thirty seconds duration.

### **Transmission electron microscopy**

Transmission electron microscopy (TEM) studies were conducted using a FEI Tecnai G2 spirit instrument operating at 80 kV and equipped with a Gatan 1k CCD camera. Copper TEM grids were surface-coated in-house to yield a thin film of amorphous carbon. For samples prepared in *n*-dodecane the grids were then loaded with dilute copolymer dispersions (0.2 % w/w) and imaged without staining. For aqueous samples the grids were plasma glow-discharged for 20 seconds to create a hydrophilic surface prior to being loaded with dilute copolymer dispersion (0.2 % w/w). The sample-loaded grids were soaked in 0.75% w/w uranyl formate solution (15 µl) for 20 seconds in order to improve contrast.

### **Laser diffraction**

The volume-average droplet ( $D[4,3]$ ) diameter was determined using a Malvern Mastersizer 2000 instrument equipped with a small volume Hydro 2000SM sample dispersion unit (ca. 100 ml), a He–Ne laser operating at 633 nm, and a solid-state blue laser operating at 466 nm. The stirring rate was adjusted to 1,000 rpm in order to avoid creaming or sedimentation of the droplets during analysis. After each measurement, the cell was rinsed twice with isopropyl alcohol. The glass walls of the cell were carefully wiped to avoid cross contamination and the laser was aligned centrally to the detector prior to data acquisition.

### **Optical microscopy**

Optical microscopy images were recorded using a Motic DMBA300 digital biological microscope equipped with a built-in camera and analysed using Motic Images Plus 2.0 ML software.

### Fluorescence microscopy

Fluorescence microscopy images were recorded on a Zeiss Axio Scope A1 microscope fitted with an AxioCam 1Cm1 monochrome camera using Zeiss filter set 43 HE (excitation 550/25 nm and emission 605/70 nm). Images were captured and processed using ZEN lite 2012 software.

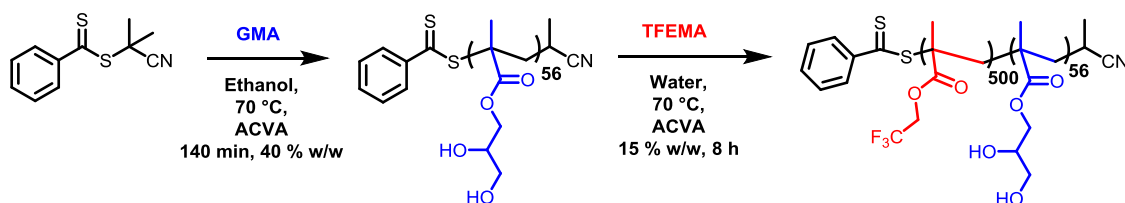
### UV/Vis absorption spectroscopy

Visible spectra were recorded in transmittance mode between 800 and 400 nm for selected Pickering emulsions using a UV 1800 Shimadzu spectrophotometer. UV spectra were recorded using the same instrument.

## 6.3 Results and discussion

### 6.3.1 Nanoparticle synthesis and refractive index matching

A PGMA macro-CTA was prepared *via* RAFT solution polymerisation in ethanol at 70 °C using 2-cyano-2-propyl dithiobenzoate (CPDB). This near-monodisperse precursor (DP = 56;  $M_w/M_n = 1.20$ ) was then chain-extended *via* the RAFT aqueous emulsion polymerisation of TFEMA at 15 % w/w solids (target DP = 500), according to (Scheme 6.1).



**Scheme 6.1:** Synthesis of a PGMA<sub>56</sub> macro-CTA, *via* solution polymerisation of GMA in ethanol using CPDB, and subsequent chain extension with TFEMA in water.

<sup>1</sup>H and <sup>19</sup>F NMR spectroscopy studies confirmed a mean diblock composition of PGMA<sub>56</sub>-PTFEMA<sub>500</sub>, while GPC analysis indicated that  $M_n = 72,000 \text{ g mol}^{-1}$  and  $M_w/M_n = 1.25$ . TEM analysis confirmed a well-defined spherical morphology for these diblock copolymer nanoparticles (see Figure 6.1) and DLS studies indicated a Z-average diameter of 101 nm.

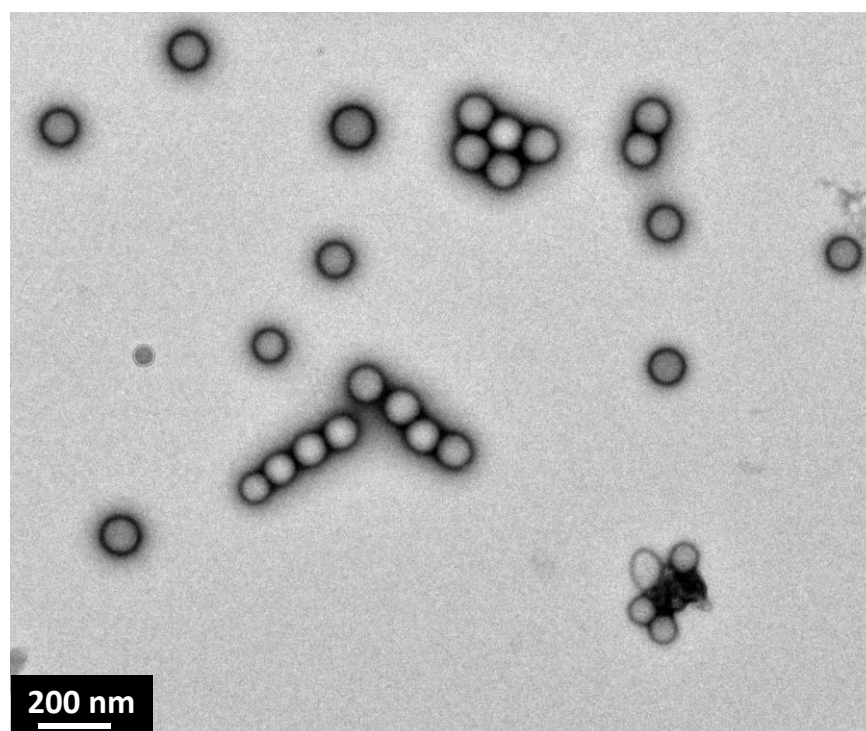


**Figure 6.1:** Transmission electron micrograph of a PGMA<sub>56</sub>-PTFEMA<sub>500</sub> latex prepared *via* RAFT aqueous emulsion polymerisation.

The as-synthesised 15 % w/w aqueous dispersion of PGMA<sub>56</sub>-PTFEMA<sub>500</sub> nanoparticles was highly turbid, as expected given the relatively large refractive index difference between the major PTFEMA component (1.42) and pure water (1.33). To produce a highly transparent dispersion, sucrose was gradually added to a 2.0 % w/w aqueous dispersion of PGMA<sub>56</sub>-PTFEMA<sub>500</sub> nanoparticles in order to achieve isorefractivity (**Figure 6.2a**). The ensuing reduction in turbidity could be conveniently monitored by visible absorption spectroscopy (**Figure 6.2b**). As the aqueous sucrose concentration was increased from zero up to approximately 50 % w/w, the transmittance of the aqueous dispersion at 400 nm increased dramatically from approximately 0 % up to 98 %. However, higher sucrose concentrations led to a *reduction* in transmission. Thus, 50.5 % w/w sucrose corresponds to a contrast-matched dispersion with maximum transmittance. This indicates that the refractive index of these sterically-stabilised nanoparticles is approximately 1.42 (i.e. the same as that of a 50.5 % w/w aqueous sucrose solution, see **Figure 6.3**).<sup>52</sup> Hence this parameter is primarily governed by the refractive index of the core-forming PTFEMA block and the influence of the highly solvated PGMA stabiliser chains is negligible.

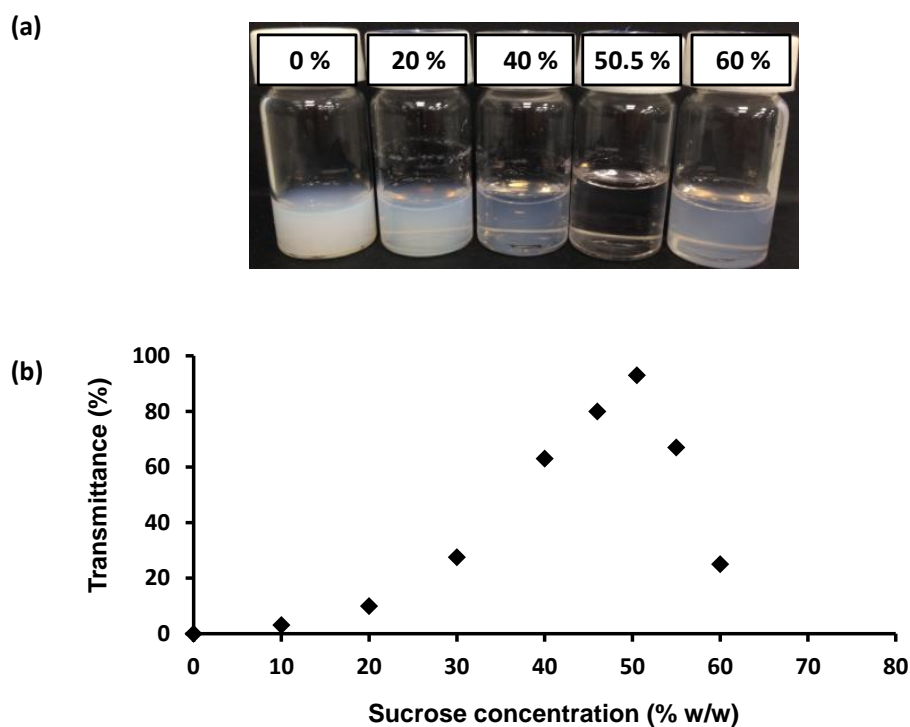


**Figure 6.2:** (a) Digital photographs of PGMA<sub>56</sub>-PTFEMA<sub>500</sub> diblock copolymer nanoparticles at a fixed concentration of 2 % w/w, dispersed in aqueous sucrose solutions with varying concentrations of sucrose. The number above each vial indicates the concentration of sucrose (% w/w) in each case. (b) Transmittance data obtained at 400 nm for a 2.0 % w/w dispersion of PGMA<sub>56</sub>-PTFEMA<sub>500</sub> nanoparticles as a function of sucrose concentration.

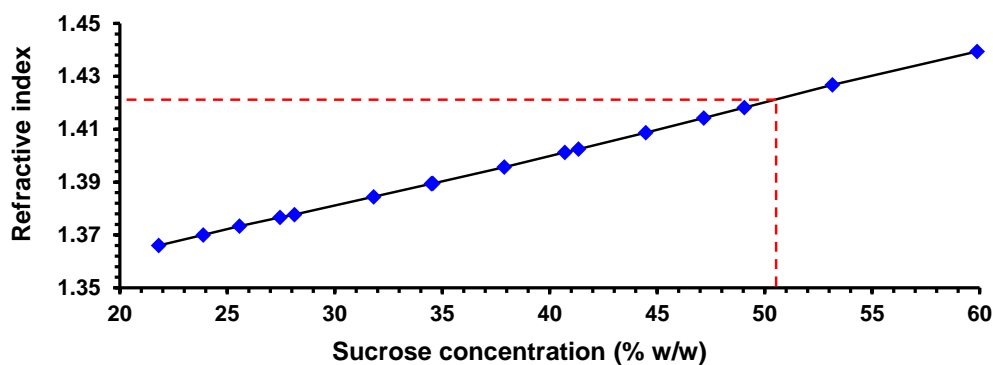


**Figure 6.3:** Refractive index vs. sucrose concentration, obtained from the literature,<sup>52</sup> for a range of aqueous sucrose concentrations. The dashed red line indicates that the refractive index of a 50.5 % w/w aqueous sucrose solution (i.e. contrast-matched with PGMA<sub>56</sub>-PTFEMA<sub>500</sub>) is 1.42.

Similar experiments using glycerol instead of sucrose confirmed that a similarly transparent dispersion could be obtained when the aqueous continuous phase contained 65 % w/w of the alcoholic co-solvent (see **Figure 6.4**).

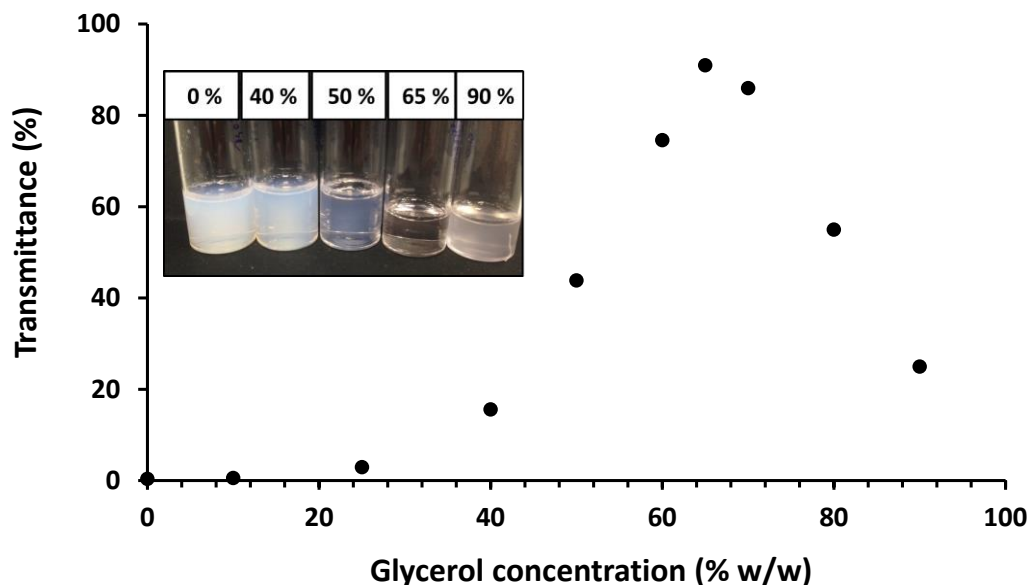


**Figure 6.4:** Transmittance data obtained at 400 nm for a 2.0 % w/w dispersion of PGMA<sub>56</sub>-PTFEMA<sub>500</sub> nanoparticles as a function of glycerol concentration. The inset is a digital photograph of select dispersions used to obtain the data shown in the graph. The number above each vial indicates the concentration of glycerol present in each dispersion (% w/w).

This observation is consistent with the literature: the refractive index of such a glycerol-rich aqueous solution is known to be approximately 1.42 (Figure 6.5).<sup>53</sup> It is perhaps noteworthy that the latter formulation may be of potential interest for transparent cosmetics formulations, since glycerol is cheap, non-toxic and a well-known humectant.<sup>54</sup>

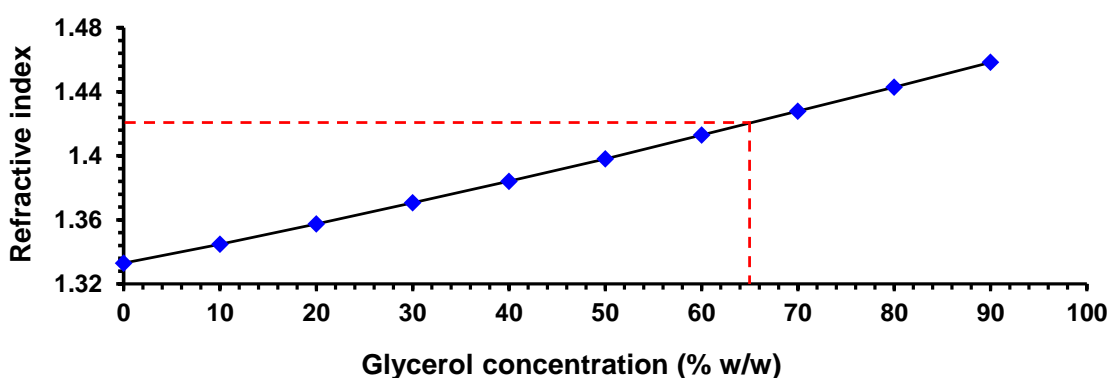


**Figure 6.5:** Refractive index vs. glycerol concentration, obtained from the literature,<sup>53</sup> for a range of aqueous glycerol concentrations. The dashed red line indicates that the refractive index of a 65 % w/w aqueous glycerol solution (i.e. contrast-matched with PGMA<sub>56</sub>-PTFEMA<sub>500</sub>) is 1.42.

### 6.3.2 Preparation of isorefractive Pickering emulsions

For emulsification experiments, a series of isorefractive aqueous sucrose or glycerol dispersions of PGMA<sub>56</sub>-PTFEMA<sub>500</sub> nanoparticles were prepared at copolymer concentrations ranging from 1.2 % to 3.5 % w/w. Each of these dispersions were then homogenised in turn with an equal volume of *n*-dodecane at 9,000 rpm for 2 min to produce contrast-matched Pickering emulsions. A schematic representation of this process, using sucrose, is shown in Figure 6.6.

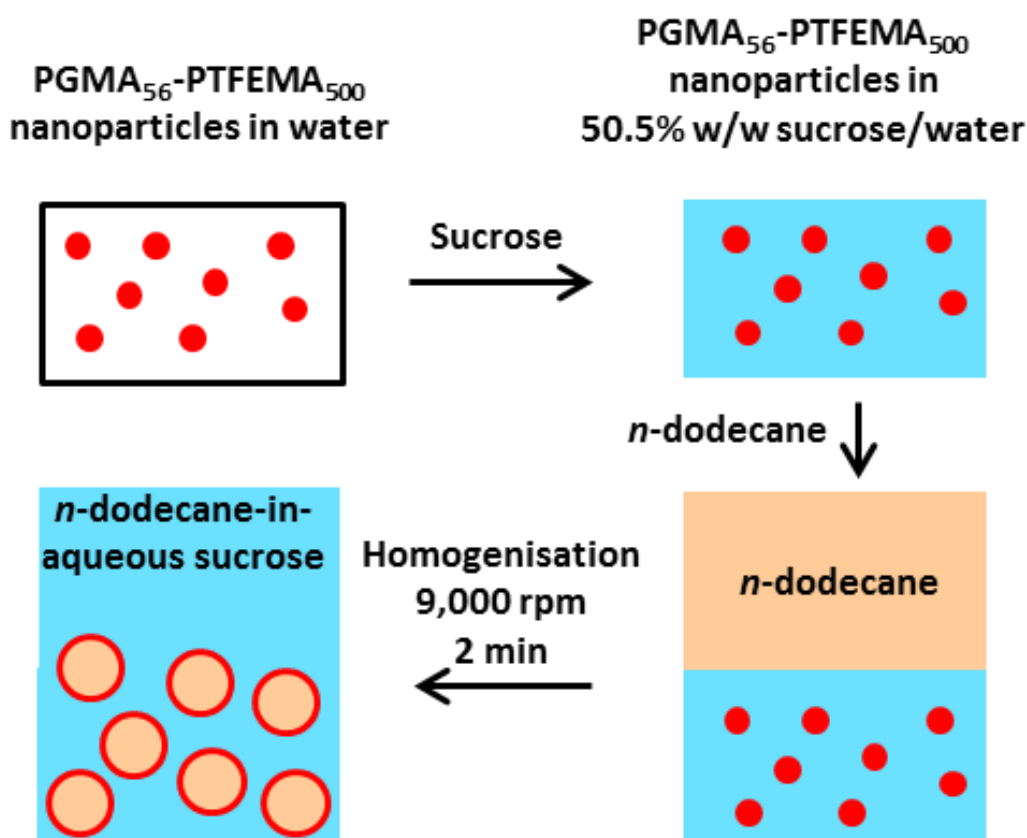


**Figure 6.6:** Schematic preparation of of *n*-dodecane-in-50.5 % w/w aqueous sucrose Pickering emulsions with 1.2 – 3.5 % w/w spherical nanoparticles dispersed in the continuous phase prior to homogenisation.

A digital photograph (**Figure 6.7a**) of an *n*-dodecane-in-50.5 % aqueous sucrose Pickering emulsion prepared using 1.20 % w/w PGMA<sub>56</sub>-TFEMA<sub>500</sub> nanoparticles serves to illustrate the remarkably high transparency that can be achieved. Visible absorption spectroscopy studies indicated an average transmittance of 96 % at 20 °C (see **Figure 6.7a**).

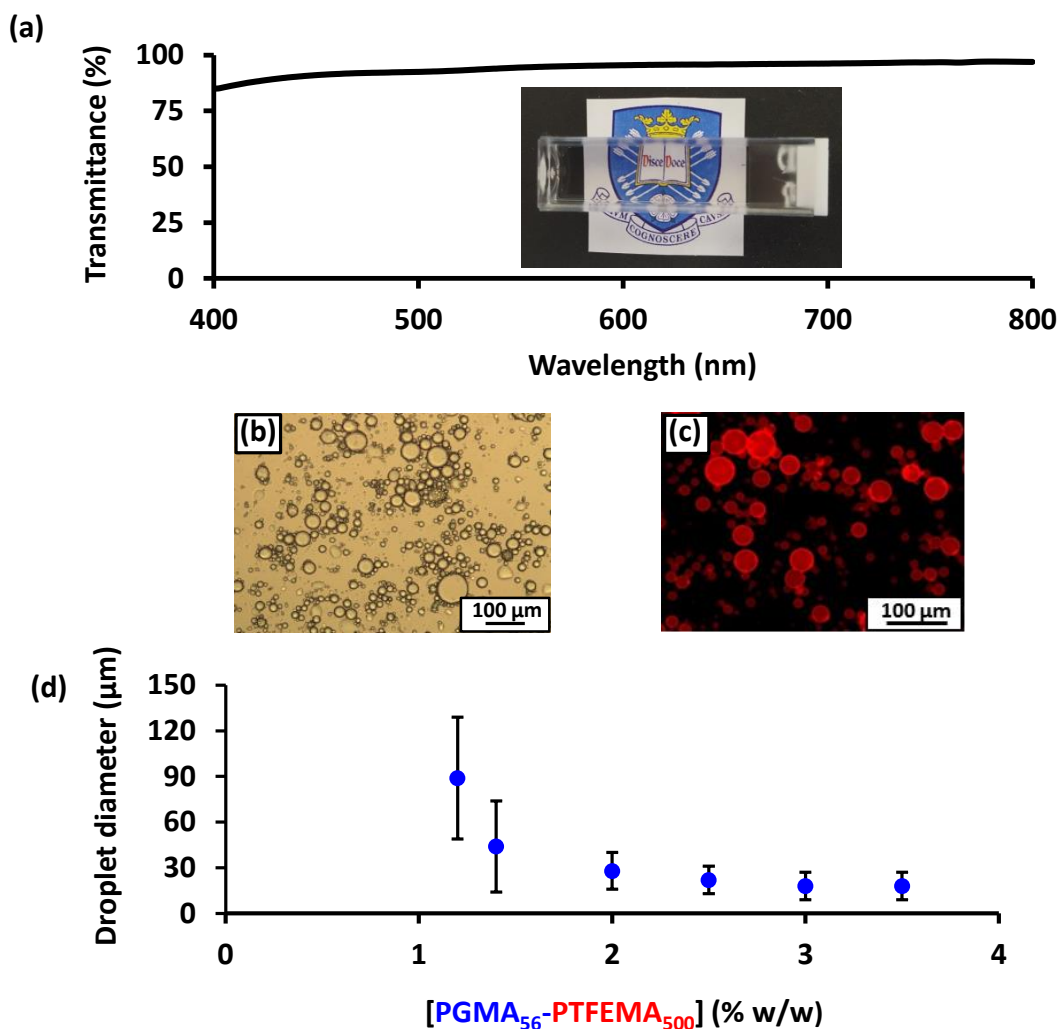


**Figure 6.7:** (a) Digital photograph of *n*-dodecane-in-50.5 % w/w aqueous sucrose Pickering emulsion prepared using 1.2 % w/w PGMA<sub>56</sub>-PTFEMA<sub>500</sub> spherical nanoparticles and the corresponding transmittance data. (b) Optical micrograph obtained for the same emulsion after dilution using pure water. (c) Fluorescence micrograph of this emulsion with the hydrophobic dye, Nile Red, dissolved in the *n*-dodecane droplet phase. (d) Variation in volume-average droplet diameter (as determined by laser diffraction) vs. PGMA<sub>56</sub>-PTFEMA<sub>500</sub> copolymer concentration. The error bars represent the standard deviation of each mean volume-average diameter.

Optical microscopy was used to confirm that stable Pickering emulsions had been formed. Initially, the *n*-dodecane droplets could not be observed, because of the almost perfect iso refractivity. This problem was overcome by diluting each Pickering emulsion with pure water (rather than ~ 50 % aqueous sucrose solution) prior to visual inspection. This protocol resulted in sufficient contrast to visualise the oil droplets (see **Figure 6.7b**). The ease of dilution of the Pickering emulsions using pure water indicated that the aqueous sucrose solution was indeed the continuous phase, as expected. This was confirmed by conductivity studies and is consistent with the observation that the less dense *n*-dodecane droplets (density of *n*-dodecane = 0.75 g cm<sup>-3</sup>)<sup>50</sup>

gradually creamed on standing at 20 °C. Laser diffraction studies performed on dilute emulsions indicated that large polydisperse droplets with a mean diameter of  $89 \pm 40 \mu\text{m}$  were produced when using 1.20 % w/w PGMA<sub>56</sub>-PTFEMA<sub>500</sub> nanoparticles. Using a higher nanoparticle concentration of 3.5 % w/w leads to the formation of smaller droplets of  $20 \pm 9 \mu\text{m}$  diameter. These observations were corroborated by dissolving Nile Red in *n*-dodecane prior to homogenisation: this hydrophobic water-insoluble dye enables the resulting Pickering emulsions to be imaged *via* fluorescence microscopy (**Figure 6.7c**). The pronounced upturn in droplet diameter on lowering the nanoparticle concentration (**Figure 6.7d**) is characteristic of a Pickering emulsifier and has been widely reported in the literature.<sup>55–61</sup>

Similar experiments conducted using 65 % glycerol instead of ~ 50 % aqueous sucrose also produced highly-transparent Pickering emulsions with a maximum mean transmittance of 94 % being achieved when utilising 1.5 % w/w nanoparticles.

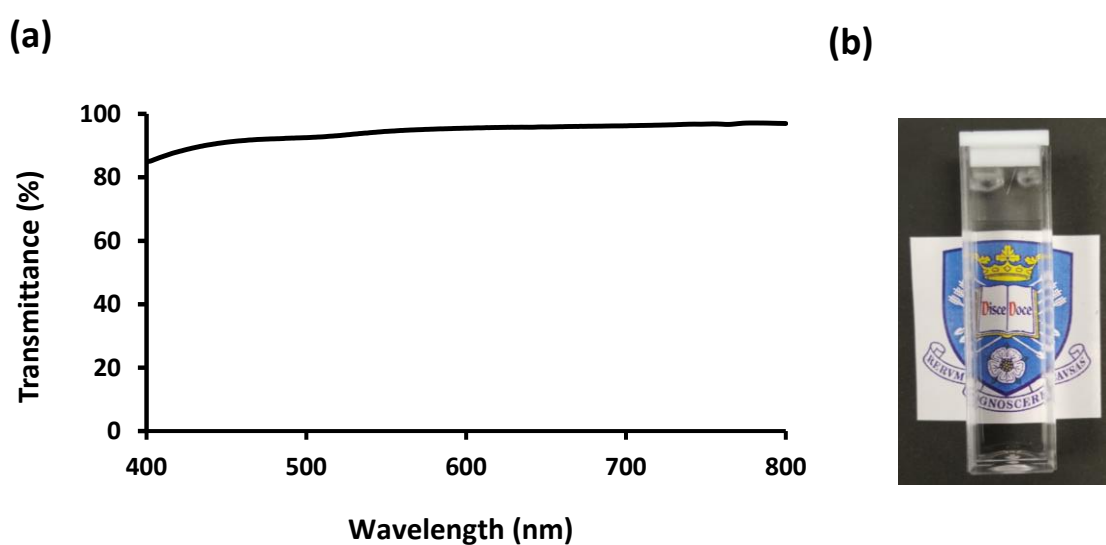


**Figure 6.8:** (a) Transmission data obtained for a *n*-dodecane-in-65 % aqueous glycerol Pickering emulsion prepared with 1.5 % w/w PGMA<sub>56</sub>-PTFEMA<sub>500</sub> spherical nanoparticles. (b) Digital photograph of same emulsion.

Optical microscopy, conducted after dilution in pure water, confirmed the presence of well-defined spherical droplets. Furthermore, the addition of Nile Red to the *n*-dodecane, prior to homogenisation, facilitated fluorescence microscopy studies to be performed. Such studies indicated that well-defined droplets were present, and therefore supported the observations made by optical microscopy. Finally, laser diffraction experiments performed upon a series of dilute emulsions confirmed that an increase in droplet diameter occurs upon decreasing the nanoparticle

concentration with which the emulsions were prepared. This provides evidence that the copolymers are adsorbing at the interface as intact particles, rather than breaking up and adsorbing as diblock copolymer chains.

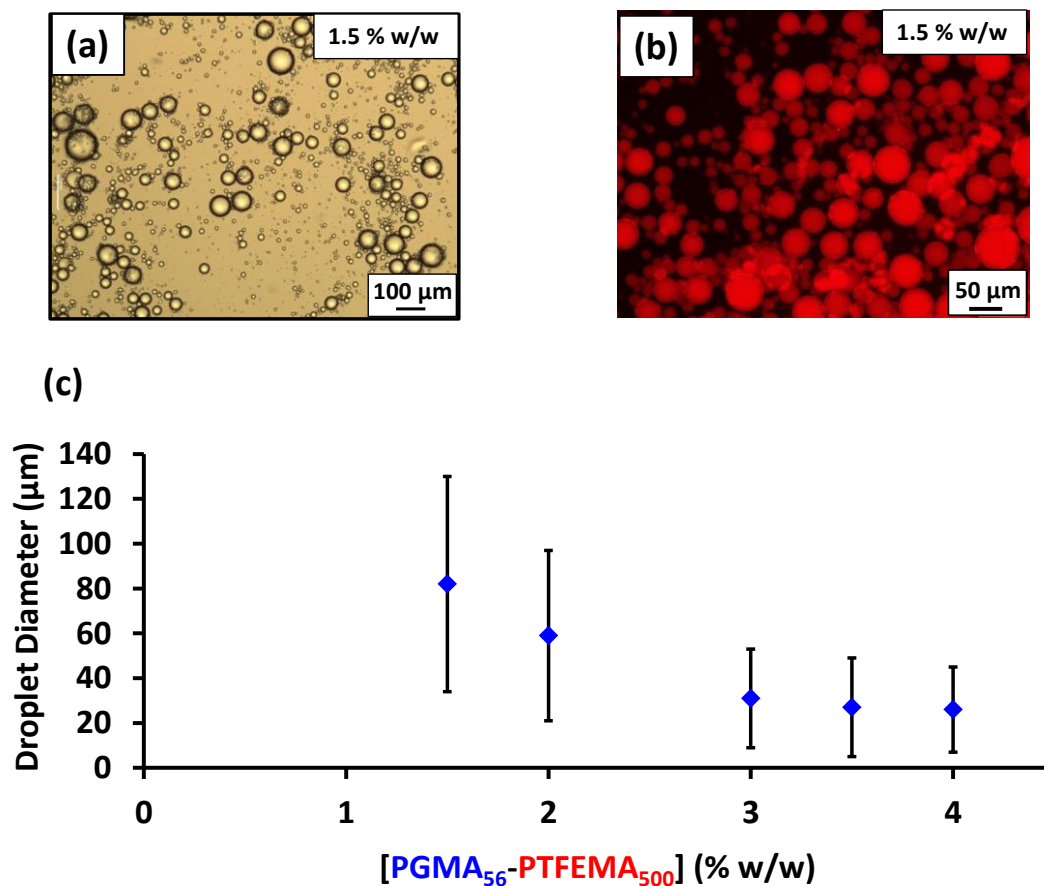


**Figure 6.9:** (a) Optical microscopy image obtained, after dilution in water, for an n-dodecane-in-65 % aqueous glycerol Pickering emulsion prepared with 2 % PGMA<sub>56</sub>-PTFEMA<sub>500</sub> spherical nanoparticles. (b) Fluorescence micrograph of the same emulsion prepared with Nile Red in the n-dodecane phase. (c) Droplet diameter vs. particle concentration, obtained by laser diffraction, obtained for a series of PGMA<sub>56</sub>-PTFEMA<sub>500</sub>-stabilised n-dodecane-in-65 % glycerol Pickering emulsions.

### 6.3.3 Control experiments with non-isorefractive nanoparticles

To investigate the importance of contrast-matching the nanoparticles as well as the two immiscible liquids, the same PGMA<sub>56</sub> macro-CTA was also used to conduct the RAFT aqueous emulsion polymerisation of benzyl methacrylate, as described previously by Cunningham and co-workers.<sup>62</sup> PBzMA was selected for the core-forming block as its refractive index of 1.57<sup>63</sup> is significantly higher than that of PTFEMA, n-dodecane and ~ 50 % aqueous sucrose (each approximately 1.42). <sup>1</sup>H NMR spectroscopy analysis indicated more than 99% BzMA

conversion, while DLS studies indicated a Z-average diameter of 102 nm for the resulting PGMA<sub>56</sub>-PBzMA<sub>300</sub> nanoparticles, which is comparable to that of the PGMA<sub>56</sub>-TFEMA<sub>500</sub> nanoparticles. Thus, the former nanoparticles are *not* contrast-matched to the two iso refractive immiscible liquids, so this new formulation serves as a useful control experiment. Sucrose was added to a 10 % w/w aqueous dispersion of PGMA<sub>56</sub>-PBzMA<sub>300</sub> nanoparticles to obtain a final sucrose concentration of 50.5 % w/w. This dispersion was then diluted using 50.5 % aqueous sucrose to produce a final copolymer concentration of 1.20 % w/w, followed by homogenisation with an equal volume of *n*-dodecane at 9000 rpm for 2 min. Optical microscopy studies confirmed that a stable Pickering emulsion was formed, with laser diffraction analysis indicating a mean droplet diameter of  $40 \pm 18 \mu\text{m}$  (see **Figure 6.10b**). However, in this case visible absorption spectroscopy studies of the Pickering emulsion indicated a mean transmittance of approximately 0 % across the entire wavelength range, which is characteristic of a highly turbid emulsion (see **Figure 6.10a**).

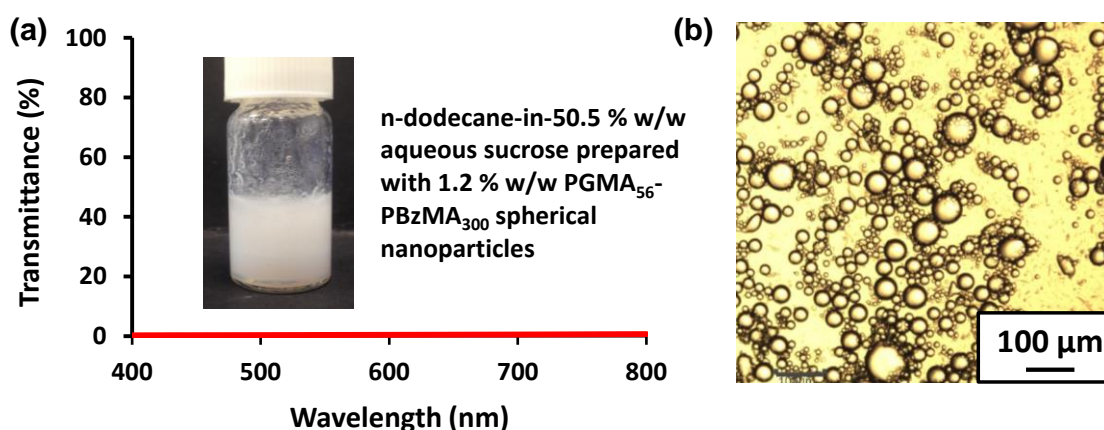


**Figure 6.10:** (a) Transmittance data obtained between 400 and 800 nm for an *n*-dodecane-in-50.5 % aqueous sucrose Pickering emulsion prepared with non-iso refractive PGMA<sub>56</sub>-PBzMA<sub>300</sub> spherical nanoparticles. A photograph of the emulsion is shown in the inset. (b) Optical micrograph of the emulsion shown in (a) after dilution in pure water.

Similar experiments using 65 % w/w aqueous glycerol instead of sucrose also produced conventional turbid emulsions with an average transmittance of 0 % across the visible spectrum (see **Figure 6.11**). Hence these control experiments confirm the importance of contrast-matching the nanoparticle emulsifier in addition to using iso refractive immiscible liquids if highly transparent Pickering emulsions are desired.

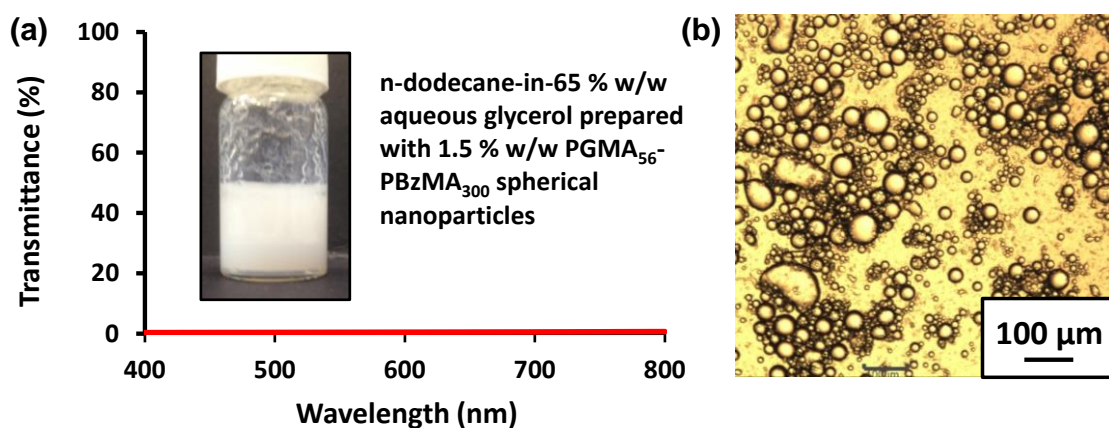


**Figure 6.11:** (a) Transmittance data obtained between 400 and 800 nm for an n-dodecane-in-50.5 % aqueous sucrose Pickering emulsion prepared with non-isorefractive PGMA<sub>56</sub>-PBzMA<sub>300</sub> spherical nanoparticles. A photograph of the emulsion is shown in the inset. (b) Optical micrograph of the emulsion shown in (a) after dilution in pure water.

### 6.3.4 Isorefractive Pickering double emulsions

Having rationally designed transparent oil-in-water Pickering emulsions, highly transparent Pickering *double* emulsions were pursued. Various examples of conventional (i.e. turbid) Pickering double emulsions have been reported<sup>64,65</sup> and potential applications for the encapsulation of various actives have been suggested.<sup>66–68</sup> According to the literature,<sup>40,69,70</sup> such formulations require the design and use of *hydrophobic* nanoparticles to supplement the *hydrophilic* PGMA<sub>56</sub>-PTFEMA<sub>500</sub> nanoparticles. This is because the former nanoparticles are required to stabilise water-in-oil emulsions,<sup>34</sup> whereas the latter invariably favour the formation of oil-in-water emulsions (*vide supra*). Thus a poly(lauryl methacrylate)<sub>39</sub> (PLMA)<sub>39</sub> macro-CTA was used to synthesise new hydrophobic PLMA<sub>39</sub>-PTFEMA<sub>800</sub> nanoparticles *via* RAFT dispersion polymerisation of TFEMA at 10 % w/w in *n*-dodecane, using a PISA formulation similar to that reported by Fielding and co-workers.<sup>51</sup> Both <sup>19</sup>F and <sup>1</sup>H NMR spectroscopy indicated > 99% TFEMA conversion. DLS studies indicated near-monodisperse nanoparticles with a Z-average diameter of 93 nm, while TEM studies confirmed a well-defined spherical morphology. This PLMA<sub>39</sub>-PTFEMA<sub>800</sub> dispersion was highly transparent even at 10 % w/w solids, suggesting that the refractive index of the nanoparticles is essentially the same as that of *n*-dodecane (1.42).

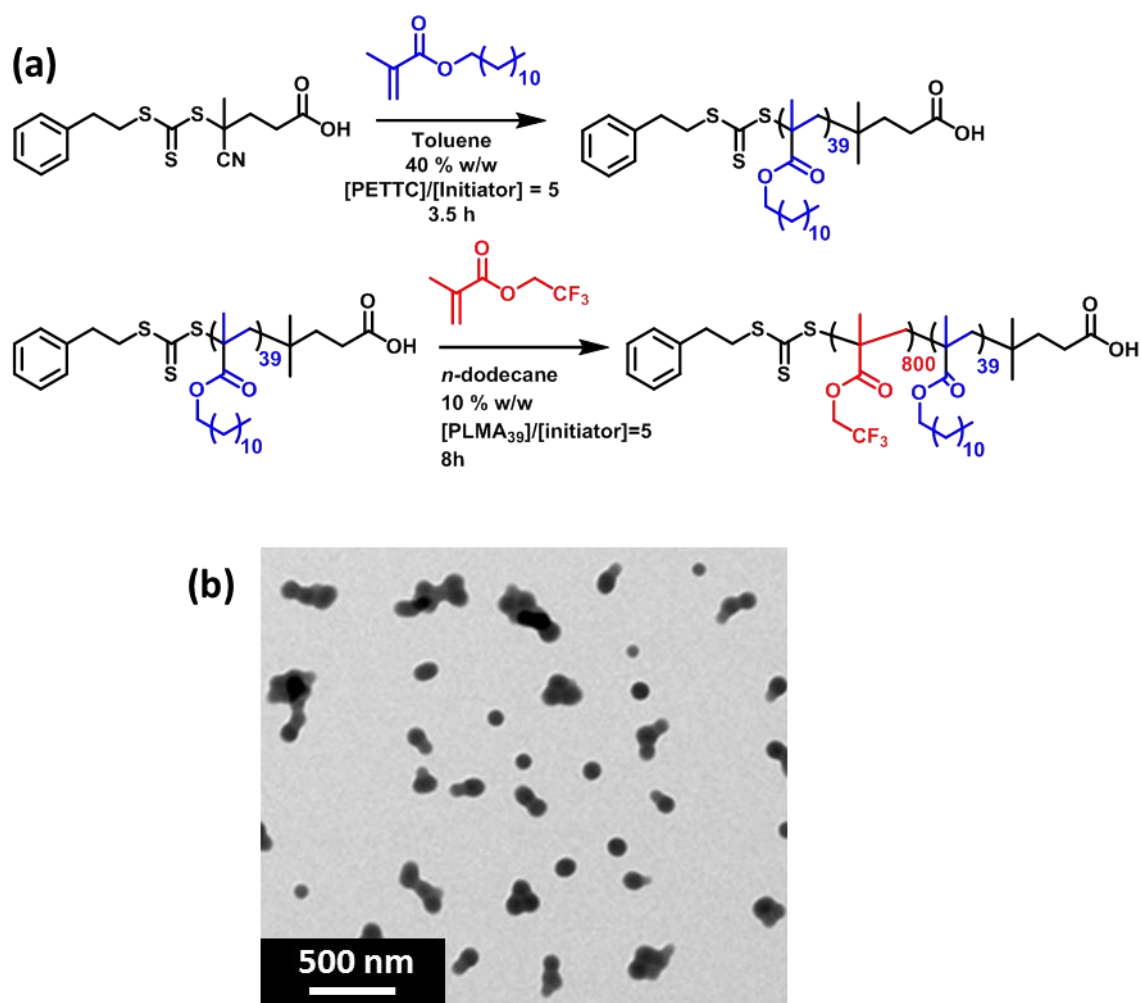


**Figure 6.12:** (a) Synthesis of PLMA<sub>39</sub> macro-CTA *via* RAFT solution polymerisation in toluene and subsequent chain extension with TFEMA *via* RAFT solution polymerisation in *n*-dodecane. (b) TEM image obtained for PLMA<sub>39</sub>-PTFEMA<sub>800</sub> spherical nanoparticles prepared in *n*-dodecane.

Pickering double emulsions were then prepared as follows. First, the precursor oil-in-water emulsion was prepared using 2.0 % w/w *hydrophilic* PGMA<sub>56</sub>-PTFEMA<sub>500</sub> nanoparticles dispersed in a 50.5 % w/w aqueous sucrose solution, an *n*-dodecane volume fraction of 0.50 and a shear rate of 24,000 rpm. These conditions were selected to produce the smallest possible droplets ( $23 \pm 12 \mu\text{m}$  diameter as judged by laser diffraction) in order to maximise the probability of their encapsulation within the aqueous droplets formed during the second-stage emulsification. This precursor emulsion was then homogenised with an equal volume of *n*-dodecane containing 2.0 % w/w *hydrophobic* PLMA<sub>39</sub>-PTFEMA<sub>800</sub> nanoparticles at a shear rate of 7,000 rpm. Laser diffraction analysis of the resulting Pickering double emulsion indicated a mean aqueous droplet diameter of  $120 \pm 68 \mu\text{m}$ . A digital photograph of the final Pickering double emulsion confirms

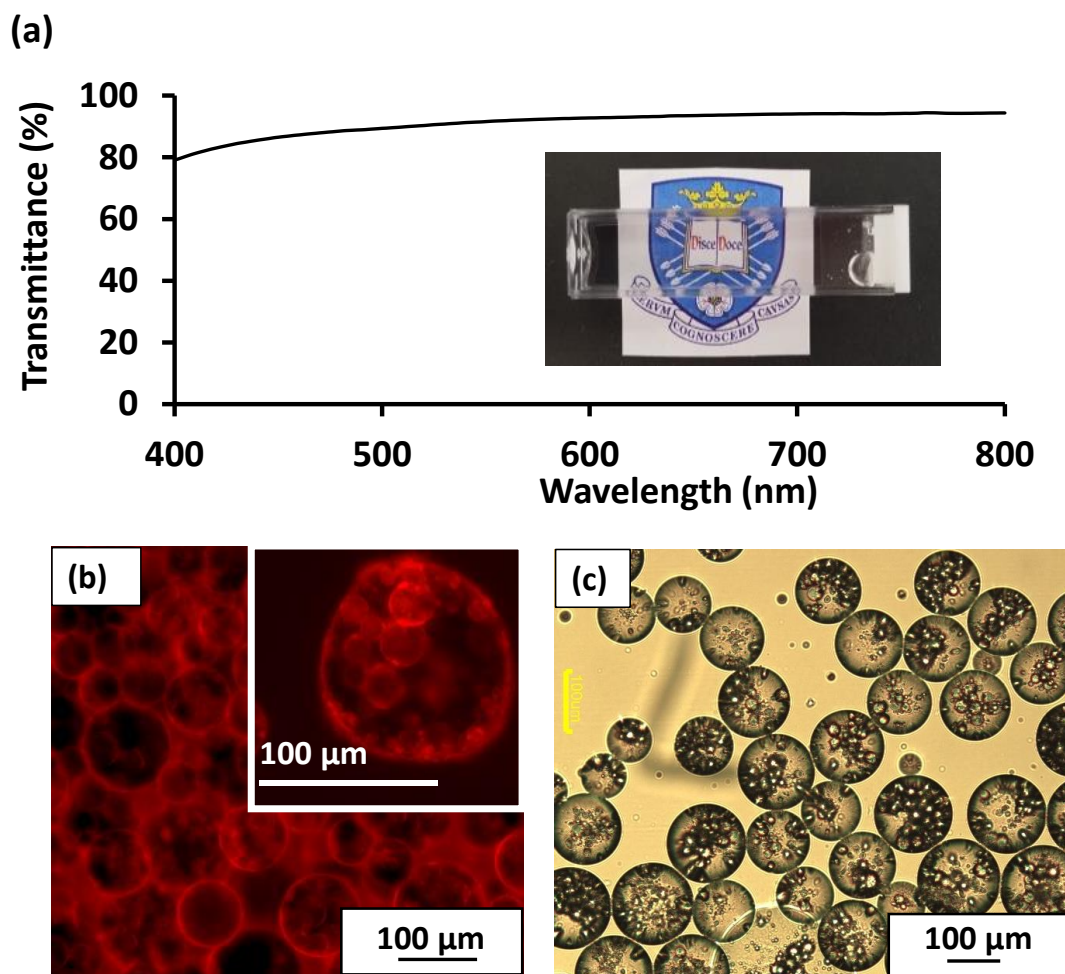


**Figure 6.13:** (a) Transmittance data obtained between 400 and 800 nm for an *n*-dodecane-in-50.5 % aqueous sucrose-in-*n*-dodecane Pickering double emulsion. The internal oil-in-water

its relatively high transparency, with visible absorption spectroscopy studies indicating a mean transmittance of 89 % (**Figure 6.13a**). Dissolving Nile Red in both the initial batch of *n*-dodecane (i.e. that used to generate the oil-in-water precursor emulsion), and also the second batch of *n*-dodecane enabled imaging *via* fluorescence microscopy (**Figure 6.13b**). These studies confirmed successful formation of a Pickering double emulsion comprising relatively small *n*-dodecane droplets within larger droplets of ~ 50 % w/w aqueous sucrose, with *n*-dodecane forming the continuous phase. These observations were consistent with sedimentation of the relatively dense aqueous droplet phase on standing. Although prone to sedimentation on standing, laser diffraction studies confirmed that these Pickering double emulsions nevertheless remained stable with respect to coalescence after storage for up to 3 days at 20 °C. Image analysis of fluorescence micrographs recorded for these double emulsions using ImageJ software indicated that the inner *n*-dodecane droplets had a mean diameter of approximately 21 μm, which is comparable to that observed for the precursor single emulsion ( $23 \pm 12$  μm as judged by laser diffraction). This

suggests that no significant change in droplet diameter occurred during the second-stage homogenisation. Finally, the above double emulsification protocol was repeated using pure water (i.e. in the absence of any sucrose) to provide sufficient contrast for optical microscopy studies, which confirmed that the aqueous droplets contained much smaller *n*-dodecane droplets within them (see **Figure 6.13c**).

## 6.4 Conclusions

Highly transparent oil-in-water Pickering emulsions can be prepared by the judicious addition of sucrose or glycerol to an aqueous dispersion of relatively low refractive index PGMA<sub>56</sub>-PTFEMA<sub>500</sub> nanoparticles, followed by high shear homogenisation with an isorefractive oil such as *n*-dodecane. The resulting contrast-matched emulsions can exhibit up to 96 % transmittance and are stable for months on standing at 20 °C. Control experiments conducted with relatively high refractive index nanoparticles (e.g. PGMA<sub>56</sub>-PBzMA<sub>300</sub>) confirm that contrast-matching the aqueous phase with the oil phase is a necessary but not sufficient criterion for a highly transparent Pickering emulsion. This is because if the nanoparticles are not also contrast-matched to the two liquid phases, they scatter light sufficiently strongly to generate substantial turbidity.

Complementary highly transparent water-in-oil emulsions can be prepared using contrast-matched hydrophobic PLMA<sub>39</sub>-PTFEMA<sub>800</sub> nanoparticles prepared in *n*-dodecane. Moreover, the judicious combination of these two types of hydrophilic and hydrophobic nanoparticle emulsifiers enables the production of an oil-in-water-in-oil Pickering double emulsion that exhibits a mean transmittance of almost 90% across the visible spectrum. Such studies serve to illustrate the remarkable versatility and tremendous potential offered by polymerisation-induced self-assembly (PISA) for the *rational design* of organic nano-objects of tunable size, morphology and surface chemistry as bespoke Pickering emulsifiers.

## 6.5 References

- (1) Ramsden, W. Separation of Solids in the Surface-Layers of Solutions and “Suspensions” (Observations on Surface-Membranes, Bubbles, Emulsions, and Mechanical Coagulation). -- Preliminary Account. *Proc. R. Soc. London* **1903**, 72, 156–164.
- (2) Pickering, S. U. CXCVI.—Emulsions. *J. Chem. Soc., Trans.* **1907**, 91, 2001–2021.
- (3) Aveyard, R.; Binks, B. P.; Clint, J. H. Emulsions Stabilised Solely by Colloidal Particles. *Adv. Colloid Interface Sci.* **2003**, 100–102, 503–546.
- (4) Binks, B. P.; Lumsdon, S. O. Catastrophic Phase Inversion of Water-in-Oil Emulsions Stabilized by Hydrophobic Silica. *Langmuir* **2000**, 16, 2539–2547.
- (5) Binks, B. P.; Lumsdon, S. O. Effects of Oil Type and Aqueous Phase Composition on Oil-water Mixtures Containing Particles of Intermediate Hydrophobicity. *Phys. Chem. Chem.*

- Phys.* **2000**, *2*, 2959–2967.
- (6) Manga, M. S.; Cayre, O. J.; Williams, R. A.; Biggs, S.; York, D. W. Production of Solid-Stabilised Emulsions through Rotational Membrane Emulsification: Influence of Particle Adsorption Kinetics. *Soft Matter* **2012**, *8*, 1532–1538.
  - (7) Madivala, B.; Vandebril, S.; Fransaer, J.; Vermant, J. Exploiting Particle Shape in Solid Stabilized Emulsions. *Soft Matter* **2009**, *5*, 1717–1727.
  - (8) Aveyard, R.; Binks, B. P.; Fletcher, P. D. I.; Rutherford, C. E. Measurement Monodisperse of Contact Angles of Spherical Particles with Surfactant Solutions. *Colloids Surfaces A Physicochem. Eng. Asp.* **1994**, *83*, 89–98.
  - (9) Schulman, J. H.; Leja, J. Control of Contact Angles at the Oil-Water-Solid Interfaces. Emulsions Stabilized by Solid Particles (BaSO<sub>4</sub>). *Trans. Faraday Soc.* **1954**, *50*, 598–605.
  - (10) Chen, T.; Colver, P. J.; Bon, S. A. F. Organic–Inorganic Hybrid Hollow Spheres Prepared from TiO<sub>2</sub>-Stabilized Pickering Emulsion Polymerization. *Adv. Mater.* **2007**, *19*, 2286–2289.
  - (11) Williams, M.; Armes, S. P.; York, D. W. Clay-Based Colloidosomes. *Langmuir* **2012**, *28*, 1142–1148.
  - (12) Cauvin, S.; Colver, P. J.; Bon, S. A. F. Pickering Stabilized Miniemulsion Polymerization: Preparation of Clay Armored Latexes. *Macromolecules* **2005**, *38*, 7887–7889.
  - (13) Bon, S. A. F.; Colver, P. J. Pickering Miniemulsion Polymerization Using Laponite Clay as a Stabilizer. *Langmuir* **2007**, *23*, 8316–8322.
  - (14) Binks, B. P.; Lumsdon, S. O. Pickering Emulsions Stabilized by Monodisperse Latex Particles: Effects of Particle Size. *Langmuir* **2001**, *17*, 4540–4547.
  - (15) Aveyard, R.; Binks, B. P.; Clint, J. H.; Fletcher, P. D. I.; Horozov, T. S.; Neumann, B.; Paunov, V. N.; Annesley, J.; Botchway, S. W.; Nees, D.; et al. Measurement of Long-Range Repulsive Forces between Charged Particles at an Oil-Water Interface. *Phys. Rev. Lett.* **2002**, *88*, 246102–246105.
  - (16) Thompson, K. L.; Armes, S. P.; Howse, J. R.; Ebbens, S.; Ahmad, I.; Zaidi, J. H.; York, D. W.; Burdis, J. A. Covalently Cross-Linked Colloidosomes. *Macromolecules* **2010**, *43*, 10466–10474.
  - (17) Thompson, K. L.; Armes, S. P.; York, D. W.; Burdis, J. A. Synthesis of Sterically-Stabilized Latexes Using Weil-Defined Poly(glycerol Monomethacrylate) Macromonomers. *Macromolecules* **2010**, *43*, 2169–2177.
  - (18) Fujii, S.; Cai, Y.; Weaver, J. V. M.; Armes, S. P. Syntheses of Shell Cross-Linked Micelles Using Acidic ABC Triblock Copolymers and Their Application as pH-Responsive Particulate Emulsifiers. *J. Am. Chem. Soc.* **2005**, *127*, 7304–7305.
  - (19) Binks, B. P.; Murakami, R.; Armes, S. P.; Fujii, S. Temperature-Induced Inversion of Nanoparticle-Stabilized Emulsions. *Angew. Chemie* **2005**, *117*, 4873–4876.
  - (20) Madivala, B.; Fransaer, J.; Vermant, J. Self-Assembly and Rheology of Ellipsoidal Particles at Interfaces. *Langmuir* **2009**, *25*, 2718–2728.
  - (21) Reynaert, S.; Moldenaers, P.; Vermant, J. Control over Colloidal Aggregation in Monolayers of Latex Particles at the Oil-Water Interface. *Langmuir* **2006**, *22*, 4936–4945.
  - (22) Velev, O. D.; Furusawa, K.; Nagayama, K. Assembly of Latex Particles by Using Emulsion Droplets as Templates .1. Microstructured Hollow Spheres. *Langmuir* **1996**, *12*, 2374–2384.
  - (23) Velev, O. D.; Furusawa, K.; Nagayama, K. Assembly of Latex Particles by Using Emulsion Droplets as Templates .2. Ball-like and Composite Aggregates. *Langmuir* **1996**, *12*, 2385–2391.
  - (24) Velev, O.; Nagayama, K. Assembly of Latex Particles by Using Emulsion Droplets. 3. Reverse (Water in Oil) System. *Langmuir* **1997**, *7463*, 1856–1859.
  - (25) Cayre, O. J.; Biggs, S. Hollow Microspheres with Binary Porous Membranes from Solid-Stabilised Emulsion Templates. *J. Mater. Chem.* **2009**, *19*, 2724–2728.
  - (26) Yuan, Q.; Cayre, O. J.; Fujii, S.; Armes, S. P.; Williams, R. A.; Biggs, S. Responsive Core-

- Shell Latex Particles as Colloidosome Microcapsule Membranes. *Langmuir* **2010**, *26*, 18408–18414.
- (27) Andresen, M.; Stenius, P. Water-in-oil Emulsions Stabilized by Hydrophobized Microfibrillated Cellulose. *J. Dispers. Sci. Technol.* **2007**, *28*, 837–844.
- (28) Lee, K.; Blaker, D.; Murakami, R. Phase Behavior of Medium and High Internal Phase Water-in-Oil Emulsions Stabilized Solely by Hydrophobized Bacterial Cellulose Nano Fibrils. *Langmuir* **2014**, *30*, 452–460.
- (29) Kalashnikova, I.; Bizot, H.; Cathala, B.; Capron, I. New Pickering Emulsions Stabilized by Bacterial Cellulose Nanocrystals. *Langmuir* **2011**, *27*, 7471–7479.
- (30) Kalashnikova, I.; Bizot, H.; Bertocini, P.; Cathala, B.; Capron, I. Cellulosic Nanorods of Various Aspect Ratios for Oil in Water Pickering Emulsions. *Soft Matter* **2013**, *9*, 952–959.
- (31) Van Hooghten, R.; Imperiali, L.; Boeckx, V.; Sharma, R.; Vermant, J. Rough Nanoparticles at the Oil–water Interfaces: Their Structure, Rheology and Applications. *Soft Matter* **2013**, *9*, 10791–10798.
- (32) Noble, P. F.; Cayre, O. J.; Alargova, R. G.; Velez, O. D.; Paunov, V. N. Fabrication Of “hairy” colloidosomes with Shells of Polymeric Microrods. *J. Am. Chem. Soc.* **2004**, *126*, 8092–8093.
- (33) Fujii, S.; Read, E. S.; Binks, B. P.; Armes, S. P. Stimulus-Responsive Emulsifiers Based on Nanocomposite Microgel Particles. *Adv. Mater.* **2005**, *17*, 1014–1018.
- (34) Finkle, P.; Draper, H. D.; Hildebrand, J. H. The Theory of Emulsification. *J. Am. Chem. Soc.* **1923**, *45*, 2780–2788.
- (35) Paunov, V. N. Novel Method for Determining the Three-Phase Contact Angle of Colloid Particles Adsorbed at Air - Water and Oil - Water Interfaces. *Langmuir* **2003**, *19*, 7970–7976.
- (36) Arnaudov, L. N.; Cayre, O. J.; Stuart, M. a C.; Stoyanov, S. D.; Paunov, V. N. Measuring the Three-Phase Contact Angle of Nanoparticles at Fluid Interfaces. *Phys. Chem. Chem. Phys.* **2010**, *12*, 328–331.
- (37) Isa, L.; Lucas, F.; Wepf, R.; Reimhult, E. Measuring Single-Nanoparticle Wetting Properties by Freeze-Fracture Shadow-Casting Cryo-Scanning Electron Microscopy. *Nat. Commun.* **2011**, *2*, 438–447.
- (38) Hunter, T. N.; Jameson, G. J.; Wanless, E. J.; Dupin, D.; Armes, S. P. Adsorption of Submicrometer-Sized Cationic Sterically Stabilized Polystyrene Latex at the Air-Water Interface: Contact Angle Determination by Ellipsometry. *Langmuir* **2009**, *25*, 3440–3449.
- (39) Safouane, M.; Langevin, D.; Binks, B. P. Effect of Particle Hydrophobicity on the Properties of Silica Particle Layers at the Air-Water Interface. *Langmuir* **2007**, *23*, 11546–11553.
- (40) Binks, B. P. Particles as Surfactants—similarities and Differences. *Curr. Opin. Colloid Interface Sci.* **2002**, *7*, 21–41.
- (41) Sun, J. Z.; Erickson, M. C. E.; Parr, J. W. Refractive Index Matching and Clear Emulsions. *J. Cosmet. Sci.* **2005**, *56*, 253–265.
- (42) Hibberd, D. J.; Mackie, A. R.; Moates, G. K.; Penfold, R.; Watson, A. D.; Barker, G. C. Preparation and Characterisation of a Novel Buoyancy and Refractive Index Matched Oil-in-Water Emulsion. *Colloids Surfaces A Physicochem. Eng. Asp.* **2007**, *301*, 453–461.
- (43) Husband, F. A.; Garrod, M. J.; Mackie, A. R.; Burnett, G. R.; Wilde, P. J. Adsorbed Protein Secondary and Tertiary Structures by Circular Dichroism and Infrared Spectroscopy with Refractive Index Matched Emulsions. *J. Agric. Food Chem.* **2001**, *49*, 859–866.
- (44) Ashby, N. P.; Binks, B. P. Pickering Emulsions Stabilised by Laponite Clay Particles. *Phys. Chem. Chem. Phys.* **2000**, *2*, 5640–5646.
- (45) Binks, B. P.; Rodrigues, J. A. Enhanced Stabilization of Emulsions due to Surfactant-Induced Nanoparticle Flocculation. *Langmuir* **2007**, *23*, 7436–7439.
-

- (46) Binks, B. P.; Elliott, R.; Fletcher, P. D. I.; Johnson, A. J.; Thompson, M. A. ( 19 ) United States ( 12 ) Patent Application Publication ( 10 ) Pub . No . : US 2014 / 0031522 A1 Related U â€™™ S â€™™ Apphcation Data. No. Non-aqueous solid stabilized emulsions, US Patent. No: 0242016A1 August 2014.
- (47) Thompson, K. L.; Lane, J. A.; Derry, M. J.; Armes, S. P. Non-Aqueous Isorefractive Pickering Emulsions. *Langmuir* **2015**, *31*, 4373–4376.
- (48) Thompson, K. L.; Fielding, L. A.; Mykhaylyk, O. O.; Lane, J. A.; Derry, M. J.; Armes, S. P. Vermicious Thermo-Responsive Pickering Emulsifiers. *Chem. Sci.* **2015**, *6*, 4207–4214.
- (49) Yoshioka, H.; Itoh, Y.; Kiyomori, A.; Era, M.; Oki, Y. Fluorene-Based Chromophore for Degradation-Recoverable Solid-State Dye Laser. *Opt. Mater. Express* **2013**, *3*, 176–183.
- (50) Aralaguppi, M. I.; Jadar, C. V.; Aminabhavi, T. M. Density, Refractive Index, Viscosity, and Speed of Sound in Binary Mixtures of Cyclohexanone with Hexane, Heptane, Octane, Nonane, Decane, Dodecane, and 2,2,4-Trimethylpentane. *J. Chem. Eng. Data* **1999**, *44*, 435–440.
- (51) Fielding, L. A.; Derry, M. J.; Ladmiral, V.; Rosselgong, J.; Rodrigues, A. M.; Ratcliffe, L. P. D.; Sugihara, S.; Armes, S. P. RAFT Dispersion Polymerization in Non-Polar Solvents: Facile Production of Block Copolymer Spheres, Worms and Vesicles in N-Alkanes. *Chem. Sci.* **2013**, *4*, 2081–2087.
- (52) Charles, D. F. Refractive Indices of Sucrose-Water Solutions in the Range from 24 to 53% Sucrose. *Anal. Chem.* **1965**, *37*, 405–406.
- (53) Hoyt, L. F. New Table of the Refractive Index of Pure Glycerol at 20°C. *Ind. Eng. Chem.* **1934**, *26*, 329–332.
- (54) Loden, M.; Wessman, W. The Influence of a Cream Containing 20% Glycerin and Its Vehicle on Skin Barrier Properties. *Int. J. Cosmet. Sci.* **2001**, *23*, 115–119.
- (55) Frelichowska, J.; Bolzinger, M.-A.; Chevalier, Y. Effects of Solid Particle Content on Properties of O/w Pickering Emulsions. *J. Colloid Interface Sci.* **2010**, *351*, 348–356.
- (56) Chevalier, Y.; Bolzinger, M.-A. Emulsions Stabilized with Solid Nanoparticles: Pickering Emulsions. *Colloids Surfaces A Physicochem. Eng. Asp.* **2013**, *439*, 23–34.
- (57) Binks, B. P.; Whitby, C. P. Silica Particle-Stabilized Emulsions of Silicone Oil and Water: Aspects of Emulsification. *Langmuir* **2004**, *20*, 1130–1137.
- (58) Midmore, B. Effect of Aqueous Phase Composition on the Properties of a Silica-Stabilized W/O Emulsion. *J. Colloid Interface Sci.* **1999**, *213*, 352–359.
- (59) Arditty, S.; Schmitt, V.; Giermanska-Kahn, J.; Leal-Calderon, F. Materials Based on Solid-Stabilized Emulsions. *J. Colloid Interface Sci.* **2004**, *275*, 659–664.
- (60) Mable, C. J.; Warren, N. J.; Thompson, K. L.; Mykhaylyk, O. O.; Armes, S. P. Framboidal ABC Triblock Copolymer Vesicles: A New Class of Efficient Pickering Emulsifier. *Chem. Sci.* **2015**, *6*, 6179–6188.
- (61) Thompson, K. L.; Mable, C. J.; Cockram, A.; Warren, N. J.; Cunningham, V. J.; Jones, E. R.; Verber, R.; Armes, S. P. Are Block Copolymer Worms More Effective Pickering Emulsifiers than Block Copolymer Spheres? *Soft Matter* **2014**, *10*, 8615–8626.
- (62) Cunningham, V. J.; Alswieleh, A. M.; Thompson, K. L.; Williams, M.; Leggett, G. J.; Armes, S. P.; Musa, O. M. Poly(glycerol monomethacrylate)–Poly(benzyl Methacrylate) Diblock Copolymer Nanoparticles via RAFT Emulsion Polymerization: Synthesis, Characterization, and Interfacial Activity. *Macromolecules* **2014**, *47*, 5613–5623.
- (63) Katritzky, A. R.; Sild, S.; Karelson, M. Correlation and Prediction of the Refractive Indices of Polymers by QSPR. *J. Chem. Inf. Comput. Sci.* **1998**, *38*, 1171–1176.
- (64) Maeda, H.; Okada, M.; Fujii, S.; Nakamura, Y.; Furuzono, T. Pickering-Type Water-in-Oil-in-Water Multiple Emulsions toward Multihollow Nanocomposite Microspheres. *Langmuir* **2010**, *26*, 13727–13731.
- (65) Sekine, T.; Yoshida, K.; Matsuzaki, F.; Yanaki, T.; Yamaguchi, M. A Novel Method for Preparing Oil-in-Water-in-Oil Type Multiple Emulsions Using Organophilic

- Montmorillonite Clay Mineral. *J. Surfactants Deterg.* **1999**, *2*, 309–315.
- (66) Lee, D.; Weitz, D. A. Double Emulsion-Templated Nanoparticle Colloidosomes with Selective Permeability. *Adv. Mater.* **2008**, *20*, 3498–3503.
- (67) Cunha, A. G.; Mougel, J. B.; Cathala, B.; Berglund, L. a.; Capron, I. Preparation of Double Pickering Emulsions Stabilized by Chemically Tailored Nanocelluloses. *Langmuir* **2014**, *30*, 9327–9335.
- (68) Lee, D.; Weitz, D. A. Nonspherical Colloidosomes with Multiple Compartments from Double Emulsions. *Small* **2009**, *5*, 1932–1935.
- (69) Thompson, K. L.; Mable, C. J.; Lane, J. A.; Derry, M. J.; Fielding, L. A.; Armes, S. P. Preparation of Pickering Double Emulsions Using Block Copolymer Worms. *Langmuir* **2015**, *31*, 4137–4144.
- (70) Williams, M.; Armes, S. P.; Verstraete, P.; Smets, J. Double Emulsions and Colloidosomes-in-Colloidosomes Using Silica-Based Pickering Emulsifiers. *Langmuir* **2014**, *30*, 2703–2711.

## Chapter 7: Conclusions and future work

The work conducted in this thesis is primarily concerned with PISA syntheses conducted in silicone oil, a hitherto unexplored area. Polymerisation of a tertiary amine methacrylate (DMA) using a PDMS macro-CTA facilitated the production of spheres, worms or vesicles in a cyclic silicone solvent, D5. Perhaps surprisingly, DMA was unique amongst the various monomers examined in enabling access to the full range of diblock copolymer morphologies. Particular attention was given to the worm-like micelles, which formed free-standing gels in D5 at ambient temperature. In addition, similar worms are synthesised in D4, HDMS and *n*-dodecane. Moreover, it was demonstrated that such worms are efficient viscosity modifiers for these solvents. Given the prevalence of silicone oils in personal care products and cosmetics, such worms may offer a new route towards oil thickening for such applications. One technical barrier here is the incomplete DMA monomer conversions achieved in these particular syntheses which was as low as 90 % in some cases. Given the malodour and potential toxicity of DMA, the acceptable levels of this monomer should be no greater than a few hundred ppm in such applications. Therefore, increasing the DMA conversions of these PISA syntheses is essential for potential commercialisation. One approach, often used industrially, is to add excess of initiator at the end of the polymerisation which oligomerises any unreacted monomer. This route may be advantageous as it is also likely to cleave the CTA end-group, which would be desirable for personal care applications. An alternative approach would be to use a dual initiator system, each with distinctly different half-lives. The polymerisation could then be conducted at a temperature appropriate for one initiator, then the reaction temperature would be increased so that the second initiator becomes active under monomer-starved conditions.

Like many diblock copolymer worms synthesised by PISA, PDMS<sub>66</sub>-PDMA<sub>100</sub> worms proved to be thermoresponsive, exhibiting a worm-to-sphere transition on heating to 110 °C. This is attributed to the surface plasticisation of the PDMS core-forming block by hot D5 solvent. This morphological transition was characterised by variable temperature <sup>1</sup>H NMR, DLS, TEM, SAXS and rheology. It was determined that whilst degelation happens at 33 °C, further heating up to temperatures of 110 °C are required to achieve a full worm-to-sphere transition. Recently, Derry *et al.* have shown that for PSMA-PBzMA prepared in mineral oil, irreversible vesicle-to-worm transitions are possible upon heating to 150 °C.<sup>1</sup> An interesting extension of the work described in Chapter 3 would be to investigate the possibility of PDMS<sub>66</sub>-PDMA vesicles undergoing a similar (ir)reversible worm-to-sphere transition. This could be probed using variable-temperature SAXS, TEM and rheology. Such a transition could lead to irreversible silicone-oil thickening upon heating, which may be attractive for industrial applications.

In addition to investigating such thermoresponsive behaviour, the feasibility of cross-linking PDMS-PDMA nanoparticles *via* their tertiary amine-functional nanoparticle cores was explored. This was attempted by adding BIEE, an alkyl diiodide, to a dispersion of either spheres, worms or vesicles. When cross-linked *via* quaternisation, the PDMS<sub>66</sub>-PDMA nanoparticles become sufficiently robust as to withstand being dispersed in a good solvent for both blocks. Furthermore, the cross-linked PDMS<sub>66</sub>-PDMA<sub>100</sub> worms form significantly stronger gels and exhibit no thermoresponse. To determine whether or not this increase in gel strength is due to worm-stiffening, the SAXS patterns of both the cross-linked and linear precursor worms could be fit to an appropriate worm-like micelle model. Such analysis would enable the worm persistence length to be determined, which is a measure of their stiffness.

One unexpected and perplexing problem that emerged from Chapter 2 was that utilising the PDMS<sub>66</sub> macro-CTA for the RAFT dispersion polymerisation of BzMA in D5 resulted solely in kinetically-trapped spheres. In contrast, Lopez-Oliva *et al.* demonstrated that when the same PDMS<sub>66</sub>-PBzMA formulations were targetted in *n*-heptane rather than D5, spheres worms or vesicles could be obtained.<sup>2</sup> This observation suggests that the subtle change in solvency (from *n*-heptane vs. D5) has a profound effect on the resulting copolymer morphology. In general, if a particular PISA formulation is limited to kinetically-trapped spheres, a useful approach is to reduce the DP of the stabiliser block. This has the effect of shifting the phase boundaries towards worms and vesicles. For the PDMS<sub>66</sub> macro-CTA, however, this was not feasible. This is because this macro-CTA was only available over a very limited DP range. Therefore, efforts were made to overcome this problem by synthesising new relatively short macro-CTAs based on a silicone-containing methacrylic monomer, SiMA. Pleasingly, such macro-CTAs facilitate access to spheres, worms or vesicles when chain-extended with BzMA in D5. Furthermore, unlike the PDMS<sub>66</sub>-PDMA diblock copolymers described in Chapter 1, PSiMA<sub>13</sub>-PBzMA<sub>x</sub> worms and vesicles were available at much lower concentrations (5 and 10 % w/w, respectively). Moreover, PSiMA<sub>13</sub>-PBzMA<sub>57</sub> worms synthesised at 5 % w/w still formed free-standing gels. This new formulation may offer a significant advantage for personal care applications, for which using a lower copolymer concentration to achieve a similar thickening performance is desirable. Furthermore, this formulation did not suffer as badly from the problem of incomplete monomer conversions, as was observed with DMA. This is highly desirable for any application for which residual free-monomer must be minimised.

Although this PSiMA-PBzMA formulation offered many advantages, it does suffer from certain drawbacks. Particularly, copolymer molecular weight distributions of the diblocks broadened over time. One plausible explanation for this observation is that the PSiMA stabilisers are cross-

linking over time due to silanol impurities present within SiMA monomer. In the future, it would be interesting to investigate whether such a cross-linking mechanism could actually enhance some of the physical properties of the particle. For example, does the gel strength of the worms increase over time as a result of cross-linking? In addition, it would also be useful to find a means to purify the monomer in order to prevent the diblock copolymers cross-linking.

In general, the first half of this Thesis is focused on the PISA synthesis and characterisation of diblock copolymer nanoparticles in silicone oil. The latter half, however, is focused on the interfacial activity of some of these nanoparticles at various liquid-liquid interfaces. It was demonstrated, for example, that PSiMA-PBzMA spherical nanoparticles prepared directly in DM5 can stabilise oil-in-DM5 Pickering emulsions. A range of natural oils were investigated for such formulations, and several suitable candidates were determined, such as sunflower oil and castor oil. These components are often found in personal care products, and such surfactant-free Pickering emulsions are of some industrial interest.

Utilising nanoparticles with a statistical copolymer core of BzMA and LMA enabled a broader range of oils to be stabilised as droplets. These additional oils included macadamia oil, linseed oil, pumpkin seed oil and olive oil. It was hypothesised that the resulting nanoparticle cores are more wettable by these natural oils. To confirm this, a worthwhile future experiment could be conducted to measure the contact angles of these different nanoparticles *in situ*. In addition, it would also be interesting to investigate whether or not this strategy works for a range of different nanoparticle/liquid combinations. For example, does copolymerising a hydrophilic monomer into the core of a hydrophobic particle make the resulting particles more wettable by water? If this turns out to be a generic approach, it may provide a platform technology by which to synthesise bespoke Pickering emulsifiers with highly tuneable wettability. A further interesting follow-up study would be to prepare PSiMA-PBzMA worms in DM5 to examine their Pickering emulsifier performance for oil-in-oil emulsions. If this system behaves like similar systems reported for water-in-oil Pickering emulsions,<sup>3</sup> it is likely that such worms will be more efficient than the equivalent spheres. Therefore, this may offer a route to achieving similar Pickering emulsifier performance at a lower copolymer concentration.

Both oil-in-water and water-in-oil Pickering emulsions were studied in the final Chapter of this thesis. RAFT aqueous emulsion polymerisation was utilised to prepare hydrophilic PGMA-PTFEMA spherical nanoparticles. This semi-fluorinated core-forming block was chosen, in particular, because it has a relatively low refractive index when compared to most other methacrylic polymers.<sup>4</sup> This presented a unique opportunity to match the refractive index of the

resulting nanoparticles to that of the aqueous phase by addition of either glycerol or sucrose. Using this isorefractive dispersion, in conjunction with *n*-dodecane, enabled the production of highly transparent oil-in-water Pickering emulsions with an average transmission of more than 95 % across the entire visible spectrum. Furthermore, by synthesising the analogous PLMA-PTFEMA spherical nanoparticles *via* RAFT dispersion polymerisation in *n*-dodecane, a second set of isorefractive hydrophobic nanoparticles were produced. When used in conjunction with the hydrophilic nanoparticles, highly transparent Pickering double emulsions could be prepared. It would be interesting to investigate whether a similar approach could be used to produce highly transparent oil-in-oil Pickering emulsions. Given that the refractive index of liquids such as glycerol (1.4731)<sup>5</sup> and sunflower oil (1.474)<sup>6</sup> are remarkably similar, all that would be required is a similarly matched core-forming block. One obvious possibility here could be poly(*n*-butyl methacrylate), which has a refractive index of around 1.48 at 20 °C.<sup>4</sup>

## 7.1 References

- (1) Derry, M. J.; Mykhaylyk, O. O.; Armes, S. P. A Vesicle-to-Worm Transition Provides a New High-Temperature Oil Thickening Mechanism. *Angew. Chemie* **2017**, *129*, 1772–1776.
- (2) Lopez-Oliva, A. P.; Warren, N. J.; Rajkumar, A.; Mykhaylyk, O. O.; Derry, M. J.; Doncom, K. E. B.; Rymaruk, M. J.; Armes, S. P. Polydimethylsiloxane-Based Diblock Copolymer Nano-Objects Prepared in Nonpolar Media via RAFT-Mediated Polymerization-Induced Self-Assembly. *Macromolecules* **2015**, *48*, 3547–3555.
- (3) Thompson, K. L.; Mable, C. J.; Cockram, A.; Warren, N. J.; Cunningham, V. J.; Jones, E. R.; Verber, R.; Armes, S. P. Are Block Copolymer Worms More Effective Pickering Emulsifiers than Block Copolymer Spheres? *Soft Matter* **2014**, *10*, 8615–8626.
- (4) Katritzky, A. R.; Sild, S.; Karelson, M. Correlation and Prediction of the Refractive Indices of Polymers by QSPR. *J. Chem. Inf. Comput. Sci.* **1998**, *38*, 1171–1176.
- (5) Hoyt, L. F. New Table of the Refractive Index of Pure Glycerol at 20°C. *Ind. Eng. Chem.* **1934**, *26*, 329–332.
- (6) Ghanei, R.; Moradi, G. R.; TaherpourKalantari, R.; Arjmandzadeh, E. Variation of Physical Properties during Transesterification of Sunflower Oil to Biodiesel as an Approach to Predict Reaction Progress. *Fuel Process. Technol.* **2011**, *92*, 1593–1598.